UNIVERSITY OF CALIFORNIA SAN DIEGO

On the mechanisms of axis specification in *Hydra*

A dissertation submitted in partial satisfaction of the
requirements for the degree
Doctor of Philosophy

in

Bioengineering

by

Rui Wang

Committee in charge:

Professor Eva-Maria S. Collins, Chair
Professor Adam Engler, Co-Chair
Professor Patrick Diamond
Professor Andrew McCulloch
Professor Karl Willert

2021

The dissertation of Rui Wang is approved, and it is acceptable in quality and form for publication on microfilm and electronically.

University of California San Diego

2021

EPIGRAPH

The second Labour which he undertook was the slaying of the Lernaean Hydra, springing from whose single body were fashioned a hundred necks, each bearing the head of a serpent. And when one head was cut off, the place where it was severed put forth two others; for this reason it was considered to be invincible, and with good reason, since the part of it which was subdued sent forth a two-fold assistance in its place.

Against a thing so difficult to manage as this Heracles devised an ingenious scheme...

—Diodorus Siculus, Library of History 4.11.5 (trans. Oldfather)

TABLE OF CONTENTS

LIST OF FIGURES

LIST OF TABLES

LIST OF SUPPLEMENTAL FILES

ACKNOWLEDGEMENTS

I would like to acknowledge Professor Eva-Maria Collins for her mentorship throughout my thesis studies, and her support as chair of my committee. I would also like to acknowledge Professor Adam Engler for being my co-chair in the Bioengineering department, and all of my committee members for their thougthful advice and valuable discussions. Finally I would like to thank all the members of the Collins Lab for their assistance with experiments, helpful discussions, and moral support throughout this long process.

Chapter 3, in full, is a reformatted reprint of material as it appears in Biophysical Journal, 2019. (Wang, R., Goel, T., Khazoyan, K., Sabry, Z., Quan, H.J., Diamond, P.H. and Collins, E.M.S. Mouth Function Determines The Shape Oscillation Pattern In Regenerating Hydra Tissue Spheres. Biophysical Journal, 117(6), pp.1145-1155.) Use of this manuscript in this dissertation is covered by the rights permitted to the authors by Elsevier. The dissertation author was the co-primary author of this paper.

Chapter 4, in full, is a reformatted reprint of material as it appears in PloS one, 2019. (Goel, T., Wang, R., Martin, S., Lanphear, E. and Collins, E.M.S., 2019. Linalool acts as a fast and reversible anesthetic in Hydra. PloS one, 2019). Use of this manuscript in this dissertation is covered by the rights permitted to the authors by PloS. The dissertation author was the co-primary author of this paper.

Chapter 5, in full, is a reprint of material as it appears in Developmental Biology 2020. (Wang, R. and Collins, E.M.S. A novel lateral grafting technique for studying patterning in Hydra. Developmental Biology, 2020, and Wang, R., Steele, R.E., and Collins, E.M.S. Wnt signaling determines body axis polarity in regenerating Hydra tissue fragments.

Developmental Biology, 2020). Use of these manuscripts in this dissertation is covered by the rights permitted to the authors by Elsevier. The dissertation author was the primary author of these papers.

VITA

2015	B. S. in Biological Engineering, Massachusetts Institute of Technology
2016-2017	Graduate Teaching Assistant, University of California San Diego
2021	Ph.D. in Bioengineering, University of California San Diego

PUBLICATIONS

Wang, R., Goel, T., Khazoyan, K., Sabry, Z., Quan, H.J., Diamond, P.H. and Collins, E.M.S., 2019. Mouth Function Determines The Shape Oscillation Pattern In Regenerating Hydra Tissue Spheres. Biophysical journal, 117(6), pp.1145-1155.

Goel, T., Wang, R., Martin, S., Lanphear, E. and Collins, E.M.S., 2019. Linalool acts as a fast and reversible anesthetic in Hydra. PloS one, 14(10), p.e0224221.

Wang, R. and Collins, E.M.S., 2020. A novel lateral grafting technique for studying patterning in Hydra. Developmental Biology, 462(1), pp. 60-65.

Wang, R., Steele, R.E., and Collins, E.M.S., 2020. Wnt signaling determines body axis polarity in regenerating Hydra tissue fragments. Developmental Biology, 467(1-2), pp. 88-94.

ABSTRACT OF THE DISSERTATION

On the mechanisms of axis specification in *Hydra*

by

Rui Wang

Doctor of Philosophy in Bioengineering

University of California San Diego, 2021

Professor Eva-Maria S. Collins, Chair
Professor Adam Engler, Co-Chair

The freshwater cnidarian *Hydra* owes its long history in experimental biology to its unique potential to address questions regarding the formation of complex patterns in biological systems. Its regenerative abilities enable grafting and transplantation experiments in the adult animal, which allowed researchers to probe and quantify the signaling gradients defining its body axis even prior to the advent of modern biochemical techniques. Furthermore, its ability to regenerate a complete animal from cell aggregates offers an easily studied *de novo* axis specification event. *Hydra*'s body plan is sufficiently simple that quantitative

modeling is feasible. Several such models of pattern formation have been developed that can reproduce experimental observations of transplantations and regeneration. However, the quantitative experimental data needed to definitively test their core premises have remained largely out of reach, representing a major limitation on *Hydra*'s broader relevance.

In this dissertation, I leverage recent advances in molecular biology combined with adaptations of classical experiments to provide some of this quantitative validation. Existing models of *Hydra* patterning make two core assumptions: that a shift in oscillation pattern is a close approximation for biochemical specification of the body axis, and that tissue pieces can be used in lieu of cell aggregates for model testing and validation. We show the oscillation pattern shift is the result of a functional mouth structure rather than a close marker for a biochemical axis specification event. Further, we demonstrate that morphogen gradients encode axis information in the body of *Hydra* at a scale of several hundred microns, indicating that small tissue fragments do not exhibit an axis specification event as previously assumed. These findings demonstrate the need to reevaluate existing models. In addition, I aimed to develop new tools to enable further research. I developed transgenic strains introducing a new fluorescent protein to the system, and created plasmid constructs for a fluorescent fusion protein reporter for *in vivo* quantitative imaging. I also gathered preliminary data in support of innexins as regulators of patterning. This dissertation thus presents several valuable experimental findings on the nature of axis specifications in *Hydra*, and lays foundations for future quantitative studies.

Chapter 1

Introduction

Morphogenesis and patterning are key areas of interest in developmental biology. In particular, the processes by which an organism determines its body axes from an initially isotropic state have yet to be fully understood. Determining how axis specification is executed and regulated has implications for our basic understanding of developmental processes, as well as for studies of regeneration and tissue engineering.

Morphogen gradients formed by secretion and degradation of signaling molecules [50] are known to control patterning in model systems as diverse as *Drosophila*, *Xenopus*, zebrafish and chick [41]. More recently, studies have shown that mechanical cues can impact pattern formation and cell differentiation. Mechanotransduction pathways translating mechanical force into biochemical signals play roles in a range of developmental processes, with evidence of mechanical strain regulating embryonic development in organisms including *Drosophila*, *Xenopus* and mouse [10], as well as for shear stress from fluid flow directing in vascular development [35] and left-right symmetry breaking in zebrafish [9] and mouse [29].

Challenges in isolating the contributions of possible mechanotransduction pathways are in large part due to a question of complexity: *in vivo* studies face challenges due to the difficulty of studying single factors in a massively interconnected system, and limitations on the experiments that are possible without disrupting or killing the organism. *In vitro* systems solve several of these challenges, but are often oversimplifications: the isolation of one aspect of the living system often means that results thus obtained are not fully relevant in the full organism.

To address these challenges we employ the freshwater cnidarian *Hydra vulgaris*: a powerful model system amenable to mathematical modeling as well as mechanical and biomolecular manipulation [11]. The ability to easily conduct and image a wide array of experimental manipulations typically limited to *in vitro* systems in a complete animal offers a unique chance to study the core mechanisms of patterning.

1.1 *Hydra* as a model organism

Hydra vulgaris is a small freshwater cnidarian with a worldwide distribution [45]. *Hydra* has a simple body plan: it has a tubular body column with an adhesive foot on one end, and a head at the other. The head consists of a mouth at the tip of the conical hypostome, ringed by several tentacles (Fig. 1.1A). It reproduces asexually by budding from the lower body column, and is also capable of sexual reproduction when stressed [39].

Hydra is composed of three self-renewing stem cell lineages - endodermal, ectodermal and interstitial. The endoderm and ectoderm are epithelial tissue layers, with the ectoderm on the exterior of the animal and the endoderm on the interior. They are separated by a

layer of extracellular matrix called the mesoglea. The interstitial cell lineage is distributed throughout the body and gives rise to a range of cell types, including gland cells, neurons, and nematocytes. [44]

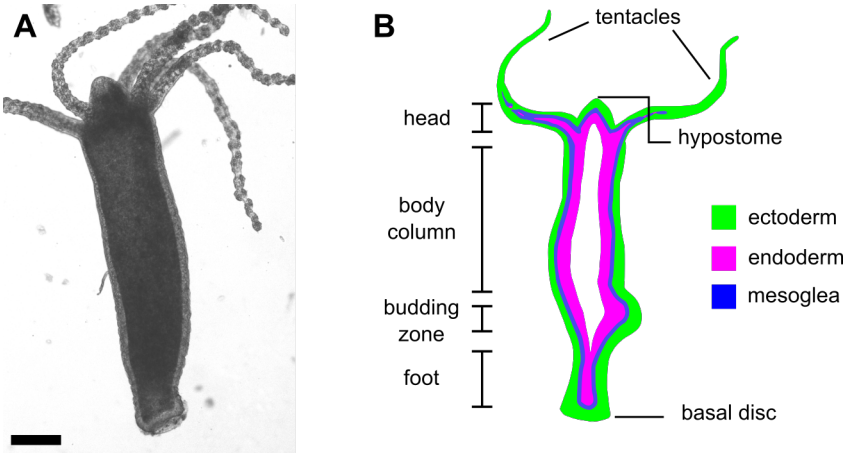

Figure 1.1: Anatomy of *Hydra vulgaris*. A. Photograph of adult *Hydra*. Scale bar 0.25 mm. B. Diagram of adult *Hydra* with anatomical features and epithelial tissue layers labeled.

Hydra represents a powerful model system for studies of regeneration and patterning, and has been used as such for centuries [23]. Its greatest asset in this regard is its fantastic ability to regenerate. *Hydra*'s tolerance of surgical manipulation and easy acceptance of transplanted tissue made it particularly well suited to the study of morphogenesis and patterning via tissue grafts. Early experiments established that *Hydra*'s hypostome is an organizer, and determined some of the characteristics of this organizer [5, 51]. Organizers are defined as small groups of cells that direct differentiation and/or patterning of the surrounding tissue via secreted signals, and are known to play critical roles in embryonic development [1]. Further transplantation experiments found that the head organizer both induces head formation at short range (head activation) and inhibits the formation of further organizers at a longer range (head inhibition) [25, 26].

Beyond surgical manipulations, *Hydra* is also capable of regeneration of an entire new animal: tissue fragments larger than approximately 270-300 cells can regenerate into complete animals [36], and even aggregates of dissassociated cells can give rise to new animals if properly cared for [13] (Fig. 1.2).

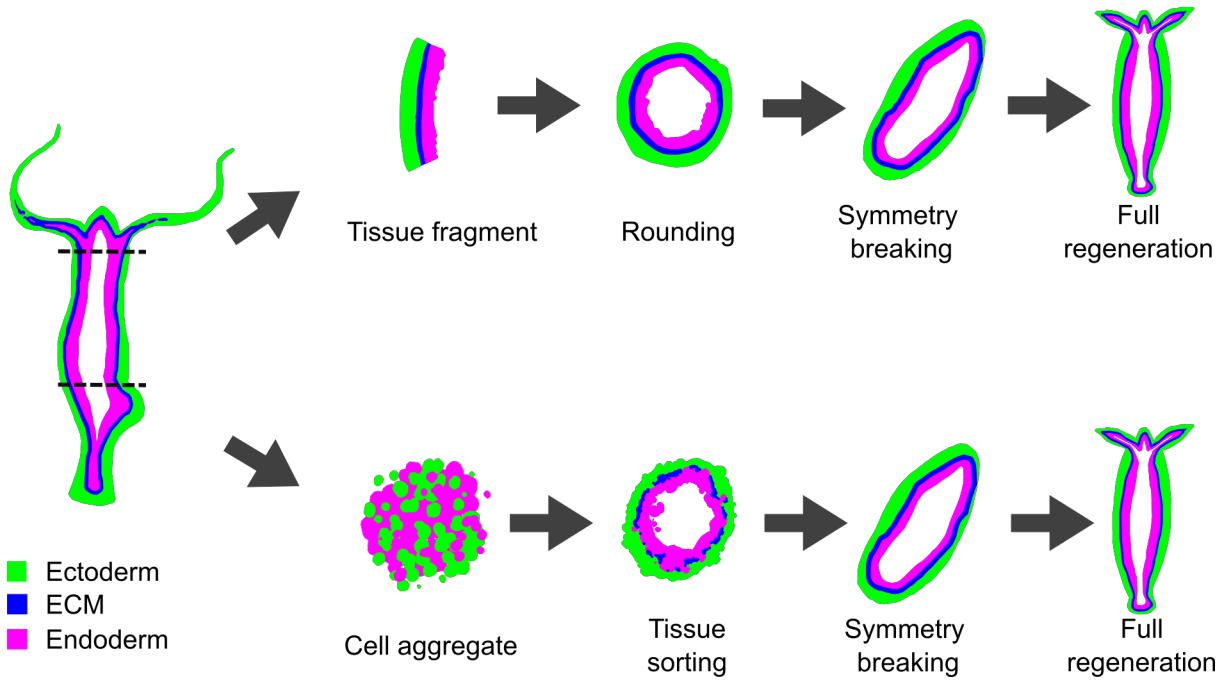

Figure 1.2: *Hydra* has powerful regenerative abilities. Cut tissue fragments fold and round into spheroids. Cell aggregates sort their epithelial layers, then hollow to form a spheroid. In both cases the spheroid undergoes osmotically-driven mechanical oscillations and regenerates into a full animal.

Regeneration of an entire animal from an apparently disordered state represents a *de novo* pattern formation event that can be triggered at will and easily observed *in vivo* - a rarity in the world of experimental biology. This feature, along with a very simple body plan and data from transplantation experiments for easy validation made *Hydra* a favored subject for attempts at quantitative models of patterning.

Hydra was one of the systems that inspired Alan Turing to create his foundational reaction-diffusion model of morphogenesis in 1952 [46]. Later, Gierer and Meinhardt used Turing's work as a basis to develop a reaction-diffusion model of *Hydra* patterning [14] that accurately reproduced the results of transplantation experiments. The Gierer-Meinhardt model is a reaction-diffusion model involving an activator and an inhibitor:

$$\frac{\delta a}{\delta t} = \rho_0 \rho + c\rho \frac{a^2}{h} - \mu_a a + D_a \frac{\delta^2 a}{\delta x^2}$$

$$\frac{\delta h}{\delta t} = c' \rho' a^2 - \mu_h h + D_h \frac{\delta^2 h}{\delta x^2}$$

Here a is a short-range autocatalytic activator, and h is a long-range inhibitor. q represents activator source density, q' represents inhibitor source density, μ_a and μ_h are decay rates, and D_a, D_h are diffusion constants. q_0, c, and c' are constants. This model is capable of reproducing the results of head transplantation experiments with a good degree of accuracy, and can simulate establishing a stable pattern form a homogeneous starting state given only a small initial perturbation [14].

Semi-quantitative probing of the head activation and inhibition gradients [25, 26] demonstrated that the head inhibition effect is strongest near the head organizer. Additionally, it was found that the relative length scales of head activation and inhibition match the

Gierer-Meinhardt model's predictions quite well [43]. This represented a promising quantitative model of patterning in *Hydra* well in advance of the genetic and molecular tools necessary to study pattern formation directly.

The sequencing of the *Hydra* genome in 2010 [7] enabled us to revisit these fundamental questions with modern tools. Transgenic reporter strains created by embryo microinjection of plasmid constructs allow *in vivo* visualization of gene expression [20]. In addition, it it was discovered that *Hydra* shares many key developmental genes and pathways with higher organisms. A key discovery is that the canonical Wnt signaling pathway is highly conserved. In *Hydra*, Wnt3 was found to set the head organizer [18] and to match the predicted qualities of the head activator [28].

This dissertation takes advantage of these recent advances to develop new methods, and revisit open questions regarding *Hydra* patterning. I experimentally test two core assumptions that existing mathematical models make regarding axis specification in regenerating *Hydra*. I also present work towards the development of new fluorescent reporter strains suitable for the *in vivo* observation of morphogens, and present preliminary data regarding a possible novel aspect of morphogenesis in *Hydra*. In this way I hope to advance the field's knowledge, and contribute to the groundwork required to fully realize *Hydra*'s potential as a model system.

1.2 Quantitative study of proposed axis specification marker

Two relatively recent models purporting to quantitatively describe the process of patterning in *Hydra* exist. These models are motivated by the fact that the secreted inhibitor molecule predicted by Gierer and Meinhardt [14] has yet to be conclusively identified. It is entirely possible that even if the reaction-diffusion model accurately describes experimental results, there is no single molecule responsible for all the functions ascribed to the inhibitor. Therefore, these models propose a mechanism by which tissue strain regulates Wnt signaling.

A possible mechanotransduction pathway was a promising avenue of inquiry for two main reasons. Firstly, mechanical regulation of development in general and Wnt signaling in particular is observed in a range of other model organisms. Wnt-β-catenin signaling is known to be mechanically activated in maintaining progenitor cells in developing joints in the mouse [21, 17], as well as in mesoderm specification in *Drosophila* and zebrafish [6]. The presence of this mechanism in both insects and fish suggests that it may be common to all bilaterians, and the conservation of the mechanosensitive β-catenin phosphorylation in even more phylogenetically diverse organisms hints that mechanical activation of Wnt-β-catenin signaling may in fact be common to all metazoans [6]. Secondly, regenerating spheroids of *Hydra* tissue were observed to undergo osmotically-driven cycles of swelling and rupture, representing repetitive tissue strain. Shape analysis of the spheroid could be used to detect elongation representing a body axis, and it was noted that an axis became detectable at a similar time to a marked shift in oscillation frequency and amplitude [37]. Therefore, a feedback between mechanical cues and biochemical signaling seemed feasible.

Soriano *et al.* first theorized that the missing inhibitor functions could be fulfilled by a feedback between mechanical force and biochemical signaling [37]. In their model, they propose a direct relation between tissue strain and the diffusion coefficient of one of the morphogens. Morphogen concentration dynamics are still modeled using the Gierer-Meinhardt model, with axis specification defined as the time at which a stable morphogen gradient is formed.

Mercker *et al.* then further explored this idea and proposed a variant of the model [27], in which a feedback mechanism exists between tissue stretch and morphogen diffusion. Under this model, the local diffusion coefficient is a function of tissue strain, while the elastic modulus of the tissue is a function of morphogen concentration. In this way a domain of high morphogen expression consistent with the head organizer forms at an area of high tissue deformation, corresponding with one end of the gradually elongating spheroid.

The main weakness of these studies is a lack of solid experimental validation. *Hydra* spheroid regeneration suffers from a lack of easily quantified, well-understood regeneration milestones that could be used to constrain the models. Thus, both Soriano *et al.* and Mercker *et al.* assume that the oscillation pattern shift represents a close approximation for biochemical specification of the body axis. The authors of both models acknowledge that the true axis specification event likely occurs slightly earlier, but posit that the correlation is still sufficiently close to allow the use of oscillation pattern shift as a model constraint.

While the oscillation pattern has the advantage of being relatively simple to quantify via 2-dimensional imaging, both its biological cause and its timing relative to the formation of biochemical gradients remained unknown. Absent this information it is difficult to experimentally validate or disprove the mechanotransduction pathway proposed by the models.

Therefore, I aimed to investigate and better define this behavior.

In chapter 2 of this work, I describe the testing and development of methods to enable quantitative study of the oscillation pattern. In chapter 3, I utilize these techniques combined with additional biological manipulations to demonstrate that the pattern shift is an artifact caused by the animal's use of its mouth to regulate internal pressure. As a head organizer must be established far in advance of the formation of a functional mouth structure, this highlights the urgent need for retuning the existing models or exploring alternatives.

1.3 Encoding and inheritance of axis information

Having shown one core assumption of existing quantitative models to be inaccurate, it was prudent to confirm other assumptions used in model validation. A second potential area of concern is the idea that both aggregates and sufficiently small tissue pieces undergo a *de novo* axis specification event during regeneration. This is potentially critical due to the use of tissue fragments to generate the experimental data used in model construction and validation [37, 38, 27].

A 2017 study challenges the equivalence between tissue fragments and aggregates by claiming that the former inherit axis information from the parental animal via the organization of contractile actin structures known as myonemes [24]. While the experiments in this work do not definitively establish a causal link between myoneme structure and axis inheritance, they do clearly illustrate that organized domains of myonemes are retained in small tissue fragments, persist throughout regeneration, and are correlated with the direction of the eventual body axis. We were able to independently verify the presence of organized

myonemes in small fragments via imaging of the tissue spheroids used in chapter 3 [49]. It is clear that small tissue fragments retain some amount of structure throughout regeneration, and cannot be assumed to begin as isotropic spheroids in the way that cell aggregates presumably do.

Determining the mechanism and robustness of the axis inheritance effect are therefore urgent concerns. Establishing the means by which axis information is encoded in *Hydra* tissue would provide valuable direction in considering the design of future studies of body axis specification. Notably, if the myoneme theory is correct it represents a new direction that needs to be explored and a mechanism that is not known in any other model organism. Testing for a causal link between myoneme structure and the direction of the inherited axis would be very challenging within the limitations of existing methods. A significant advance on the grafting techniques previously used to probe axis information was therefore necessary.

Chapter 4 of this work represents the quantification of a new safe and reversible anesthetic for *Hydra*, linalool, and a review of existing anesthetics in the field demonstrating that linalool is superior for most imaging and surgical manipulation applications. In chapter 5, I use linalool to develop a novel grafting technique that allows investigation of effects running perpendicular to the body axis. I then use this technique to test the theory that actin structure encodes axis information, and find that biochemical signaling gradients override actin structure in setting the regenerated body axis even when the differential is limited to what naturally occurs within the animal's body column. This work definitively proves that biochemical signaling encodes body axis information even on the scale of small tissue fragments. This supports the theory that tissue pieces do not experience a *de novo* axis specification event, and indicates that further efforts to probe the nature of patterning in

Hydra should focus on morphogen gradients.

1.4 Development of new reporter strains

The advent of a fully sequenced *Hydra* genome [7] opened a vast array of possible explorations using modern molecular biology techniques, including methods for the creation of transgenic strains.

The most robust technique, used to produce reporter strains now widely used throughout the field, consists of embryo microinjection of plasmid constructs [20]. Due to *Hydra*'s ability to incorporate foreign DNA this approach reliably yields transgenic animals. A relatively simple example of this approach is constructs with the *Hydra* actin promoter driving constitutive expression of fluorescent proteins (FPs). Combining endoderm and ectoderm expressing different fluorescent proteins allows easy *in vivo* differentiation of the lineages [15]. Constructs can also use the promoters of genes of interest for *in vivo* visualization of gene expression. Examples of such strains include HyWnt3, a Wnt critical to the head organizer [28], and HyBra2, a T-box gene directly regulated by Wnt [15].

Beyond visualization of gene expression, choice of promoter and of the protein or sequence being expressed can be used to achieve a range of useful outcomes. Promoters specific to certain cell types can be coupled with fluorescent markers to visualize these cells and their activity. Strains using neuron-specific promoters to drive calcium indicators have been used to visualize the contraction activity of epithelial tissue [40] and to track the activity of discrete neuron subpopulations within *Hydra*'s nerve net [8, 30, 31]. LifeAct-GFP lines [2] allow visualization of myoneme structure *in vivo* [24]. Driving a gene of interest with

the actin promoter can be used to overexpress a protein, as seen in β-catenin [12] and lamin [22] overexpression strains. In addition, knockdown of a gene using the same approach to express an shRNA has also been reported [22]. Finally, these authors also report the successful use of a tetracycline-inducible promoter [22], which could enable manipulations that would otherwise be lethal.

These manipulations clearly show the power of the plasmid construct approach. However, with regards to the study of pattern formation in *Hydra* it has several critical limitations. Almost all existing strains are a promoter of interest directly driving a fluorescent protein. This is a potentially serious flaw, especially in the case of diffusing morphogens where expression domain is not well correlated with protein localization. Fluorescent fusion proteins have been created, but are of limited use as they are not driven by their native promoters. Finally, strains made by plasmid microinjection are not helpful in studies of the native protein.

In chapter 6 of this work I present the development of several new transgenic strains aimed at addressing these issues. I successfully established new strains expressing the yellow fluorescent protein YPet driven by the actin promoter in both endoderm and ectoderm. I begin the process of creating a triply-labeled strain to enable simultaneous imaging of all three stem cell lineages, serving as a proof of concept for co-visualization of multiple genes. I also created constructs using the promoter of Sp5, a candidate Wnt inhibitor, to drive either a fluorescent protein alone or a Sp5-fluorescent protein fusion. These new transgenics and future strains like them will be instrumental in obtaining quantitative data necessary for the retuning of existing models or the construction of new ones.

1.5 Exploring alternate patterning mechanisms

The Gierer-Meinhardt model of *Hydra* patterning [14] was developed far in advance of detailed biochemical knowledge. As the field advanced some aspects of this early model were validated - particularly findings suggesting that Wnt3 matches the predicted behaviors of the activator molecule [18, 28]. However, other aspects remained elusive: while a graded head inhibition effect clearly exists [25, 42] the predicted diffusing inhibitor has yet to be conclusively identified. Proteins matching some of the predicted characteristics have been studied: dkk is a secreted Wnt antagonist [3, 16] but is not expressed near the head organizer. Sp5 is known to be a Wnt inhibitor in other systems and has recently been characterized as such in *Hydra* [48]. It is expressed near the head but is not secreted. The inability to identify a single secreted morphogen responsible for head inhibition despite ever-increasing molecular biology efforts emphasizes the necessity of investigating alternate methods of regulating axis specification.

Gap junctions represent promising candidates for unexplored components of the Wnt signaling pathway. Connexins have been shown to be targets of and to regulate Wnt-β-catenin signaling in mammalian systems (ex. [47, 19]). A smaller body of work in invertebrate models has also shown gap junctions as targets of Wnt signaling [4], and evidence of patterning defects in response to gap junction inhibition [34, 32, 33]. *Hydra* is known to have a number of innexin genes, several of which are expressed in gradients that are strongest near the head and weaken down the body column - a pattern similar to that of the predicted inhibitor.

In chapter 7 of this work I explore gap junctions as a possible component of the Wnt

signaling pathway. I have established expression patterns for three candidate innexins, and obtained a wide range of preliminary data suggesting that several methods of perturbing Wnt signaling can alter innexin expression in *Hydra*. Future work in this area will focus on quantitatively confirming innexins as targets of Wnt signaling, and determining whether Wnt signaling and patterning can be affected by perturbing innexin function or expression.

Bibliography

[1] Claire Anderson and Claudio D. Stern. "Organizers in Development". In: *Current Topics in Developmental Biology*. Vol. 117. Academic Press Inc., Dec. 2016, pp. 435–454. DOI: 10.1016/bs.ctdb.2015.11.023.

[2] Roland Aufschnaiter, Roland Wedlich-Söldner, Xiaoming Zhang, and Bert Hobmayer. "Apical and basal epitheliomuscular F-actin dynamics during Hydra bud evagination". In: *Biology Open* 6.8 (Aug. 2017), pp. 1137–1148. ISSN: 20466390. DOI: 10.1242/bio.022723.

[3] René Augustin, André Franke, Konstantin Khalturin, Rainer Kiko, Stefan Siebert, Georg Hemmrich, and Thomas C.G. Bosch. "Dickkopf related genes are components of the positional value gradient in Hydra". In: *Developmental Biology* 296.1 (Aug. 2006), pp. 62–70. ISSN: 00121606. DOI: 10.1016/j.ydbio.2006.04.003.

[4] Reinhard Bauer, Corinna Lehmann, Bernhard Fuss, Franka Eckardt, and Michael Hoch. "The Drosophila gap junction channel gene innexin 2 controls foregut development in response to Wingless signalling". In: *Journal of Cell Science* 115.9 (2002), pp. 1859–1867. ISSN: 00219533.

[5] Ethel Nicholson Browne. "The production of new hydranths in Hydra by the insertion of small grafts". In: *Journal of Experimental Zoology* 7.1 (Aug. 1909), pp. 1–23. ISSN: 0022-104X. DOI: 10.1002/jez.1400070102.

[6] Thibaut Brunet, Adrien Bouclet, Padra Ahmadi, Démosthène Mitrossilis, Benjamin Driquez, Anne Christine Brunet, Laurent Henry, Fanny Serman, Gaëlle Béalle, Christine Ménager, Frédéric Dumas-Bouchiat, Dominique Givord, Constantin Yanicostas, Damien Le-Roy, Nora M. Dempsey, Anne Plessis, and Emmanuel Farge. "Evolutionary conservation of early mesoderm specification by mechanotransduction in Bilateria". In: *Nature Communications* 4.1 (Nov. 2013), pp. 1–15. ISSN: 20411723. DOI: 10.1038/ncomms3821.

[7] Jarrod A. Chapman, Ewen F. Kirkness, Oleg Simakov, Steven E. Hampson, Therese Mitros, Thomas Weinmaier, Thomas Rattei, Prakash G. Balasubramanian, Jon Borman, Dana Busam, Kathryn Disbennett, Cynthia Pfannkoch, Nadezhda Sumin, Granger G. Sutton, Lakshmi Devi Viswanathan, Brian Walenz, David M. Goodstein, Uffe Hellsten, Takeshi Kawashima, Simon E. Prochnik, Nicholas H. Putnam, Shengquiang Shu, Bruce Blumberg, Catherine E. Dana, Lydia Gee, Dennis F. Kibler, Lee Law, Dirk Lindgens, Daniel E. Martinez, Jisong Peng, Philip A. Wigge, Bianca Bertulat, Corina Guder, Yukio Nakamura, Suat Ozbek, Hiroshi Watanabe, Konstantin Khalturin, Georg Hemmrich, André Franke, René Augustin, Sebastian Fraune, Eisuke Hayakawa, Shiho Hayakawa, Mamiko Hirose, Jung Shan Hwang, Kazuho Ikeo, Chiemi Nishimiya-Fujisawa, Atshushi Ogura, Toshio Takahashi, Patrick R.H. Steinmetz, Xiaoming Zhang, Roland Aufschnaiter, Marie Kristin Eder, Anne Kathrin Gorny, Willi Salvenmoser, Alysha M. Heimberg, Benjamin M. Wheeler, Kevin J. Peterson, Angelika Böttger, Patrick Tischler, Alexander Wolf, Takashi Gojobori, Karin A. Remington,

Robert L. Strausberg, J. Craig Venter, Ulrich Technau, Bert Hobmayer, Thomas C.G. Bosch, Thomas W. Holstein, Toshitaka Fujisawa, Hans R. Bode, Charles N. David, Daniel S. Rokhsar, and Robert E. Steele. "The dynamic genome of Hydra". In: *Nature* 464.7288 (2010), pp. 592–596. ISSN: 00280836. DOI: 10.1038/nature08830.

[8] Christophe Dupre and Rafael Yuste. "Non-overlapping Neural Networks in Hydra vulgaris". In: *Current Biology* 27.8 (Apr. 2017), pp. 1085–1097. ISSN: 0960-9822. DOI: 10.1016/J.CUB.2017.02.049.

[9] Jeffrey J. Essner, Jeffrey D. Amack, Molly K. Nyholm, Erin B. Harris, and H. Joseph Yost. "Kupffer's vesicle is a ciliated organ of asymmetry in the zebrafish embryo that initiates left-right development of the brain, heart and gut". In: *Development* 132.6 (Mar. 2005), pp. 1247–1260. ISSN: 09501991. DOI: 10.1242/dev.01663.

[10] Emmanuel Farge. *Mechanotransduction in Development*. Vol. 95. Academic Press, Jan. 2011, pp. 243–265. DOI: 10.1016/B978-0-12-385065-2.00008-6.

[11] Brigitte Galliot. "The hydra model system". In: *International Journal of Developmental Biology* 56.6-8 (2012), pp. 407–409. ISSN: 02146282. DOI: 10.1387/ijdb.120094bg.

[12] Lydia Gee, Julia Hartig, Lee Law, Jörg Wittlieb, Konstantin Khalturin, Thomas C.G. G Bosch, and Hans R. Bode. "β-catenin plays a central role in setting up the head organizer in hydra". In: *Developmental Biology* 340.1 (Apr. 2010), pp. 116–124. ISSN: 0012-1606.

[13] A Gierer, S Berking, H Bode, C N David, K Flick, G Hansmann, H Schaller, and E Trenkner. "Regeneration of hydra from reaggregated cells". In: *Nature New Biology* 239.91 (1972), pp. 98–101. ISSN: 00900028. DOI: 10.1038/newbio239098a0.

[14] A. Gierer and Hans Meinhardt. "A theory of biological pattern formation". In: *Kybernetik* 12.1 (1972), pp. 30–39. ISSN: 03401200. DOI: 10.1007/BF00289234.

[15] K. M. Glauber, C. E. Dana, S. S. Park, D. A. Colby, Y. Noro, T. Fujisawa, A. R. Chamberlin, and R. E. Steele. "A small molecule screen identifies a novel compound that induces a homeotic transformation in Hydra". In: *Development* 142.11 (2015), pp. 2081–2081. ISSN: 0950-1991. DOI: 10.1242/dev.126235.

[16] Corina Guder, Sonia Pinho, Tanju G. Nacak, Heiko A. Schmidt, Bert Hobmayer, Christof Niehrs, and Thomas W. Holstein. "An ancient Wnt-dickkopf antagonism in Hydra". In: *Development* 133.5 (Mar. 2006), pp. 901–911. ISSN: 09501991. DOI: 10.1242/dev.02265.

[17] Julie R. Hens, Kimberly M. Wilson, Pamela Dann, Xuesong Chen, Mark C. Horowitz, and John J. Wysolmerski. "TOPGAL mice show that the canonical Wnt signaling pathway is active during bone development and growth and is activated by mechanical loading in vitro". In: *Journal of Bone and Mineral Research* 20.7 (July 2005), pp. 1103–1113. ISSN: 08840431. DOI: 10.1359/JBMR.050210.

[18] Bert Hobmayer, Fabian Rentzsch, Kerstin Kuhn, Christoph M Happel, Christoph Cramer Von Laue, Petra Snyder, Ute Rothbächer, and Thomas W Holstein. "WNT signalling molecules act in axis formation in the diploblastic metazoan Hydra". In: *Nature* 407.6801 (2000), pp. 186–189. ISSN: 00280836. DOI: 10.1038/35025063.

[19] Xiaoming Hou, Mohammad R. A. Khan, Mark Turmaine, Christopher Thrasivoulou, David L Becker, and Aamir Ahmed. "Wnt signaling regulates cytosolic translocation of connexin 43". In: *American Journal of Physiology-Regulatory, Integrative and Comparative Physiology* 317.2 (Aug. 2019), R248–R261. ISSN: 0363-6119. DOI: 10.1152/ajpregu.00268.2018.

[20] Celina E. Juliano, Haifan Lin, and Robert E. Steele. "Generation of Transgenic Hydra by Embryo Microinjection". In: *Journal of Visualized Experiments* 91 (2014), e51888. ISSN: 1940-087X. DOI: 10.3791/51888.

[21] Joy Kahn, Yulia Shwartz, Einat Blitz, Sharon Krief, Amnon Sharir, Dario A. Breitel, Revital Rattenbach, Frederic Relaix, Pascal Maire, Ryan B. Rountree, David M. Kingsley, and Elazar Zelzer. "Muscle Contraction Is Necessary to Maintain Joint Progenitor Cell Fate". In: *Developmental Cell* 16.5 (May 2009), pp. 734–743. ISSN: 15345807. DOI: 10.1016/j.devcel.2009.04.013.

[22] Alexander Klimovich, Jörg Wittlieb, and Thomas C.G. Bosch. "Transgenesis in Hydra to characterize gene function and visualize cell behavior". In: *Nature Protocols* 14.7 (July 2019), pp. 2069–2090. ISSN: 17502799. DOI: 10.1038/s41596-019-0173-3.

[23] Sylvia G. Lenhoff and Howard M. Lenhoff. *Hydra and the Birth of Experimental Biology - 1744*. Pacific Grove CA: Boxwood Press, 1986, p. 192. ISBN: 0940168014.

[24] Anton Livshits, Lital Shani-Zerbib, Yonit Maroudas-Sacks, Erez Braun, and Kinneret Keren. "Structural Inheritance of the Actin Cytoskeletal Organization Determines the Body Axis in Regenerating Hydra". In: *Cell Reports* 18.6 (Feb. 2017), pp. 1410–1421. ISSN: 22111247. DOI: 10.1016/j.celrep.2017.01.036.

[25] Harry K. MacWilliams. "Hydra transplantation phenomena and the mechanism of Hydra head regeneration. I. Properties of the head inhibition". In: *Developmental Biology* 96.1 (Mar. 1983), pp. 217–238. ISSN: 00121606. DOI: 10.1016/0012-1606(83)90324-X.

[26] Harry K. MacWilliams. "Hydra transplantation phenomena and the mechanism of Hydra head regeneration. II. Properties of the head activation". In: *Developmental Biology* 96.1 (Mar. 1983), pp. 239–257. ISSN: 00121606. DOI: 10.1016/0012-1606(83)90325-1.

[27] Moritz Mercker, Alexandra Köthe, and Anna Marciniak-Czochra. "Mechanochemical Symmetry Breaking in Hydra Aggregates". In: *Biophysical Journal* 108.9 (2015), pp. 2396–2407. ISSN: 15420086. DOI: 10.1016/j.bpj.2015.03.033.

[28] Yukio Nakamura, Charisios D Tsiairis, Suat Özbek, and Thomas W Holstein. "Autoregulatory and repressive inputs localize Hydra Wnt3 to the head organizer." In:

Proceedings of the National Academy of Sciences of the United States of America 108.22 (2011), pp. 9137–42. ISSN: 1091-6490. DOI: 10.1073/pnas.1018109108.

[29] Shigenori Nonaka, Hidetaka Shiratori, Yukio Saijoh, and Hiroshi Hamada. "Determination of left-right patterning of the mouse embryo by artificial nodal flow". In: *Nature* 418.6893 (July 2002), pp. 96–99. ISSN: 00280836. DOI: 10.1038/nature00849.

[30] Yukihiko Noro, Hiroshi Shimizu, Katsuhiko Mineta, and Takashi Gojobori. "A single neuron subset governs a single coactive neuron circuit in Hydra vulgaris, representing a prototypic feature of neural evolution". In: *bioRxiv* (Nov. 2020), p. 2020.11.22.392985. DOI: 10.1101/2020.11.22.392985.

[31] Yukihiko Noro, Seungshic Yum, Chiemi Nishimiya-Fujisawa, Christina Busse, Hiroshi Shimizu, Katsuhiko Mineta, Xiaoming Zhang, Thomas W. Holstein, Charles N. David, Takashi Gojobori, and Toshitaka Fujisawa. "Regionalized nervous system in Hydra and the mechanism of its development". In: *Gene Expression Patterns* 31 (Jan. 2019), pp. 42–59. ISSN: 18727298. DOI: 10.1016/j.gep.2019.01.003.

[32] Néstor J. Oviedo and Michael Levin. "Smedinx-11 is a planarian stem cell gap junction gene required for regeneration and homeostasis". In: *Development* 134.17 (Sept. 2007), pp. 3121–3131. ISSN: 09501991. DOI: 10.1242/dev.006635.

[33] Néstor J. Oviedo, Junji Morokuma, Peter Walentek, Ido P. Kema, Man Bock Gu, Joo Myung Ahn, Jung Shan Hwang, Takashi Gojobori, and Michael Levin. "Long-range neural and gap junction protein-mediated cues control polarity during planarian regeneration". In: *Developmental Biology* 339.1 (Mar. 2010), pp. 188–199. ISSN: 1095564X. DOI: 10.1016/j.ydbio.2009.12.012.

[34] T. Harshani Peiris and Néstor J. Oviedo. *Gap junction proteins: Master regulators of the planarian stem cell response to tissue maintenance and injury*. Jan. 2013. DOI: 10.1016/j.bbamem.2012.03.005.

[35] Beth L. Roman and Kerem Pekkan. "Mechanotransduction in embryonic vascular development". In: *Biomechanics and Modeling in Mechanobiology* 11.8 (Nov. 2012), pp. 1149–1168. ISSN: 16177959. DOI: 10.1007/s10237-012-0412-9.

[36] Hiroshi Shimizu, Yasuji Sawada, and Tsutomu Sugiyama. "Minimum tissue size required for hydra regeneration". In: *Developmental Biology* 155.2 (Feb. 1993), pp. 287–296. ISSN: 00121606. DOI: 10.1006/dbio.1993.1028.

[37] Jordi Soriano, Cyril Colombo, and Albrecht Ott. "Hydra molecular network reaches criticality at the symmetry-breaking axis-defining moment". In: *Physical Review Letters* 97.25 (2006). ISSN: 00319007. DOI: 10.1103/PhysRevLett.97.258102.

[38] Jordi Soriano, Sten Rüdiger, Pramod Pullarkat, and Albrecht Ott. "Mechanogenetic Coupling of Hydra Symmetry Breaking and Driven Turing Instability Model". In: *Biophysical Journal* 96.4 (Feb. 2009), pp. 1649–1660. ISSN: 0006-3495. DOI: 10.1016/J.BPJ.2008.09.062.

[39] Tsutomu Sugiyama and Toshitaka Fujisawa. "Genetic analysis of developmental mechanisms in Hydra I. Sexual reproduction of Hydra magnipapillata and isolation of mutants". In: *Development, Growth & Differentiation* 19.3 (1977), pp. 187–200. ISSN: 1440169X. DOI: 10.1111/j.1440-169X.1977.00187.x.

[40] John R. Szymanski and Rafael Yuste. "Mapping the Whole-Body Muscle Activity of Hydra vulgaris". In: *Current Biology* 29.11 (2019), 1807–1817.e3. ISSN: 09609822. DOI: 10.1016/j.cub.2019.05.012.

[41] Tetsuya Tabata and Yuki Takei. "Morphogens, their identification and regulation". In: *Development* 131.4 (Feb. 2004), pp. 703–712. ISSN: 09501991. DOI: 10.1242/dev.01043.

[42] Jun Takano and Tsutomu Sugiyama. "Genetic analysis of developmental mechanisms in hydra. VIII. Head-activation and head-inhibition potentials of a slow-budding strain (L4)". In: *Development* 78.1 (1983).

[43] U Technau, C Cramer von Laue, F Rentzsch, S Luft, B Hobmayer, H R Bode, and T W Holstein. "Parameters of self-organization in Hydra aggregates." In: *Proceedings of the National Academy of Sciences of the United States of America* 97.22 (Oct. 2000), pp. 12127–31. ISSN: 0027-8424. DOI: 10.1073/pnas.97.22.12127.

[44] Ulrich Technau and Robert E. Steele. "Evolutionary crossroads in developmental biology: Cnidaria". In: *Development* 138.8 (Apr. 2011), pp. 1447–1458. ISSN: 09501991. DOI: 10.1242/dev.048959.

[45] James H. Thorp and Alan P. Covich. *Ecology and Classification of North American Freshwater Invertebrates*. Academic Press, 2010, p. 1056. ISBN: 9780123748553. DOI: 10.1016/C2009-0-02669-5.

[46] A. M. Turing. "The chemical basis of morphogenesis". In: *Bulletin of Mathematical Biology* 52.1-2 (Jan. 1990), pp. 153–197. ISSN: 00928240. DOI: 10.1007/BF02459572.

[47] Marcel A.G. Van der Heyden, Martin B. Rook, Monique M.P. Hermans, Gert Rijksen, Johannes Boonstra, Libert H.K. Defize, and Olivier H.J. Destrée. "Identification of connexin43 as a functional target for Wnt signalling". In: *Journal of Cell Science* 111.12 (May 1998), pp. 1741–1749. ISSN: 00219533.

[48] Matthias C. Vogg, Leonardo Beccari, Laura Iglesias Ollé, Christine Rampon, Sophie Vriz, Chrystelle Perruchoud, Yvan Wenger, and Brigitte Galliot. "An evolutionarily-conserved Wnt3/β-catenin/Sp5 feedback loop restricts head organizer activity in Hydra". In: *Nature Communications* 10.1 (Dec. 2019), pp. 1–15. ISSN: 20411723. DOI: 10.1038/s41467-018-08242-2.

[49] Rui Wang, Tapan Goel, Kate Khazoyan, Ziad Sabry, Heng J. Quan, Patrick H. Diamond, and Eva Maria S. Collins. "Mouth Function Determines the Shape Oscillation Pattern in Regenerating Hydra Tissue Spheres". In: *Biophysical Journal* 117.6 (Sept. 2019), pp. 1145–1155. ISSN: 15420086. DOI: 10.1016/j.bpj.2019.07.051.

[50] Ortrud Wartlick, Anna Kicheva, and Marcos González-Gaitán. *Morphogen gradient formation.* Sept. 2009. DOI: 10.1101/cshperspect.a001255.

[51] T. Yao. "Studies on the organizer problem in Pelmatohydra oligactis. I. The induction potency of the implants and the nature of the induced hydranth". In: *J. Exp. Biol* 21.1 (1945), pp. 147–150.

Chapter 2

Locking of regenerated body axis direction via applied temperature gradient

2.1 Introduction

Quantitative modeling of the axis specification event has long been a goal of the *Hydra* field. Several studies have utilized time lapse imaging and shape analysis of regenerating spheroids to obtain quantitative measurements of regeneration [5, 2]. However, 2-dimensional imaging of a mostly-spherical 3-dimensional object capable of rotating freely presents numerous challenges: mainly, the difficulty of tracking any features and the possibility that regions of interest may not be consistently captured.

It has been claimed that the axis direction of regenerating *Hydra* tissue fragments can be manipulated by the application of an external temperature gradient [4]. The authors

find that the tissue pieces align their regenerated axis to the gradient, with the strength of the effect increases when the steepness of the gradient is increased. Finally, they find that the axis-locking effect only occurs when the gradient is applied early in the regeneration process. Taken together, Soriano *et al.* draw the conclusion that the axis specification event occurs within a specific time window early in regeneration and that the process is influenced by temperature.

Replicating this method to lock the axis of a regenerating *Hydra* would be extremely useful to any attempt at studying the axis specification process. Creating an apparatus in which the default axis direction is fixed greatly simplifies the problem of analyzing and comparing images of different animals. Furthermore, the impacts on patterning of any perturbations applied within this system could easily be assessed by whether they alter or override the axis locking effect. Thus, it could be used to quickly and quantitatively evaluate a range of mechanical and pharmacological perturbations. Impacts on axis direction could be directly assessed via shape analysis, while impacts on biochemical gradients could be observed with the addition of epifluorescent imaging and reporter strains.

2.2 Materials and Methods

2.2.1 *Hydra* strains and tissue fragments

Hydra medium (HM), culture conditions, and feeding procedures are as previously described [6]. Tissue fragments were also prepared as previously described [6] - in brief, the head and foot were removed, the body column tissue was cut into rings, and each ring was

separated into 3-4 fragments and allowed to heal. The resulting spheroids were selected to have a radius of approximately 200 μm.

Hydra vulgaris "watermelon" (AEP expressing GFP in the ectoderm and DsRed2 in the endoderm) [1] and a strain with the HyWnt3 promoter driving EGFP [3] were used to test fluorescent imaging.

2.2.2 Imaging apparatus

An apparatus was constructed capable of imaging multiple regenerating tissue fragments on a temperature gradient in both brightfield and epifluorescence channels. This apparatus was used in an attempt to reproduce the axis direction results described by Soriano *et al.* [4]. If successful, it was to be combined with transgenic reporter strains to test and validate existing quantitative models of *Hydra* patterning.

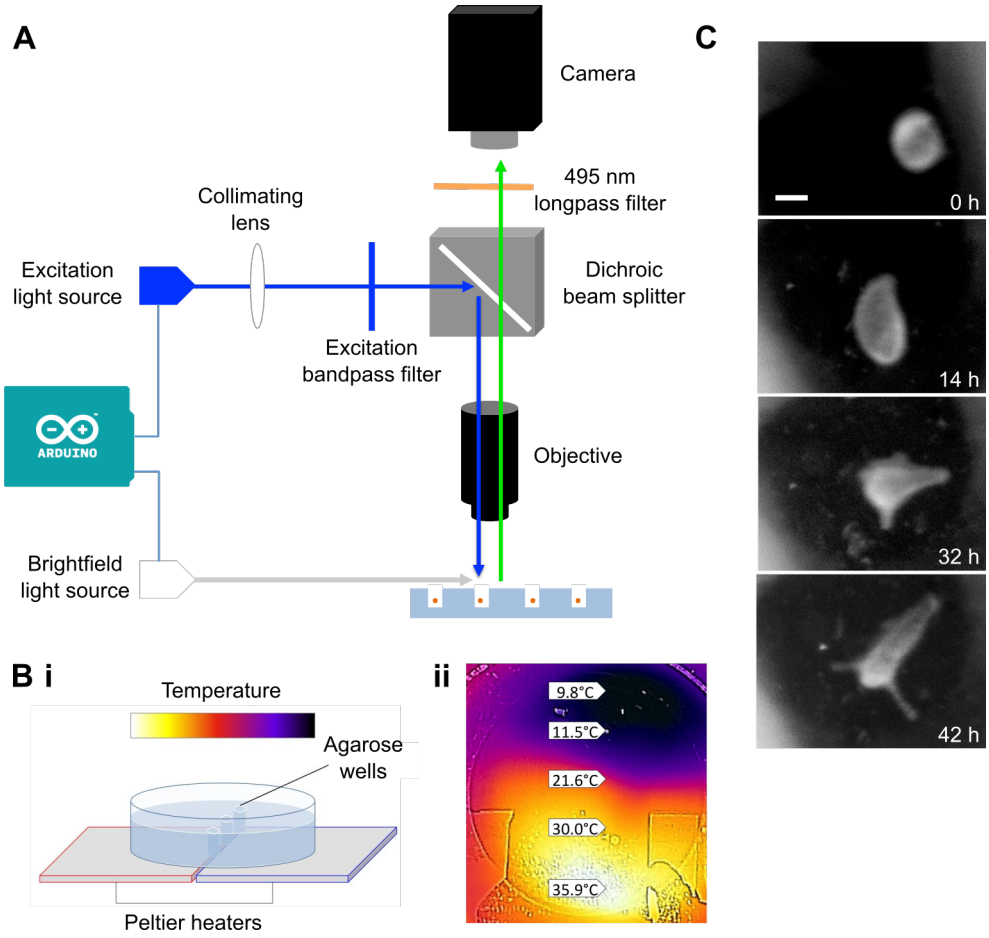

Figure 2.1: Temperature gradient and imaging apparatus. A. Block diagram of optics. B. Temperature gradient. i. Diagram of Peltier heater arrangement. ii. Thermal image showing temperature gradient formed in dish. C. Representative images from time series of tissue piece, showing progression from spheroid to fully regenerated animal. Scale bar 150 μm.

The imaging apparatus consists of optics (Fig. 2.1A) mounted on a linear rail, enabling automated movement over a dish placed on Peltier heating elements to create the temperature gradient (Fig. 2.1B).

The optics were designed to enable both brightfield and epifluorescence imaging. This was achieved using a dichroic mirror (Thorlabs, Newton NJ, MD499) in a cube mount (ThorLabs CM1-DCH). The excitation light source consisted of a 3W royal blue LED (Sparkfun, Boulder CO, COM-13107), mounted in a 25 mm lens tube with a collimating lens and an excitation filter (ThorLabs MF469-35). Collimated and filtered light from this LED was reflected from the dichroic mirror through a 4X microscope objective and onto the sample. Emitted light passed back through the microscope objective and beam splitter, then through a longpass emission filter (ThorLabs FGL495) to a camera (Basler, Ahrensberg, Germany, A641F). Illumination for brightfield imaging consisted of a 3w white LED (Sparkfun COM-13105) mounted outside the main light path, focused on the sample dish.

The optical components were fixed to a focusing rail from a stereo microscope. This was them bolted to a gantry plate on an aluminum extrusion. The plate was moved along the extrusion by a 28STH32 NEMA-11 stepper motor (Phidgets Inc., Calgary AB, Canada) controlled by a 1067_0B control board (Phidgets Inc.).

Movement of the platform was controlled by using MATLAB (Mathworks, Natick MA) to interface with the Phidgets control software. Illumination was controlled using an Arduino Uno, with the ability to use one light source at a time. For each well, the platform moves to position, activates the white LED, captures a brightfield image, deactivates the white LED, activates the blue LED, captures a fluorescent image, deactivates the blue LED, and moves to the next position. When all wells have been imaged, it returns to the first

well and pauses such that image sets are captured 5 minutes apart. This enables time lapse imaging of tissue pieces over the full course of regeneration (Fig. 2.1C).

The apparatus was tested on transgenic lines expressing GFP in the ectoderm, and GFP driven by the HyWnt3 promoter. In both cases it was confirmed that the GFP signal could be detected.

Peltier heaters (TEC1-12703) were used to create a temperature gradient, with a goal of a gradient centered at 20°C with a drop of 0.6-0.9°C across a 1 mm well as described in [4]. The heating elements were arranged side by side with opposing polarities such that one heated and one cooled, and both powered with DC current from an adjustable power supply.

To hold the regenerating animals over the Peltiers, a plastic hair comb with 1 mm teeth was used to cast wells using 1% agarose in a rectangular glass container(25 mm wide x 75 mm long x 15 mm high) constructed from glass microscope slides and aquarium silicone. This container was loaded with a *Hydra* tissue fragment in each well, and the HM removed. The container was completely filled with a solution of 1.25% methylcellulose (Sigma-Aldrich, St. Louis MO) in HM, and covered with a ThermalSeal RT sealing film (Excel Scientific, Victorville CA) to prevent evaporation and enable clear imaging. The bottom of the container was spray painted black to improve image contrast. The container was placed directly onto the Peltier elements with the row of wells directly between the two elements. The temperature gradient across the wells was tuned by imaging with a FLIR thermal camera on an iPhone 5 (Apple Inc., Cupertino CA), and adjusting the input voltage to the Peltier elements until the desired differential was achieved.

2.2.3 Image analysis

Code to analyze the acquired images was initially written in MATLAB, and later ported to Python (Anaconda distribution) by Kate Khazoyan to take advantage of differences in watershedding algorithms. The code navigates to a folder containing the raw images and increments through them, pausing for user input. The number of images processed between pauses, whether watershedding is used, and watershedding parameters can be adjusted by the user at each pause (Fig. 2.2A). This allows accurate analysis of data sets that require different parameters at different points, as well as constant user supervision to prevent major failures such as oversegmenting or targeting the wrong object from appearing in the final data sets. For each image the code binarizes the original image, uses image opening and closing to remove small artifacts, then uses watershedding to eliminate items such as ejected cell debris in contact with the tissue sphere. It then fits an ellipse to the regenerating animal. The code returns the area of the animal, the aspect ratio as calculated from the major and minor axes of the fit ellipse, and the angle of the major axis (Fig. 2.2B). It also returns the radius of the circle with an equivalent area to the animal.

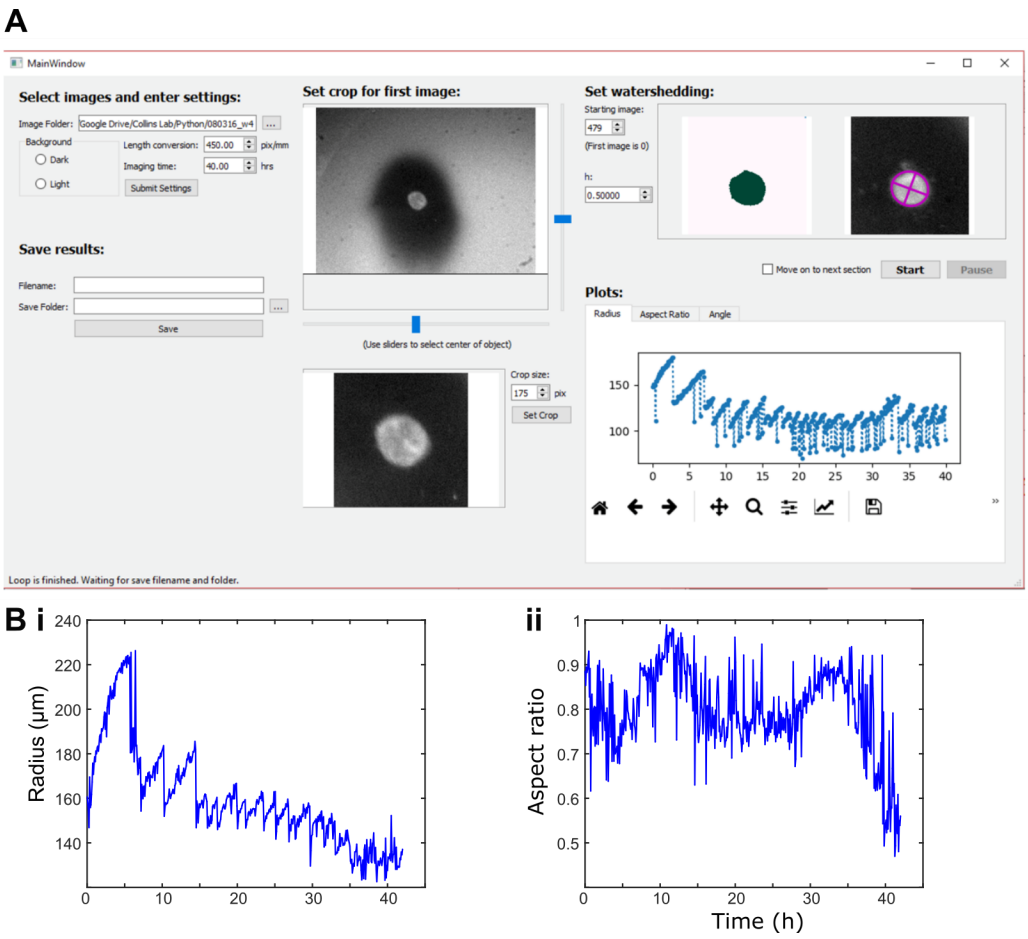

Figure 2.2: Representative image analysis output. A. GUI of analysis script while running, showing image cropping, ellipse fit, and radius plot in progress. B. Example output plots transferred into MATLAB for analysis. i. radius. ii. Aspect ratio.

2.3 Results and Discussion

The imaging and shape analysis methods developed while investigating axis direction were critically useful to subsequent investigations. Of particular note was the ability to create plots of radius and aspect ratio over time. These capabilities were key to our subsequent work investigating the claim that a change in the oscillation patterns of tissue pieces acts as an easily measured regeneration milestone [5, 2]. The area measurement can be used to observe and quantify the mechanical oscillations, while a decrease in aspect ratio represents the animal beginning to elongate along its new axis. As the oscillation pattern shift was theorized to be linked to an axis specification event, quantifying and studying it has the potential to shed significant light on the patterning process.

Despite the success of our image quantification techniques, the reported axis specification effect was not reproducible under the temperature gradient conditions previously published. We were successfully able to create a gradient of 0.9°C across a single well, a differential which was reported to cause virtually all animals form an axis within 30° of the gradient direction[4].

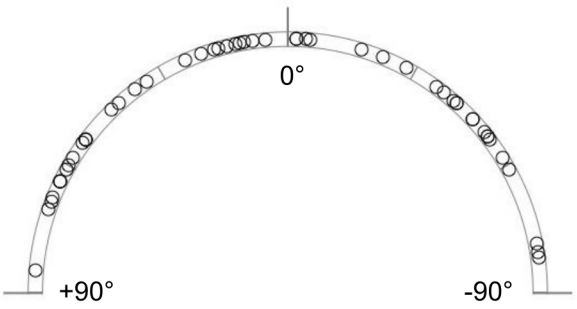

Figure 2.3: Failure to reproduce published temperature gradient results. Direction of regenerated axes of tissue pieces in a 0.9°C gradient. 0° is parallel to the gradient; +/- 90° is perpendicular. Each circle represents one animal, n = 51 animals total.

The direction of the regenerated axis appears random at a temperature differential of 0.9°C across the wells (Fig. 2.3). This is in contrast to published results, where the effect is visible at a differential of 0.6°C and increases in strength with steeper gradients[4]. It is possible that the published results are highly dependent upon the quality of the apparatus. Soriano *et al.* had access to advanced fabrication capabilities, with the chamber containing the samples and transmitting the temperature gradient to them being machined from a solid piece of sapphire glass. In addition, not designing their apparatus to accommodate multiple regenerating animals per experiment likely allowed greater control and standardization of the temperatures experienced by each tissue fragment.

With the resources and materials available to us, the only significant improvements to the gradient possible would have been to attempt active regulation of the Peltier elements. This could have been achieved by using thermistors to detect the temperature on each side of the gradient, and using the Arduino to read temperature and adjust the voltage supplied to the Peltiers. Alternatively, it would have been possible to explore options for machining the sample chamber from glass or a different nontoxic, thermally conductive material. If our apparatus had simply produced a much weaker version of the axis-setting effect, further improvements would certainly have been worth pursuing. However, a complete lack of any observable effects of applied temperature gradient on axis direction cast serious doubt on whether it would be possible to produce a strong axis setting effect with a reasonable investment of time and resources.

Using axis setting in conjunction with mechanical or biological perturbations to quickly and accurately screen for factors impacting patterning requires an axis setting effect that is very reliable and at least reasonably strong. Thus, the axis-locking aspect of this

project was abandoned at this juncture.

2.4 Acknowledgements

I would like to thank Kate Khazoyan for assistance with experiments and significant contributions to the image analysis code. I would also like to thank Jerry Quan for his work on data analysis and statistics.

Bibliography

[1] K. M. Glauber, C. E. Dana, S. S. Park, D. A. Colby, Y. Noro, T. Fujisawa, A. R. Chamberlin, and R. E. Steele. "A small molecule screen identifies a novel compound that induces a homeotic transformation in Hydra". In: *Development* 142.11 (2015), pp. 2081–2081. ISSN: 0950-1991. DOI: 10.1242/dev.126235.

[2] Moritz Mercker, Alexandra Köthe, and Anna Marciniak-Czochra. "Mechanochemical Symmetry Breaking in Hydra Aggregates". In: *Biophysical Journal* 108.9 (2015), pp. 2396–2407. ISSN: 15420086. DOI: 10.1016/j.bpj.2015.03.033.

[3] Yukio Nakamura, Charisios D Tsiairis, Suat Özbek, and Thomas W Holstein. "Autoregulatory and repressive inputs localize Hydra Wnt3 to the head organizer." In: *Proceedings of the National Academy of Sciences of the United States of America* 108.22 (2011), pp. 9137–42. ISSN: 1091-6490. DOI: 10.1073/pnas.1018109108.

[4] Jordi Soriano, Cyril Colombo, and Albrecht Ott. "Hydra molecular network reaches criticality at the symmetry-breaking axis-defining moment". In: *Physical Review Letters* 97.25 (2006). ISSN: 00319007. DOI: 10.1103/PhysRevLett.97.258102.

[5] Jordi Soriano, Sten Rüdiger, Pramod Pullarkat, and Albrecht Ott. "Mechanogenetic Coupling of Hydra Symmetry Breaking and Driven Turing Instability Model". In: *Biophysical Journal* 96.4 (Feb. 2009), pp. 1649–1660. ISSN: 0006-3495. DOI: 10.1016/J.BPJ.2008.09.062.

[6] Rui Wang, Tapan Goel, Kate Khazoyan, Ziad Sabry, Heng J. Quan, Patrick H. Diamond, and Eva Maria S. Collins. "Mouth Function Determines the Shape Oscillation Pattern in Regenerating Hydra Tissue Spheres". In: *Biophysical Journal* 117.6 (Sept. 2019), pp. 1145–1155. ISSN: 15420086. DOI: 10.1016/j.bpj.2019.07.051.

Chapter 3

Mouth Function Determines the Shape Oscillation Pattern in Regenerating *Hydra* Tissue Spheres

3.1 Abstract

Hydra is a small freshwater polyp capable of regeneration from small tissue pieces and from aggregates of cells. During regeneration, a hollow bilayered sphere is formed that undergoes osmotically driven shape oscillations of inflation and rupture. These oscillations are necessary for successful regeneration. Eventually, the oscillating sphere breaks rotational symmetry along the future head-foot axis of the animal. Notably, the shape oscillations show an abrupt shift from large-amplitude, long-period oscillations to small-amplitude, short-period oscillations. It has been widely accepted that this shift in oscillation pattern is linked to symmetry breaking and axis formation, and current theoretical models of *Hydra*

symmetry breaking use this assumption as a model constraint. However, a mechanistic explanation for the shift in oscillation pattern is lacking. Using *in vivo* manipulation and imaging, we quantified the shape oscillation dynamics and dissected the timing and triggers of the pattern shift. Our experiments demonstrate that the shift in the shape oscillation pattern in regenerating *Hydra* tissue pieces is caused by the formation of a functional mouth and not by shape symmetry breaking as previously assumed. Thus, model assumptions must be revised in light of these new experimental data, which can be used to constrain and validate improved theoretical models of pattern formation in *Hydra*.

3.2 Significance

Hydra spheres originating from tissue pieces or aggregates of body column cells undergo dramatic osmotically driven shape oscillations during regeneration. Previous works proposed a causal link between a characteristic abrupt shift in the frequency of shape oscillations of regenerating spheres and *de novo* axis specification via the establishment of morphogen gradients. Here, we break this link by demonstrating that regeneration without an oscillation pattern shift is possible and that the shift is a direct consequence of mouth function and its use in osmoregulation. Because the link between oscillation dynamics and axis specification was a key assumption in current models of *Hydra* regeneration, our results indicate that we must reexamine the mechanisms driving pattern formation in *Hydra*.

3.3 Introduction

Hydra is a small (∼1 cm long), transparent, radially symmetric freshwater cnidarian polyp (Fig. 3.1 A). It consists of a cylindrical body column with a tentacle ring and a dome-shaped hypostome containing the mouth on one end and a foot that anchors the animal to the substrate on the other. Hydra is composed of only two tissue layers: an outer ectodermal epithelium and an inner endodermal epithelium, separated by a basal lamina called the mesoglea. Body shape is regulated by contractile processes on the epithelial cells called myonemes, which are oriented longitudinally along the head-foot axis in the ectoderm and circumferentially in the endoderm [43]. This simple anatomy, combined with the ability to regenerate a complete polyp from tissue pieces and from aggregates of body column cells, made *Hydra* an important model system for biologists and physicists alike to study regeneration, axis formation, and patterning [17].

One of the earliest attempts at modeling axial patterning in Hydra was made by Alfred Gierer and Hans Meinhardt [20], who proposed a reaction-diffusion model consisting of a short-range head activator, a long-range head inhibitor, and a gradient for the activator source. The model qualitatively explains pattern formation from a homogeneous starting state. However, a lack of quantitative experimental data has limited progress on validation and refinement of this and subsequent models [30]. Recently, the availability of a fully sequenced genome [11], various transgenic reporter lines [23, 21] and CRISPR genome editing tools [29] has allowed researchers to reexamine earlier models and studies of *Hydra* regeneration and gain new insights.

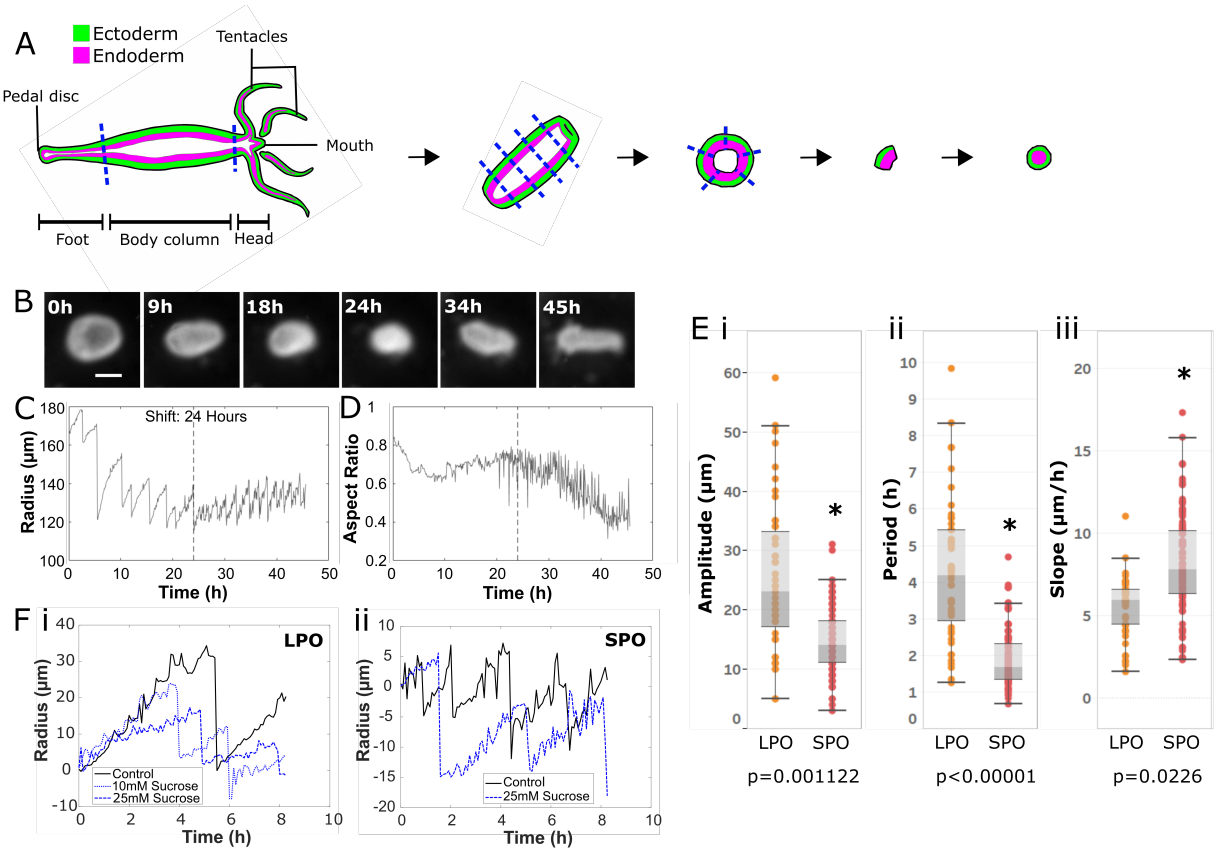

Figure 3.1: Generation of tissue spheres and quantification of oscillation dynamics. (A) Preparation of tissue pieces from a Hydra polyp (see Materials and Methods) is shown. (B) Representative images of regenerating tissue spheres at various time points during regeneration are shown. In the 45 h image, the regenerated head with tentacles is to the left. Scale bars, 150 μm. (C) Shown is a plot of effective radius, calculated as the radius of a circle with an area equal to that of the tissue piece, as a function of time for the sphere shown in (B). (D) Shown is a plot of aspect ratio as a function of time for the same tissue sphere. The dashed line indicates the time of shift from LPO to SPO. (E) Box-whisker plots of (i) amplitudes, (ii) time periods, and (iii) slopes for LPOs and SPOs for body column tissue pieces regenerating in HM are shown. The asterisk indicates a statistically significant difference from LPO (p ¡ 0.05): amplitude p = 0.0011; period p ¡ 1e-5; slope p = 0.0226. (F) A plot of effective radius (adjusted to set initial radius to zero) as a function of time at different sucrose concentrations in the external medium during (i) LPOs and (ii) SPOs is shown.

Here, we revisit a striking phenomenon that occurs during *Hydra* regeneration from tissue pieces [35] and aggregates of cells [19]. As they regenerate, both tissue pieces and aggregates form a hollow bilayered sphere with ectodermal cells on the outside and endodermal cells on the inside. These *Hydra* spheres undergo osmotically driven cycles of swelling and subsequent rupture, referred to as shape oscillations [24, 16]. The shape oscillations are sawtooth shaped, consisting of cycles of a long inflation phase followed by an abrupt deflation of the sphere due to local tissue rupture [33]. The inflation phase is caused by the uptake of water and the active pumping of sodium ions into the lumen of the sphere [2]. Initially, inflation is isotropic. The *Hydra* sphere's aspect ratio, defined as the ratio of the minor axis to the major axis of an ellipse fit to the sphere, is close to unity. As time progresses, the swelling becomes increasingly anisotropic: the aspect ratio decreases with sharp dips during deflation of the hollow sphere. The regenerating animal breaks spherical symmetry to establish a body axis and develops a mouth and tentacles by 48 h [16].

Previous studies have utilized different definitions and criteria for symmetry breaking. First, morphological, or shape symmetry breaking, refers to the tissue sphere becoming ellipsoidal, which has been quantified by shape analysis either through a decrease in the aspect ratio of an ellipsoid fit to the tissue sphere [38] or as changes in the Fourier modes of the two-dimensional contour of the tissue over time [16]. Second, biochemical symmetry breaking involves spatial patterning of morphogens such as Wnt3 [22] to specify a body axis and the position of the head, foot, and tentacles. Finally, structural symmetry breaking involves the reorganization of supracellular structures such as myonemes [28]. Although these aspects have been studied individually and feedback between morphological and biochemical symmetry breaking has been proposed by some studies [30, 38, 18], the lack of tools to

visualize morphogen gradients in vivo has prevented researchers from demonstrating a causal connection.

It has long been hypothesized that shape symmetry breaking coincides with or occurs shortly after the morphogen patterning proposed by Gierer and Meinhardt [20], leading models to use the time of oscillation pattern shift as the time of biochemical symmetry breaking. To the best of our knowledge, the mechanism underlying the oscillation pattern shift has not been determined. Sato-Maeda and Tashiro [33] were the first to probe the connection between shape oscillations and axis formation two decades ago. They reported the sawtooth shape of the oscillations and described a method of detecting shape symmetry breaking in cell aggregates by quantifying the divergence of orthogonal radii as the regenerating animal elongated along one axis. This approach represented a measure of body axis formation that could be quantitatively linked to other morphological fluctuations. Fütterer et al. [16] subsequently analyzed the shape of regenerating *Hydra* spheres originating from tissue pieces in greater detail, using Fourier decomposition to reveal three distinct temporal stages: 1) large-amplitude, long-period oscillations (LPOs) of the zeroth mode (size of the tissue piece); 2) small-amplitude, short-period oscillations (SPOs) of the zeroth mode associated with fluctuations of the second mode (elongation); and 3) strong in- crease in the second mode during contractions. They reported that shape anisotropy always occurred after the completion of LPOs, suggesting a correlation between oscillation dynamics and formation of the body axis as implied by shape symmetry breaking [16].

Hydra spheres derived from cell aggregates and from small tissue pieces exhibit similar oscillation dynamics. It was also reported that regenerating spheres reoriented their body axes in alignment with an applied temperature gradient regardless of their origin, so long

as the gradient was applied before the onset of SPOs [37]. Consequently, it was conjectured that both tissue pieces and cell aggregates begin from a homogenous state and must break symmetry *de novo*. The idea that the pattern shift occurs at the same time as biochemical symmetry breaking was supported by the finding that the time of pattern shift from LPO to SPO coincides with the emergence of critical scaling in the patch size distribution of the *Hydra* head-specific gene ks1 [37]. Secondly, β-catenin, which acts as a mechanotransducer in other model organisms [8], is involved in *Hydra* head specification via the canonical Wnt pathway [7, 6]. Because the timing of oscillation pattern shift at 24 h [22] was comparable to the timing of the emergence of expression patches of Wnt3, the earliest known marker expressed during *Hydra* head regeneration [25, 32], in larger cell aggregates, Soriano et al. [38] concluded that the oscillation pattern shift must also coincide with the establishment of biochemical asymmetry. Consequently, it has been proposed that β-catenin may link the mechanical forces caused by tissue stretch or rupture with biochemical patterning in *Hydra* [38]. This remains to be experimentally verified, but the theory is attractive because of the known role of mechanotransduction pathways in a wide range of morphogenetic and developmental processes [13].

Thus, the pattern shift was regarded as a reliable and easily detectable marker of the morphological and biochemical symmetry breaking event in both aggregates and small tissue pieces [37]. Because of this apparent link, subsequent theoretical models by Soriano et al. [38] and Mercker et al. [30] coupled tissue mechanics with reaction-diffusion of morphogens to explain axis formation in *Hydra*. Both authors acknowledge that equating the time of oscillation pattern shift to that of biochemical symmetry breaking is a possible overestimation but use this assumption to constrain their models for lack of viable alternatives.

Recently, the assumption that both small tissue pieces and aggregates break symmetry *de novo* has been challenged. It was shown that spheres derived from small tissue pieces inherit the parent animal's myoneme organization and, as such, have structural asymmetry from the beginning [28]. How this structural asymmetry relates to morphological or biochemical symmetry breaking remains elusive. However, it suggests that regenerating tissue spheres possess a predetermined body axis, which is incompatible with existing models of *Hydra* regeneration, assuming that small regenerating tissue fragments and regenerating aggregates both begin from an isotropic state and exhibit a true symmetry breaking event. In light of this apparent paradox in the existing literature, there is a need to determine the cause of the LPO-SPO shift and understand its relevance.

Here, we use *in vivo* manipulation and imaging to quantify shape oscillation dynamics and experimentally dissect the timing and triggers of the pattern shift. First, we demonstrate that both LPOs and SPOs are driven by osmotic pressure, suggesting that the observed differences do not arise from different swelling mechanisms but from changes in the local yield strength of the tissue spheres. Consistent with this idea, we find that the site of tissue rupture is random during LPOs but conserved during SPOs, suggesting the existence of a fixed mechanical weak point during SPOs. We demonstrate that this weak spot is the mouth. Furthermore, we show that mouth structure alone is insufficient to cause an oscillation pattern shift because tissue pieces derived from nerve-free animals, which are unable to open their mouths, regenerate fully but exhibit only LPOs. Additionally, tissue pieces derived from the heads of normal animals containing a functional mouth were found to exhibit only SPOs, whereas tissue pieces from the heads of nerve-free animals with a structurally normal but nonfunctional mouth only exhibit LPOs. Together, these experiments demonstrate that the

shift in oscillation pattern observed in regenerating *Hydra* tissue pieces is caused by the onset of mouth function. Therefore, the pattern shift is an indicator of active control of mouth opening, providing an easily observable readout for an important regeneration milestone. In addition to providing a mechanistic explanation for shape oscillation dynamics, this study also allowed us to estimate a lower bound for the tissue yield strength, a parameter which may prove useful for future models of *Hydra* regeneration.

3.4 Materials and Methods

3.4.1 *Hydra* strains and culture

Hydra vulgaris strain AEP, *Hydra vulgaris* (formerly *Hydra magnipapillata* strain 105) strain sf-1 (temperature-sensitive interstitial stem cells), *Hydra vulgaris* strain A10 (chimera consisting of *Hydra vulgaris* epithelial cells and sf-1 interstitial cells) [34], and *Hydra vulgaris* "watermelon" (AEP expressing GFP in the ectoderm and DsRed2 in the endoderm) [21] were used for experiments. Polyps were kept in *Hydra* medium (HM) composed of 1 mM $CaCl_2$ (Spectrum Chemical, New Brunswick, NJ), 0.1 mM $MgCl_2$ (Sigma-Aldrich, St. Louis, MO), 0.03 mM KNO_3 (Fisher Scientific, Waltham, MA), 0.5 mM $NaHCO_3$ (Fisher Scientific, Hampton, NH), and 0.08 mM $MgSO_4$ (Fisher Scientific) prepared with MilliQ water, with pH between 7 and 7.3, at 18°C in a Panasonic incubator (Panasonic MIR-554, Kadoma, Japan) in the dark. The *Hydra* were fed three times per week with *Artemia* nauplii (Brine Shrimp Direct, Ogden, UT). Animals were cleaned daily using published procedures [27].

3.4.2 Generation of nerve-free *Hydra*

Nerve-free *Hydra* were generated using either of two methods. Watermelon animals were made nerve free as described by Tran et al. [40]. Briefly, the animals were incubated in 0.4% colchicine (Acros Organics, Thermo Fisher Scientific, Waltham, MA) in HM for 8 h in the dark. This 8 h incubation was then repeated 3 weeks after the first treatment. Colchicine-treated *Hydra* are susceptible to bacterial infection, so the animals were kept in HM supplemented with 50 μg/mL rifampicin (EMD Millipore, Burlington, MA) at 18°C in the dark in the incubator. Nontransgenic nerve-free animals were generated by heat shock treatment of the sf-1 and A10 strains [34, 39, 15]. Sf-1 and A10 animals were heat shocked in an incubator at 29°C in the dark for 48 h and then moved back into the 18°C incubator. All nerve-free animals were force fed and "burped" as per the protocol described in Tran et al. [40].

3.4.3 Preparation of tissue pieces

Tissue pieces were cut with a scalpel (Sklar Instruments, West Chester, PA) from the body columns of adult nonbudding *Hydra* starved for 24 h, as shown in Fig. 3.1 A. The head was amputated immediately below the tentacles. A second cut was made above the foot to isolate the body column. Depending on the size of the resulting body column piece, one to three cross-sectional cuts were made to extract rings. The rings were cut into four or more pieces and allowed to round up in HM for 2 h (measured from the time of initial excision of the body column piece). Once rounded up, tissue pieces were selected by size (<200 μm radius) by visual examination under a stereo microscope for use in experiments (Fig. 3.1 A).

3.4.4 Preparation of head and foot tissue pieces

Head tissue pieces were prepared under a stereo microscope. The animals' heads were removed immediately below the tentacle ring, and then the tentacle bases were excised. The remaining head tissue pieces were given 1 h to round up and placed individually into custom-made agarose wells for time-lapse imaging. Foot tissue pieces were prepared by cutting the animals immediately above the basal disk and allowing the resulting tissue pieces to round up for 2 h. In both cases, rounded tissue pieces of the same approximate size as body column tissue pieces were selected for imaging.

3.4.5 Imaging of shape oscillations

Regenerating tissue pieces were placed in agarose wells made using a 1% solution of agarose or low melting point agarose (Invitrogen, Carlsbad, CA) in HM. The two types of agarose were used interchangeably. To make the wells, molten agarose solution was poured into 30 mm Falcon petri dishes (Thermo Fisher Scientific), and a comb with 1-mm-wide teeth was placed vertically into the dishes to create wells. Once the agarose had solidified, the comb was removed, the wells were filled with HM, and the tissue pieces were moved into the wells using a pipette. Imaging was accomplished using an Invitrogen EVOS FL Auto 2 microscope (Thermo Fisher Scientific) and the Invitrogen EVOS FL Auto 2.0 Imaging System software. Images were acquired every 5 min and stored as Tagged Image File Format files. Viability of the tissue pieces was assayed by observing the presence of a body axis at 48 h and the formation of tentacles and mouth opening upon presentation of *Artemia* at 96 h.

3.4.6 Altering osmolarity of HM

To test the effect of changes in osmotic pressure on regenerating tissue pieces, tissue pieces were prepared and imaged as described above. However, the tissue pieces were kept in sucrose-supplemented HM for imaging instead of HM. Sucrose (Sigma-Aldrich) was added to HM to final concentrations of 10 or 25 mM. Rifampicin (EMD Millipore) was added to a final concentration of 50 μg/mL to prevent bacterial growth in the presence of sucrose.

3.4.7 Injections of microbeads and rupture site tracking

Tissue pieces were incubated at room temperature until at least 5 h after cutting to allow them to round up and form an internal cavity. An agarose trough for microinjection was cast as previously described [12]. Hollow tissue spheres were placed in the trough in HM and injected with 1 μm green fluorescent (excitation/emission: 468/508 nm) microbeads (Thermo Fisher Scientific G0100) using a WPI Pneumatic PicoPump (PV 820) (Sarasota, FL) and needles pulled using a Sutter Instrument P-1000 (Novato, CA). Successfully injected spheres were placed in agarose wells and imaged for 24 h as described above. The resulting videos were used to determine the location of rupture events by tracking the locations of ejection of fluorescent beads relative to a fixed feature on the sphere. The smaller of the two angles between the fixed feature and the rupture location was recorded.

3.4.8 Visualization of myoneme arrangement in the head

Nerve-free *Hydra* prepared by heat shock treatment of strain A10 and untreated controls were fixed and stained with rhodamine-phalloidin (Biotium, Fremont, CA). The

polyps were relaxed in 1 mL of 1 mM linalool (Sigma-Aldrich) in HM for 10 min (https://www.biorxiv.org/content/10.1101/584946v1) and then fixed in 4% paraformaldehyde (Thermo Fisher Scientific) in HM for 20 min at room temperature. They were washed with HM thrice for 10 min each before being incubated overnight at 4°C in rhodamine-phalloidin diluted 1:100 in HM. The fixed stained samples were washed 5 times for 10 min each with HM. They were then placed on 22 × 40 mm glass coverslips (Corning, Corning, NY), which had a piece of double-sided tape (3M, Maplewood, MN) running along the short edges of the coverslips. These coverslips were then sealed by placing 22 × 22 mm glass coverslips (Fisher Scientific) on top, and the samples were imaged using an Olympus IX81 inverted microscope (Olympus Corporation, Tokyo, Japan) with an ORCA-ER camera (Hamamatsu Photonics, Hamamatsu, Japan). Slidebook version 5 (Intelligent Imaging Innovations, Denver, CO) was used to interface with the microscope and acquire z-stacks. Maximum intensity projections of the z-stacks were used to determine the orientation of the myonemes.

3.4.9 Oscillation analysis

Images collected using the EVOS microscopes were opened in ImageJ (http://imagej.nih.gov/ij/; National Institutes of Health, Bethesda, MD), and full regeneration was verified. Full regeneration was defined as the regenerated tissue piece exhibiting a well-defined body axis, head formation, and tentacle growth. Only tissue pieces that showed full regeneration were included in further analysis. The obtained images were processed to extract the radius of the tissue piece as a function of time as described in the next paragraph. Only those tissue spheres whose minimum radius was $\leq$150 μm were included

in further analysis. This cutoff was chosen based on the literature, in which it has been suggested that spheres with <200 μm average minimum radius, defined as the average of the minimum radii across oscillation cycles for a single tissue sphere, exhibited a pattern shift [38].

Each image set was analyzed using built-in functions in a custom Python script (Python 3.7.0; Python Software Foundation). The script first applies morphological image opening and closing to distinguish the sphere from the background, followed by watershed segmentation to detect and eliminate ejected cell debris (Fig. 3.S1). If the script failed to segment the raw image set, debris was removed from the images by manually tracing over the debris in ImageJ before analysis. For each image in a set, the script traces the boundary of the regenerating tissue to determine its area. Effective radius is calculated as the radius of the circle having the same area as the tissue piece. Shape is approximated by fitting an ellipse to the two-dimensional contour of the tissue piece and recording major and minor axes to determine the aspect ratio. Effective volume of the tissue piece was determined as the volume of an ellipsoid obtained by revolution of the fit ellipse about its major axis as described in Soriano et al. [37]. We found that the effective radius and the effective volume, normalized so that the minimum radius and volume are unity, qualitatively show the same temporal dynamics (Fig. 3.S2). Subsequent processing and analysis of the data were carried out in MATLAB 2017b (The MathWorks, Natick, MA). The code is available online at `https://github.com/Collinslab-swat/Oscillation-Analysis.git`. The existence and timing of oscillation pattern shift in a data set was determined by having five researchers independently examine the radius-time plots for the data set and provide an estimate of the presence and timing of the shift. The data set was accepted as having a shift at a particular

time if there was consensus of at least four of the researchers, defined as all scores being within a 4 h interval.

After shift presence and timing were determined, the amplitude, time period, and slope of each oscillation were extracted. The amplitude was defined as the difference between maximum and minimum radius during the inflation phase. The time period was defined as the time difference between the beginning of the inflation phase and end of the deflation phase. The swelling rate (slope) was obtained from a linear fit to the inflation phase of the oscillation.

As individual oscillations within a single biological replicate cannot be considered independent and their parameters are not normally distributed, we calculated the median values for each biological replicate and used these as inputs in our statistical analysis.

A two-sided Mann-Whitney U test was used to determine whether two sets of oscillation parameters originated from the same distribution. A p-value of 0.05 or lower rejects the null hypothesis that the two samples were drawn from the same distribution. For all conditions other than body column tissue pieces taken from wild-type animals regenerating in HM, the oscillations were classified as LPO or SPO based on comparison to wild-type LPO and SPO time periods. We used time periods for classifying an oscillation as LPO or SPO because the time periods are fairly consistent across biological replicates and the LPO time period distribution has very little overlap with the SPO time period distribution.

3.4.10 Calculation of the yield strength of the tissue

The *Hydra* tissue sphere was treated as a linear elastic hollow spherical shell. Then, the elastic pressure experienced by the sphere is given by the following:

$$P = 2Eh\frac{A}{R_0^2(1-\nu)}$$

Here, E is the Young's modulus of the tissue, ν is the Poisson's ratio, h is the thickness of the shell, A is the amplitude of the sphere at the time of rupture, and R_0 is the minimum radius of the sphere. The tissue was assumed to be incompressible, so $\nu = 0.5$. However, the results are not strongly dependent on the choice of ν. For example, if $\nu = 0.25$ is used, as in Kücken et al. [24], the pressure is only reduced by a factor of 1.5. For the Young's modulus, a value of 185 N/m^2 was used based on experiments by Veschgini et al. [42], who measured the response of tissue spheres to uniaxial compression. The median values of minimum radius and amplitude were used, with $R_0 = 119$ μm and $A = 28$ μm for LPOs and $A = 15.5$ μm for SPOs, respectively. The shell thickness, h, was obtained from images presented in Buzgariu et al. [9] and was found to be 25 μm. The size of the hole caused by rupture was estimated from images that captured debris leaving the tissue sphere during a rupture event. The narrowest portion of the debris immediately adjacent to the sphere was averaged over three events and treated as an upper limit approximation of the size of the exit point, yielding a mean diameter of 26 μm, corresponding to one to two cell diameters.

3.4.11 Comparison of the oscillation parameters to previously published values

Published histograms of the slopes during LPOs and SPOs were taken from Soriano et al. [38]. Using the freely available WebPlotDigitizer (`https://automeris.io/WebPlotDigitizer/`), we converted the histograms into frequency distribution tables, calculated medians for the slopes for LPO and SPO, and compared those to the medians we calculated for our data. Because histograms were not available for time periods and amplitudes, we used other published plots of radius and volume over time to obtain time periods and amplitudes. The median time periods were obtained after digitizing the volume over time plot in Soriano et al. [37]. Median amplitudes were also obtained in the same manner from the radius over time plot in Kücken et al. [24]. We used medians as the summary statistic for the data because the data distributions were nonnormal.

3.5 Results and Discussion

As a freshwater animal, *Hydra* experiences a continuous inflow of water from the medium, through the tissues and into the gastric cavity [3, 1]. The resulting internal pressure is periodically relieved by opening of the mouth [10]. Regenerating *Hydra* spheres initially lack a mouth and therefore must relieve pressure from water accumulation by passive tissue rupture. This creates an oscillatory pattern of gradual osmotically driven swelling and rapid deflation due to tissue rupture, followed by healing of the rupture site. These cycles of swelling and rupture show an abrupt shift in oscillation pattern from LPOs to SPOs,

coincident with a change in the aspect ratio of the regenerating *Hydra* sphere.

3.5.1 LPOs and SPOs have distinct oscillation parameters but a common driving mechanism

To examine the cause of the observed shift in oscillation pattern, we prepared tissue spheres (Fig. 3.1 A) and imaged them over the course of regeneration (Video S1). We only analyzed data from tissue spheres that regenerated fully, showing a defined body axis with head and tentacles (Fig. 3.1 B). A shift in oscillation pattern was observed to coincide with a gradual decline in aspect ratio (Fig. 3.1 C, D), as previously reported [24, 16, 38]. From these radius-versus-time plots (Fig. 3.1 C), we extracted amplitude, period, and swelling rate (slope) for LPOs and SPOs (see Materials and Methods) and found all parameters to differ significantly between the two oscillation types (Fig. 3.1 E). A comparison of our data to the literature [24, 38] using the medians of the oscillation parameters (see Materials and Methods) shows similar differences in these three parameters between LPO and SPO.

The median amplitudes observed for LPOs and SPOs (Table 3.1) correspond to changes of 25% and 15%, respectively, in the radius of the tissue spheres. Because a sphere's radius scales linearly with the linear size of the epithelial cells, we infer that the cells undergo linear deformations of 25% during LPOs and 15% during SPOs. Although these are significant cell deformations, similar and more extreme deformations are observed during mouth opening in intact polyps over the course of tens of seconds [10]. These numbers illustrate the remarkable deformability of *Hydra* tissue.

Table 3.1: Summary of oscillation parameters. Parameters are reported as the median of biological replicates with the first and third quartiles.
[a] Indicates significant difference from wild-type SPOs at p<0.01.
[b] Indicates significant difference from wild-type SPOs at p<0.05.
[c] Indicates significant difference from wild-type LPOs at p<0.01.
[d] Indicates significant difference from wild-type LPOs at p<0.05.

	Period Length (h)	Amplitude (μm)	Slope (μm/h)	Number of Biological Replicates
Wild-type (HM) LPO	4.2 (3.7, 5.8)[a]	28.0 (21.0, 36.3)[a]	6.3 (5.6, 7.1)[b]	15
Wild-type (HM) SPO	1.8 (1.5, 1.9)[c]	15.5 (13.0, 19.7)[c]	7.5 (6.7, 9.8)[d]	15
Sucrose 10 mM 2 h	2.3 (1.9, 3.0)[a,c]	13.5 (10.9, 19.1)[c]	4.9 (4.4, 6.3)[a]	14
Sucrose 25 mM 2h	3.0 (2.8, 4.3)[a]	14.3 (11.7, 19.8)[c]	3.5 (3.1, 4.1)[a,c]	17
Sucrose 25 mM 24 h	4.1 (2.7, 4.5)[a]	21.2 (13.5, 29.2)	4.0 (3.6, 5.0)[a,c]	15
Wild-type head tissue piece	1.1 (0.9, 1.4)[a,c]	8.7 (6.3, 12.1)[b,c]	9.7 (7.4, 10.9)[d]	4
Foot tissue piece	2.8 (2.3, 4.0)[a]	21.0 (14.2, 30.3)	7.6 (5.5, 7.9)	5

Previous studies and models assumed that both LPOs and SPOs are driven solely by osmotic pressure [30, 24]. However, this was only experimentally tested for LPOs [24]. To verify that SPOs are also osmotically driven, we incubated tissue pieces in hypertonic medium made by adding 10 or 25 mM sucrose to HM. Because the osmolarity between the inside and the outside of a tissue sphere equilibrates after several rupture events, we began incubation either 2 h postamputation to probe the effect of altered osmotic pressure on LPOs or 24 h postamputation to probe its effect on SPOs. Consistent with previous work [24], we observed a concentration-dependent decrease in swelling rates during the LPO cycle in the 2 h postamputation treatments (Table 3.1). Similarly, we obtained a decrease in slope in the 24 h postamputation treatment with 25 mM sucrose. Moreover, the increase in slope from LPOs to SPOs was not affected by sucrose concentrations (Table 3.1).

This suggests that SPOs are also primarily osmotically driven and that the increased rate of inflation is due to a secondary mechanism, such as a change in tissue properties associated with regeneration (e.g., an increase in tissue permeability to water or an increase in the number or activity of ion pumps), as previously suggested [16]. As slopes are even further increased in head tissue piece oscillations, the change may be linked to the development of a head, which has been reported to differ in terms of cell composition and matrix thickness [44].

The decrease in maximum amplitude of SPOs compared to LPOs indicates that the pressure required to trigger a rupture event has decreased. This can be explained either by the weakening of the tissue's tearing strength (globally or locally) or the rupture becoming an actively controlled process. Both of these are attributes of the *Hydra* mouth. The mouth is a structural weak spot because it has a thinner mesoglea and an absence of myonemes running

across it [44]. The mouth also allows for active pressure release in the intact polyp through the control of the nervous system [10]. Soriano et al. [37] proposed the first possibility, suggesting that the formation of a protomouth created a weak spot, but this idea was not tested experimentally.

3.5.2 Rupture site becomes constant as regeneration progresses

To determine whether a fixed rupture site consistent with a permanent mechanical defect appears during regeneration, we used fluorescent microbead injections to visualize the rupture site in oscillating tissue spheres (Fig. 3.2 A, B). We observed that cell debris was frequently ejected from spheres throughout the regeneration process and thus conclude that the introduction of microbeads does not represent a significant alteration to natural behavior (Fig. S4). Because rupture events can no longer be visualized after all beads are ejected from a sphere, we injected 5 h postamputation to track rupture events during LPOs or 24 h postamputation to track ruptures during SPOs. We observed that rupture sites are randomly distributed in spheres injected at 5 h (Fig. 3.2 Ci) but are significantly more localized in spheres injected at 24 h (Fig. 3.2 Cii). We compared rupture site locations for both LPOs and SPOs to data drawn from a uniform distribution using a two-sample Kolmogorov-Smirnov test and found that the 5 h data are not significantly different from a uniform distribution ($p = 0.9702$), whereas the 24 h data are ($p = 1.0047e\text{-}07$.) This suggests that a mechanical weak spot in the tissue sphere forms as regeneration proceeds.

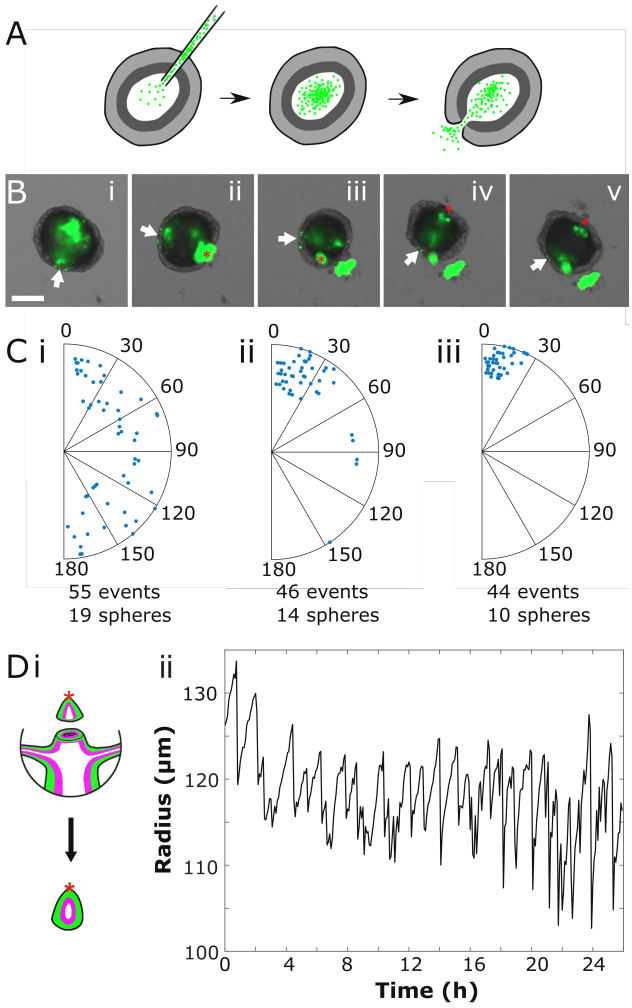

Figure 3.2: The rupture site becomes constant with head development. (A) An experiment schematic shows injection of fluorescent microbeads into a hollow sphere. Beads are ejected from the sphere during rupture events. (B) A representative image series of sphere ejecting beads during successive ruptures is shown. The white arrow indicates the feature used to track rotation, and the red asterisk represents the observed rupture site (see Materials and Methods). Scale bars, 100 μm. (C) Shown is the location of the rupture site relative to the first rupture, with each radius representing a single sphere. (i) Beginning 5 h after cutting is shown. (ii) Beginning 24 h after cutting is shown. (iii) Head tissue pieces containing the mouth of the parent animal are shown. (D) (i) A schematic illustrating the creation of a head tissue piece is shown. The red asterisk indicates the location of the mouth. (ii) Representative oscillation plot of a head tissue piece is shown.

To confirm that this structural weak point corresponded to the *Hydra* mouth, we tracked ruptures in excised head tissue pieces. These were created by excising the intact mouth of the parent animal and a small amount of surrounding tissue, then allowing the piece to round in the same way as a body column tissue piece (Fig. 3.2 Di). Head tissue pieces are not viable long term because of being composed mainly of terminally differentiated cells, but they remain healthy for at least 24 h and exhibit trackable oscillations during that time (Fig. 3.2 Dii). They also retain the parental mouth structure, which can be visualized via phalloidin staining (Fig. S5). We found that these head piece spheres had an invariant rupture site (Fig. 3.1 Ciii), supporting the idea that the emergence of a fixed rupture site is coincident with mouth development during regeneration. Finally, to confirm a link between the mouth and oscillation dynamics, we analyzed the oscillations of head pieces and found that they only exhibit SPOs as seen from the distribution of time periods (Fig. 3.2 Dii; Table 3.1). These data demonstrate that the presence of a mouth in a tissue piece is sufficient for SPOs.

Because it had been proposed that the aboral pore acts as a second weak point in the intact animal that may be used for pressure regulation [36], we also imaged foot tissue pieces containing the entire basal disk (Fig. 3.1 A). Foot tissue pieces showed oscillation parameters with a greater similarity to LPOs than to SPOs (Table 3.1). The statistically significant difference in period between foot tissue pieces and SPOs indicates that the presence of an aboral pore does not increase rupture frequency in the same way the presence of a mouth does. Thus, the aboral pore does not play a role in regulating osmotic pressure during regeneration. We suspect that the similarity in the swelling rate between the foot piece and body tissue piece SPOs results from a difference in tissue composition in the foot.

Both the hypostomal region and the basal disk have significantly higher proportions of epitheliomuscular and nerve cells than the body column [5], which may cause differences in mechanical properties or permeability.

In summary, these results support the hypothesis that ruptures during LPOs are caused by osmotically driven inflation until the yield strength of the tissue is reached, resulting in random rupture locations. In contrast, SPOs are caused by the development of a mouth structure, creating a permanent, localized weak point on the sphere. This is consistent with previous observations that insertion of head tissue into cell aggregates decreases the time required for a shift to SPOs to occur [38]. The presence of a head organizer would allow the aggregate to more rapidly define a head and develop a mouth, resulting in a faster oscillation pattern shift. Whether the forming mouth acts solely as a mechanical defect, as previously suggested [37], or actively regulates osmotic pressure cannot be distinguished based on these data.

3.5.3 Mouth function is required for a shift to SPO

To determine whether the mouth plays an active osmoregulatory role in regenerating tissue spheres, we decouple mouth function from mouth structure by examining nerve-free *Hydra*, which are capable of complete regeneration but are unable to open their mouths to relieve pressure or respond to chemical stimuli [3, 26, 14]. In contrast to normal animals, nerve-free *Hydra* take on a characteristic bloated appearance [40] (Fig. 3.3 A) because of their inability to relieve internal pressure by mouth opening. The mouth appears morphologically normal in nerve-free animals (Fig. 3.3 B), suggesting that lack of function is caused by the

absence of neurons and thus an inability to sense pressure [14]. Body column tissue spheres derived from nerve-free animals showed only LPOs, with a period slightly longer than LPOs in wild-type spheres (Fig. 3.3 C; Table 3.2). The small difference in parameters may be due to differences in tissue strength given that nerve-free animals lack all cell types derived from the interstitial cell lineage: neurons, gland cells, and nematocytes [4]. Although it has been suggested that nerve-free animals may use an alternate, slower regeneration pathway for regeneration than enervated animals [31], we observe that nerve-free animals are able to form a head and tentacles within 72 h without ever exhibiting SPO behavior (Figs. 3.3 C and S3; Video S2). Thus, nerve-free animals break shape symmetry and have a clearly specified axis without ever experiencing SPOs.

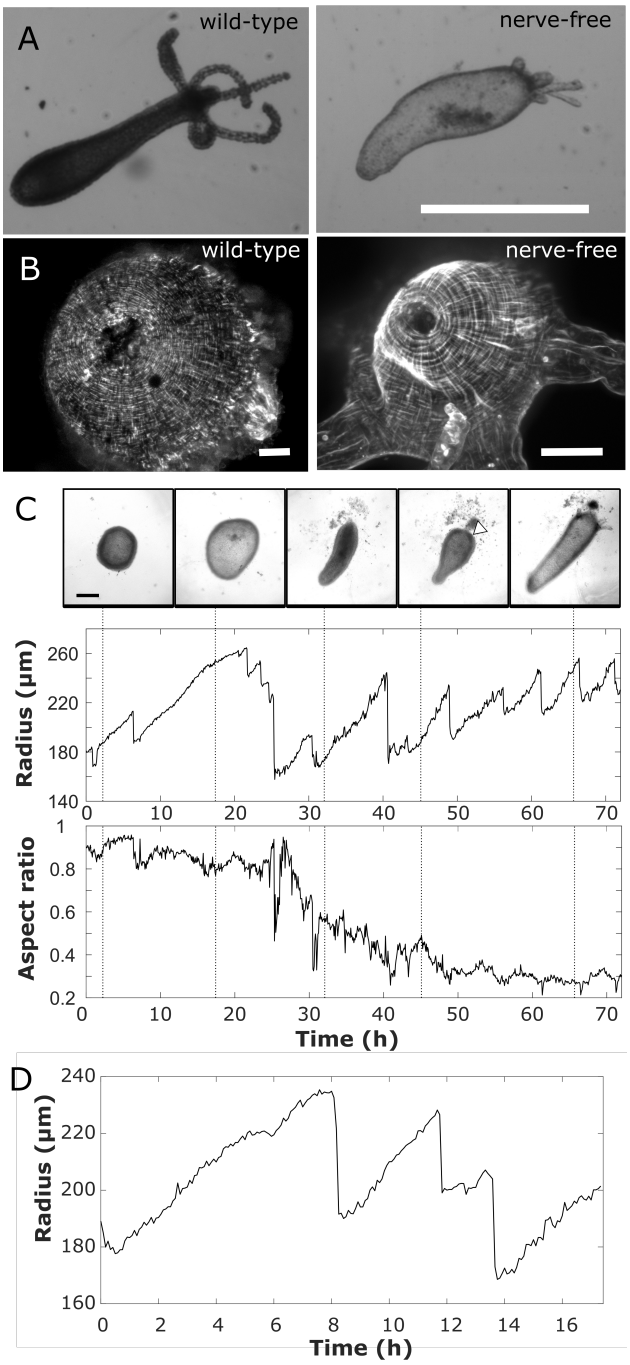

Figure 3.3: Mouth opening impacts oscillation dynamics. (A) Shown is a comparison between wild-type and nerve-free polyps, showing characteristic bloated phenotype of nerve-free *Hydra* (scale bars, 1 mm). (B) A comparison of myoneme organization in the hypostome of wild-type and nerve-free animals (scale bars, 50 μm) is shown. (C) Full regeneration of a nerve-free tissue sphere showing only LPOs (the time periods of all the oscillations are much greater than that of SPOs) is shown. Representative images are taken at times indicated on radius and aspect ratio plots. Scale bars, 200 μm. (D) A representative oscillation plot of nerve-free head tissue sphere showing only LPOs is shown.

Table 3.2: Oscillation Parameters for Various Experimental Conditions. Parameters are reported as the median of biological replicates with the first and third quartiles.
[a] Indicates significant difference from wild-type SPOs at $p<0.01$.
[b] Indicates significant difference from wild-type SPOs at $p<0.05$.
[c] Indicates significant difference from wild-type LPOs at $p<0.01$.
[d] Indicates significant difference from wild-type LPOs at $p<0.05$.

	Period Length (h)	Amplitude (μm)	Slope (μm/h)	Number of Biological Replicates
Wild-type body column tissue pieces LPO	4.2 (3.7, 5.8)[a]	28.0 (21.0, 36.3)[a]	6.3 (5.6, 7.1)[b]	15
Wild-type body column tissue pieces SPO	1.8 (1.5, 1.9)[c]	15.5 (13.0, 19.7)[c]	7.5 (6.7, 9.8)[d]	15
Wild-type head tissue pieces	1.1 (0.9, 1.4)[a,c]	8.7 (6.3, 12.1)[b,c]	9.7 (7.4, 10.9)[d]	4
Nerve-free body column pieces	6.6 (5.6, 9.3)[a,c]	28.5 (25.8, 37.7)[a]	4.1 (3.3, 4.5)[a]	11
Nerve-free head tissue pieces	3.2 (2.8, 4.0)[a]	20.8 (16.0, 29.9)	6.5 (5.5, 7.8)	4

Because it is still possible that the development of mouth structures is delayed in nerve-free *Hydra*, we use excised head pieces from nerve-free *Hydra* containing the mouth to fully decouple mouth structure from mouth function. If the presence of a mouth structure was sufficient to increase rupture frequency, we would expect to observe SPOs in spheres derived from nerve-free head pieces as we do in untreated wild-type head pieces (Fig. 3.2 D). Alternatively, if active control of the mouth structure is necessary for SPOs to occur, nerve-free head pieces should not show SPOs. We observe that spheres from nerve-free head pieces show only LPOs (Fig. 3.3 D; Table 3.2) and therefore conclude that mouth function is a requirement for the occurrence of SPOs.

Taken together, these data demonstrate that the shift in oscillation pattern observed in regenerating *Hydra* tissue spheres is caused by the formation of a functional mouth and its use in osmoregulation. A tissue sphere derived from a wild-type polyp initially exhibits LPOs in which rupture is dictated by the yield strength of the tissue. Rupture events in this regime are randomly located because mechanical failure is equally likely to occur at any point on the sphere. Approximately 24 h into the regeneration process, we observed the development of a functional mouth, which allows for active osmoregulation, causing the shift to SPOs.

3.5.4 Implications for theoretical models of *Hydra* regeneration

Various attempts have been made to model axis determination from a homogenous initial state in *Hydra* spheres. The core of these models lies in some form of feedback between morphogen concentrations and mechanical properties of the tissue such as elasticity. The

dynamics of the morphogen concentrations are modeled using the Gierer-Meinhardt model [20], whereas feedback between mechanics and the morphogens is modeled using a relation between tissue stretch and morphogen diffusion. In the model proposed by Soriano et al. [38], this takes the form of a linear relationship between tissue strain and the diffusion coefficient of one of the morphogens. Axis formation is posited to occur when a stable morphogen gradient is established (a consequence of the diffusion coefficient exceeding a certain threshold [38]), which makes the timescale for gradient formation much shorter than the timescale for shape oscillations. In a more recent model by Mercker et al. [30], the local diffusion coefficient is a function of the local area strain of the tissue, and the elastic modulus is a function of morphogen concentration. This allows for a growth instability: high local strain causes accumulation of the morphogen and morphogen accumulation allows for higher local strains in response to the same stress [30].

To date, there are no quantitative experimental data on concentration patterns of morphogens, their diffusion constants, or the feedback between morphogen concentration and mechanical properties in *Hydra*. Therefore, models rely entirely on relations between morphological parameters, such as swelling rate, initial tissue size, and the time of shape symmetry breaking, to constrain model parameters and validate predictions. The results presented here force us to reconsider the assumption that the time of shape and biochemical symmetry breaking always coincide with the time of the oscillation pattern shift from LPO to SPO. Nerve-free tissue pieces only exhibit LPOs but nevertheless break shape symmetry and specify a body axis (Fig. 3.3 C; Fig. S3). This demonstrates that one of the key observables used to constrain the existing models is not universally applicable. Instead, we show that the shift in the oscillation pattern is caused by a change in local yield strength

of the tissue because of mouth formation, a property whose variation is not considered by existing models.

We estimate the local yield strength of the tissue by treating it as an elastic shell (see Materials and Methods). The order of magnitude estimate is made using only quantities that can be measured or calculated from experimental data presented here or elsewhere in the literature, except for Poisson's ratio, which does not affect the order of magnitude (see Materials and Methods). The estimated elastic pressure inside the sphere at the time of rupture is on the order of 20 Pa during LPOs. Because the pressure scales linearly with oscillation amplitude (see Materials and Methods) and the SPO amplitude is approximately half the LPO amplitude, the pressure at the time of rupture during SPOs is 10 Pa acting on an area of the order of two to three cell diameters across. Therefore, the elastic force must be on the order of a few nano-Newtons at the time of rupture during SPOs.

The magnitude of this force is comparable to that exerted by myonemes to create a mouth opening [10] and to the separation force associated with tight junctions involved in cell-cell adhesion [41]. Although the sources of the elastic forces estimated here for SPOs are different from those involved in mouth opening, they act on the same tissue producing the same effect (breaking cell-cell contacts to create an opening), suggesting that the estimates are reasonable. We thus provide an experimentally determined value that can be used to constrain the maximum stress associated with tissue rupture in models.

We can infer that axis specification must precede mouth function. Previous work shows that Wnt3 expression occurs by 24 h in large aggregates that give rise to multiple body axes [22] or by 1.5 h after amputation in a decapitated animal [25]. Because a tissue piece retains more structure than an aggregate but less than a decapitated animal, we expect

Wnt3 signaling to be established between these times. By combining these constraints with the time of the oscillation pattern shift as an upper bound, we can improve our estimate of the time of axis specification over that used in previous models.

Finally, although this and other recent works [24, 16, 28] have focused on regenerating spheres originating from tissue pieces, the oscillation behavior of spheres originating from cell aggregates should be revisited. A direct comparison of the results from these two starting scenarios is likely to provide further insights into the mechanisms that drive regeneration and patterning. Exploring these possibilities and leveraging them to improve existing models should be the next step in our attempt to understand axis specification in *Hydra*.

3.6 Conclusions

During *Hydra* regeneration from small tissue pieces or aggregated cells, a hollow bi-layered sphere forms that undergoes dramatic shape oscillations. A switch in oscillation pattern, from long-period, large-amplitude to short-period, small-amplitude oscillations, occurs approximately 1 day into regeneration. Because previous explanations for the shift in oscillation pattern have recently been invalidated, we reexamined this fundamental process during *Hydra* regeneration from tissue spheres and demonstrate that the oscillation pattern shift is a direct consequence of the onset of mouth function and its use in osmoregulation. This allows us to infer the development of an important physiological function through a morphological readout. The results from this work also enable the field to reexamine and improve existing models of *Hydra*regeneration that rely on the concurrence of the shift in oscillation pattern and decrease in aspect ratio to constrain model parameters.

3.7 Acknowledgements

Chapter 3, in full, is a reformatted reprint of material as it appears in Biophysical Journal, 2019. (Wang, R., Goel, T., Khazoyan, K., Sabry, Z., Quan, H.J., Diamond, P.H. and Collins, E.M.S. Mouth Function Determines The Shape Oscillation Pattern In Regenerating Hydra Tissue Spheres. Biophysical Journal, 117(6), pp.1145-1155.) Use of this manuscript in this dissertation is covered by the rights permitted to the authors by Elsevier. The dissertation author was the co-primary author of this paper.

Bibliography

[1] Dale J Benos and Robert D Prusch. "Osmoregulation in Hydra: Column contraction as a function of external osmolality". In: *Comparative Biochemistry and Physiology – Part A: Physiology* 44.4 (Apr. 1973), pp. 1397–1400. ISSN: 03009629. DOI: 10.1016/0300-9629(73)90280-6.

[2] Dale J. Benos, R. Gary Kirk, William P. Barba, and Marcia M. Goldner. "Hyposmotic fluid formation in Hydra". In: *Tissue and Cell* 9.1 (Jan. 1977), pp. 11–22. ISSN: 00408166. DOI: 10.1016/0040-8166(77)90045-3.

[3] Dale J. Benos and Robert D. Prusch. "Osmoregulation in fresh-water Hydra". In: *Comparative Biochemistry and Physiology – Part A: Physiology* 43.1 (Sept. 1972), pp. 165–171. ISSN: 03009629. DOI: 10.1016/0300-9629(72)90478-1.

[4] H R Bode. *The interstitial cell lineage of hydra: A stem cell system that arose early in evolution*. June 1996.

[5] H. Bode, S. Berking, C. N. David, A. Gierer, H. Schaller, and E. Trenkner. "Quantitative analysis of cell types during growth and morphogenesis in Hydra". In: *Wilhelm Roux Archiv für Entwicklungsmechanik der Organismen* 171.4 (Dec. 1973), pp. 269–285. ISSN: 0949944X. DOI: 10.1007/BF00577725.

[6] Hans Bode. "Axis Formation in Hydra". In: *Annual Review of Genetics* 45.1 (Dec. 2011), pp. 105–117. ISSN: 0066-4197. DOI: 10.1146/annurev-genet-102209-163540.

[7] Mariya Broun, Lydia Gee, Beate Reinhardt, and Hans R Bode. "Formation of the head organizer in hydra involves the canonical Wnt pathway". In: *Development* 132.12 (2005), pp. 2907–2916. DOI: 10.1242/dev.01848.

[8] Thibaut Brunet, Adrien Bouclet, Padra Ahmadi, Démosthène Mitrossilis, Benjamin Driquez, Anne Christine Brunet, Laurent Henry, Fanny Serman, Gaëlle Béalle, Christine Ménager, Frédéric Dumas-Bouchiat, Dominique Givord, Constantin Yanicostas, Damien Le-Roy, Nora M. Dempsey, Anne Plessis, and Emmanuel Farge. "Evolutionary conservation of early mesoderm specification by mechanotransduction in Bilateria". In: *Nature Communications* 4.1 (Nov. 2013), pp. 1–15. ISSN: 20411723. DOI: 10.1038/ncomms3821.

[9] W Buzgariu, S Al Haddad, S Tomczyk, Y Wenger, and B Galliot. "Multi-functionality and plasticity characterize epithelial cells in Hydra." eng. In: *Tissue barriers* 3.4 (2015), e1068908. ISSN: 2168-8362 (Print). DOI: 10.1080/21688370.2015.1068908.

[10] Jason A. Carter, Callen Hyland, Robert E. Steele, and Eva Maria S. Collins. "Dynamics of Mouth Opening in Hydra". In: *Biophysical Journal* 110.5 (2016), pp. 1191–1201. ISSN: 15420086. DOI: 10.1016/j.bpj.2016.01.008.

[11] Jarrod A. Chapman, Ewen F. Kirkness, Oleg Simakov, Steven E. Hampson, Therese Mitros, Thomas Weinmaier, Thomas Rattei, Prakash G. Balasubramanian, Jon Bor-

man, Dana Busam, Kathryn Disbennett, Cynthia Pfannkoch, Nadezhda Sumin, Granger G. Sutton, Lakshmi Devi Viswanathan, Brian Walenz, David M. Goodstein, Uffe Hellsten, Takeshi Kawashima, Simon E. Prochnik, Nicholas H. Putnam, Shengquiang Shu, Bruce Blumberg, Catherine E. Dana, Lydia Gee, Dennis F. Kibler, Lee Law, Dirk Lindgens, Daniel E. Martinez, Jisong Peng, Philip A. Wigge, Bianca Bertulat, Corina Guder, Yukio Nakamura, Suat Ozbek, Hiroshi Watanabe, Konstantin Khalturin, Georg Hemmrich, André Franke, René Augustin, Sebastian Fraune, Eisuke Hayakawa, Shiho Hayakawa, Mamiko Hirose, Jung Shan Hwang, Kazuho Ikeo, Chiemi Nishimiya-Fujisawa, Atshushi Ogura, Toshio Takahashi, Patrick R.H. Steinmetz, Xiaoming Zhang, Roland Aufschnaiter, Marie Kristin Eder, Anne Kathrin Gorny, Willi Salvenmoser, Alysha M. Heimberg, Benjamin M. Wheeler, Kevin J. Peterson, Angelika Böttger, Patrick Tischler, Alexander Wolf, Takashi Gojobori, Karin A. Remington, Robert L. Strausberg, J. Craig Venter, Ulrich Technau, Bert Hobmayer, Thomas C.G. Bosch, Thomas W. Holstein, Toshitaka Fujisawa, Hans R. Bode, Charles N. David, Daniel S. Rokhsar, and Robert E. Steele. "The dynamic genome of Hydra". In: *Nature* 464.7288 (2010), pp. 592–596. ISSN: 00280836. DOI: 10.1038/nature08830.

[12] P Culp, C Nüsslein-Volhard, and N Hopkins. "High-frequency germ-line transmission of plasmid DNA sequences injected into fertilized zebrafish eggs". In: *Proceedings of the National Academy of Sciences* 88.18 (Sept. 1991), pp. 7953–7957. ISSN: 0027-8424. DOI: 10.1073/PNAS.88.18.7953.

[13] Emmanuel Farge. *Mechanotransduction in Development*. Vol. 95. Academic Press, Jan. 2011, pp. 243–265. DOI: 10.1016/B978-0-12-385065-2.00008-6.

[14] Helen Forrest. "Lack of Dependence of the Feeding Reaction in Hydra on Reduced Glutathion". In: *The Biological Bulletin* 122.3 (June 1962), pp. 343–361. DOI: 10.2307/1539235.

[15] Toshitaka Fujisawa. "Hydra regeneration and epitheliopeptides". In: *Developmental Dynamics* 226.2 (2003), pp. 182–189. ISSN: 10588388. DOI: 10.1002/dvdy.10221.

[16] C Fütterer, C Colombo, F Jülicher, and A Ott. "Morphogenetic oscillations during symmetry breaking of regenerating ¡i¿Hydra vulgaris¡/i¿ cells". In: *Europhysics Letters (EPL)* 64.1 (2003), pp. 137–143. ISSN: 0295-5075. DOI: 10.1209/epl/i2003-00148-y.

[17] Brigitte Galliot. *The hydra model system*. 2012. DOI: 10.1387/ijdb.120094bg.

[18] Andrea Gamba, Mario Nicodemi, Jordi Soriano, and Albrecht Ott. "Critical behavior and axis defining symmetry breaking in hydra embryonic development". In: *Physical Review Letters* 108.15 (Apr. 2012), p. 158103. ISSN: 00319007. DOI: 10.1103/PhysRevLett.108.158103.

[19] A Gierer, S Berking, H Bode, C N David, K Flick, G Hansmann, H Schaller, and E Trenkner. "Regeneration of hydra from reaggregated cells". In: *Nature New Biology* 239.91 (1972), pp. 98–101. ISSN: 00900028. DOI: 10.1038/newbio239098a0.

[20] A. Gierer and Hans Meinhardt. "A theory of biological pattern formation". In: *Kybernetik* 12.1 (1972), pp. 30–39. ISSN: 03401200. DOI: 10.1007/BF00289234.

[21] K. M. Glauber, C. E. Dana, S. S. Park, D. A. Colby, Y. Noro, T. Fujisawa, A. R. Chamberlin, and R. E. Steele. "A small molecule screen identifies a novel compound that induces a homeotic transformation in Hydra". In: *Development* 142.11 (2015), pp. 2081–2081. ISSN: 0950-1991. DOI: 10.1242/dev.126235.

[22] Bert Hobmayer, Fabian Rentzsch, Kerstin Kuhn, Christoph M Happel, Christoph Cramer Von Laue, Petra Snyder, Ute Rothbächer, and Thomas W Holstein. "WNT signalling molecules act in axis formation in the diploblastic metazoan Hydra". In: *Nature* 407.6801 (2000), pp. 186–189. ISSN: 00280836. DOI: 10.1038/35025063.

[23] Celina E. Juliano, Haifan Lin, and Robert E. Steele. "Generation of Transgenic Hydra by Embryo Microinjection". In: *Journal of Visualized Experiments* 91 (2014), e51888. ISSN: 1940-087X. DOI: 10.3791/51888.

[24] Michael Kücken, Jordi Soriano, Pramod A. Pullarkat, Albrecht Ott, and Ernesto M. Nicola. "An osmoregulatory basis for shape oscillations in regenerating Hydra". In: *Biophysical Journal* 95.2 (July 2008), pp. 978–985. ISSN: 15420086. DOI: 10.1529/biophysj.107.117655.

[25] Tobias Lengfeld, Hiroshi Watanabe, Oleg Simakov, Dirk Lindgens, Lydia Gee, Lee Law, Heiko A Schmidt, Suat Özbek, Hans Bode, and Thomas W Holstein. "Multiple Wnts are involved in Hydra organizer formation and regeneration". In: *Developmental Biology* 330.1 (2009), pp. 186–199. DOI: http://dx.doi.org/10.1016/j.ydbio.2009.02.004.

[26] H M LENHOFF. "Activation of the feeding reflex in Hydra littoralis. I. Role played by glutathione and quantitative assay of the feeding reflex". In: *The Journal of general physiology* 45.2 (Nov. 1961), pp. 331–344. ISSN: 00221295. DOI: 10.1085/jgp.45.2.331.

[27] Howard M. Lenhoff and Ray DuBois Brown. "Mass culture of hydra: an improved method and its application to other aquatic invertebrates". In: *Laboratory Animals* 4.1 (Apr. 1970), pp. 139–154. ISSN: 0023-6772. DOI: 10.1258/002367770781036463.

[28] Anton Livshits, Lital Shani-Zerbib, Yonit Maroudas-Sacks, Erez Braun, and Kinneret Keren. "Structural Inheritance of the Actin Cytoskeletal Organization Determines the Body Axis in Regenerating Hydra". In: *Cell Reports* 18.6 (Feb. 2017), pp. 1410–1421. ISSN: 22111247. DOI: 10.1016/j.celrep.2017.01.036.

[29] Mark Lommel, Anja Tursch, Laura Rustarazo-Calvo, Benjamin Trageser, and Thomas W Holstein. "Genetic knockdown and knockout approaches in Hydra". In: *bioRxiv* (2017), p. 230300. DOI: 10.1101/230300.

[30] Moritz Mercker, Alexandra Köthe, and Anna Marciniak-Czochra. "Mechanochemical Symmetry Breaking in Hydra Aggregates". In: *Biophysical Journal* 108.9 (2015), pp. 2396–2407. ISSN: 15420086. DOI: 10.1016/j.bpj.2015.03.033.

[31] Marijana Miljkovic-Licina, Simona Chera, Luiza Ghila, and Brigitte Galliot. "Head regeneration in wild-type hydra requires de novo neurogenesis." In: *Development (Cambridge, England)* 134.6 (Mar. 2007), pp. 1191–201. ISSN: 0950-1991. DOI: 10.1242/dev.02804.

[32] Yukio Nakamura, Charisios D Tsiairis, Suat Özbek, and Thomas W Holstein. "Autoregulatory and repressive inputs localize Hydra Wnt3 to the head organizer." In: *Proceedings of the National Academy of Sciences of the United States of America* 108.22 (2011), pp. 9137–42. ISSN: 1091-6490. DOI: 10.1073/pnas.1018109108.

[33] Mika Sato-Maeda and Hideo Tashiro. "Development of Oriented Motion in Regenerating Hydra Cell Aggregates". In: *Zoological Science* 16.2 (1999), pp. 327–334. ISSN: 0289-0003. DOI: 10.2108/zsj.16.327.

[34] Hiroshi Shimizu, Osamu Koizumi, and Toshitaka Fujisawa. "Three digestive movements in Hydra regulated by the diffuse nerve net in the body column". In: *Journal of Comparative Physiology A* 190.8 (Aug. 2004), pp. 623–630. ISSN: 0340-7594. DOI: 10.1007/s00359-004-0518-3.

[35] Hiroshi Shimizu, Yasuji Sawada, and Tsutomu Sugiyama. "Minimum tissue size required for hydra regeneration". In: *Developmental Biology* 155.2 (Feb. 1993), pp. 287–296. ISSN: 00121606. DOI: 10.1006/dbio.1993.1028.

[36] Hiroshi Shimizu, Yasuharu Takaku, Xiaoming Zhang, and Toshitaka Fujisawa. "The aboral pore of hydra: Evidence that the digestive tract of hydra is a tube not a sac". In: *Development Genes and Evolution* 217.8 (2007), pp. 563–568. ISSN: 0949944X. DOI: 10.1007/s00427-007-0165-0.

[37] Jordi Soriano, Cyril Colombo, and Albrecht Ott. "Hydra molecular network reaches criticality at the symmetry-breaking axis-defining moment". In: *Physical Review Letters* 97.25 (2006). ISSN: 00319007. DOI: 10.1103/PhysRevLett.97.258102.

[38] Jordi Soriano, Sten Rüdiger, Pramod Pullarkat, and Albrecht Ott. "Mechanogenetic Coupling of Hydra Symmetry Breaking and Driven Turing Instability Model". In: *Biophysical Journal* 96.4 (Feb. 2009), pp. 1649–1660. ISSN: 0006-3495. DOI: 10.1016/J.BPJ.2008.09.062.

[39] T. Sugiyama and T. Fujisawa. "Genetic analysis of developmental mechanisms in hydra. II. Isolation and characterization of an interstitial cell-deficient strain". In: *Journal of Cell Science* Vol. 29.1 (1978), pp. 35–52. ISSN: 00219533.

[40] Cassidy M. Tran, Sharon Fu, Trevor Rowe, and Eva Maria S. Collins. "Generation and long-term maintenance of nerve-free hydra". In: *Journal of Visualized Experiments* 2017.125 (2017). ISSN: 1940087X. DOI: 10.3791/56115.

[41] S. R.K. Vedula, T. S. Lim, P. J. Kausalya, E. Birgit Lane, G. Rajagopal, W. Hunziker, and C. T. Lim. "Quantifying forces mediated by integral tight junction proteins in cell-cell adhesion". In: *Experimental Mechanics* 49.1 (Feb. 2009), pp. 3–9. ISSN: 00144851. DOI: 10.1007/s11340-007-9113-1.

[42] M. Veschgini, F. Gebert, N. Khangai, H. Ito, R. Suzuki, T. W. Holstein, Y. Mae, T. Arai, and M. Tanaka. "Tracking mechanical and morphological dynamics of regenerating Hydra tissue fragments using a two fingered micro-robotic hand". In: *Applied Physics Letters* 108.10 (Mar. 2016), p. 103702. ISSN: 0003-6951. DOI: 10.1063/1.4943402.

[43] David L. West. "The epitheliomuscular cell of hydra: Its fine structure, three-dimensional architecture and relation to morphogenesis". In: *Tissue and Cell* 10.4 (1978), pp. 629–646. ISSN: 00408166. DOI: 10.1016/0040-8166(78)90051-4.

[44] Richard L. Wood. "The fine structure of the hypostome and mouth of hydra - I. Scanning electron microscopy". In: *Cell and Tissue Research* 199.2 (1979), pp. 307–317. ISSN: 0302766X. DOI: 10.1007/BF00236141.

3.8 Supplemental Information

The supplemental information may be accessed online at: https://ars.els-cdn.com/content/image/1-s2.0-S000634951930668X-mmc1.pdf

3.8.1 Supplementary Figures

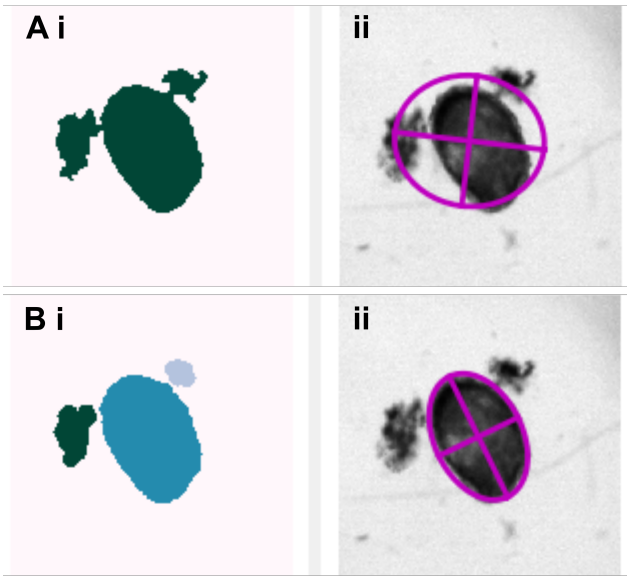

Figure 3.S1: Representative images from image analysis of regenerating tissue spheres. (A) Prior to image segmentation using watershedding. i. Debris and tissue piece identified as single object. ii. Raw image with fitted ellipse. (B) After image segmentation using watershedding. i. Debris and tissue piece identified as separate objects. ii. Raw image with fitted ellipse. The ellipse fit in the bottom right panel was used for analysis.

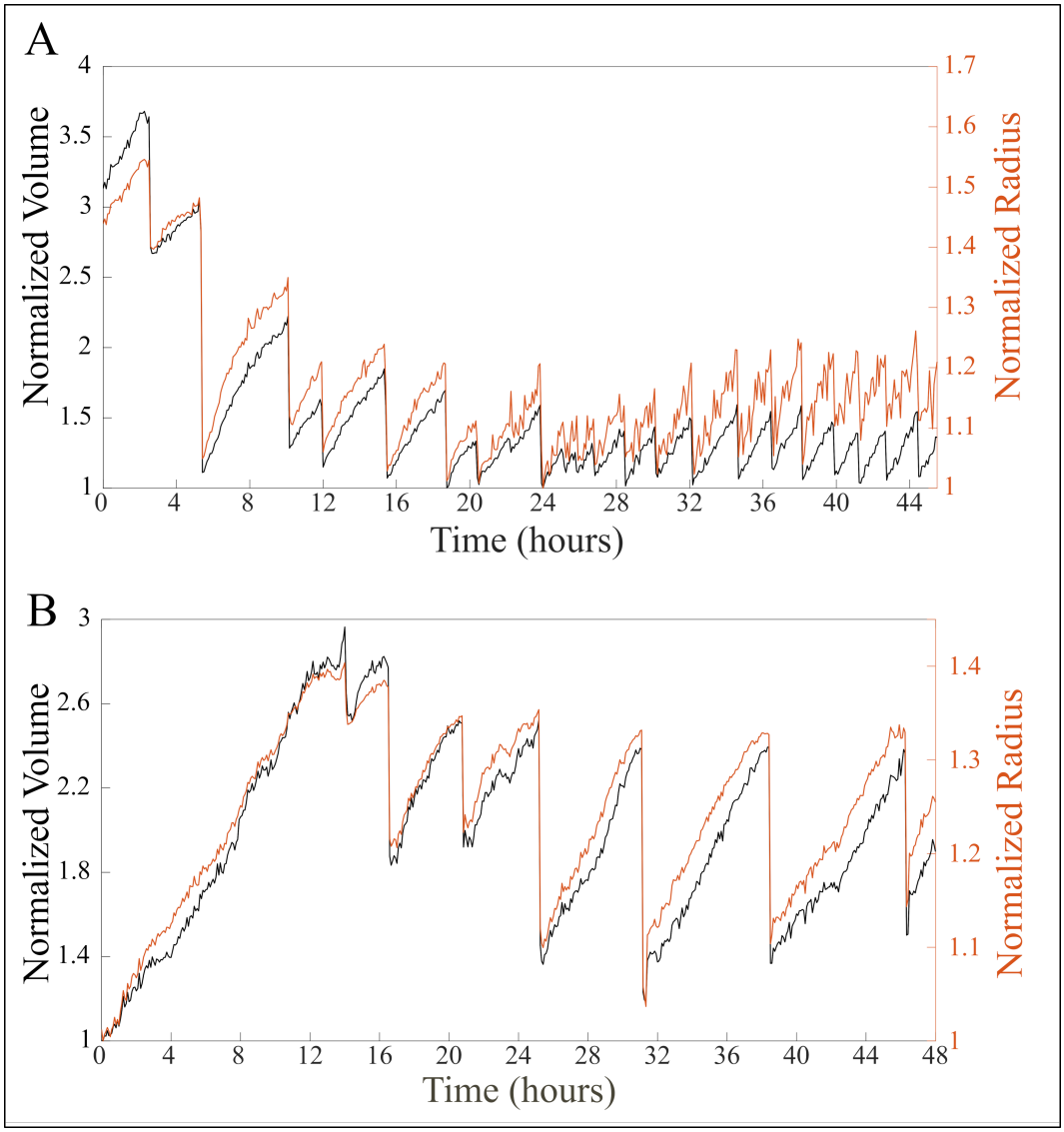

Figure 3.S2: Effective radius and volume dynamics are not qualitatively different. (A) Wildtype tissue piece displaying an oscillation pattern shift. Radius plotted in red, calculated volume plotted in black. Both were normalized by dividing by the respective minimum values. (B) Tissue piece from a nerve-free animal only displaying LPOs. Normalized radius plotted in red,normalized calculated volume plotted in black.

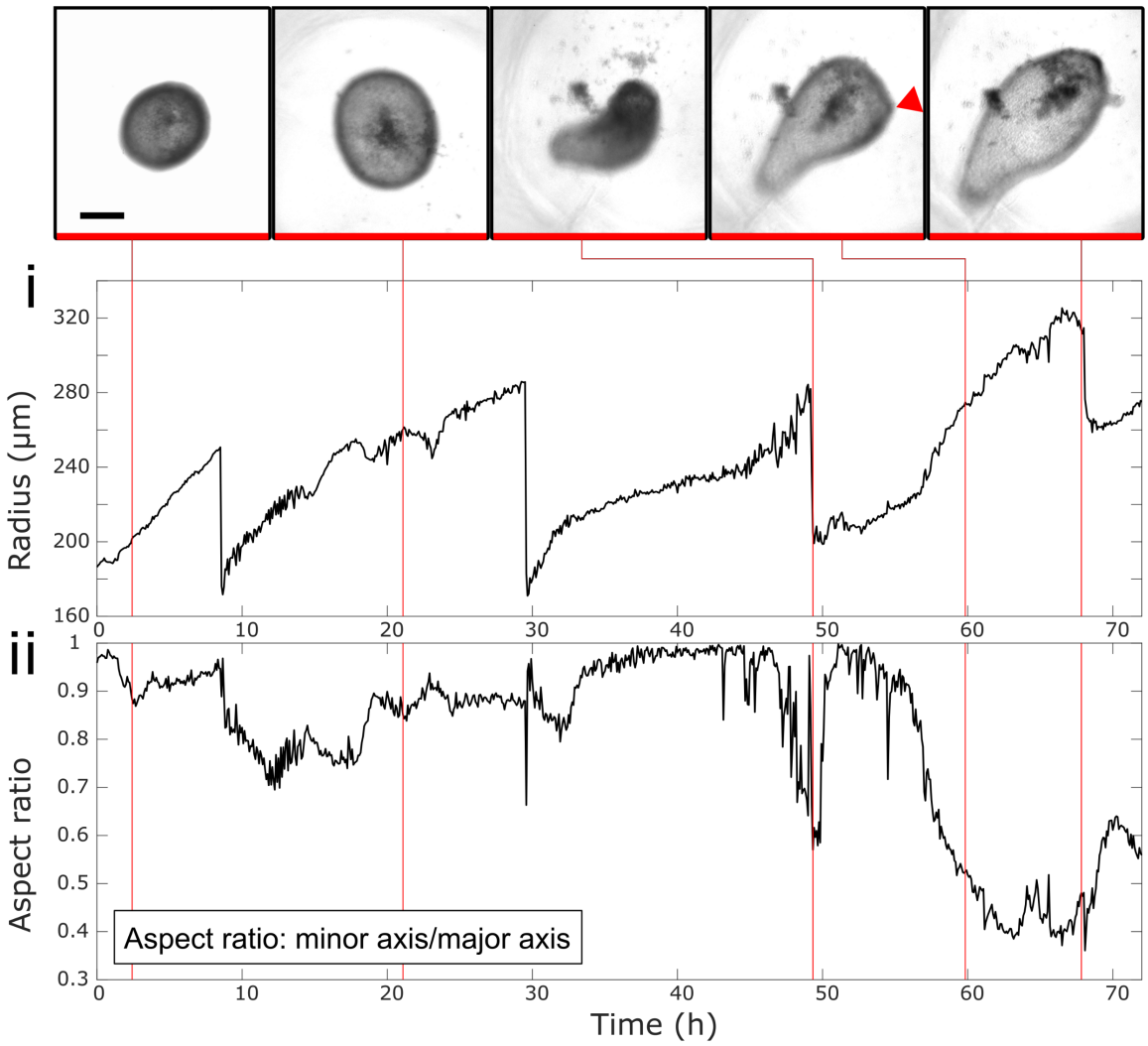

Figure 3.S3: Regeneration of head structures in nerve-free tissue piece over the course of 72 h. i.Radius and ii. aspect ratio plots for regeneration of nerve-free tissue piece, with representative images indicated by red lines. Shape symmetry is broken before 48h and the appearance of tentacle buds is observed around 60h. Red arrowhead indicates first visible tentacle bud. Scale bar 200 μm.

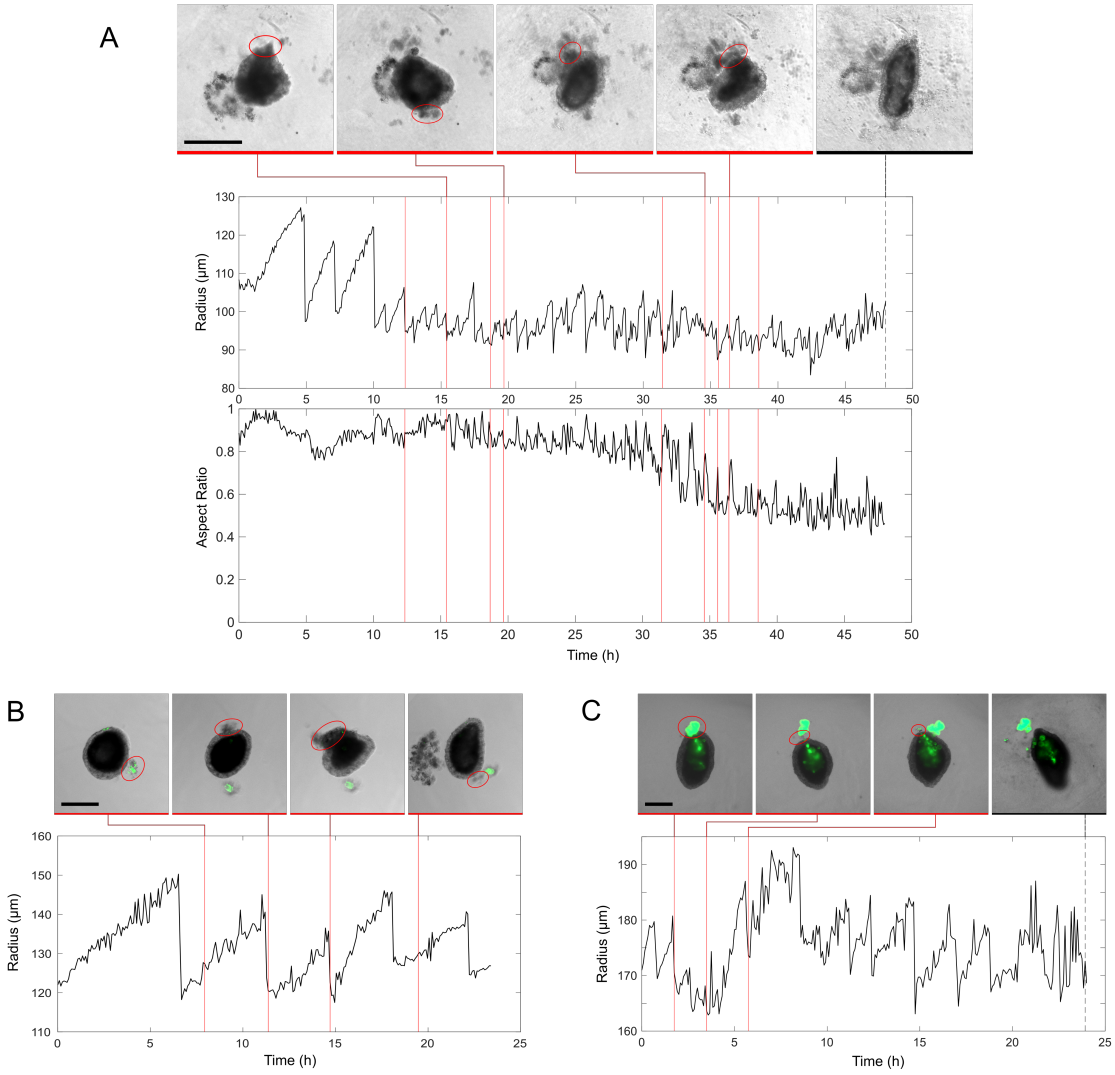

Figure 3.S4: Debris is ejected throughout the regeneration process. (A) Cell debris ejected from an un-injected tissue piece. Red lines on radius and aspect ratio plots indicate the earliest frame in which a new piece of ejected debris can be clearly observed. Image series illustrate representative rupture events, with new debris circled in red. Dashed black line and associated image indicate the last frame of the video, showing the presence of a body axis. (B) Tissue piece injected with microbeads 5 h after cutting. 4 trackable rupture events with ejection of both beads and cell debris are observed. Images have been rotated to standardize the orientation of the tissue piece. Oscillations resemble LPOs and rupture site is not conserved. (C) Tissue piece injected with microbeads 24 h after cutting. 3 trackable rupture events with ejection of both beads and cell debris are observed. Images have been rotated to standardize the orientation of the tissue piece. Rupture site is conserved, and oscillations resemble SPOs. The last frame of the video shows the tissue piece is oblong with a conical hypostome structure.Scale bars 200 μm.

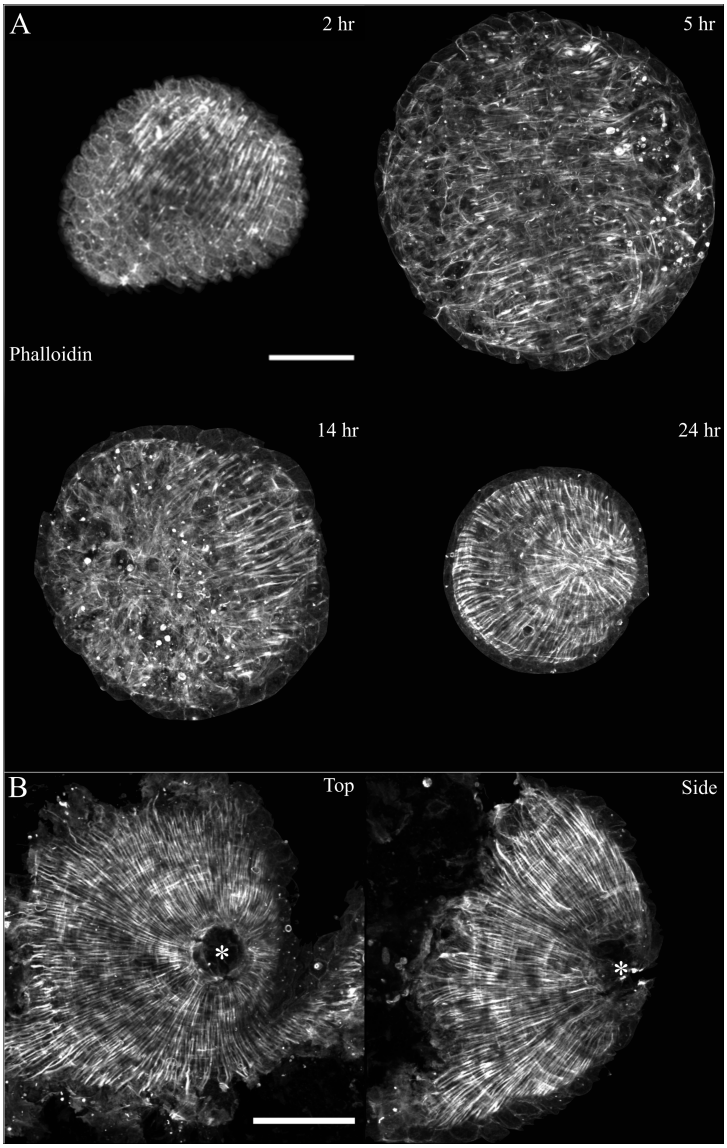

Figure 3.S5: Retention of myoneme structure in tissue pieces. (A) Body column tissue pieces fixed and stained with phalloidin 2, 5, 14 and 24h after cutting. (B) Phalloidin staining of head pieces 5h after excision showing retention of normal myoneme organization of the mouth. Damage to the aboral side of the piece (on the left in the side view) occurs during mounting due to the conical shape of head pieces and does not accurately represent the live state. Scale bars 100 μm

3.8.2 Supplementary Movies

Movie 1. Regeneration of wildtype tissue piece. Raw video of the tissue piece represented in Figure S4 A. Scale bar 200 μm, total time 48 h. Recorded at 1 frame every 5 minutes (0.003 fps), playback at 10 fps.

Movie 2. Regeneration of nerve-free tissue piece. Raw video of the tissue piece represented in Figure 3.3, sowing formation of body axis and head structures. Scale bar 200 μm, total time 72h. Recorded at 1 frame every 5 minutes (0.003 fps), playback at 10 fps.

Chapter 4

Linalool acts as a fast and reversible anesthetic in *Hydra*

4.1 Abstract

The ability to make transgenic Hydra lines has allowed for quantitative *in vivo* studies of *Hydra* regeneration and physiology. These studies commonly include excision, grafting and transplantation experiments along with high-resolution imaging of live animals, which can be challenging due to the animal's response to touch and light stimuli. While various anesthetics have been used in *Hydra* studies, they tend to be toxic over the course of a few hours or their long-term effects on animal health are unknown. Here, we show that the monoterpenoid alcohol linalool is a useful anesthetic for *Hydra*. Linalool is easy to use, non-toxic, fast acting, and reversible. It has no detectable long-term effects on cell viability or cell proliferation. We demonstrate that the same animal can be immobilized in linalool multiple times at intervals of several hours for repeated imaging over 2–3 days. This uniquely allows

for *in vivo* imaging of dynamic processes such as head regeneration. We directly compare linalool to currently used anesthetics and show its superior performance. Linalool will be a useful tool for tissue manipulation and imaging in *Hydra* research in both research and teaching contexts.

4.2 Introduction

Abraham Trembley's careful and systematic studies on *Hydra* regeneration, published in his Memoires in 1744, brought this freshwater cnidarian into the spotlight of biological research [52]. *Hydra* is an optically transparent polyp a few millimeters in length. It consists of a hollow cylindrical body column with a head on one end, consisting of a ring of tentacles and a dome-shaped hypostome, and an adhesive basal disk on the other end. *Hydra* is composed of only a small number of cell types originating from three (ectodermal, endodermal and interstitial) stem cell lineages [7]. This anatomical simplicity, continuous cell turnover in the adult [17], and the ability to regenerate from small fragments of the body column or even from aggregates of cells [32, 81] render *Hydra* a powerful system for studies of development [86], stem cell biology [24, 11], and regeneration [12, 31, 21, 69]. Furthermore, *Hydra* has a relatively simple nervous system [14, 8], consisting of a few thousand cells [23] that are organized in three neuronal networks [26], making it an attractive system to study neuron development [67, 50] and neuronal control of behavior [26, 37].

Exploiting *Hydra*'s patterning processes and regenerative abilities via sophisticated excision and grafting studies has been a mainstay of *Hydra* research since Trembley's original experiments. This "cut-and-paste" approach has provided fundamental insights into *Hydra*

biology. For example, the excision and subsequent threading of body column rings onto fishing line allowed researchers to probe questions about oral-aboral polarization [1]. Grafting of hypostomes into body columns showed that the tip of the hypostome acts as a head organizer [13, 97] long before the head organizer was biochemically analyzed [9]. Transplantation experiments were used to characterize the properties and dynamics of head inhibition [59] and estimate the length scales of head activation and inhibition [91], which helped validate the Gierer-Meinhardt model of axial patterning [33] decades before *in vivo* visualization of cells or proteins was possible in *Hydra*.

However, despite its many advantages, *Hydra* has not become a mainstream model organism due to the lack of genetic tools. This has changed in the last decade with access to a fully assembled *Hydra* genome [19], single cell RNAseq data [83], and the development of molecular tools that allow for the generation of transgenic lines [44, 34, 96]. Because of these tools, numerous recent studies have been able to address longstanding open questions that could not previously be answered. For example, the recent creation of a transgenic line expressing GCaMP6s in the interstitial lineage allowed visualization of neural activity in real time in freely behaving animals and led to the discovery of multiple discrete networks of neurons linked to specific behaviors [26]. Transgenic animals have also enabled biomechanics studies to settle key biological questions regarding the mechanism driving cell sorting during regeneration from cell aggregates [21] and the functioning of the *Hydra* mouth [18].

As *Hydra* research continues to dig deeper into such questions in the living animal, future studies will require ever more precise and repeatable manipulations, high resolution live imaging, or a combination thereof to fully exploit transgenic strains and other new technologies. Because *Hydra* is in a continuous dynamic state of extension-contraction and

responds rapidly to stimuli such as touch and light [75], a reversible way of slowing or preventing the animal's movements would greatly facilitate these kinds of experiments. The search for a reliable and reversible relaxant in *Hydra* has driven the field to explore an array of compounds, with the most prominent being urethane [58, 5, 64, 89, 15], heptanol [85, 73], and chloretone [3, 56, 57, 49]. Urethane and heptanol have broad effects on *Hydra*. Urethane reverses the transepithelial potential, causing adverse effects upon several hours of exposure [58]. Heptanol blocks epithelial gap junction communication in the body column [90]. Chloretone is reportedly nervous-system specific, but *Hydra* was observed to develop tolerance to the anesthetic within hours of exposure [49]. Thus, existing anesthetics have limitations and there is an urgent need for an alternative that reliably immobilizes *Hydra* without causing tolerance or adverse health effects.

Here, we report on linalool as a novel, safe and fully reversible anesthetic for *Hydra*. Linalool is a monoterpenoid alcohol found in flowers and frequently used in cosmetic products [2]. It has been shown to have anesthetic or sedative activity in mice [54], catfish [39] and flatworms [10]. Linalool exists in two enantiomeric for ms with different pharmacological effects. In humans, the (S)-enantiomer causes an increase in heart rate while the (R)-enantiomer works as a stress relieving agent [41]. In contrast, in catfish the (S)- enantiomer acts as a sedative [39]. Here, we demonstrate that a racemic mixture of linalool enables live imaging of *Hydra*, including the acquisition of fluorescence time-lapse movies and multichannel z-stacks at high magnification. Linalool is fast acting – a 1 mM solution of linalool anesthetizes an animal within 10 min of exposure, with recovery occurring in approximately the same time after removal from the solution. Because anesthesia using linalool is reversible, the same animal can be imaged consecutively over the course of days,

enabling dynamic studies of long-term processes such as head regeneration and budding. Furthermore, linalool facilitates the rapid execution of precise tissue manipulations such as tissue excisions and grafting. Linalool has been reported to be a cytostatic agent in cancer cells *in vitro* [74]; therefore, we also investigated this possibility in *Hydra*. We found no significant effects of prolonged (3-day) continuous linalool exposure on budding rates, mitotic activity, or cell viability. In contrast, 3-day continuous exposure to linalool partially suppressed regeneration in amputated animals, but regeneration could be rescued by removal of the anesthetic. Thus, linalool may also be a useful tool for manipulating regeneration dynamics. In conclusion, we find that linalool outperforms other currently used anesthetics and enables *in vivo* manipulations and live imaging of *Hydra* with precision and ease of use.

4.3 Results and Discussion

4.3.1 Linalool is a fast acting and reversible anesthetic

Intact polyps in *Hydra* Medium (HM) continuously exhibit body shape changes such as contractions, extensions, bending, as well as tentacle movements [37, 45], which complicates *in vivo* manipulations and imaging. In contrast, animals incubated in 1 mM linalool (LL) for 10 min appear relaxed, with tentacles splayed out and the mouth assuming a conical shape (Fig 4.1A).

Figure 4.1: Linalool as an anesthetic. A. Representative images of *Hydra* polyps before (i. extended, ii. contracted) and after (iii) incubation in 1 mM linalool (abbreviated to LL). Scale bar: 200 μm. B. 3 hr incubation in linalool concentrations exceeding 3 mM causes lethality. Each point represents a single technical replicate containing 8–10 animals. C. Box plot showing time of full extension after last observed contraction burst during 65 min incubation in linalool concentrations up to 1 mM. 1mM linalool takes 7.53 min (5.44, 9.03) (median (25^{th} percentile, 75^{th} percentile)) to anesthetize the animals. (*), (**) and (***) indicate statistically significant difference from 0 mM linalool at $p<0.05$, $p<0.01$ and $p<0.001$ respectively (Mann-Whitney U test). Data from 3 technical replicates containing 3–4 animals each for every concentration. Each data point corresponds to one animal. D. Box plot showing time of first observed contraction burst during 120 min recovery in HM following 65 min of anesthesia in linalool. Animals recover in 12.77 min (7.72, 15.13) (median (25^{th} percentile, 75^{th} percentile)) after incubation in 1mM linalool. (*), (**) and (***) indicate statistically significant difference from 0 mM linalool at $p<0.05$, $p<0.01$ and $p<0.001$ respectively (Mann-Whitney U test). Data from 3 technical replicates containing 4 animals each for every concentration. Each data point corresponds to one animal. E. Pinch response. i. *Hydra* polyp in HM. ii. Polyp in HM shows a global body column contraction in response to pinching. iii. *Hydra* polyp incubated in 1 mM linalool for 10 min. iv. Anesthetized polyp shows only local swelling after pinch, indicated by black arrowhead. Images representative of $n = 5$ animals per replicate in 2 technical replicates. F. 30 min feeding response in 4-day starved polyp. i. *Hydra* polyps in HM readily capture and ingest *Artemia* (brine shrimp), with multiple *Artemia* clearly visible within the body column of each animal. ii. *Hydra* polyps incubated in linalool for 10 min prior to introduction of *Artemia* have a strongly reduced reaction, and only rarely ingest *Artemia*. White arrowheads indicate *Artemia* inside polyps. Several animals have not ingested prey at all, and those that have contain a maximum of one *Artemia* each. Scale bars for E, F: 1 mm.

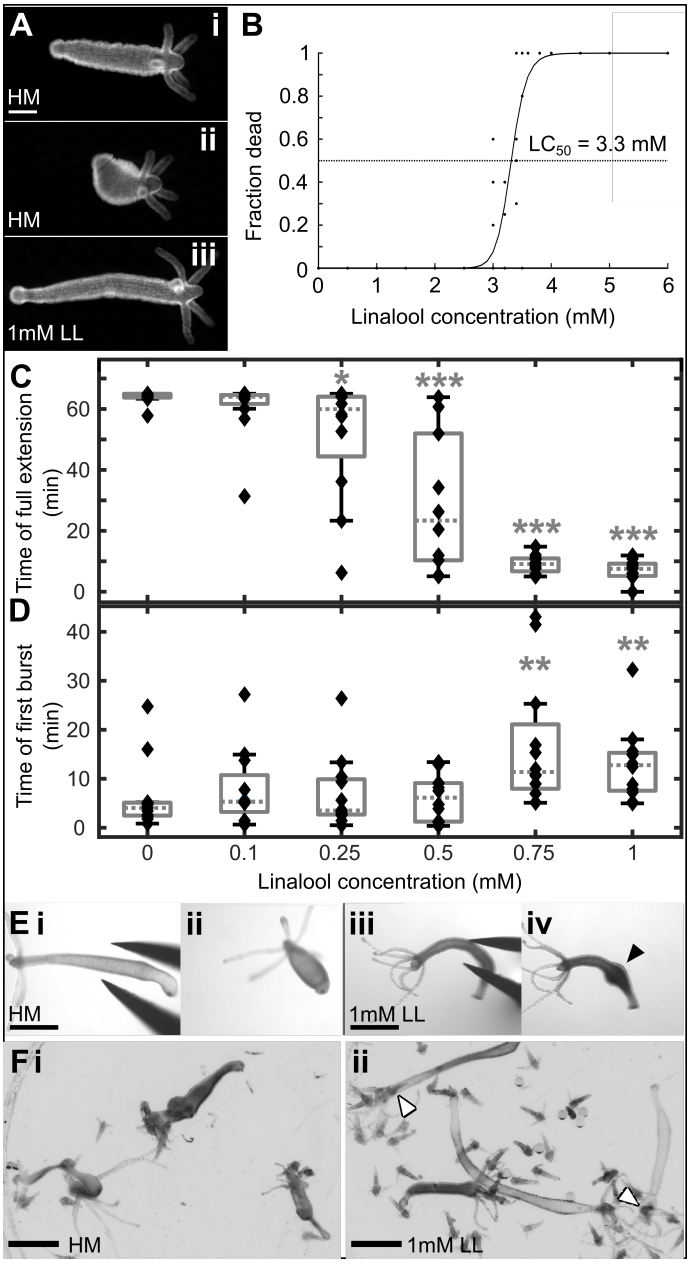
A
i
HM
ii
HM
iii
1mM LL
B
Fraction dead
LC50 = 3.3 mM
Linalool concentration (mM)
C
Time of full extension (min)
D
Time of first burst (min)
Linalool concentration (mM)
E i
HM
ii
iii
1mM LL
iv
F i
HM
ii
1mM LL

We investigated the effect of various linalool concentrations on animal health within 3 hours of incubation (Fig 4.1B) and found that concentrations $\geq$ 2 mM caused negative health effects on the animals, such as an abnormal body shape, contracted tentacles, and partial disintegration (S1 Fig). Death was observed at concentrations of 3 mM and beyond, following the 3 h exposure. We determined the LC_{50} to be 3.31 mM (95% confidence interval 3.27 mM to 3.36 mM) using the same approach as in [36]. We then empirically determined the optimal working concentration for linalool by measuring and comparing induction and recovery times for different sublethal concentrations.

No negative health effects were observed at or below 1mM linalool. Induction time of anesthesia decreased with increasing concentration of linalool to about 10 min at 1mM (Fig 4.1C), while recovery time remained between 10–20 min for all concentrations tested (Fig 4.1D). After a 1 h incubation in 1 mM linalool, polyps regained their spontaneous contractions in about 13.0 (8.8, 17.2) min (mean (95% confidence interval), n = 12 across 3 technical replicates) (Fig 4.1D). Therefore, we determined that the highest tolerated dose, 1 mM, was the best concentration to use in experiments.

Polyps incubated in 1 mM linalool for 10 min no longer exhibit the "pinch response", a global longitudinal contraction that is observed upon gently squeezing the body column of a polyp in HM with forceps (Fig 4.1Ei and Fig 4.1Eii, S1 Movie). Polyps in 1 mM linalool swelled at the site of pinching but did not contract globally (Fig 4.1Eiii and Fig 4.1Eiv). However, upon being returned to HM, the polyps regained their response to pinching within 5 min (n = 18, across 3 replicates, Fig 4.S2A). Taken together, these results demonstrate that linalool prevents both spontaneous and mechanically induced contractions in *Hydra*.

Mechanically induced body column contractions are known to be mediated by the

ectodermal epithelial layer, and epithelial (nerve-free) animals in HM retain their pinch response despite lacking spontaneous contraction behaviors [90]. Therefore, to determine whether linalool affected epithelial cells directly, we tested whether nerve-free *Hydra* exhibited a pinch response in linalool. As was the case for enervated polyps, nerve-free animals lost their pinch response in linalool (S2 Movie). The loss of both spontaneous and mechanically induced contractions, in both enervated (Fig 4.1Eiii and Fig 4.1Eiv) and nerve free animals (S2 Movie) upon treatment with linalool suggests that linalool affects both the neuronal and epithelial cells.

However, 1 mM linalool does not completely paralyze the animal—we observed that some anesthetized individuals were able to capture and ingest *Artemia* (brine shrimp), although very inefficiently compared to controls (Fig 4.1F). We quantified the feeding response by adapting the protocol by [62]. While we found *Artemia* readily stuck to the tentacles of most animals, only 2 out of 9 animals in 1 mM linalool ingested 1 *Artemia* each in 30 min, whereas the median number of *Artemia* ingested by each animal incubated in HM was significantly higher ($p = 0.00028$, Mann-Whitney U test) with 13 (11, 16; 25^{th} percentile, 75^{th} percentile) for $n = 9$ polyps across 2 technical replicates. (Fig 4.S2D).

The effect of linalool treatment on mechanically induced contraction and the ability to feed was rapidly reversed by moving the polyps back into HM. Following a 10 min incubation in 1 mM linalool, polyps regained the mechanically induced pinch response within 5 min of return to HM ($n = 18$ across 3 technical replicates; Fig 4.S2A). The ability to capture and ingest *Artemia* was restored within 15 min of HM incubation following a 10–15 min incubation in 1 mM linalool, as quantified by the fraction of polyps that were able to capture and ingest *Artemia* at different time points after the linalool incubation (Fig 4.S2C).

4.3.2 1 mM linalool enables precise tissue manipulations

Recent studies have shown that the regeneration outcome in *Hydra* could be influenced by the geometry of tissue pieces excised from the body column [55]. Making precise cuts is also useful for manual sections of the body column for use in immunohistochemistry and histology. To test whether linalool allowed for improved precision of cuts and thus would be a useful tool for such studies, we compared the excision of tissue rings from animals incubated in HM with those incubated in 1 mM linalool. When sectioning animals to obtain pieces of body column tissue, the application of linalool did not drastically improve the average thickness of the sections (Fig 4.2Av), but significantly reduced the time required to section the animals from 99 ± 45 s (mean ± standard deviation (SD), n = 13 across 3 technical replicates) per animal in HM to 40 ± 9 s (mean ± SD, n = 16 across 5 technical replicates) per animal in 1 mM linalool (p = 0.00002, 2-tailed t-test) (Fig 4.2Aiv). The reductions in variability and in average time are due to the suppression of the animal's natural contractile response to touch, removing the need to wait for the polyp to extend following each cut.

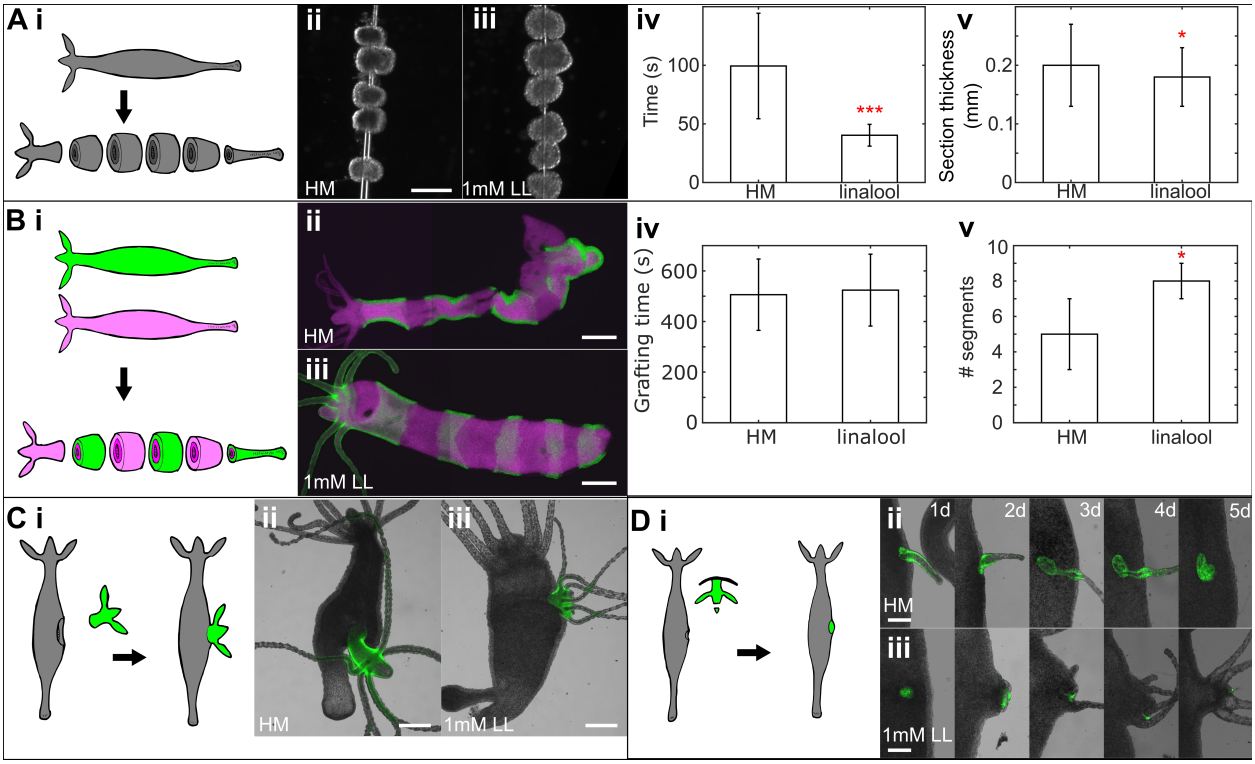

Figure 4.2: Linalool improves outcomes of surgical manipulations in *Hydra*. A. Sectioning of body column. i. Experimental schematic. ii. Sections cut in HM. iii. Sections cut in linalool. Scale bar: 400 μm iv. Time required to section a polyp in Hydra medium (HM) (90 $\pm$ 45 s (mean $\pm$ SD), n = 13, across 3 technical replicates) and in 1 mM linalool (40 $\pm$ 9 s, n = 16, across 5 technical replicates). v. Thickness of body column sections cut in HM (0.20 $\pm$ 0.07 mm (mean $\pm$ SD), n = 66 sections, 15 polyps across 4 technical replicates) and in 1mM linalool (0.18 $\pm$ 0.05 mm, n = 99 sections, 19 polyps across 6 technical replicates). Error bars represent SDs. (*), (**) and (***) indicate statistical significance at $p < 0.05$, $p < 0.01$ and $p < 0.001$ respectively, calculated using a 2 tailed t-test. B. "Zebra grafting". i. Experimental schematic. ii. Representative animal grafted and healed in HM. iii. Representative animal grafted and healed in linalool. Scale bars: 400 μm. All grafts are shown in S3 Fig. iv. Time taken to assemble grafts in HM (506 $\pm$ 141 s (mean $\pm$ SD)) and in 1 mM linalool (524 $\pm$ 142) (n = 8, across 2 technical replicates each for HM and 1 mM linalool). v. Number of segments in completed graft in HM (5 $\pm$ 2 (mean $\pm$ SD)) and in 1 mM linalool (8 $\pm$ 1) (n = 8, across 2 technical replicates each for HM and 1 mM linalool). Error bars represent SDs. (*) indicates statistically significant difference from grafts in HM at $p < 0.05$ (2-tailed t-test). C. Head transplantation into gastric region. i. Experimental schematic. ii. Representative animal grafted and healed in HM. iii. Representative animal grafted and healed in 1mM linalool. Scale bars: 400 μm. D. Head organizer transplantation into gastric region. i. Experimental schematic. ii. Animal grafted in HM imaged daily over 5 days. iii. Animal grafted in 1 mM linalool imaged daily over 5 days. Scale bars: 200 μm. Linalool did not improve hypostome cutting times, which were 60 s (50, 69) (median, (25^{th} quartile, 75^{th} quartile), measured for n = 17 grafts) in HM and 50 s, (38, 66) (n = 17) in linalool, but slightly improved success of the induction of ectopic axes (6/25 in HM versus 11/25 in linalool) and significantly shortened grafting time to 134 s (104, 209) (n = 17) compared to 196 s (147, 258) (n = 17) in HM.

The improvements possible using linalool become more readily apparent in grafting experiments. A "zebra graft" to create a chimeric animal consisting of bands of differently labeled tissue produced a significantly better result when linalool was employed (Fig 4.2B). While the time to assemble the grafts was comparable with or without linalool treatment (Fig 4.2Biv), the average number of segments per graft was significantly higher ($p = 0.03$, 2-tailed t-test) for grafts in linalool (8 ± 1 segments per graft, $n = 8$ grafts) than those made in HM (5 ± 2 segments per graft, $n = 8$ grafts; Fig 4.2Bv). This difference is due to a combination of two effects. First, the animals do not move in linalool and second, they are extended. Thus, they are more quickly and easily cut into smaller segments, which are in turn easier to thread onto a needle. Morphology of grafts made in HM was also more frequently abnormal compared to those made in linalool (Fig 4.S3). The observed morphological abnormalities are likely due to tissue movement during healing, causing the cut edges of the pieces to become misaligned while on the needle, thus preventing the segments from healing smoothly together as described previously [80]. A similar effect was observed when grafting heads onto body columns ($n = 3$ per condition), following the procedure described in [71]. Linalool allowed more precise decapitation of the donor animal, reducing the amount of extraneous body column tissue, and guaranteed better positioning of the graft on the recipient animal. Grafts carried out in HM tend to have the donor head protruding at an angle, again due to misalignment of the cut surfaces during healing (Fig 4.2C).

Finally, linalool is beneficial in hypostome grafts, carried out as previously described [88]. We conducted 25 hypostome grafts each in HM and in 1 mM linalool and scored at 4 days after grafting for retention of donor tissue and for formation of an ectopic body axis from recipient tissue with donor tissue limited to a small part of the new head (Fig 4.2Diii),

as in [13, 88]. Grafts that retained donor tissue but failed to induce an axis fell into several broad categories: donor tissue that either failed to form any structure or induced only a tentacle before being resorbed (Fig 4.2Dii), or donor tissue that formed the entirety of an ectopic head with no host tissue involvement (Fig 4.S4). We found a slight but statistically non-significant improvement in the number of grafts that induce an ectopic axis when linalool is used (6/25 in HM vs. 11/25 in linalool). For two technical replicates containing n = 16 grafts per condition, we individually recorded the time taken to excise the donor hypostome and to conduct the graft. Linalool did not significantly improve the time required to cut hypostomes ($p = 0.1221$, Mann-Whitney U test), but grafting times were significantly shorter ($p = 0.0226$, Mann-Whitney U test) in linalool, with 134 s (104, 209; median, (25^{th} quartile, 75^{th} quartile)), compared to in HM with 196 s (147, 258).

4.3.3 Incubation in 1 mM linalool enables high quality short-term fluorescence imaging

To test whether the immobilization in 1 mM linalool was sufficient to allow for *in vivo* fluorescence imaging, we imaged animals incubated in 1mM linalool under various conditions and compared the results to those obtained from imaging animals in HM.

First, we used single channel fluorescence imaging using polyps expressing GCaMP6s in the interstitial cell lineage [26], because this transgenic line allows for the visualization of individual neurons and subcellular processes such as dendrites. We imaged unconstrained animals at low magnification (Fig 4.3A, S3 Movie). Unconstrained animals in HM moved significantly during the 10 s acquisition, as shown by a maximum intensity projection of

the time series (Fig 4.3Aii). In contrast, polyps incubated in 1 mM linalool for at least 10 min only exhibited drift (Fig 4.3Aiv and 4.3Av), which can be corrected for with standard post-processing methods (Fig 4.3Avi), whereas these methods do not correct for the motion observed in the control, because the animal exhibits non-linear body shape changes (Fig 4.3Aiii).

Figure 4.3: Single channel live imaging in linalool. A. Unconstrained GCaMP6s Hydra imaged at low magnification. i. single image in HM. ii. Maximum intensity t-projection of a 10 s video in HM. iii. Rigid body correction of HM video projection. iv. Single image in 1 mM linalool. v. Maximum intensity t-projection of 10 s video in linalool. vi. Rigid body correction of linalool video projection. Scale bars: 200 μm. B. Single slice from a 7.5 μm thick z-stack of a GCaMP6s animal imaged at 60x magnification with a resolution of 0.25 μm along the z-axis at a 500 ms exposure per slice using blue excitation in (i) HM and (ii) 1 mM linalool. C. Maximum intensity projection of high magnification z-stacks in (i) HM and (ii) 1 mM linalool. Scale bars: 10 μm. D. Coefficient of variation for (i) low magnification imaging in HM (0.175 $\pm$ 0.025 (mean $\pm$ SD)) and linalool (0.143 $\pm$ 0.008) calculated from n = 10 polyps across 2 technical replicates (ii) high magnification imaging in HM (0.188 $\pm$ 0.042 (mean $\pm$ SD)) and linalool (0.121 $\pm$ 0.026) calculated from n = 6 polyps across 2 technical replicates. Error bars represent SDs. (**) indicates statistically significant difference at $p < 0.01$ as determined by a 2 tailed t-test.

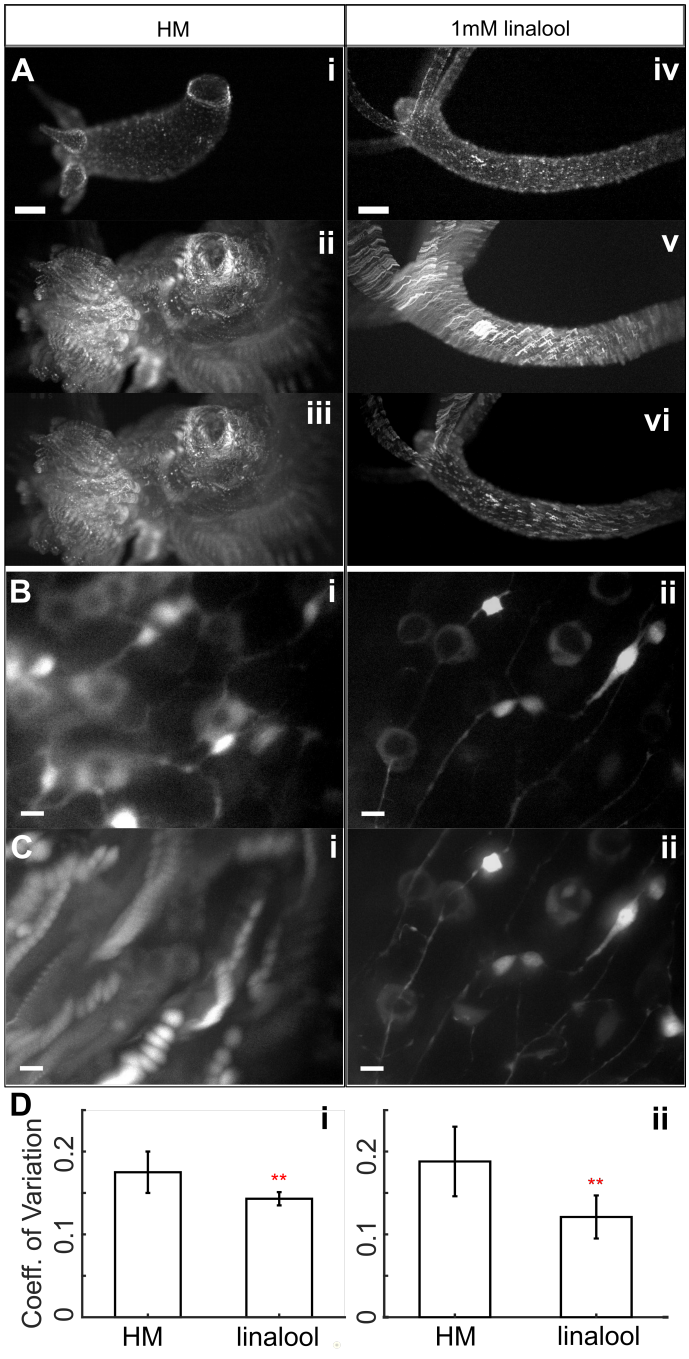
HM
1mM linalool
A
i
ii
iii
iv
v
vi
B
i
ii
C
i
ii
D
i
ii
Coeff. of Variation
0
0.1
0.2
HM
linalool
**

We also acquired 7.5 μm thick z-stacks of the body columns of intact polyps mounted in tunnel slides [18] at high magnification (Fig 4.3B and 4.3C). The image quality of individual slices was better when imaging anesthetized animals (Fig 4.3B), but the difference in stability and thus image quality becomes most evident when comparing maximum intensity projections of the entire z-stack (Fig 4.3C). The animals in linalool were sufficiently still to allow the resolution of subcellular features such as neuronal processes, whereas the animals in HM moved too much, making z-stacks impractical (Fig 4.3C and S4 Movie). As the tissue stretched and compressed anisotropically during those movements, it was not possible to correct this motion through post-processing. We quantified the motion under these two imaging conditions (HM, 1 mM linalool) using the coefficient of variation (see Methods). As expected from the images (Fig 4.3), the coefficient of variation was significantly higher for image sequences acquired in HM than for those acquired in 1 mM linalool (Table 4.S1, Fig 4.3D).

Next, we tested the performance of 10 min incubation in 1 mM linalool for the acquisition of multi-channel z-stacks at low (10x) and high magnification (60x). Control videos in HM were not attempted due to the unsatisfactory results obtained in single channel imaging as described in the preceding paragraphs (Fig 4.3). By exposing animals to 1 mM linalool in the presence of 2 mM reduced glutathione, we were able to induce mouth opening (Fig 4.4A). The animal is sufficiently still to allow for simultaneous visualization of nuclei positions and cell boundaries using different excitation wavelengths at 10x magnification. We also took 3-channel time-lapse movies of heads exposed to reduced glutathione below the activation threshold for opening to illustrate the overall stability that can be achieved using linalool, allowing for co-localization studies of dynamic processes (S5 Movie).

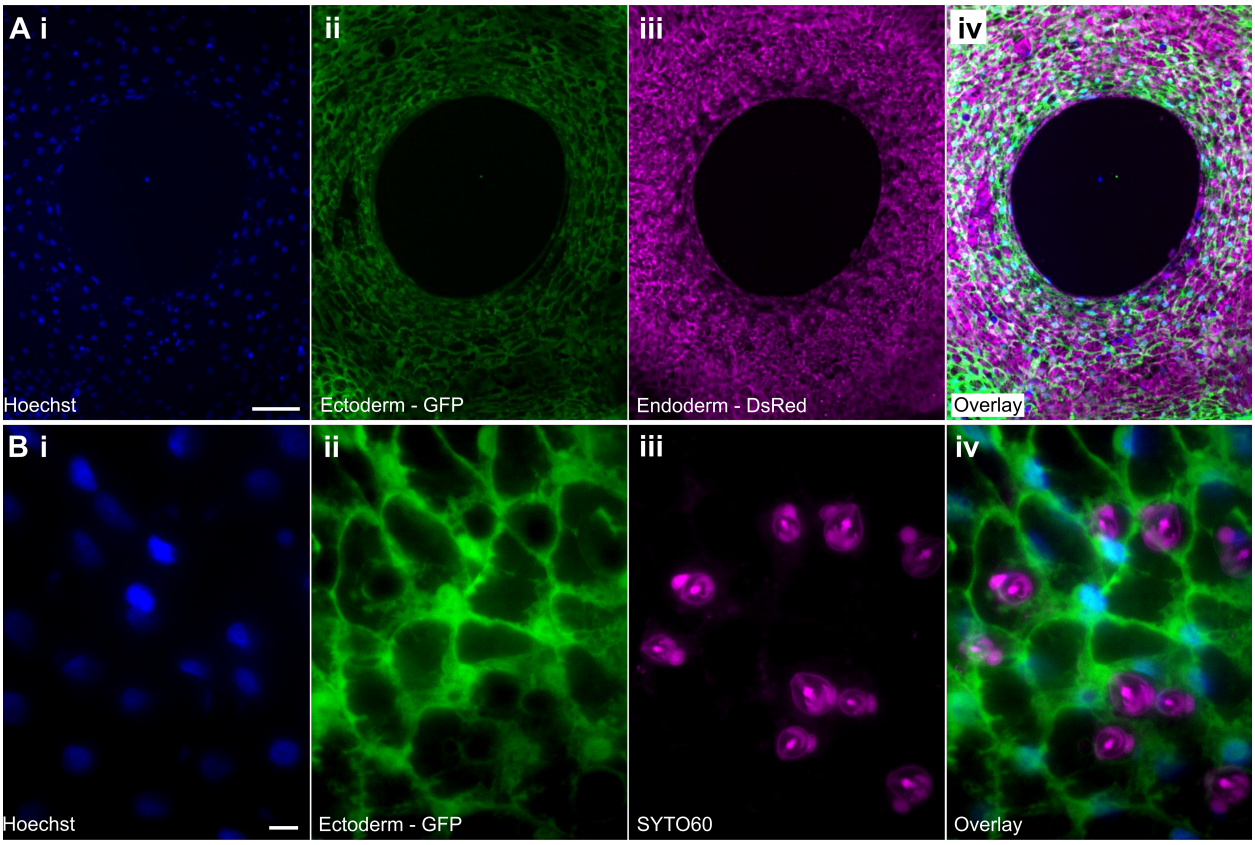

Figure 4.4: Linalool enables high resolution imaging in multiple channels. A. Low magnification maximum intensity projection of a z-stack acquired of an open Hydra mouth in 1mM linalool using i. Hoechst 33342, ii. Ectoderm—GFP, iii. Endoderm–DsRed2, iv. overlay. 5 μm slice thickness, 6 slices total. Scale bar: 100 μm. B. High magnification maximum intensity projection of a z-stack of the body column tissue acquired in 1mM linalool using i. Hoechst 33342, ii. Ectoderm–GFP, iii. Nematocysts–SYTO 60, iv. overlay. 0.25 μm z-step, 17 slices total. Scale bar: 10 μm. The reduced animal motion allows for acquisition of multiple z-slices in 3 channels.

Furthermore, we used mouth opening to test if calcium imaging was possible in linalool-treated animals. Epithelial GCaMP animals [88] incubated in 1 mM linalool for 10 min opened their mouth in response to 2 mM reduced glutathione and calcium waves could be observed (S6 Movie). We also observed local calcium signaling in the body column in response to pinching with tweezers (S8 Movie). Together, these data demonstrate that linalool does not interfere with epithelial calcium signaling and that behaviors that are not suppressed by linalool can be studied using GCaMP animals.

Finally, we tested whether animals were sufficiently immobile to obtain high quality z-stacks at high magnification (60x) in multiple channels (UV, blue, and green excitation; Fig 4.4B). Notably, when testing live dyes for this purpose, we found that the SYTO 60 red fluorescent nucleic acid stain is specific to nematocysts of all types in Hydra (Fig 4.4Biii), determined by comparing morphology of stained structures to previous descriptions of nematocyst types [28]. Thus, SYTO 60 is a useful tool for studying nematocysts *in vivo*.

While motion was not completely suppressed in 1 mM linalool and extended exposure to short wavelength light caused the animal to escape the field of view, it was nevertheless possible to achieve high quality multichannel imaging (Fig 4.4B). Thus, linalool is a useful tool for *in vivo* co-localization studies at high magnification, which are impossible to perform in HM.

4.3.4 Linalool allows for repeated short-term fluorescence imaging

A major strength of linalool as a reversible anesthetic is the ability to repeatedly anesthetize and image the same animal over the course of days, thus allowing the acquisition

of dynamic data of cellular processes in a single animal. To illustrate this capability, we decapitated transgenic HyBra2 promoter::GFP animals and allowed them to regenerate in HM. We imaged head regeneration over the course of 2 days, using repeated short-term 15 min incubations in 1 mM linalool to acquire a total of 11 high resolution images of the same animal (Fig 4.5A). When not being imaged, the regenerating animals were returned to HM. In this way we were able to observe the development of the hypostome and tentacles and also observe a gradual increase in GFP signal beginning at 24 h. The same technique of repeated linalool exposure was used to image the tissue grafts in Fig 4.2.

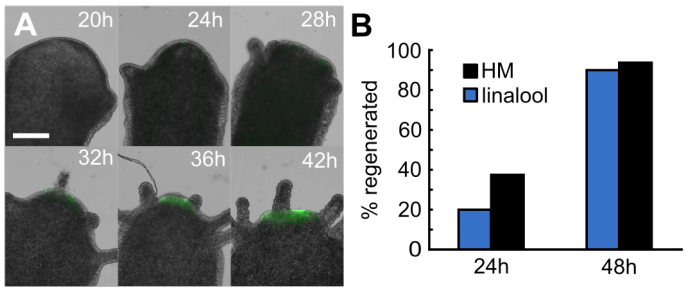

Figure 4.5: Linalool enables repeated high-resolution imaging. A. Head regeneration in a transgenic HyBra2 promoter::GFP polyp imaged at high resolution every 4 h from 12 h to 48 h. Subset of images shown. Scale bar: 0.5 mm B. Repeated anesthesia and recovery do not impact regeneration speed or outcome (n = 10 animals HM, n = 16 animals linalool, 3 technical replicates). Differences between conditions not statistically significant at p = 0.05 level (Fisher's Exact test).

We also confirmed that the timing and outcome of head regeneration in animals repeatedly anesthetized for imaging did not significantly differ from that observed in untreated controls (Fig 4.5B). Thus, linalool is a valuable tool for repeated live imaging applications, which will be useful to study long term processes, such as regeneration and budding.

4.3.5 Long-term effects of linalool

Due to the reported cytostatic effect of linalool on cancer cells in culture [74], we investigated whether linalool has similar effects in *Hydra*. The cell cycle lengths in interstitial and epithelial cells are approximately 1 [16] and 3 days [22], respectively. Therefore, we continuously incubated intact polyps for 3 days in 1 mM linalool, exchanging the solution every 24 hours to account for volatility. We did not observe significant changes in the mitotic index (Fig 4.6A) nor in the rate of cell death (Fig 4.6B) in the body column of intact polyps. Furthermore, budding seemed to occur normally, as verified using 3-day continuous time-lapse imaging (Fig 4.6C, Fig 4.S5).

Figure 4.6: Effect of long-term continuous linalool exposure. A. 3-day incubation in 1 mM linalool does not impact rate of cell division. Slices stained with DRAQ5 (nuclei) and anti-PH3 (phospho-histone H3, dividing cells). i. Representative image of body column sections from polyps incubated 3 days in HM. ii. Representative slice from polyps incubated 3 days in 1 mM linalool. iii. Percentage of dividing cells in animals incubated 3 d in HM or 1mM linalool. Mean ± SD: HM = 1.3 ± 0.6, linalool = 1.6 ± 0.8. n = 18 across 5 technical replicates. Difference not statistically significant at $p < 0.05$ (2-tailed t-test). Error bars represent SD. Scale bar: 100 μm. B. 3-day incubation in 1 mM linalool does not damage or kill cells. Representative images of polyps stained with propidium iodide after incubating for i. 3 days in HM, ii. 24 h in 0.04% colchicine, and iii. 3 days in 1 mM linalool. iv. Mean number of dead cells per animal after incubation in HM (5 ± 4, n = 38), in colchicine (31 ± 21, n = 28) and linalool (4 ± 3, n = 39). Error bars represent SD. (***) indicates statistically significant difference from linalool at $p < 0.001$ (2-tailed t-test). Scale bar: 100 μm. C. Long term incubation in linalool does not impact budding. Representative images of a budding polyp continuously incubated and imaged in 1 mM linalool. Scale bar: 500 μm. D. Long term incubation in linalool prevents head regeneration. Error bars represent SD (0 mM n = 17, 0.1 mM n = 20, 0.5 mM n = 40, 0.75 mM n = 19, 1 mM n = 19; 3 technical replicates). (*), (**) and (***) indicate statistically significant difference from 0 mM at $p < 0.05$, $p < 0.01$ and $p < 0.001$ respectively (Fisher's Exact Test). E. Recovery in HM rescues the head regeneration defect. i. Polyp incubated in HM for 68 h after decapitation. ii. Polyp incubated in 1 mM linalool for 68 h after decapitation. iii. Decapitated polyp recovered for 28 h after 3 d in 1mM linalool, iv. Polyps recovered for 3 d after 3 d in 1mM linalool. Scale bar: 1 mm. v. Head regeneration is suppressed by incubation for 3 d in 1 mM linalool. Only 14/42 polyps incubated in 1 mM linalool regenerated at least one tentacle at the end of 3 d incubation compared to 40/42 polyps in HM (across 4 technical replicates). (***) denotes that the difference is statistically significant at $p < 0.001$ (Fisher's Exact test) when comparing overall numbers. vi. Head regeneration is rescued in linalool- incubated animals after 3 d recovery in HM. 35/36 polyps incubated in 1 mM linalool regenerated heads at the end of 3 d recovery compared to 36/36 polyps in HM, across 4 technical replicates. The difference is not statistically significant at $p < 0.05$ (Fisher's Exact test) when comparing overall numbers.

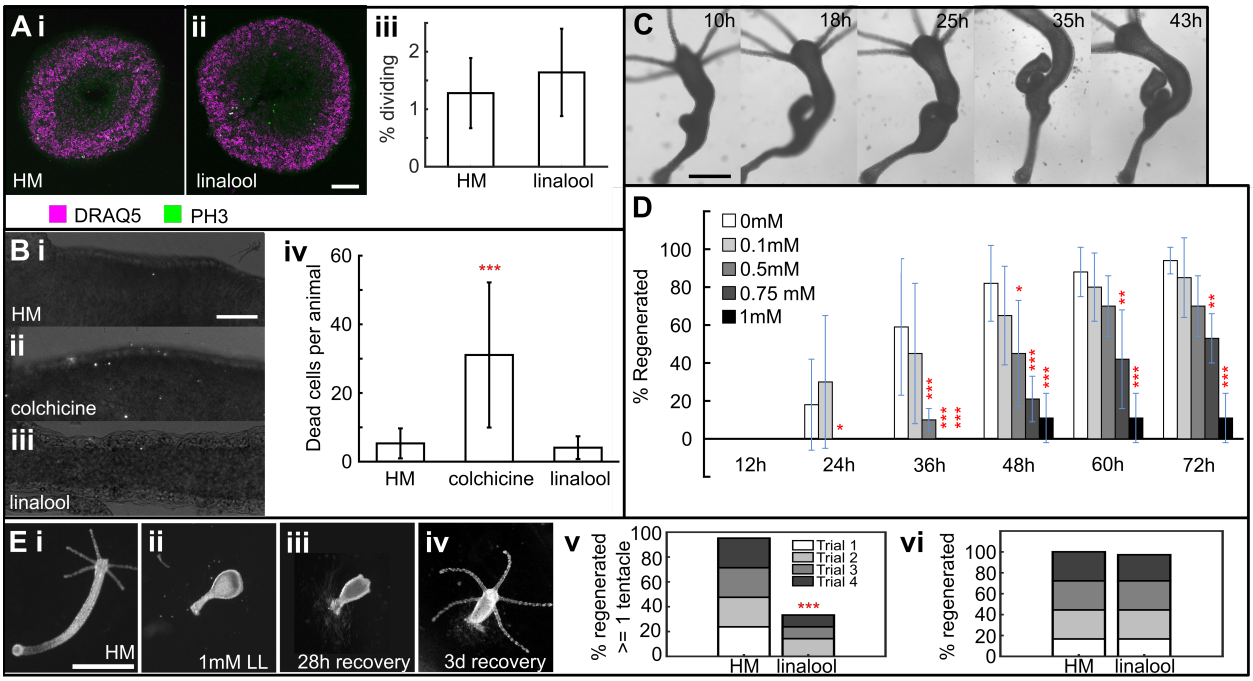
A i
ii
iii
HM
linalool
DRAQ5
PH3
% dividing
HM
linalool
C
10h
18h
25h
35h
43h
B i
HM
ii
colchicine
iii
linalool
iv
Dead cells per animal
HM
colchicine
linalool
D
0mM
0.1mM
0.5mM
0.75 mM
1mM
% Regenerated
12h
24h
36h
48h
60h
72h
E i
HM
ii
1mM LL
iii
28h recovery
iv
3d recovery
v
% regenerated >= 1 tentacle
Trial 1
Trial 2
Trial 3
Trial 4
HM
linalool
vi
% regenerated
HM
linalool

Based on these results, we attempted to image head regeneration using continuous incubation in 1 mM linalool. Continuous incubation would be advantageous compared to consecutive mounting and imaging sessions as it would minimize interaction with the sample and could be fully automated. We found that decapitated Hydra experienced a significant delay in head regeneration when continuously exposed to 1 mM linalool over the course of 3 days. Anesthetized body columns were observed to shed cells and assume a lollipop shape (Fig 4.6Ei and 4.6Eii), and a few animals disintegrated completely. A third of the animals (14/42 across 4 technical replicates) were less affected and showed 1–2 small tentacle buds at the end of 3 days (Fig 4.S6). If removed from linalool after 3 d, however, the remaining two thirds of the animals, which showed no visible signs of regeneration, recovered. Tentacle buds were observed as early as 1 d into recovery and all polyps had fully regenerated their heads after 3d of recovery (Fig 4.6E). Foot regeneration was similarly suppressed in 3-day continuous 1 mM linalool exposure and was also rescued after the animals were moved into HM (Fig 4.S7). This suggests that the effects of linalool on regeneration are not specific to the head.

The observed head regeneration delay in continuous linalool exposure was observed for concentrations as low as 0.5 mM for up to 48 h (Fig 4.6D), and at 0.75 mM, 50% of the animals did not regenerate heads within 3 days. However, since even 1 mM linalool was ineffective in sufficiently immobilizing animals to allow for long-term imaging with cellular resolution (S7 Movie), these lower concentrations are not viable alternatives.

Finally, we tested whether the inhibition of regeneration is caused by an effect on the nervous system, as it had previously been suggested that the nervous system plays a role in head regeneration [63]. To this end, we generated nerve-free animals as described in

Methods and assayed head regeneration in 1 mM linalool. Surprisingly, nerve-free animals in 1 mM linalool regenerated similarly to nerve-free animals maintained in HM. After 4 days of regeneration, 7/10 animals in HM and 4/10 in linalool showed tentacle buds across two technical replicates. By 5 days this had increased to 9/10 in HM and 6/10 in linalool (Fig 4.S8). There were no statistically significant differences in the fraction of head regenerates for both days ($p = 0.36$ for day 4 and $p = 0.30$ for day 5, Fisher's Exact test). Furthermore, nerve-free animals in linalool did not assume the lollipop shape (Fig 4.6Eii) that we observed in enervated polyps. Together, these data suggest that linalool disrupts regeneration by perturbing the function of either neurons or other cells in the interstitial lineage.

4.3.6 Comparison of linalool to other commonly used anesthetics in *Hydra* research

Whenever one introduces a new tool, it is important to compare performance with existing methods and demonstrate that the advantages of the new tool are sufficient to make its adoption worthwhile. While anesthetics were and continue to be most frequently used to relax Hydra prior to fixation for histological and immunohistochemistry studies [5, 64, 15, 38], the advent of modern molecular tools have brought with it an increased use for *in vivo* applications [89, 3, 56]. Table 4.1 provides an overview of the various anesthetics that have been reported in the literature for use in *Hydra* and examples of their respective applications.

Table 4.1: Summary of various anesthetics used to relax *Hydra*. This table is not a comprehensive summary of all *Hydra* studies that have employed anesthetics but provides an overview of examples spanning different chemicals and applications. To the best of our knowledge such a direct comparison has not previously been attempted and is thus a useful resource for the field.

Chemical	Working concentration	Application	Treatment duration	Health effects	References
Urethane	2% w/v	Determination of mechanism of urethane's action		Hyperextension; potential reversal; structural damage	[58]
	1-3% w/v	Relaxation prior to fixation	2-20 min	None reported	[5, 64] [38, 82]
	2% w/v	Fluorescence microscopy	Not reported	None reported	[89]
	$5*10^{-2}$M	Inhibition of feeding reaction	Not reported	None reported	[57]
Chlorobutanol (chloretone)	0.1-0.33% w/v in bath	Reactions to chloretone exposure on 3 *Hydra* species	several hours	No apparent damage at low concentrations; habituation	[49]
	$3*10^{-3}$M	Inhibition of feeding reaction	Not reported	None reported	[57]
	0.1% w/v	Fluorescence imaging	Not reported	None reported	[3, 56]
1-Heptanol	3mM	RNA interference	10 min at 4°C	None reported	[85]
	1% v/v	Fluorescence microscopy	Not reported	None reported	[73]
Magnesium chloride	2.5% w/v	Inhibition of feeding reaction	5 min	Extensive damage with exposure > 1 hr	[18]
Menthol	Not reported	Relaxation prior to fixation	Not reported	None reported	[43, 42]
	Not reported	Inhibition of feeding reaction	Not reported	Disintegration	[18]
MS-222	0.1%	Inhibition of feeding reaction	Not reported	None reported	[57]

Based on our literature search, the most prominent *in vivo* application of the anesthetics was fluorescence imaging using urethane, heptanol, or chloretone. We therefore compared linalool to these anesthetics. To this end we studied whether there were any differences in morphology when *Hydra* polyps are exposed to the different substances. Although we observed variability among individual polyps exposed to the same anesthetic at a fixed concentration, both in terms of morphology and in terms of immobilization speed and strength, polyps assumed characteristic shapes upon exposure to the different chemicals (Fig 4.7A). Following a 15 min exposure, *Hydra* polyps incubated in 1 mM linalool appear relaxed with tentacles splayed outwards and had cone-shaped hypostomes (Fig 4.7Ai). This morphology does not change significantly by 60 min. Animals incubated in 0.04% heptanol appear less extended at 15 min, with contracted conical tentacles. At 60 min the body columns are contracted, and the stubby tentacles persist (Fig 4.7Aii). Exposure to 2% urethane causes animals to extend and become very thin at 15 min, though they become swollen while remaining extended by 60 min (Fig 4.7Aiii). 0.1% chloretone causes initial extension without the thinness seen in urethane, followed by the formation of swellings along the body column by 15 min and contraction of both body and tentacles by 60 min (Fig 4.7Aiv). To quantify these differences, we calculated average body length of individual animals after 10 min incubation in anesthetic as a percentage of their average length prior to anesthesia (see Methods and Fig 4.8).

We found that linalool, heptanol and urethane produced similar anesthetized lengths at 10min, while chloretone showed a statistically significant increase in length at the 5% level and some hyperextended animals (Fig 4.8A and 4.8D). Because this length measure does not account for the other morphological characteristics described above (e.g. the contracted

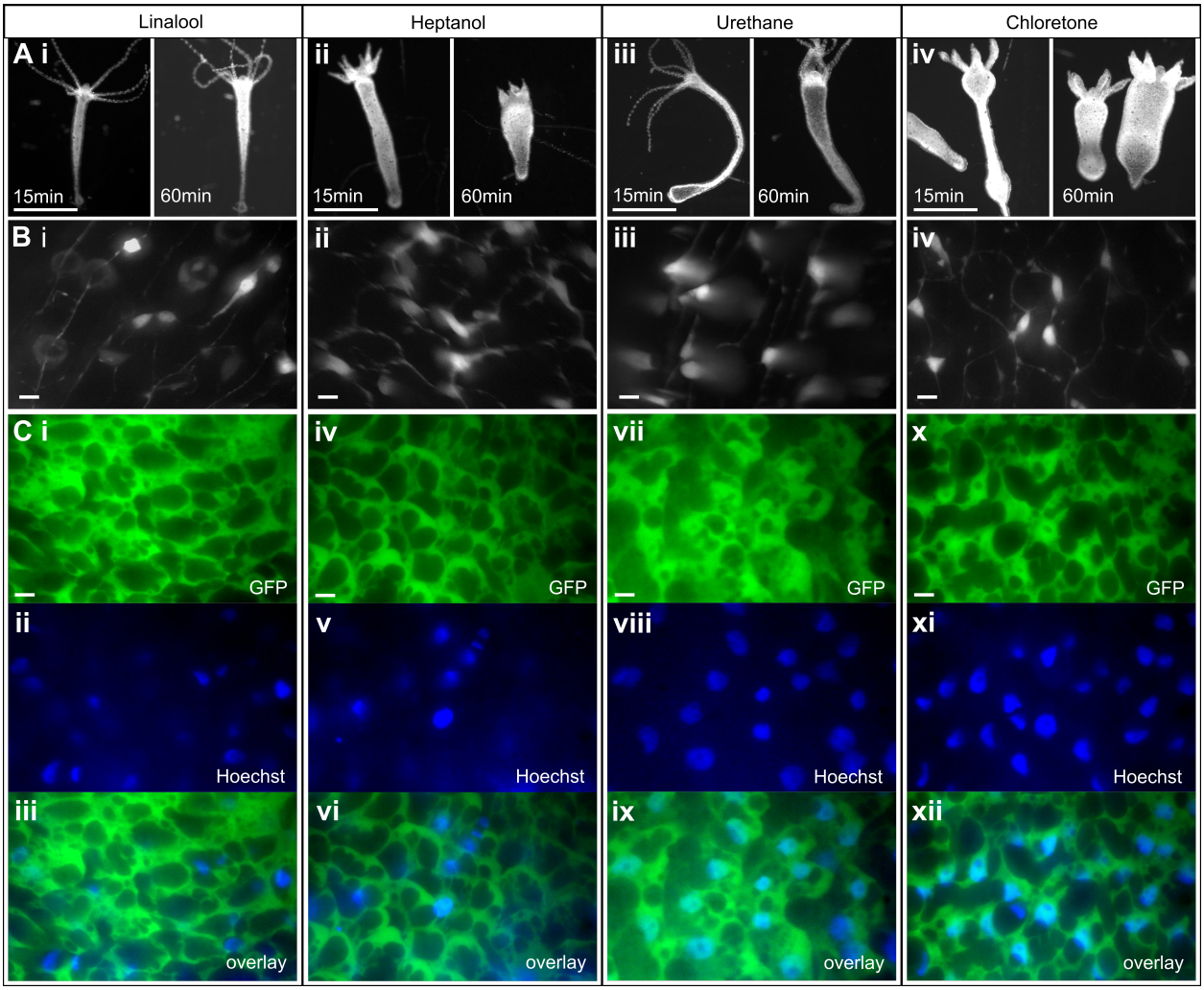

Figure 4.7: Comparison of various *Hydra* anesthetics. A. Comparisons of the same animal after 15 min and 60 min of anesthetic exposure. i. 1 mM linalool, ii. 0.04% heptanol, iii. 2% urethane, iv. 0.1% chloretone. Scale bars: 1 mm. B. Maximum intensity projections of GCaMP6s animals at 60x magnification in each anesthetic. Scale bars: 10 μm. C. Maximum intensity projections of two-channel images of watermelon animals stained with Hoechst nuclear dye at 60x magnification. GFP channel, DAPI channel, and merge (overlay) shown for each anesthetic. Scale bars: 10 μm.

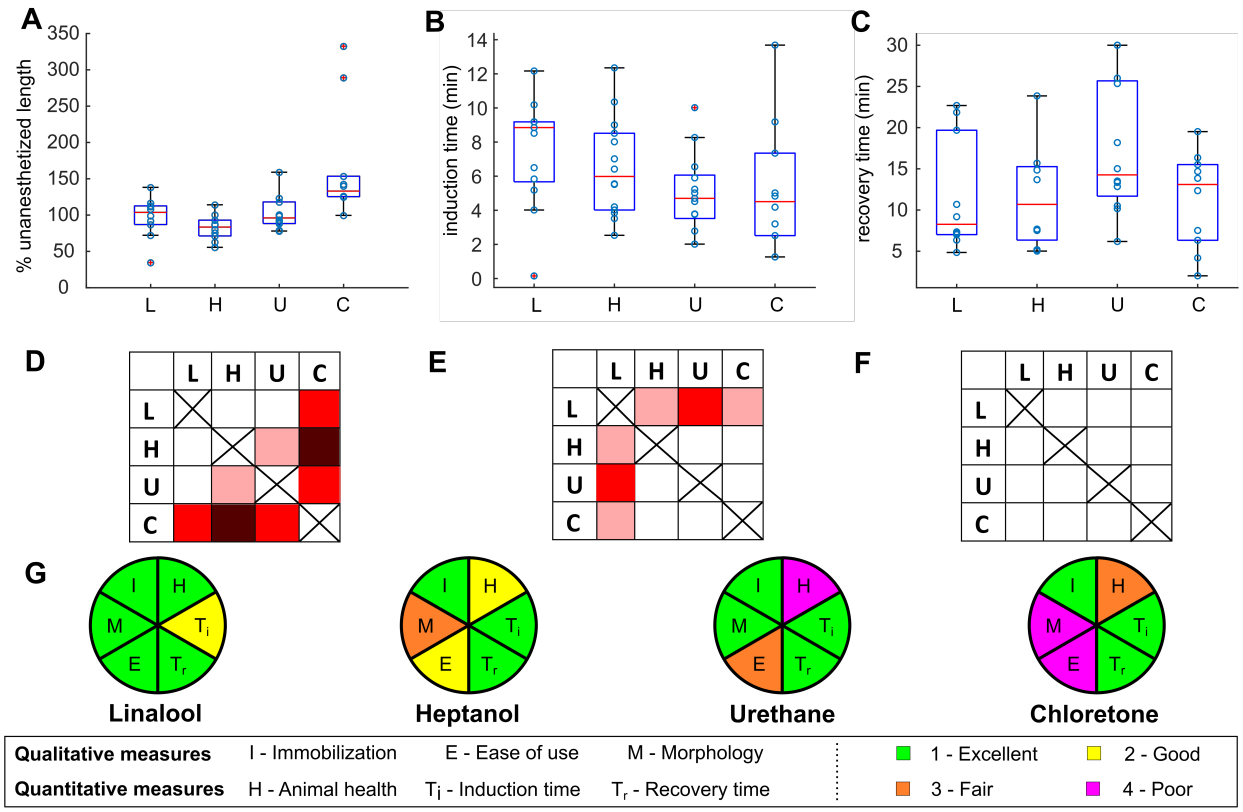

Figure 4.8: *Hydra* response to 1mM linalool (L), 0.04% heptanol (H), 2% urethane (U), and 0.1% chloretone (C). A. Percent length of anesthetized *Hydra* polyps compared to their natural state at 10min incubation. n = 10 animals per condition across 2 technical replicates. Anesthetized lengths similar to the average lengths in HM were recorded in linalool at 103% (87, 112; median (25^{th} percentile, 75^{th} percentile)), heptanol at 83% (71, 93) and urethane at 96% (88, 118), while chloretone-treated animals hyperextended at 133% (125, 153). B. Induction times across 2 technical replicates. Linalool n = 13, heptanol n = 14, urethane n = 13, chloretone n = 10. Linalool's median induction time was 9 min (6, 9) (median (25^{th} percentile, 75^{th} percentile)) and thus significantly longer than that of heptanol at 6 min (4, 9), urethane at 5 min (4, 6) and chloretone at 5 min (3, 7). C. Recovery times across 2 technical replicates. Linalool n = 10, heptanol n = 8, urethane n = 12, chloretone n = 10. Median recovery time was 8 min (7, 17) for linalool, 11 min (7, 15) for heptanol, 14 min (12, 26) for urethane and 13 min (7, 15) for chloretone. (D-F) Pairwise statistical comparisons of data shown in A-C. Pink, red and dark red indicate a statistically significant difference at $p<0.05$, $p<0.01$ and $p<0.001$ respectively, determined using the Mann-Whitney U test between pairs of anesthetics. D. Comparison between percent length distributions. E. Comparison between induction time distributions. F. Comparison between recovery time distributions. G. Overview of the four anesthetics tested, scored on degree of immobilization, animal health following anesthesia, time to induce anesthesia, time to recover from anesthesia, morphology, and ease of use (see Methods).

tentacles in heptanol or the formation of bumps in the body column of chloretone-treated animals) nor for the changes in morphology that were observed for heptanol and chloretone over time, we also qualitatively compared the body shapes of the anesthetized animals (Fig 4.7A) to those of untreated animals. Because the morphologies in linalool and urethane were the most similar to the untreated body morphology and did not change much over the course of 60 min incubation, we ranked morphology in linalool and urethane as the best, followed by heptanol (contracted body and tentacles, changing shape), and chloretone (hyperextended, contracted tentacles, bumps, changing shape).

Because most published studies specified only the concentration of anesthetic used and not the incubation time, we used concentrations that have been reported in the literature to be effective for the different anesthetics and measured induction and recovery times for direct comparison to linalool. Anesthesia in linalool is induced slower than in other anesthetics (Fig 4.8B and 4.8E). Recovery times were statistically similar between all anesthetics, with most polyps resuming normal activity within 10–20 min post-exposure (Fig 4.8C and 4.8F).

Finally, we compared the effects of long-term exposure to the different anesthetics. First, we tested a 3-day exposure to the anesthetics without changing the medium, as would be necessary for long term immobilization for continuous imaging, as in the example shown in Fig 4.6C for 1 mM linalool. While 1 mM linalool does not negatively affect intact polyps (Fig 4.6), all polyps disintegrated within 24 h upon continuous exposure to 2% urethane (Fig 4.S9). Under the same conditions, chloretone caused disintegration in 50% of the animals after 24 h, with most polyps disintegrating by 72 h (Fig 4.S9). The animals that survived the 3-day chloretone treatment without solution exchange had a fairly normal morphology and pinch response, potentially due to a developed tolerance, as previously suggested [49].

Heptanol was not lethal to *Hydra* over 3 days (Fig 4.S9), but as with chloretone the animals regained normal morphology and pinch response by the third day.

Subsequently we tested a 3-day incubation with media changes every 24 h, to determine whether performance could be improved by constant refreshing of the anesthetic. As seen with the previous experiment, polyps in urethane died within the first 24 h and polyps in linalool were still alive at the end of 72 h. Survival in chloretone was reduced as all polyps had died by 48 h. Similarly, only about 60% of the polyps survived in heptanol by 72 h (Fig 4.S9).

We also compared the performance of these various anesthetics for single and dual channel high magnification fluorescent live imaging of GCaMP6s (Fig 4.7B) and WM animals labeled with Hoechst (Fig 4.7C), respectively and did not observe a notable difference in image quality between the anesthetics.

Using these comparative data, we ranked the performance of the anesthetics in the six categories we tested (Fig 4.8G and Methods): ease of use, animal morphology upon exposure to anesthetic, induction and recovery times, immobilization/imaging quality, and negative health effects. As liquids, heptanol and linalool solutions are easier and quicker to prepare than urethane or chloretone, which are supplied as solids (see Methods). Morphology is closest to normal and remains stable over the course of at least 1 hour incubation in urethane and linalool (Fig 4.7A and Fig 4.8A and 4.8D). Induction was slightly slower in linalool compared to the other three anesthetics (Fig 4.8B and 4.8E), but recovery times after short-term exposure were similar (Fig 4.8C and 4.8F). All anesthetics tied regarding immobilization/imaging quality (Fig 4.7B and 4.7C). Linalool stands out with the least negative health effects–in contrast to the situation in the other anesthetics, not a single animal

died in linalool at the end of 3-day exposures (Fig 4.S9), making linalool the compound of choice for multi-day applications. In summary, linalool ties for best on 3/6 criteria and scores best for 2/6. Thus, based on these six criteria, linalool's overall performance is superior to currently used anesthetics.

4.4 Discussion

Our results show that linalool is a fast-acting, reversible anesthetic for Hydra. It is non-toxic and simple to use, and its pleasant smell makes working with it an enjoyable experience. Incubation in 1 mM linalool does not completely immobilize the animal, as mouth opening and feeding are still observed (Figs 4.1F and 4.4A); although, feeding is extremely impaired (Fig 4.1F, Fig 4.S2). While *Artemia* frequently get stuck to the tentacles of animals incubated in linalool, few are ingested. This suggests that while nematocyte and mouth function may be normal in linalool-treated animals (Fig4.4A), the movement of food into the body cavity is impaired. As digestive movements have previously been shown to require nervous system function [79], this impairment may be a direct consequence of linalool's effect on the Hydra nervous system, as suggested by our data. Our experiments in wildtype and nerve-free animals show the absence of both spontaneous and mechanically induced body column contractions, implying that linalool affects both nervous system and epithelial cells.

In terms of applications, a 10 min incubation in 1 mM linalool significantly decreased polyp movement, allowing for fine surgical manipulations with superior precision, efficiency, and long-term success compared to their execution in HM (Fig 4.2). Thus, linalool is a useful

tool for grafting and tissue manipulations, especially for novice researchers. We achieved significantly improved fluorescent imaging when compared to HM and were able to acquire high quality single- and multi-channel fluorescent z-stacks and time lapse movies (Fig 4.4 and S3–S6 Movies). Comparable high-quality fluorescence in vivo imaging has previously only been possible using chloretone [56], which, as we show here, is not without negative side effects (Fig 4.8 and Fig 4.S9), or using custom microfluidics [3] and Polydimethylsiloxane (PDMS) chips [25].

Additionally, we showed that linalool enables repeated short-term imaging of the same specimen over the course of days, allowing us to visualize the dynamics of graft development and head regeneration in individuals (Fig 4.2Diii and Fig 4.5A). We were able to achieve fluorescent imaging with sub-cellular resolution (Fig 4.3), which suggests that one could study cellular migration processes over the course of days. Furthermore, induced mouth opening and induced local body column contraction in linalool treated epithelial GCaMP animals demonstrated that linalool does not interfere with epithelial calcium signaling and that GCaMP animals can be used to study behaviors that are not suppressed by linalool. Therefore, given linalool's lack of toxicity and ease of use, linalool is likely to become a popular tool by making *in vivo* fluorescence imaging over broad contexts accessible to *Hydra* researchers.

When compared to other currently used anesthetics, 1 mM linalool is superior in terms of ease of preparation, handling, and disposal. Linalool and heptanol are alcohols and supplied as liquids; thus, working solutions are made up within minutes. Because heptanol has a strong smell, however, preparation in the fume hood may be preferred. Urethane and chloretone are powders and therefore the preparation of stock solutions requires more time

and safety precautions, such as working in a fume hood. Chloretone also needs to be heated to dissolve. Regarding overall toxicity, linalool is considered non-toxic at the concentrations employed here [53]. Chloretone is also comparably non-toxic at the concentrations used here [66], whereas urethane is a known carcinogen [95, 77, 76]. Heptanol is a teratogen [6] and considered to have aquatic toxicity [84], and long-term low-dose exposure causes abnormal patterning phenotypes, such as two-headed animals in freshwater planarians [65]. Thus, linalool provides a clear advantage in terms of ease of use and lack of toxicity.

Linalool also has an advantage in anesthetized animal morphology (Fig 4.7A). Animals extend in linalool and in urethane and maintain their shape for at least 1 hour, facilitating precision cuts and grafting experiments (Fig 4.2); in contrast, animals in heptanol or chloretone appear contracted and misshapen and change morphology over time (Fig 4.7Aii and 4.7Aiv). As grafting requires precise manipulations that are most easily executed on an evenly extended animal, chloretone and heptanol are suboptimal for such applications. The morphological differences that we observed between the various anesthetics can be important when choosing an anesthetic for a specific application. The demonstrated lack of cellular damage or other harm to the animal with linalool provides an advantage for repeated imaging or for particularly sensitive experiments.

In terms of long-term applications, we find that a 3-day continuous exposure without media exchange is lethal in urethane within 24 h, partially lethal in chloretone, and harmless in linalool and heptanol. Surviving chloretone and heptanol-treated animals showed normal morphology and pinch response, whereas linalool-treated animals do not. The observed detrimental effect on animal health of urethane may be due to an overly broad mechanism of action that impacts other aspects of the animal's physiology. Urethane has been shown

to act in *Hydra* by reversing the sodium polarity across the cell membrane, leading to structural damage [58]. While chloretone has been proposed to act directly on nerves [49], its mechanism of action in *Hydra* remains unclear. It is possible that the gross anatomical changes that are observed in exposure to chloretone cause functional problems that ultimately cause death. Heptanol is a gap junction blocker that effectively blocks ectodermal epithelial cell-cell communication in the body column at 0.04% v/v [90]. As a small alcohol, its effect may be lost over long incubations due to its volatility. Exchanging the media every 24 h drastically changed the outcome of incubation in chloretone and heptanol, with all chloretone-treated and most heptanol-treated animals dying within 3 days. This result suggests that the survival and loss of anesthesia seen in animals incubated 72 h in heptanol or chloretone without medium changes is due to evaporation or degradation of the chemical, and that continuous exposure to active concentrations is toxic to the animals. In summary, these data suggest that urethane, chloretone, and heptanol cannot be used for continuous 3-day exposure and long-term imaging. Thus, for long-term experiments, linalool is the only viable option among the four anesthetics tested.

In contrast to intact polyps, regenerating body columns continuously exposed to 1 mM linalool over 3 days showed abnormal morphology (Fig 4.6Eii) and suppressed regeneration (Fig 4.6D). Both, head and foot regeneration were delayed (Fig 4.6E and Fig 4.S7). Affected animals healed their wounds but did not develop the structures associated with the missing body part–decapitated animals mostly did not form tentacles or hypostomes, and animals lacking feet did not regain a peduncle or the ability to adhere to the substrate. A small fraction of animals showed one or two tentacle buds at 3 days of regeneration in 1mM linalool (Fig 4.S6), whereas some animals died under the same conditions, suggesting sen-

sitivity differences among individuals of the same strain. Regeneration could be rescued by transferring the regenerating animals back to HM after linalool exposure (Fig 4.6E). While these findings prevent the use of linalool for continuous long-term imaging of regeneration, they indicate that linalool could potentially be a useful tool for regeneration studies if the mechanism of action can be elucidated.

Because nerve-free animals in linalool do not show delayed regeneration (Fig 4.S8), these data suggest that nerve or interstitial cells are the target for the regeneration defect. The precise role of the interstitial cell lineage in regeneration and morphogenesis is unknown. Nerve-free *Hydra* are capable of regeneration and budding [60]. Marcum and Campbell propose several possible explanations for this observation – 1. that nerve cells are not involved in development, 2. that nerve cells modulate developmental processes initiated by epithelial cells, 3. that nerve cells play an essential role in patterning but that their absence can be compensated for, or 4. that nerve and epithelial cells both have critical but overlapping roles in development. Head regeneration is delayed in *Hydra* treated with double-stranded RNA from a gene encoding a neuronal progenitor marker [63]. The authors take this result to support the third possibility laid out by Marcum and Campbell – that neurons are critical for regeneration, but that in their complete absence nerve-free animals can employ an alternate pathway. Our finding that linalool strongly suppresses head regeneration in wild type animals while having no effect on nerve-free animals supports this idea that neuronal signals play an important role for head regeneration under normal circumstances. It will be exciting to dissect this relationship between nerve signaling and axial patterning. One possible starting point for investigation is linalool's known mechanism of action in other systems.

Linalool has been found to inhibit glutamatergic signaling in the central nervous system [27] and to modify nicotinic receptors at neuromuscular junctions in rodents, leading to modulated acetylcholine release [72]. While it is unclear whether the mechanism of anesthesia in *Hydra* is the same as that in rodents, the cellular machinery targeted is sufficiently conserved that this is a possibility. *Hydra* has been shown to possess GABA receptors [70], and to have specific glutamate-binding abilities likely corresponding to at least two types of glutamate receptors [4]. GABA, glutamate, and their agonists and antagonists have been shown to influence behaviors such as contraction bursts [46], as well as nematocyst activity [48]. On the other hand, *Hydra* homogenate was found to contain an enzyme that hydrolyzes acetylcholine [29]. Nicotinic acetylcholinesterase antagonists were found to decrease contraction bursts while a muscarinic acetylcholinergic antagonist increased them [47]. A cDNA sequence for acetylcholinesterase has also been cloned, though its expression and localization have not been confirmed [89]. Thus, the targets of linalool's mechanism of action appear to be conserved between *Hydra* and rodents, though further mechanistic studies will be needed to confirm a shared mode of action.

Finally, because different species are used in *Hydra* research, we also tested the suitability of linalool as a reversible anesthetic in other *Hydra* species – *H. oligactis* and *H. viridissima*. The results for induction and recovery times and effects on pinch and feeding responses are summarized in S10 Fig. We found similar effects as observed for *Hydra vulgaris* (Fig 4.S10) and conclude that linalool effectively anesthetizes these other *Hydra* species.

In summary, linalool offers a range of advantages over other available anesthetics by enabling new applications such as long term or repeated imaging while also being usable as a pre-fixation relaxant in the same way as current options. Linalool's lack of toxicity to both

Hydra and researchers and the ease of use and preparation compared to current anesthetics render it an attractive tool for *Hydra* experimentation in the teaching setting. Excitingly, linalool makes grafting experiments that can provide fundamental insights into regeneration and biological patterning accessible to students with no previous experience with *Hydra*.

4.5 Materials and Methods

4.5.1 *Hydra* strains and culture

We used the *Hydra vulgaris* AEP strain [61, 92] and various transgenic lines derived from this strain: GCaMP6s, expressing the calcium sensor GCaMP6s in interstitial cells [26]; Epithelial GCaMP, expressing GCaMP6s in the endoderm cells [88], Wnt, expressing GFP under control of the Wnt3 promoter [40]; HyBra, expressing GFP under control of the HyBra2 promoter [35]; "Watermelon" (WM) animals [35] expressing GFP in the ectoderm and DsRed2 in the endoderm with both genes under control of an actin gene promoter; *Hydra vulgaris* strain A10 (chimera consisting of *Hydra vulgaris* (formerly *Hydra magnipapillata* strain 105) epithelial cells and sf-1 interstitial cells, which are temperature sensitive interstitial cells [79]; and a line originating from a single animal that was obtained by recombining AEP ectoderm and watermelon endoderm following tissue separation [21] and named "Frank" by the undergraduate student who created it. The Frank line has unlabeled ectoderm and DsRed2-expressing endoderm. *Hydra viridissima* and *Hydra oligactis* were generously provided by Dr. Rob Steele.

Hydra strains were maintained in mass cultures in *Hydra* medium (HM) composed of

1 mM $CaCl_2$ (Spectrum Chemical, New Brunswick, NJ), 0.1 mM $MgCl_2$ (Sigma-Aldrich, St. Louis, MO), 0.03 mM KNO_3 (Fisher Scientific, Waltham, MA), 0.5 mM $NaHCO_3$ (Fisher Scientific), and 0.08 mM $MgSO_4$ (Fisher Scientific) prepared with MilliQ water, with a pH between 7 and 7.3. Cultures were maintained at 18°C in the dark in a Panasonic incubator (Panasonic MIR-554, Tokyo, Japan) save the *H. oligactis* and *H. viridissima* which were kept on a windowsill at room temperature. The cultures were fed 2-3x/week with *Artemia* nauplii (brine shrimp) from the San Francisco Bay or from the Great Salt Lake (Brine Shrimp Direct, Ogden, UT). Animals were cleaned daily using standard cleaning procedures [51]. Asexual, non-budding polyps starved for at least 24 h were used for experiments unless stated otherwise.

4.5.2 Generation of nerve-free *Hydra*

To generate nerve-free *Hydra*, A10 polyps were heat-shocked in an incubator (Fisher Scientific 615F) at 28–29°C in the dark for 72 h and then moved back into the 18°C incubator [79, 87, 30]. All nerve-free animals were subsequently force-fed and "burped" as described previously [94] for three to four weeks, in which time they lost nematocytes, as well as feeding and mouth opening behaviors.

4.5.3 Preparation of anesthetic solutions

Stock solutions were made in HM at concentrations of 1 mM linalool (Sigma-Aldrich), 0.04% heptanol (Acros Organics, Fisher Scientific), 2% urethane (Sigma-Aldrich), or 0.1% chloretone hemihydrate (Sigma-Aldrich). Linalool and heptanol were prepared fresh daily by

adding to HM and shaking vigorously for 1 min to dissolve and, stored at room temperature. Urethane and chloretone solutions were stored at 4°C for a few days and pre-warmed to room temperature before usage. Anesthetic solutions were prepared at room temperature, except for chloretone, which was prepared with slight heating.

4.5.4 Linalool viability assay

24 h starved polyps were incubated in 6-well plates (Genesee Scientific, El Cajon, CA), 8 or 10 animals per well in 2 mL of different concentrations of linalool (0–10 mM) at room temperature for 3 h. Below concentrations of 3 mM and above 3.6 mM, 4 technical replicates were performed for each concentration. Between 3 mM and 3.6 mM, 6 technical replicates were performed at each concentration. The fraction of live animals was scored at the end of the assay. To obtain the LC_{50} value, the fraction of dead animals (1 - fraction of live animals) was plotted against the linalool concentration. The data were fitted to the Hill equation as in [36]:

$$y = \frac{1}{1 + \frac{LC50}{x}^{Hill-coefficient}}$$

Here, y is the fraction of dead animals and x is the concentration of linalool in millimolar. The fit was generated using the curve fitting application in MATLAB (MathWorks, Natick, MA, USA) to obtain the mean LC_{50} value and the 95% confidence intervals.

4.5.5 Characterizing short term efficacy of anesthetics

1–5 intact *Hydra* polyps were incubated per well in a flat bottom 6-well plate (Eppendorf, Hamburg, Germany) filled with 8 mL of HM or respective anesthesia. If more than 2 polyps were used, 40 μm or 100 μm Falcon cell strainers (Fisher Scientific) were used in the well to allow for quicker transfer of the animals from HM to anesthesia and vice versa. In some experiments, all wells were imaged simultaneously, and polyps were stained with neutral red (1:400,000 w/v; Fisher Scientific) in HM for 90 s at room temperature prior to the experiment to enhance contrast during imaging. The 6-well plate was imaged from the top using a Basler A601f-2 camera (Basler Inc., Exton, PA) attached to a 25 mm TV lens C22525KP with adjustable focal length (Pentax, Tokyo, Japan) for 65 min at 1 fps using Basler pylon camera software. Lighting was provided by a model A4S light box (ME456, Amazon, Seattle, WA). After 65 min, the cell strainers were moved to a new well and 8 mL of HM were added to each well. Following this, the plate was imaged for 2 h. In other experiments, individual wells were imaged on a stereo microscope using a Flea-3 camera (FLIR Integrated Imaging Solutions Inc, Wilsonville, OR) controlled by a custom MATLAB script. To obtain representative images at higher magnification, anesthetized *Hydra* were imaged in a 35 mm tissue culture dish with a Leica MZ16FA microscope (Leica Microsystems Inc., Buffalo Grove, IL) equipped with a SPOT RT3 camera (SPOT Imaging, Sterling Heights, Michigan), using the SPOT 5.1 software (SPOT Imaging) at 15 min and at 60 min exposure.

A range of sublethal linalool concentrations (0 mM, 0.1 mM, 0.25 mM, 0.5 mM, 0.75 mM,1 mM) were tested. Working concentrations for other anesthetics were 2% urethane, 0.04% heptanol, or 0.1% chloretone, with induction imaged for at least 20 min and recovery

for at least 30 min. At least 10 animals were assayed for each condition, in at least 3 technical replicates. Time of induction of anesthesia was considered to be the time at which the animal stopped extending further after its last spontaneous contraction, and time of recovery was considered to be the timing of complete contraction in the first contraction burst observed after returning the polyps to HM. Due to the complex behavior of *Hydra* and the subjectivity of these measures, calculated times for induction and recovery should be considered estimates rather than conclusive values.

4.5.6 Body column length of *Hydra* in anesthetics

24 h starved polyps were imaged for 10 min in HM to observe both extended and contracted states of the moving polyp to calculate an average body length ((max+min)/2). The polyps were then transferred to 1 mM linalool, 2% urethane, 0.04% heptanol, or 0.1% chloretone and imaged for an additional 20 min. We averaged the minimum and maximum body lengths of *Hydra* in the last 10 min of recording in each anesthetic. Average body length in the anesthetic was divided by the average in HM to find the % body length for each anesthetic to determine whether the polyps were hyperextended (>100%) or contracted (<100%) compared to their "normal" length. Because *Hydra* doesn't have a fixed body shape or length due to constant extension and contraction, this normal length is somewhat arbitrary; it nevertheless allows us to compare the effects of the various anesthetics.

4.5.7 Feeding and pinch responses in linalool

24 h starved polyps were incubated in 1 mM linalool for 10 min in a 60 mm tissue culture dish (VWR International, Radnor, PA). Each animal was pinched using a pair of Dumont No. 5 forceps (Fine Surgical Tools, Foster City, CA) to determine presence or absence of a contractile response while in the linalool solution.

To evaluate how quickly the pinch response would be restored after removal from 1 mM linalool, six 1-day starved Hydra were incubated in 1 mM linalool for either 10 min or 30 min in a 30 mm diameter dish. After incubation they were moved over to the lid of a 30 mm dish containing 3 mL Hydra medium with a glass pipet and their behavior was recorded on a Leica Wild M3C dissection microscope, equipped with a Flea-3 camera. Three independent replicates were performed for each 10 min and 30 min exposure, with 6 biological replicates per technical replicate.

To assay whether animals exhibited a feeding response in linalool, 4-day starved polyps were first incubated for 10 min in HM or 1 mM linalool. Meanwhile, 30 *Artemia* were counted and added to a well of a 96-well plate (Eppendorf) either in HM or 1 mM linalool. A picture of the well was taken using a Flea-3 camera attached to a stereo microscope to record the number of *Artemia* in the well. A single polyp was then added to the well and left undisturbed for 30 min. At the end of 30 minutes, the number of *Artemia* ingested were counted, either by pulling the ingested *Artemia* out of the animal's body cavity using forceps in the case of the *H. viridissima* or by counting the number of freely floating *Artemia* in the dish.

To assay how long anesthetized animals took to regain a feeding response once re-

moved from linalool, 5 animals were incubated in 1mM linalool for 10-15 min. A single individual was added to a small drop (60–80 μl) of HM containing approx. 70–80 *Artemia*. All 5 animals were imaged using a Leica dissection microscope and Flea-3 camera at regular intervals to determine whether the *Hydra* started eating *Artemia*. The number of animals eating at 5, 10, and 15 min were recorded. Eating was determined as having an enlarged body column due to ingestion of *Artemia*. Three technical replicates with 5 animals each were performed.

4.5.8 Cross sections and "zebra grafts"

48–72 h starved Wnt and Frank polyps were used to assay sectioning. Polyps were placed in the lids of 35 mm dishes in either HM or 1 mM linalool for at least 10 min. Rings of tissue were excised from the body column using a scalpel 10 blade. The rings were strung onto glass needles pulled from microcapillaries (World Precision Instruments, Sarasota, FL) using a P-1000 micropipette puller (Sutter Instrument, Novato, CA) and imaged with a Leica MZ16FA microscope equipped with a SPOT RT3 camera, using the SPOT 5.1 software. The time taken to cut the sections was measured for each polyp. The thickness of each section was measured using Fiji [78] by measuring the length of the thickest part of the cross section.

"Zebra grafts" (n = 10 per condition) were created using WM and Frank animals. One animal of each kind was used to make one graft. The animals were placed in a 100 mm petri dish (Spectrum Scientifics, Philadelphia, PA) filled with either HM or 1 mM linalool in HM. A small piece of filter paper (2x2 mm) was cut and threaded onto a size 00 enameled insect pin (Austerlitz, Carolina Biological) and the pin placed into the dish. One animal

was decapitated, and the head threaded onto the pin mouth first using forceps such that the cut edge of the tissue faced towards the point of the pin. The second animal was then decapitated, and the head discarded. A ring of tissue was cut as thinly as possible from the body column of the second animal and threaded onto the pin, followed by a ring from the first animal. Alternating rings of tissue were cut and placed on the pin until the body columns of both animals were used up, at which point one of the feet was threaded onto the pin to complete the chimera. A second piece of filter paper was threaded onto the pin, and forceps used to gently move the two pieces of paper together in order to force all the rings into contact with each other. These chimeras were allowed to heal on the pins for 2 h, then gently pushed off the pins with forceps, transferred to clean 35 mm dishes full of HM, and allowed to further heal overnight before imaging. Two grafts were then imaged using an Invitrogen EVOS FL Auto microscope (Thermo Fisher Scientific) and the Invitrogen EVOS FL Auto Imaging System software. Since the entire graft did not fit in a single field of view, multiple images were taken and stitched together in Inkscape 0.92.3 which is an opensource vector graphics editor. The other grafts were imaged using an Olympus IX81 inverted microscope (Olympus Corporation, Tokyo, Japan) with an ORCA-ER camera (Hamamatsu Photonics, Hamamatsu, Japan) and slidebook software version 5.0 (Intelligent Imaging Innovations, Denver, CO). The number of segments in each graft and the time taken to cut sections of the parent animals and assemble the graft on the pin was recorded.

Grafting of heads into the body column was accomplished using WM and unlabeled animals using an approach similar to the insect pin method described above. The WM animal was decapitated, and a slit cut in the side of the unlabeled animal. The pin was passed through the WM head hypostome first, then through the wound in the unlabeled

polyp and out through the body wall on the other side. Care was taken when positioning the filter paper pieces to avoid pushing the donor head into the recipient body cavity. Animals were allowed to heal for 2 h, then removed from the pins and placed in dishes of clean HM to heal overnight before imaging. Grafting of head organizers into the body column was accomplished without pins. Head organizers were obtained by anesthetizing a WM animal in linalool, removing the head, then excising the tentacle bases to leave only a small fragment of tissue containing the tip of the hypostome. A small slit was cut in the body column of an unlabeled animal, and forceps used to place the hypostome piece into the slit. Animals were allowed to heal for 2 h before transfer to dishes of clean HM. Successful grafts were imaged every 24 h to determine whether an ectopic body axis was induced.

4.5.9 Fluorescence imaging in 1 mM linalool and in other anesthetics

All fluorescence imaging was done using the Olympus IX81 inverted microscope with the ORCA-ER camera. Slidebook software was used to interface with the microscope and acquire z-stacks and time-lapse images. Anesthesia incubations were performed as described earlier.

Hydra expressing GCaMP6s in nerve cells and WM Hydra were used for fluorescence imaging. For low magnification single channel imaging, a GCaMP6s animal was allowed to move freely in a drop of either HM or 1 mM linalool on a 40 mm x 24 mm glass coverslip (Fisher Scientific) and was imaged in the GFP channel with a 50 ms exposure using a 4x objective (Olympus). Images were recorded every 100 ms for 10 s to obtain a time lapse

movie. Rigid body correction of z-stacks was accomplished using a previously described algorithm [93]. For high-magnification single channel imaging, GCaMP6s animals were mounted in tunnel slides prepared as described in [18]. Neurons in the body column of GCaMP6s animals were imaged by taking z-stacks of the tissue in the GFP channel (500 ms exposure; z-step size of 0.25 μm), using a 60x oil immersion objective (Olympus).

For imaging calcium activity during mouth opening, 4–5 day starved epithelial GCaMP animals were incubated in 1 mM linalool for 10 minutes. The animals were then decapitated and the hypostomes mounted in tunnel slides. Mouth opening was induced by flushing in 2 mM reduced glutathione (Sigma-Aldrich) diluted in 1 mM linalool into the tunnel slide [18]. Images were taken every 400 ms with an 80 ms exposure using a 10x objective (Olympus) in the GFP channel.

For calcium imaging using a pinch response, 5 epithelial GCaMP animals were used. A single polyp was moved into a 60 mm petri dish with HM. Response to pinch was recorded on the Leica MZ16FA microscope equipped with the SPOT RT3 camera at 5 fps. The same polyp was then moved into a second 60 mm petri dish containing 1 mM linalool and incubated at room temperature for 10 minutes. Pinch response was then recorded in the same way it was done for HM.

For low-magnification multi-channel imaging, WM animals were incubated in Hoechst 33342 (Thermo-Fisher Scientific) diluted 1:500 in 1 mM linalool for 15 minutes in the dark. The animals were then decapitated and the hypostome mounted in a tunnel slide. Z-stacks were taken in DAPI, GFP and RFP channels with a step size of 2.99 μm using a 10x objective.

For high-magnification multi-channel imaging, RWM animals were first incubated in SYTO 60 red fluorescent nucleic acid stain (Invitrogen) diluted to 10 μM in HM for 1 h at

room temperature in the dark. 2 quick washes in 1 mL HM followed, as well as a 15 min incubation in the dark at room temperature in 1:250 Hoechst 33342 diluted in 1 mM linalool. Body columns of the animals were imaged in the DAPI, RFP and DRAQ5 channels with a 60x oil immersion objective. For high magnification two-channel imaging, Hoechst 33342 (Thermo-Fisher Scientific) was diluted 1:500 in 1 mL of the respective anesthetic solution and WM animals were incubated for 15 min at room temperature in the dark. Individuals were mounted on tunnel slides and imaged.

For long term imaging, whole polyps were placed in 35 mm plastic dishes in 2 mL 1 mM linalool solution. They were imaged unconstrained with no stage movement once every 5 minutes for 24 h using an Invitrogen EVOS FL Auto microscope.

4.5.10 Quantification of movement of samples during imaging

To quantify the amount of movement of the samples during imaging, the z-stacks obtained by imaging GCaMP6s animals at 60x and t-stacks obtained by imaging them at 4x were projected using a SD projection in Fiji. The mean gray value of the projection was obtained and divided by the mean grey value of the first image of the z-stack or t-stack to calculate the coefficient of variation.

4.5.11 Regeneration and budding assays

Polyps were decapitated with a scalpel just below the tentacle ring for head regeneration and above the budding zone for foot regeneration assays. In one experiment, the decapitated animals were placed in 600 μL of 0 mM (control), 0.1 mM, 0.25 mM, 0.5 mM,

0.75 mM, or 1 mM linalool in HM. Head regeneration was scored by the appearance of the first tentacle on a decapitated animal. 8 animals were kept at each concentration in a 48-well plate (Eppendorf) and imaged in brightfield at 4x with the Invitrogen EVOS Fl Auto 2. Head regeneration was scored every 12 h for 72 h. The lid of the plate was removed for imaging and the solutions were changed every 24 h. In another experiment, decapitated polyps were placed individually into the wells of a 24-well plate (Eppendorf), filled either with 500 μl HM or 1 mM linalool. Polyps were imaged approximately every 12 h and the appearance of tentacles and hypostomes were scored. After approximately 3 days, polyps were transferred into a new 24-well plate containing 500 μl fresh HM and imaged a day after transfer. Foot regeneration experiments were conducted the same way, with animals scored for the appearance of a peduncle and for the ability to adhere to the substrate. For repeated imaging of head regeneration at high magnification, animals were anesthetized in 1 mM linalool for 10 min prior to imaging and returned to HM to recover afterwards. To facilitate removal from the slides, a layer of Scotch tape was placed over the double-sided tape during construction of tunnel slides. The increased space between coverslip and slide and ability to easily lift off the coverslip after imaging allowed recovery of the animal with minimal chance of injury.

Budding was assessed by selecting healthy animals with early buds at stages 3–4 on the previously described scale [68], and incubating them in well plates as described for regeneration assays. Animals were scored for development of tentacles on the bud and formation of further buds at the end of 3 days. Long-term imaging of budding was carried out in 35 mm glass bottomed dishes (MatTek, Ashland, MA). One animal was placed onto the glass surface at the bottom of the dish in 1 mM linalool, a coverslip was laid over the

top to constrain the animal, and the dish was flooded with 1 mM linalool. Animals were imaged once per hour for 48 h using an Invitrogen EVOS FL Auto microscope.

4.5.12 Cell viability assay

Polyps were incubated for 30 min in 1 μg/mL propidium iodide in HM, washed twice in HM, then mounted on glass slides as described for live imaging of neurons. Slides were imaged on an Invitrogen EVOS FL Auto microscope in the red fluorescence channel using the Invitrogen EVOS FL Auto Imaging System software. Labeled cells were counted in the body column only and reported as number of labeled cells per animal. As a positive control, polyps were incubated in 0.04% colchicine (Acros Organics) in HM to induce cell death [20]. Animals were incubated in colchicine for a full 24 h rather than 8 h incubation followed by 16 h recovery as described.

4.5.13 Mitotic index assay

Polyps were incubated in HM or 1 mM linalool for 72 hours in 60 mm cell culture dishes at a density of 1 polyp/mL. Polyps were not fed during the experiment, but the medium was changed daily. At the end of the 72 h, one or two cross sectional segments were cut from the body column of each polyp near the head. The samples were placed on glass slides for a wet mount antibody stain. Humid chambers for staining were constructed by lining covered 100 mm Petri dishes (Spectrum Scientific) with wet paper towels and placing the slides inside the dishes. A well was created in the center of each glass slide by layering two pieces of double-sided tape across both short sides of the slide with one piece of tape

running on both long edges of the slide. The samples were placed in a drop of medium on the slide. All steps were performed at room temperature unless otherwise noted. The samples were fixed in 20 μL 4% paraformaldehyde (Sigma-Aldrich) in HM for 15 min. The samples were washed three times with 20 μL 1x PBS, followed by a 15 min permeabilization with 20 μL 0.5% PBSTx (0.5% Triton-X in 1x PBS). They were then incubated for 3.5 h in 20 μL blocking solution (1% FBS, 0.1% DMSO in 1x PBS) and placed overnight (16h) at 4°C in 30 μL anti-phospho-histone H3 (Ser10) primary antibody (Millipore Sigma, Burlington, MA) diluted 1:100 in blocking solution. On the second day, samples were washed quickly 3x with 40 μL 1x PBS, followed by four 25–35 minute washes of 20 μL 0.3% PBSTx. The samples were then incubated in a 1:1000 or 1:500 dilution of Alexa 546 rabbit IgG secondary antibody (Thermo-Fisher Scientific) for 5 h, followed by three quick and two 10 min washes of 0.3% PBSTx. To stain nuclei, the samples were incubated in DRAQ5 (Thermo-Fisher Scientific) diluted to 5 μM in 1x PBS for 15 min and then washed three times with 1x PBS. The 1x PBS was replaced with a 1:1 solution of glycerol and HM. Finally, a cover slip was placed over the samples and nail polish was used to seal the slides. Z-stacks of the cross-sections were imaged using a Leica high-resonance scanning SP5 confocal microscope with a 20x C-Apochromat 1.2 W objective.

To calculate mitotic indices, the number of Alexa 546 stained nuclei was counted for each cross section, divided by the number of nuclei stained by DRAQ5 and multiplied by 100 to obtain a percentage. Counting of Alexa 546 and DRAQ5 stained nuclei was done using Fiji. For the z-stack corresponding to each color channel, a maximum intensity z-projection was taken and binarized. The projection was then segmented using the water-shedding tool. The number of particles was counted using the Analyze Particles tool, with a size range of

10 - infinity μm^2. For Alexa 546 color channel stacks, an additional thresholding step was used before binarizing the image.

4.5.14 Comparison of different anesthetics

The different anesthetics were ranked 1–4, based on our direct comparison of their performance and the criteria described in Table 4.2. 1 was considered excellent, 2 good, 3 fair and 4 poor. The anesthetics were ranked the same if the difference in relevant values for comparison were not statistically significant.

Table 4.2: Criteria for ranking anesthetics

Readout	**Criterion**
Induction time	Ranked in increasing order of median induction times (Fig. 4.8B)
Recovery time	Ranked in increasing order of median recovery times (Fig. 4.8C)
Lethality	Ranked in decreasing order of fraction of surviving animals at the end of 3 d incubations (S9B Fig.)
Ease of use	Ranked based on availability as solid or liquid, with liquids ranking higher, and on toxicity (requiring handling in the fume hood or not).
Morphology	Ranked on basis of closeness to appearance of animals in HM. Effects such as bloating, lumps, or stubby tentacles were ranked lower (Fig. 4.7A)
Immobilization	Quality of z-projections of z-stacks of neuronal GCaMP6s animals taken at 60x (Fig. 4.7B)

4.6 Acknowledgements

Chapter 4, in full, is a reformatted reprint of material as it appears in PloS one, 2019. (Goel, T., Wang, R., Martin, S., Lanphear, E. and Collins, E.M.S., 2019. Linalool acts as a fast and reversible anesthetic in Hydra. PloS one, 2019). Use of this manuscript in this dissertation is covered by the rights permitted to the authors by PloS. The dissertation author was the co-primary author of this paper.

Bibliography

[1] Hiroshi Ando, Yasuji Sawada, Hiroshi Shimizu, and Tsutomu Sugiyama. "Pattern formation in hydra tissue without developmental gradients". In: *Developmental Biology* 133.2 (June 1989), pp. 405–414. ISSN: 0012-1606. DOI: 10.1016/0012-1606(89)90044-4.

[2] Ana Clara Aprotosoaie, Monica Hăncianu, Irina Iuliana Costache, and Anca Miron. "Linalool: A review on a key odorant molecule with valuable biological properties". In: *Flavour and Fragrance Journal* 29.4 (2014), pp. 193–219. ISSN: 10991026. DOI: 10.1002/ffj.3197.

[3] Krishna N Badhiwala, Daniel L Gonzales, Daniel G Vercosa, Benjamin W Avants, and Jacob T Robinson. "Microfluidics for electrophysiology, imaging, and behavioral analysis of: Hydra". In: *Lab on a Chip* 18.17 (2018), pp. 2523–2539. ISSN: 14730189. DOI: 10.1039/c8lc00475g.

[4] Susan L. Bellis, William Grosvenor, G. Kass-Simon, and Dennis E. Rhoads. "Chemoreception in Hydra vulgaris (attenuata): initial characterization of two distinct binding sites for l-glutamic acid". In: *Biochimica et Biophysica Acta (BBA) - Biomembranes* 1061.1 (Jan. 1991), pp. 89–94. ISSN: 0005-2736. DOI: 10.1016/0005-2736(91)90272-A.

[5] Dale J. Benos, R.Gary Kirk, William P. Barba, and Marcia M. Goldner. "Hyposmotic fluid formation in Hydra". In: *Tissue and Cell* 9.1 (Jan. 1977), pp. 11–22. ISSN: 0040-8166. DOI: 10.1016/0040-8166(77)90045-3.

[6] Giovanni Bernardini, Claudio Vismara, Patrizia Boracchi, and Marina Camatini. "Lethality, teratogenicity and growth inhibition of heptanol in Xenopus assayed by a modified frog embryo teratogenesis assay-Xenopus (FETAX) procedure". In: *Science of the Total Environment, The* 151.1 (July 1994), pp. 1–8. ISSN: 00489697. DOI: 10.1016/0048-9697(94)90480-4.

[7] H R Bode. *The interstitial cell lineage of hydra: A stem cell system that arose early in evolution*. June 1996.

[8] H. Bode, S. Berking, C. N. David, A. Gierer, H. Schaller, and E. Trenkner. "Quantitative analysis of cell types during growth and morphogenesis in Hydra". In: *Wilhelm Roux Archiv für Entwicklungsmechanik der Organismen* 171.4 (Dec. 1973), pp. 269–285. ISSN: 0949944X. DOI: 10.1007/BF00577725.

[9] Hans R. Bode. "The head organizer in Hydra". In: *The International Journal of Developmental Biology* 56.6-7-8 (June 2012), pp. 473–478. ISSN: 0214-6282. DOI: 10.1387/ijdb.113448hb.

[10] Tobias Boothe, Lennart Hilbert, Michael Heide, Lea Berninger, Wieland B. Huttner, Vasily Zaburdaev, Nadine L. Vastenhouw, Eugene W. Myers, David N. Drechsel, and Jochen C. Rink. "A tunable refractive index matching medium for live imaging cells,

tissues and model organisms." In: *eLife - Tools and Resources* (2017). DOI: 10.1111/jam.13772. arXiv: 1705.11170.

[11] Thomas C. G. Bosch. "Hydra and the evolution of stem cells". In: *BioEssays* 31.4 (Apr. 2009), pp. 478–486. ISSN: 02659247. DOI: 10.1002/bies.200800183.

[12] Thomas C.G. Bosch. *Why polyps regenerate and we don't: Towards a cellular and molecular framework for Hydra regeneration*. Mar. 2007. DOI: 10.1016/j.ydbio.2006.12.012.

[13] Ethel Nicholson Browne. "The production of new hydranths in Hydra by the insertion of small grafts". In: *Journal of Experimental Zoology* 7.1 (Aug. 1909), pp. 1–23. ISSN: 0022-104X. DOI: 10.1002/jez.1400070102.

[14] Allison L. Burnett and Norma A. Diehl. "The nervous system of hydra. I. Types, distribution and origin of nerve elements". In: *Journal of Experimental Zoology* 157.2 (Nov. 1964), pp. 217–226. ISSN: 0022-104X. DOI: 10.1002/jez.1401570205.

[15] Wanda Buzgariu, Yvan Wenger, Nina Tcaciuc, Ana-Paula Catunda-Lemos, and Brigitte Galliot. "Impact of cycling cells and cell cycle regulation on Hydra regeneration". In: *Developmental Biology* 433.2 (Jan. 2018), pp. 240–253. ISSN: 0012-1606. DOI: 10.1016/J.YDBIO.2017.11.003.

[16] R.D. Campbell and C.N. David. "Cell Cycle Kinetics and Development of Hydra attenuata. II. Interstitial cells". In: *Journal of Cell Science* 16.2 (1974), pp. 349–358. ISSN: 0021-9533.

[17] Richard D. Campbell. "Cell movements in Hydra". In: *American Zoologist* 14.2 (1974), pp. 523–535. ISSN: 15407063. DOI: 10.1093/icb/14.2.523.

[18] Jason A. Carter, Callen Hyland, Robert E. Steele, and Eva Maria S. Collins. "Dynamics of Mouth Opening in Hydra". In: *Biophysical Journal* 110.5 (2016), pp. 1191–1201. ISSN: 15420086. DOI: 10.1016/j.bpj.2016.01.008.

[19] Jarrod A. Chapman, Ewen F. Kirkness, Oleg Simakov, Steven E. Hampson, Therese Mitros, Thomas Weinmaier, Thomas Rattei, Prakash G. Balasubramanian, Jon Borman, Dana Busam, Kathryn Disbennett, Cynthia Pfannkoch, Nadezhda Sumin, Granger G. Sutton, Lakshmi Devi Viswanathan, Brian Walenz, David M. Goodstein, Uffe Hellsten, Takeshi Kawashima, Simon E. Prochnik, Nicholas H. Putnam, Shengquiang Shu, Bruce Blumberg, Catherine E. Dana, Lydia Gee, Dennis F. Kibler, Lee Law, Dirk Lindgens, Daniel E. Martinez, Jisong Peng, Philip A. Wigge, Bianca Bertulat, Corina Guder, Yukio Nakamura, Suat Ozbek, Hiroshi Watanabe, Konstantin Khalturin, Georg Hemmrich, André Franke, René Augustin, Sebastian Fraune, Eisuke Hayakawa, Shiho Hayakawa, Mamiko Hirose, Jung Shan Hwang, Kazuho Ikeo, Chiemi Nishimiya-Fujisawa, Atshushi Ogura, Toshio Takahashi, Patrick R.H. Steinmetz, Xiaoming Zhang, Roland Aufschnaiter, Marie Kristin Eder, Anne Kathrin Gorny, Willi Salvenmoser, Alysha M. Heimberg, Benjamin M. Wheeler, Kevin J. Peterson, Angelika

Böttger, Patrick Tischler, Alexander Wolf, Takashi Gojobori, Karin A. Remington, Robert L. Strausberg, J. Craig Venter, Ulrich Technau, Bert Hobmayer, Thomas C.G. Bosch, Thomas W. Holstein, Toshitaka Fujisawa, Hans R. Bode, Charles N. David, Daniel S. Rokhsar, and Robert E. Steele. "The dynamic genome of Hydra". In: *Nature* 464.7288 (2010), pp. 592–596. ISSN: 00280836. DOI: 10.1038/nature08830.

[20] Mihai Cikala, Bettina Wilm, Engelbert Hobmayer, Angelika Böttger, and Charles N. David. "Identification of caspases and apoptosis in the simple metazoan Hydra". In: *Current Biology* 9.17 (Sept. 1999), 959–S2. ISSN: 0960-9822. DOI: 10.1016/S0960-9822(99)80423-0.

[21] Olivier Cochet-Escartin, Tiffany T. Locke, Winnie H. Shi, Robert E. Steele, and Eva Maria S. Collins. "Physical Mechanisms Driving Cell Sorting in Hydra". In: *Biophysical Journal* 113.12 (Dec. 2017), pp. 2827–2841. ISSN: 15420086. DOI: 10.1016/j.bpj.2017.10.045.

[22] C N David and R D Campbell. "Cell cycle kinetics and development of Hydra attenuata. I. Epithelial cells." In: *Journal of Cell Science* 11.2 (1972), pp. 557–68. ISSN: 0021-9533.

[23] Charles N. David. "A quantitative method for maceration of hydra tissue". In: *Wilhelm Roux Archiv für Entwicklungsmechanik der Organismen* 171.4 (Dec. 1973), pp. 259–268. ISSN: 0949944X. DOI: 10.1007/BF00577724.

[24] Charles N. David and Susan Murphy. "Characterization of interstitial stem cells in hydra by cloning". In: *Developmental Biology* 58.2 (July 1977), pp. 372–383. ISSN: 00121606. DOI: 10.1016/0012-1606(77)90098-7.

[25] Joseph P. Dexter, Mary B. Tamme, Christine H. Lind, and Eva-Maria S. Collins. "On-chip immobilization of planarians for in vivo imaging". In: *Scientific Reports* 4.1 (May 2015), p. 6388. ISSN: 2045-2322. DOI: 10.1038/srep06388.

[26] Christophe Dupre and Rafael Yuste. "Non-overlapping Neural Networks in Hydra vulgaris". In: *Current Biology* 27.8 (Apr. 2017), pp. 1085–1097. ISSN: 0960-9822. DOI: 10.1016/J.CUB.2017.02.049.

[27] Elaine Elisabetsky, Jeanine Marschner, and Diogo Onofre Souza. "Effects of linalool on glutamatergic system in the rat cerebral cortex". In: *Neurochemical Research* 20.4 (1995), pp. 461–465. ISSN: 03643190. DOI: 10.1007/BF00973103.

[28] U. Engel, S. Oezbek, R. Engel, B. Petri, F. Lottspeich, and T. W. Holstein. "Nowa, a novel protein with minicollagen Cys-rich domains, is involved in nematocyst formation in Hydra". In: *Journal of Cell Science* 115.20 (2002), pp. 3923–3934. ISSN: 00219533. DOI: 10.1242/jcs.00084.

[29] Ida Eržen and Miro Brzin. "Cholinergic mechanisms in hydra". In: *Comparative Biochemistry and Physiology Part C: Comparative Pharmacology* 59.1 (Jan. 1978), pp. 39–43. ISSN: 0306-4492. DOI: 10.1016/0306-4492(78)90009-6.

[30] Toshitaka Fujisawa. "Hydra regeneration and epitheliopeptides". In: *Developmental Dynamics* 226.2 (Feb. 2003), pp. 182–189. ISSN: 1058-8388. DOI: 10.1002/dvdy.10221.

[31] Brigitte Galliot, Wanda Buzgariu, Quentin Schenkelaars, and Yvan Wenger. "Non-developmental dimensions of adult regeneration in hydra". In: *International Journal of Developmental Biology* 62.6-8 (June 2018), pp. 373–381. ISSN: 02146282. DOI: 10.1387/ijdb.180111bg.

[32] A Gierer, S Berking, H Bode, C N David, K Flick, G Hansmann, H Schaller, and E Trenkner. "Regeneration of hydra from reaggregated cells". In: *Nature New Biology* 239.91 (1972), pp. 98–101. ISSN: 00900028. DOI: 10.1038/newbio239098a0.

[33] A. Gierer and Hans Meinhardt. "A theory of biological pattern formation". In: *Kybernetik* 12.1 (1972), pp. 30–39. ISSN: 03401200. DOI: 10.1007/BF00289234.

[34] K. M. Glauber, C. E. Dana, S. S. Park, D. A. Colby, Y. Noro, T. Fujisawa, A. R. Chamberlin, and R. E. Steele. "A small molecule screen identifies a novel compound that induces a homeotic transformation in Hydra". In: *Development* 142.11 (2015), pp. 2081–2081. ISSN: 0950-1991. DOI: 10.1242/dev.126235.

[35] Kristine M Glauber, Catherine E Dana, Steve S Park, David A Colby, Yukihiko Noro, Toshitaka Fujisawa, A Richard Chamberlin, and Robert E Steele. "A small molecule screen identifies a novel compound that induces a homeotic transformation in Hydra." In: *Development (Cambridge, England)* 140.23 (Dec. 2013), pp. 4788–96. ISSN: 1477-9129. DOI: 10.1242/dev.094490.

[36] Danielle Hagstrom, Olivier Cochet-Escartin, Siqi Zhang, Cindy Khuu, and Eva-Maria S. Collins. "Freshwater Planarians as an Alternative Animal Model for Neurotoxicology". In: *Toxicological Sciences* 147.1 (Sept. 2015), pp. 270–285. ISSN: 1096-6080. DOI: 10.1093/toxsci/kfv129.

[37] Shuting Han, Ekaterina Taralova, Christophe Dupre, and Rafael Yuste. "Comprehensive machine learning analysis of Hydra behavior reveals a stable basal behavioral repertoire". In: *eLife* 7 (Mar. 2018). ISSN: 2050084X. DOI: 10.7554/eLife.32605.

[38] Robert E. Hausman and Allison L. Burnett. "The mesoglea of Hydra. IV. A qualitative radioautographic study of the protein component". In: *Journal of Experimental Zoology* 177.4 (Aug. 1971), pp. 435–446. ISSN: 1097010X. DOI: 10.1002/jez.1401770405.

[39] Clarissa G. Heldwein, Lenise de L. Silva, Eduarda Z. Gai, Cassiela Roman, Thaylise V.parfaut Parodi, Marilise E. Bürger, Bernardo Baldisserotto, Érico M.de M. Flores, and Berta M. Heinzmann. "S-(+)-Linalool from Lippia alba: Sedative and anesthetic for silver catfish (Rhamdia quelen)". In: *Veterinary Anaesthesia and Analgesia* 41.6 (2014), pp. 621–629. ISSN: 14672995. DOI: 10.1111/vaa.12146.

[40] Bert Hobmayer, Fabian Rentzsch, Kerstin Kuhn, Christoph M. Happel, Christoph Cramer von Laue, Petra Snyder, Ute Rothbächer, and Thomas W. Holstein. "WNT

signalling molecules act in axis formation in the diploblastic metazoan Hydra". In: *Nature* 407.6801 (Sept. 2000), pp. 186–189. ISSN: 0028-0836. DOI: 10.1038/35025063.

[41] Martina Höferl, Sabine Krist, and Gerhard Buchbauer. "Chirality Influences the Effects of Linalool on Physiological Parameters of Stress". In: *Planta Medica* 72.13 (Oct. 2006), pp. 1188–1192. ISSN: 0032-0943. DOI: 10.1055/s-2006-947202.

[42] L. A. Hufnagel, G. Kass-Simon, and M. K. Lyon. "Functional organization of battery cell complexes in tentacles of Hydra attenuata". In: *Journal of Morphology* 184.3 (June 1985), pp. 323–341. ISSN: 0362-2525. DOI: 10.1002/jmor.1051840307.

[43] Linda A. Hufnagel and M. Lynn Myhal. "Observations on a Spirochaete Symbiotic in Hydra". In: *Transactions of the American Microscopical Society* 96.3 (July 1977), p. 406. ISSN: 00030023. DOI: 10.2307/3225874.

[44] Celina E. Juliano, Haifan Lin, and Robert E. Steele. "Generation of Transgenic Hydra by Embryo Microinjection". In: *Journal of Visualized Experiments* 91 (2014), e51888. ISSN: 1940-087X. DOI: 10.3791/51888.

[45] Hiroyuki J. Kanaya, Yoshitaka Kobayakawa, and Taichi Q. Itoh. "Hydra vulgaris exhibits day-night variation in behavior and gene expression levels". In: *Zoological Letters* 5.1 (2019), pp. 1–12. ISSN: 2056306X. DOI: 10.1186/s40851-019-0127-1.

[46] G. Kass-Simon, A. Pannaccione, and P. Pierobon. "GABA and glutamate receptors are involved in modulating pacemaker activity in hydra". In: *Comparative Biochemistry and Physiology - A Molecular and Integrative Physiology* 136.2 (Oct. 2003), pp. 329–342. ISSN: 10956433. DOI: 10.1016/S1095-6433(03)00168-5.

[47] G. Kass-Simon and L. M. Passano. "A neuropharmacological analysis of the pacemakers and conducting tissues ofHydra attenuata". In: *Journal of Comparative Physiology ? A* 128.1 (1978), pp. 71–79. ISSN: 0340-7594. DOI: 10.1007/BF00668375.

[48] G. Kass-Simon and A. A. Scappaticci. "Glutamatergic and GABAnergic control in the tentacle effector systems of Hydra vulgaris". In: *Hydrobiologia* 530-531.1-3 (Nov. 2004), pp. 67–71. ISSN: 0018-8158. DOI: 10.1007/s10750-004-2647-7.

[49] WM. A. Kepner and D.L. L. Hopkins. "Reactions of Hydra to Chloretone". In: *Journal of Experimental Zoology* 38.c (Jan. 1938), pp. 951–959. ISSN: 0022-104X. DOI: 10.1002/jez.1400380403.

[50] Osamu Koizumi. "Developmental neurobiology of hydra, a model animal of cnidarians". In: *Canadian Journal of Zoology* 80.10 (Oct. 2002), pp. 1678–1689. ISSN: 0008-4301. DOI: 10.1139/z02-134.

[51] Howard M. Lenhoff and Ray DuBois Brown. "Mass culture of hydra: an improved method and its application to other aquatic invertebrates". In: *Laboratory Animals* 4.1 (1970), pp. 139–154. ISSN: 0023-6772. DOI: 10.1258/002367770781036463.

[52] Sylvia G. Lenhoff and Howard M. Lenhoff. *Hydra and the Birth of Experimental Biology - 1744*. Pacific Grove CA: Boxwood Press, 1986, p. 192. ISBN: 0940168014.

[53] C.S Letizia, J Cocchiara, J Lalko, and A.M Api. "Fragrance material review on linalool". In: *Food and Chemical Toxicology* 41.7 (July 2003), pp. 943–964. ISSN: 0278-6915. DOI: 10.1016/S0278-6915(03)00015-2.

[54] Viviane de Moura Linck, Adriana Lourenço da Silva, Micheli Figueiró, Ângelo Luis Piato, Ana Paula Herrmann, Franciele Dupont Birck, Elina Bastos Caramão, Domingos Sávio Nunes, Paulo Roberto H. Moreno, and Elaine Elisabetsky. "Inhaled linalool-induced sedation in mice". In: *Phytomedicine* 16.4 (Apr. 2009), pp. 303–307. ISSN: 0944-7113. DOI: 10.1016/J.PHYMED.2008.08.001.

[55] Anton Livshits, Lital Shani-Zerbib, Yonit Maroudas-Sacks, Erez Braun, and Kinneret Keren. "Structural Inheritance of the Actin Cytoskeletal Organization Determines the Body Axis in Regenerating Hydra". In: *Cell Reports* 18.6 (Feb. 2017), pp. 1410–1421. ISSN: 22111247. DOI: 10.1016/j.celrep.2017.01.036.

[56] Mark Lommel, Anja Tursch, Laura Rustarazo-Calvo, Benjamin Trageser, and Thomas W Holstein. "Genetic knockdown and knockout approaches in Hydra". In: *bioRxiv* (2017), p. 230300. DOI: 10.1101/230300.

[57] W. F. Loomis. "Glutathione Control Of The Specific Feeding Reactions Of Hydra". In: *Annals of the New York Academy of Sciences* 62.9 (Oct. 1955), pp. 211–227. ISSN: 17496632. DOI: 10.1111/j.1749-6632.1955.tb35372.x.

[58] M Macklin. "The effect of urethan on hydra." In: *The Biological bulletin* 150.3 (June 1976), pp. 442–52. ISSN: 0006-3185. DOI: 10.2307/1540684.

[59] Harry K. MacWilliams. "Hydra transplantation phenomena and the mechanism of Hydra head regeneration: II. Properties of the head activation". In: *Developmental Biology* 96.1 (Mar. 1983), pp. 239–257. ISSN: 0012-1606. DOI: 10.1016/0012-1606(83)90325-1.

[60] B. A. Marcum and R. D. Campbell. "Development of hydra lacking nerve and interstitial cells". In: *Journal of Cell Science* Vol. 29.1 (1978), pp. 17–33. ISSN: 00219533.

[61] V J Martin, C L Littlefield, W E Archer, and H R Bode. "Embryogenesis in hydra." In: *The Biological bulletin* 192.3 (June 1997), pp. 345–63. ISSN: 0006-3185. DOI: 10.2307/1542745.

[62] Susan McLaughlin. "Evidence that polycystins are involved in Hydra cnidocyte discharge". In: *Invertebrate Neuroscience* 17.1 (2017), p. 1. ISSN: 13542516. DOI: 10.1007/s10158-016-0194-3.

[63] Marijana Miljkovic-Licina, Simona Chera, Luiza Ghila, and Brigitte Galliot. "Head regeneration in wild-type hydra requires de novo neurogenesis." In: *Development (Cam-*

bridge, England) 134.6 (Mar. 2007), pp. 1191–201. ISSN: 0950-1991. DOI: 10.1242/dev.02804.

[64] Sandra Münder, Susanne Tischer, Maresa Grundhuber, Nathalie Büchels, Nadine Bruckmeier, Stefanie Eckert, Carolin A. Seefeldt, Andrea Prexl, Tina Käsbauer, and Angelika Böttger. "Notch-signalling is required for head regeneration and tentacle patterning in Hydra". In: *Developmental Biology* 383.1 (Nov. 2013), pp. 146–157. ISSN: 1095564X. DOI: 10.1016/j.ydbio.2013.08.022.

[65] Taisaku Nogi and Michael Levin. "Characterization of innexin gene expression and functional roles of gap-junctional communication in planarian regeneration". In: *Developmental Biology* 287.2 (Nov. 2005), pp. 314–335. ISSN: 0012-1606. DOI: 10.1016/J.YDBIO.2005.09.002.

[66] S P Nordt. "Chlorobutanol toxicity." In: *The Annals of pharmacotherapy* 30.10 (Oct. 1996), pp. 1179–80. ISSN: 1060-0280.

[67] Yukihiko Noro, Seungshic Yum, Chiemi Nishimiya-Fujisawa, Christina Busse, Hiroshi Shimizu, Katsuhiko Mineta, Xiaoming Zhang, Thomas W. Holstein, Charles N. David, Takashi Gojobori, and Toshitaka Fujisawa. "Regionalized nervous system in Hydra and the mechanism of its development". In: *Gene Expression Patterns* 31 (Jan. 2019), pp. 42–59. ISSN: 18727298. DOI: 10.1016/j.gep.2019.01.003.

[68] Joann J. Otto and Richard D. Campbell. "Budding in Hydra attenuata: Bud stages and fate map". In: *Journal of Experimental Zoology* 200.3 (June 1977), pp. 417–428. ISSN: 1097010X. DOI: 10.1002/jez.1402000311.

[69] Hendrik O. Petersen, Stefanie K. Höger, Mario Looso, Tobias Lengfeld, Anne Kuhn, Uwe Warnken, Chiemi Nishimiya-Fujisawa, Martina Schnölzer, Marcus Krüger, Suat Özbek, Oleg Simakov, and Thomas W. Holstein. "A comprehensive transcriptomic and proteomic analysis of hydra head regeneration". In: *Molecular Biology and Evolution* 32.8 (Aug. 2015), pp. 1928–1947. ISSN: 15371719. DOI: 10.1093/molbev/msv079.

[70] Paola Pierobon, Alessandra Concas, Giovanna Santoro, Giuseppe Marino, Rosario Minei, Anna Pannaccione, Maria Cristina Mostallino, and Giovanni Biggio. "Biochemical and functional identification of GABA receptors in Hydra vulgaris". In: *Life Sciences* 56.18 (Mar. 1995), pp. 1485–1497. ISSN: 0024-3205. DOI: 10.1016/0024-3205(95)00111-I.

[71] H W Rand, J F Bovard, and D E Minnich. "Localization of Formative Agencies in Hydra." In: *Proceedings of the National Academy of Sciences of the United States of America* 12.9 (Sept. 1926), pp. 565–70. ISSN: 0027-8424.

[72] L. Re, S. Barocci, S. Sonnino, A. Mencarelli, C. Vivani, G. Paolucci, A. Scarpantonio, L. Rinaldi, and E. Mosca. "Linalool modifies the nicotinic receptor-ion channel kinetics at the mouse neuromuscular junction". In: *Pharmacological Research* 42.2 (2000), pp. 177–181. ISSN: 10436618. DOI: 10.1006/phrs.2000.0671.

[73] Fabian Rentzsch, Bert Hobmayer, and Thomas W. Holstein. "Glycogen synthase kinase 3 has a proapoptotic function in Hydra gametogenesis". In: *Developmental Biology* 278.1 (Feb. 2005), pp. 1–12. ISSN: 0012-1606. DOI: 10.1016/J.YDBIO.2004.10.007.

[74] Boris Rodenak-Kladniew, Agustina Castro, Peter Stärkel, Christine De Saeger, Margarita García de Bravo, and Rosana Crespo. "Linalool induces cell cycle arrest and apoptosis in HepG2 cells through oxidative stress generation and modulation of Ras/MAPK and Akt/mTOR pathways". In: *Life Sciences* 199.February (2018), pp. 48–59. ISSN: 18790631. DOI: 10.1016/j.lfs.2018.03.006.

[75] Norman B. Rushforth, Allison L. Burnett, and Richard Maynard. "Behavior in hydra: Contraction responses of hydra pirardi to mechanical and light stimuli". In: *Science* 139.3556 (Feb. 1963), pp. 760–761. ISSN: 00368075. DOI: 10.1126/SCIENCE.139.3556.760.

[76] Katsuhisa Sakano, Shinji Oikawa, Yusuke Hiraku, and Shosuke Kawanishi. "Metabolism of carcinogenic urethane to nitric oxide is involved in oxidative DNA damage". In: *Free Radical Biology and Medicine* 33.5 (Sept. 2002), pp. 703–714. ISSN: 08915849. DOI: 10.1016/S0891-5849(02)00969-3.

[77] M H Salaman and F J Roe. "Incomplete carcinogens: ethyl carbamate (urethane) as an initiator of skin tumour formation in the mouse." In: *British journal of cancer* 7.4 (Dec. 1953), pp. 472–81. ISSN: 0007-0920.

[78] Johannes Schindelin, Ignacio Arganda-Carreras, Erwin Frise, Verena Kaynig, Mark Longair, Tobias Pietzsch, Stephan Preibisch, Curtis Rueden, Stephan Saalfeld, Benjamin Schmid, Jean-Yves Tinevez, Daniel James White, Volker Hartenstein, Kevin Eliceiri, Pavel Tomancak, and Albert Cardona. "Fiji: an open-source platform for biological-image analysis". In: *Nature Methods* 9.7 (July 2012), pp. 676–682. ISSN: 1548-7091. DOI: 10.1038/nmeth.2019.

[79] Hiroshi Shimizu, Osamu Koizumi, and Toshitaka Fujisawa. "Three digestive movements in Hydra regulated by the diffuse nerve net in the body column". In: *Journal of Comparative Physiology A* 190.8 (Aug. 2004), pp. 623–630. ISSN: 0340-7594. DOI: 10.1007/s00359-004-0518-3.

[80] Hiroshi Shimizu and Yasuji Sawada. "Transplantation phenomena in hydra: Cooperation of position-dependent and structure-dependent factors determines the transplantation result". In: *Developmental Biology* 122.1 (July 1987), pp. 113–119. ISSN: 0012-1606. DOI: 10.1016/0012-1606(87)90337-X.

[81] Hiroshi Shimizu, Yasuji Sawada, and Tsutomu Sugiyama. "Minimum tissue size required for hydra regeneration". In: *Developmental Biology* 155.2 (Feb. 1993), pp. 287–296. ISSN: 00121606. DOI: 10.1006/dbio.1993.1028.

[82] Hiroshi Shimizu, Xiaoming Zhang, Jinsong Zhang, Alexey Leontovich, Kaiyin Fei, Li Yan, and Michael P Sarras. "Epithelial morphogenesis in hydra requires de novo ex-

pression of extracellular matrix components and matrix metalloproteinases". In: *Development* 129.6 (Mar. 2002), 1521 LP –1532.

[83] Stefan Siebert, Jeffrey A. Farrell, Jack F. Cazet, Yashodara Abeykoon, Abby S. Primack, Christine E. Schnitzler, and Celina E. Juliano. "Stem cell differentiation trajectories in Hydra resolved at single-cell resolution". In: *bioRxiv* (Nov. 2018), p. 460154. DOI: 10.1101/460154.

[84] W. Slooff, J.H. Canton, and J.L.M. Hermens. "Comparison of the susceptibility of 22 freshwater species to 15 chemical compounds. I. (Sub)acute toxicity tests". In: *Aquatic Toxicology* 4.2 (Sept. 1983), pp. 113–128. ISSN: 0166-445X. DOI: 10.1016/0166-445X(83)90049-8.

[85] K. M. Smith, L. Gee, and H. R. Bode. "HyAlx, an aristaless-related gene, is involved in tentacle formation in hydra". In: *Development* 127.22 (2000), pp. 4743–4752. ISSN: 09501991.

[86] Robert E. Steele. *Developmental signaling in Hydra: What does it take to build a . Aug. 2002.* DOI: *10.1006/dbio.2002.0744*.

[87] T Sugiyama and T Fujisawa. "Genetic analysis of developmental mechanisms in hydra. II. Isolation and characterization of an interstitial cell-deficient strain". In: *Journal of Cell Science* Vol. 29.2 (Feb. 1978), pp. 35–52. ISSN: 00219533. DOI: 10.1006/dbio.2002.0744.

[88] John R. Szymanski and Rafael Yuste. "Mapping the Whole-Body Muscle Activity of Hydra vulgaris". In: *Current Biology* 29.11 (Aug. 2019), 1807–1817.e3. ISSN: 09609822. DOI: 10.1016/j.cub.2019.05.012.

[89] Toshio Takahashi and Naoya Hamaue. "Molecular characterization of Hydra acetylcholinesterase and its catalytic activity". In: *FEBS Letters* 584.3 (Feb. 2010), pp. 511–516. ISSN: 0014-5793. DOI: 10.1016/J.FEBSLET.2009.11.081.

[90] Yasuharu Takaku, Jung Shan Hwang, Alexander Wolf, Angelika Böttger, Hiroshi Shimizu, Charles N. David, and Takashi Gojobori. "Innexin gap junctions in nerve cells coordinate spontaneous contractile behavior in Hydra polyps". In: *Scientific Reports* 4.1 (May 2015), p. 3573. ISSN: 2045-2322. DOI: 10.1038/srep03573.

[91] U Technau, C Cramer von Laue, F Rentzsch, S Luft, B Hobmayer, H R Bode, and T W Holstein. "Parameters of self-organization in Hydra aggregates." In: *Proceedings of the National Academy of Sciences of the United States of America* 97.22 (Oct. 2000), pp. 12127–31. ISSN: 0027-8424. DOI: 10.1073/pnas.97.22.12127.

[92] Ulrich Technau, Michael A Miller, Diane Bridge, and Robert E Steele. "Arrested apoptosis of nurse cells during Hydra oogenesis and embryogenesis". In: *Developmental Biology* 260.1 (Aug. 2003), pp. 191–206. ISSN: 0012-1606. DOI: 10.1016/S0012-1606(03)00241-0.

[93] P Thévenaz, U E Ruttimann, and M Unser. "A Pyramid Approach to Subpixel Registration Based on Intensity". In: *IEEE Transactions on Image Processing* 7.1 (Aug. 1998), pp. 27–41. ISSN: 00121606. DOI: 10.1006/dbio.2002.0744.

[94] Cassidy M. Tran, Sharon Fu, Trevor Rowe, and Eva Maria S. Collins. "Generation and long-term maintenance of nerve-free hydra". In: *Journal of Visualized Experiments* 2017.125 (Aug. 2017), pp. 199–219. ISSN: 1940087X. DOI: 10.3791/56115.

[95] David A Tuveson and Tyler Jacks. *Modeling human lung cancer in mice: Similarities and shortcomings*. Sept. 1999. DOI: 10.1038/sj.onc.1203107.

[96] J. Wittlieb, F. Anton-Erxleben, T. C. G. Bosch, J. U. Lohmann, and K. Khalturin. "Transgenic Hydra allow in vivo tracking of individual stem cells during morphogenesis". In: *Proceedings of the National Academy of Sciences* 103.16 (Aug. 2006), pp. 6208–6211. ISSN: 0027-8424. DOI: 10.1073/pnas.0510163103.

[97] T. Yao. "Studies on the organizer problem in Pelmatohydra oligactis. I. The induction potency of the implants and the nature of the induced hydranth". In: *J. Exp. Biol* 21.1 (Aug. 1945), pp. 147–150. ISSN: 00121606. DOI: 10.1006/dbio.2002.0744.

4.7 Supporting information

The supporting information may be accessed online at: https://journals.plos.org/plosone/article?id=10.1371/journal.pone.0224221#sec025

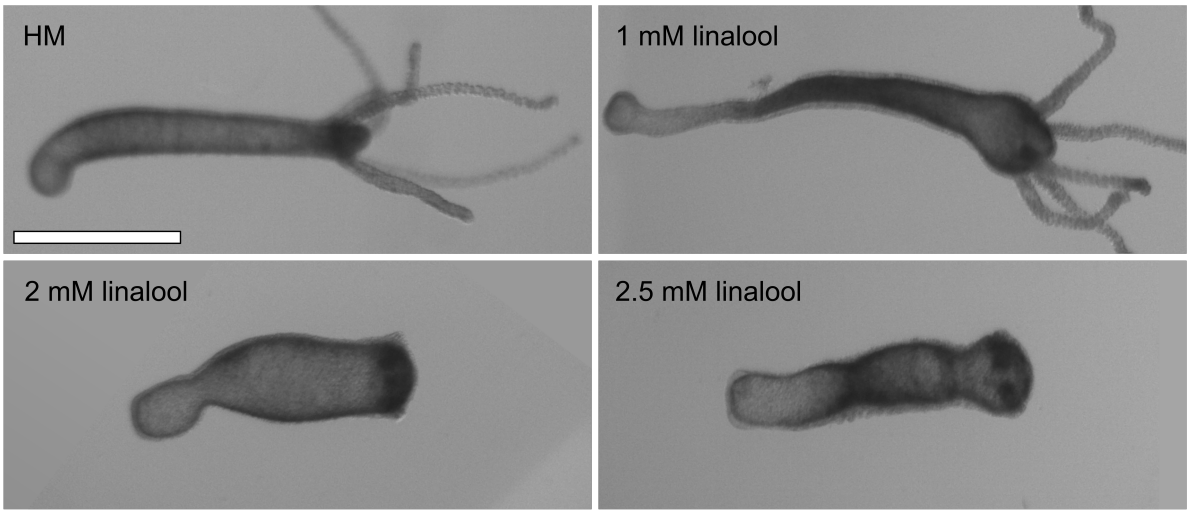

Figure 4.S1: Abnormal morphology of Hydra after 3 h incubation in linalool. Animals are contracted with stubby tentacles in concentrations of 2 mM and 2.5 mM. Images representative of 5/5 animals imaged at the different concentrations. HM denotes Hydra medium control. Scale bar: 1 mm.

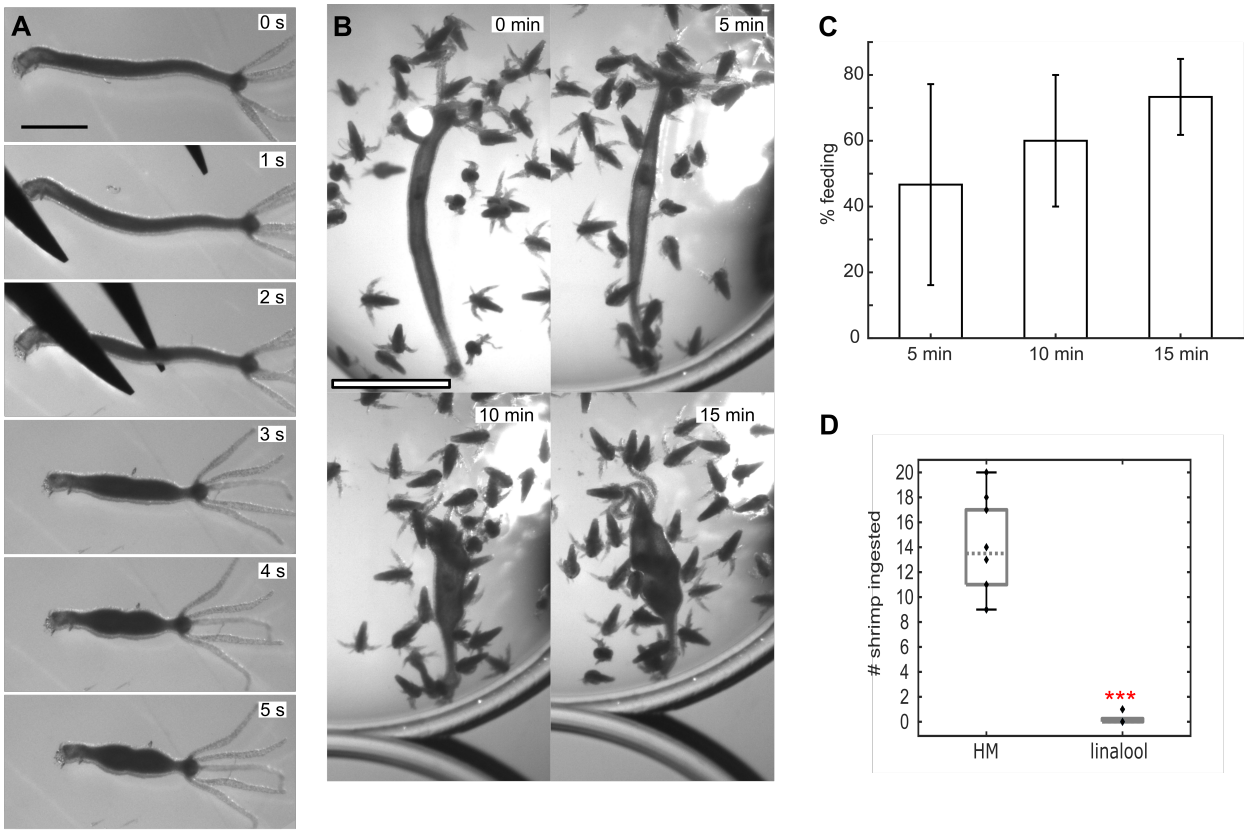

Figure 4.S2: *Hydra* pinch and feeding responses after recovery from 1 mM linalool. A. Animals display a normal pinch response after 5 min recovery in Hydra medium (HM). Image representative of 18/18 polyps across 3 technical replicates. Scale bar: 0.5 mm. B. Feeding after 0, 5, 10, and 15 min recovery in HM. Scale bar: 1mm. C. Percentage of animals that feed after 5 min (47 ± 31% (mean ± SD)), 10 min (60 ± 20%) and 15 min (73 ± 12%) recovery in HM (averages over 3 technical replicates with 5 polyps each). Error bars represent SD. D. Median number of shrimp ingested by each animal incubated in HM for 30 minutes was 13 (11, 16; 25^{th} percentile, 75^{th} percentile) for n = 9 polyps across 2 technical replicates. On the other hand, only 2 out of 9 animals (across 2 technical replicates) kept in 1 mM linalool ingested shrimp in the 30 min. Both animals ingested only one shrimp each. (***) denotes statistically significant difference at $p < 0.001$ (Mann- Whitney U test).

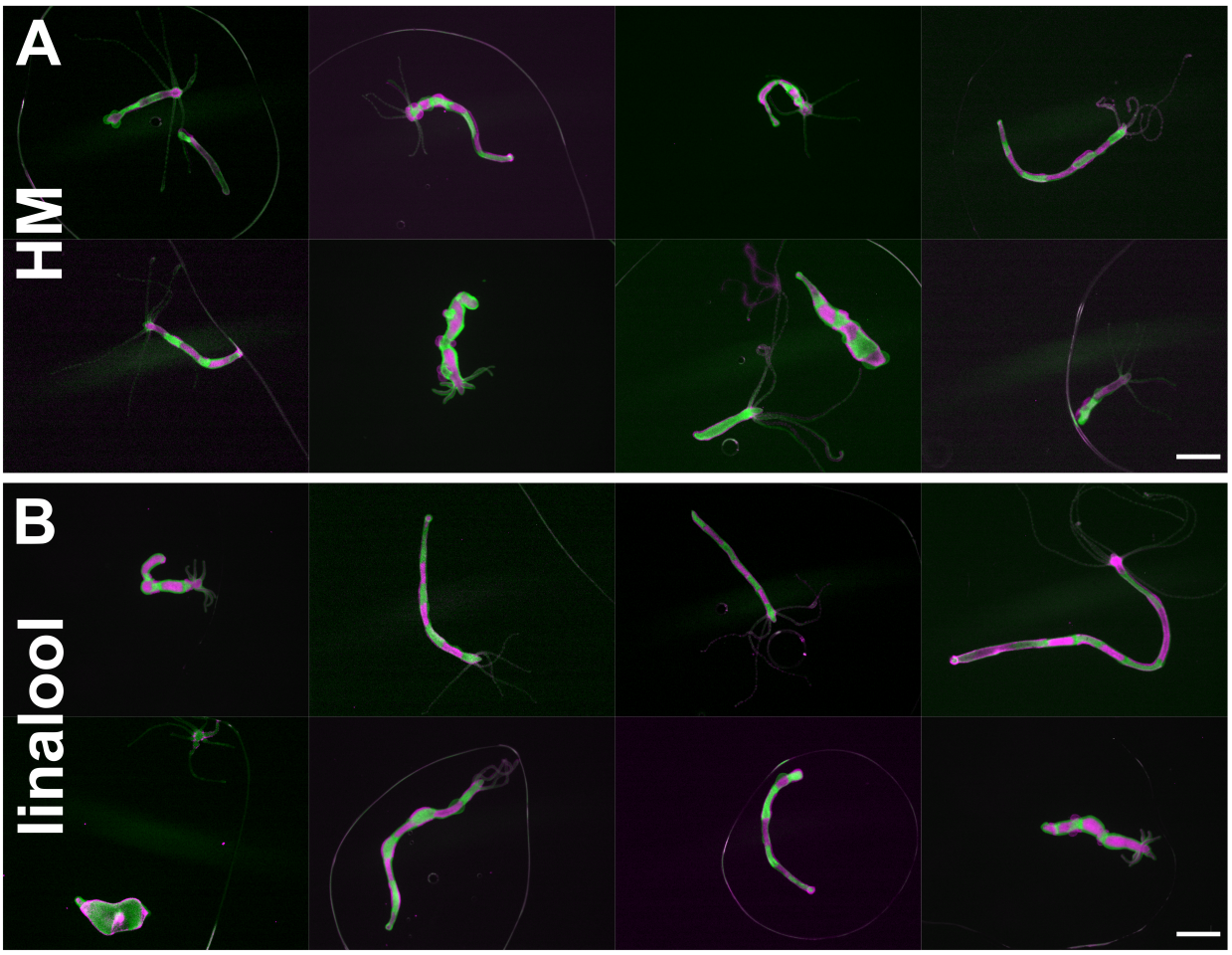

Figure 4.S3: Linalool improves outcome of zebra grafts. A. Zebra grafts conducted in *Hydra* medium (HM), imaged 24 h after grafting. Scale bar: 1 mm. B. Zebra grafts conducted in 1 mM linalool, imaged 24 h after grafting. Scale bar: 1 mm.

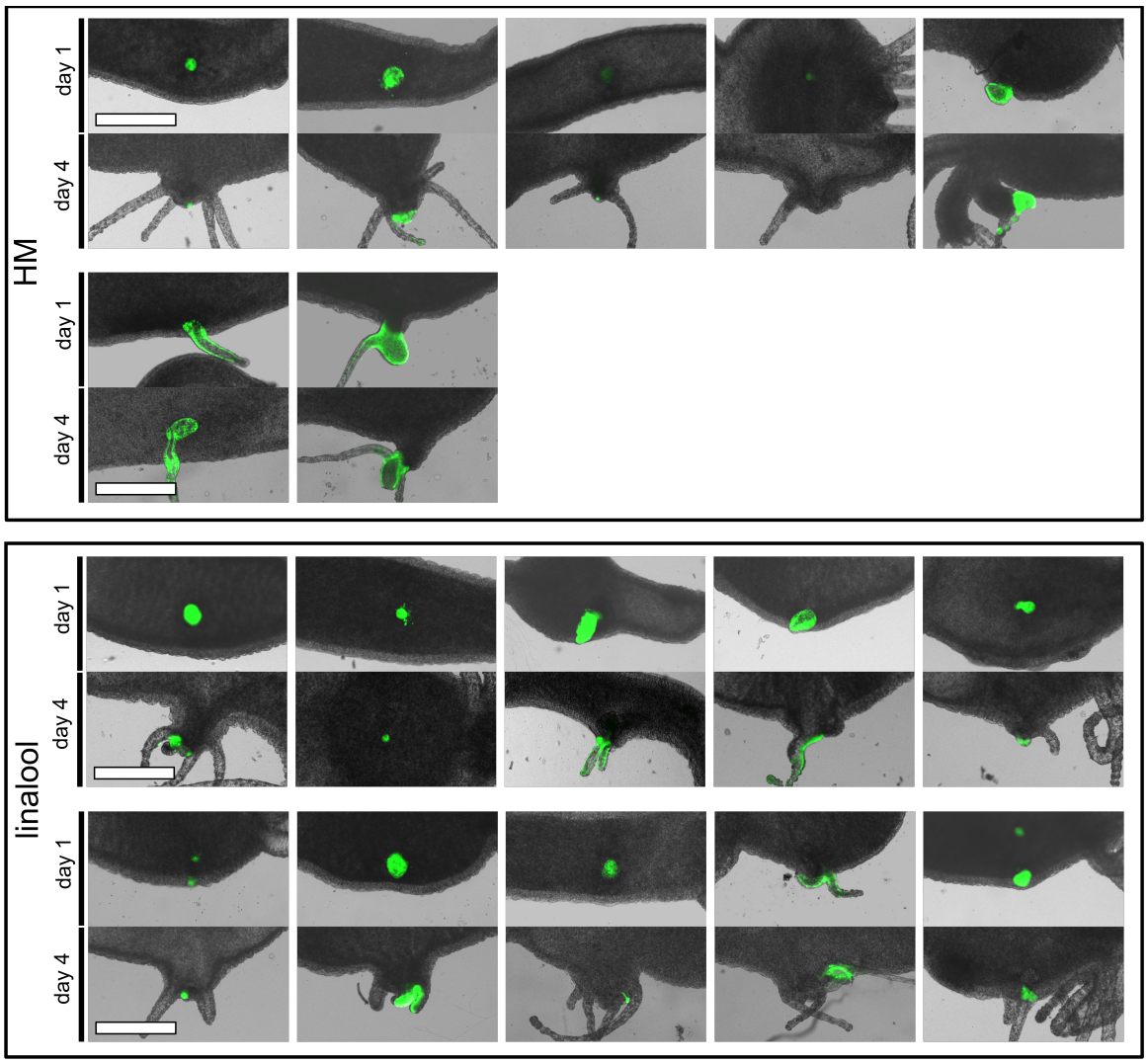

Figure 4.S4: Hypostome graft morphologies. Animals that retained the grafted tissue or formed an ectopic axis, with grafting performed in either *Hydra* medium (HM) or 1 mM linalool (from n = 17 attempts per condition) are shown. Scale bars: 0.5 mm.

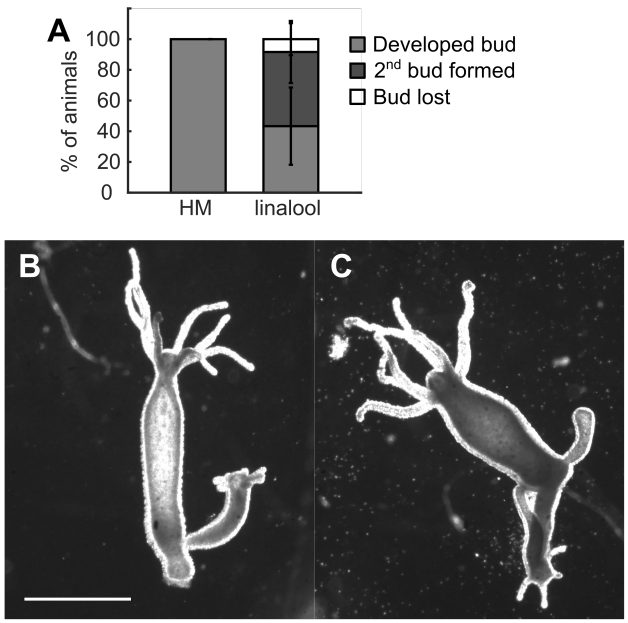

Figure 4.S5: Linalool does not impact budding rate. A. Bud development in budding animals incubated continuously for 3 d in HM or 1 mM linalool, 30 animals per condition across 3 technical replicates. There was no statistically significant difference between animals in HM and in linalool (2-tailed t-test). Error bars represent SD. B. Representative image of animal with fully developed bud. C. Representative image of animal with two buds. Scale bar: 1 mm.

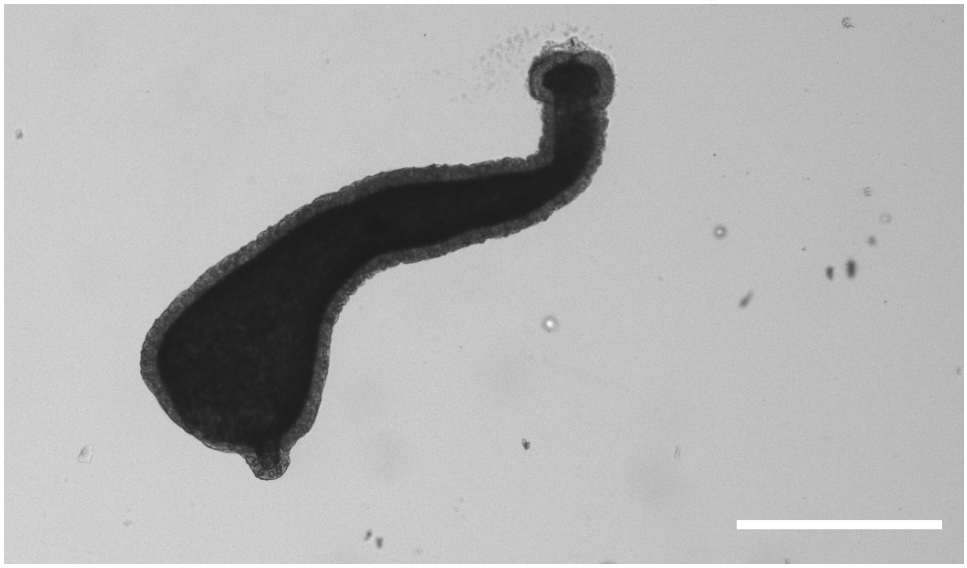

Figure 4.S6: Head regeneration in linalool. 14/42 decapitated polyps across 4 technical replicates regenerated small tentacle buds at the end of 3 d incubation in linalool. Linalool solution was changed every day. The remaining animals did not regenerate head structures. Scale bar: 0.5 mm.

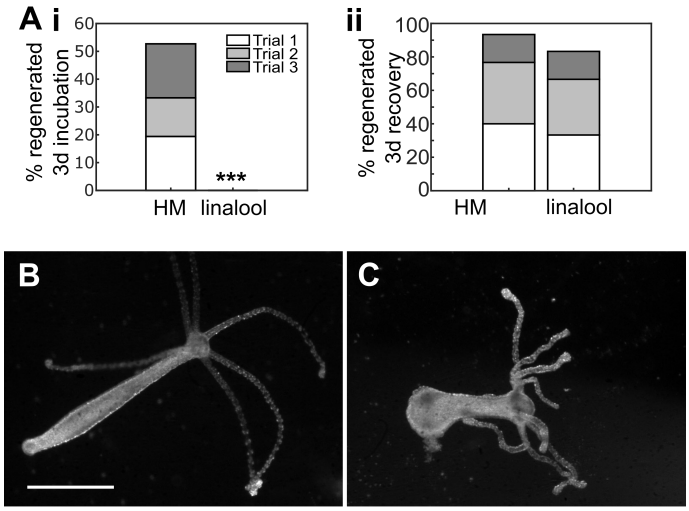

Figure 4.S7: Linalool inhibits foot regeneration. A. i. Three-day incubation in linalool prevents foot regeneration. Data from 36 polyps per condition across 3 technical replicates. (***) denotes statistically significant difference between percentage of animals with regenerated foot in HM and linalool at p ¡ 0.001 (Fisher's exact test) when comparing overall numbers. ii. Phenotype is rescued after 3d recovery in HM. Data from 30 polyps per condition across 3 technical replicates. B. Polyp incubated 3d in HM after foot amputation. C. Polyp incubated 3d in 1 mM linalool after foot amputation. Scale bar: 1 mm.

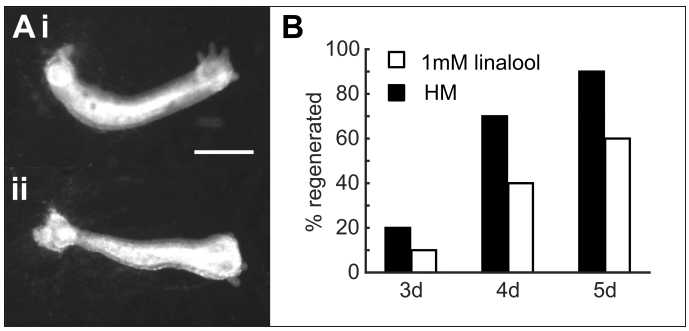

Figure 4.S8: Head regeneration in nerve-free *Hydra* is not negatively impacted by 5-day incubation in linalool. A. Representative images of nerve-free polyps regenerating their heads in i. HM and ii. linalool after 4d incubation. Scale bar: 1 mm. B. Percentage of animals with at least one regenerated tentacle over time (n = 10 animals in 2 technical replicates). There is no statistically significant difference between animals regenerating in HM compared to those regenerating in linalool (Fisher's Exact test).

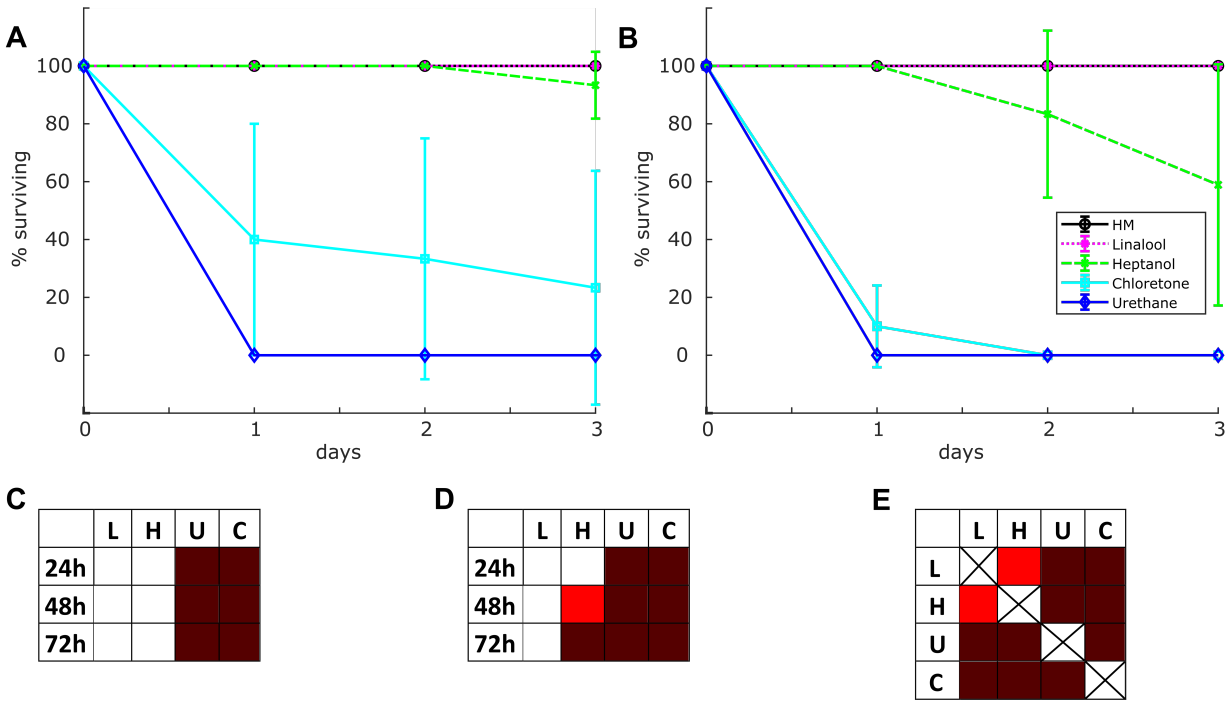

Figure 4.S9: Lethality of 3d incubation in various anesthetics. A. Incubation without changing media. n = 20 animals per condition across 3 technical replicates. Surviving heptanol and chloretone animals had a normal pinch response at 3 d. Surviving linalool animals remained anesthetized. B. Incubation with media exchanged every 24 h. n = 22 animals per condition across 3 technical replicates except for linalool and urethane where 2 technical replicates with 5 animals per replicate were performed. C. Statistical comparison of number of surviving animals at each time point in each anesthetic (without media changes) with the HM control as reference (Fisher's Exact test). D. Statistical comparison of number of surviving animals at each time point in each anesthetic (with media changes) with the HM control as reference (Fisher's Exact test). E. Pairwise statistical comparisons of number of animals surviving at the end of the 3d incubation in the anesthetics (with media changes) (Fisher's Exact test). (C-E) Pink, red and dark red indicate a statistically significant difference at $p<0.05$, $p<0.01$ and $p<0.001$ respectively, determined using the Fisher's Exact test between pairs of anesthetics.

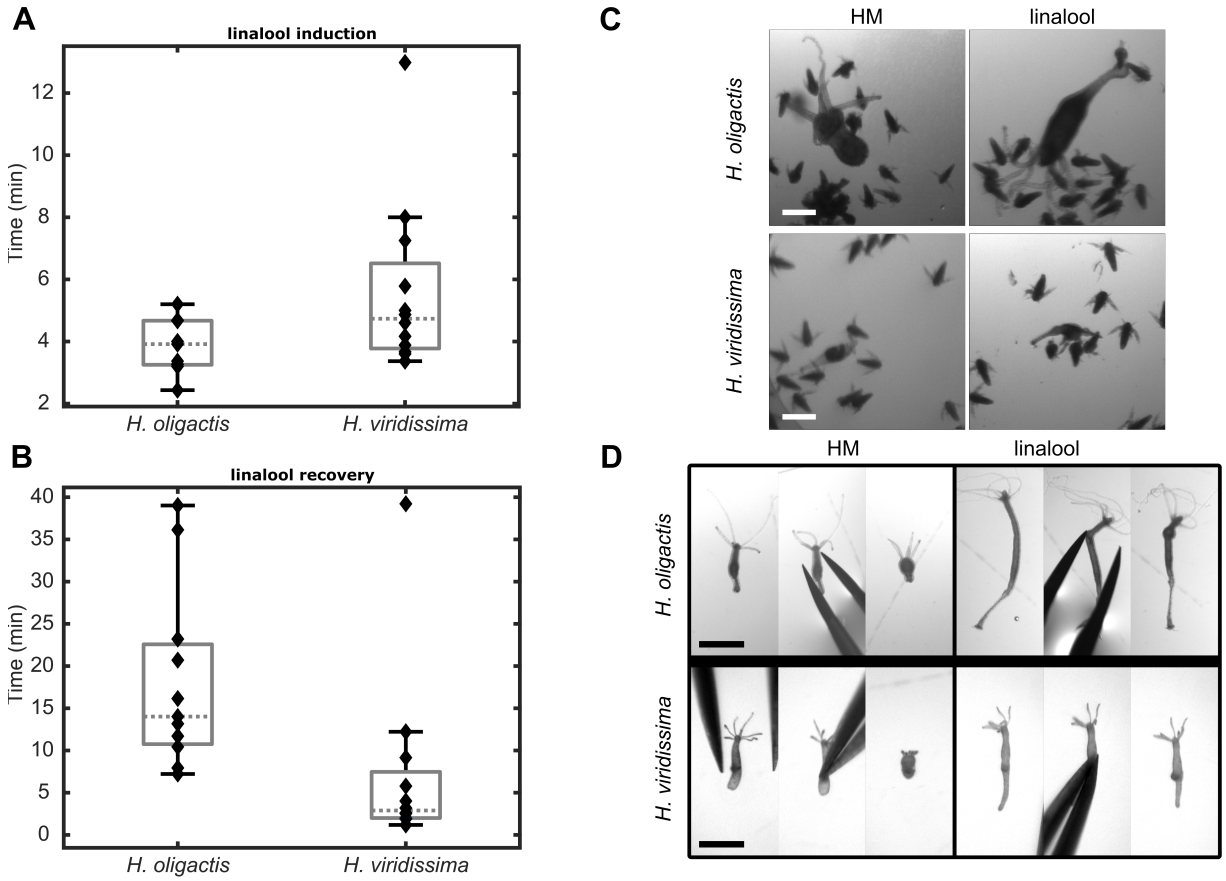

Figure 4.S10: Response of *H. oligactis* and *H. viridissima* to 1 mM linalool. A. Time for induction of anesthesia, measured as time of full extension after last observed contraction burst, in 1 mM linalool (n = 9 for *H. oligactis* across 3 technical replicates, n = 12 for *H. viridissima* across 3 technical replicates). B. Time for recovery from anesthesia, measured as time of first observed contraction burst, after being moved to HM from 1 mM linalool (n = 11 for *H. oligactis* across 3 technical replicates, n = 12 for *H. viridissima* across 3 technical replicates). C. Feeding assay. Feeding is inhibited due to linalool incubation. While animals in linalool have shrimp stuck to their tentacles, they do not have any in their body column, contrary to what is seen with animals in HM. Scale bar 0.5 mm. D. Pinch responses in HM and 1 mM linalool. Pinch response is inhibited by linalool incubation. Scale bar 1mm.

S1 Movie. 1 mM linalool prevents pinch response.
Time-lapse movie of *Hydra* polyp incubated in either *Hydra* medium (HM; left) or in 1 mM linalool for 10 minutes (right). Experimental details provided in Methods in main text. Movie is representative of 10/10 animals across 2 technical replicates. Video playback: 1fps. Scale bar: 1mm.

S2 Movie. 1 mM linalool prevents pinch response in nerve-free animals.
Time-lapse movie of nerve free Hydra polyp incubated in either *Hydra* medium (HM; left) or in 1 mM linalool for 10 minutes (right). Experimental details provided in Methods in main text. Movie is representative of 6/6 tested nerve-free animals across 2 technical replicates. Video playback: 1 fps. Scale bar: 1mm.

S3 Movie. Linalool incubation allows for low magnification time-lapse imaging.
Time-lapse movie of freely moving GCaMP6s animals in either *Hydra* medium (HM; left) or incubated for at least 10 min in 1 mM linalool (LL; right). Experimental details are provided in Methods in the main text and Fig 4.3A shows a Maximum Intensity Projection of the video. Video playback: 10 fps. Scale bar: 100 μm.

S4 Movie. Linalool allows for high magnification time-lapse imaging.
Time-lapse movie showing a z-stack through the body column of a GCaMP6s animal in either *Hydra* medium (HM; left) or incubated for at least 10 min in 1 mM linalool (LL; right). Experimental details are provided in Methods in the main text and Fig 4.2B shows a single slice and the Maximum Intensity Projection of the video. Video playback: 10 fps. Scale bar: 10 μm.

S5 Movie. Linalool treatment allows for multi-channel fluorescence time-lapse imaging.
Time-lapse movie of a 3-channel acquisition of a watermelon animal stained with Hoechst nuclear dye. The head was mounted as described in Carter et al. [18] in 1 mM linalool and flushed with 2 mM reduced glutathione to trigger a feeding reaction. While the mouth stays closed during recording, one can clearly see the quality of imaging that can be obtained in linalool, allowing for simultaneous imaging of cell shapes and nuclear positions. Video playback: 10 fps. Scale bar: 100 μm.

S6 Movie. Linalool does not interfere with calcium imaging.
Time-lapse movie showing calcium activity in epithelial GCaMP animal during chemically induced mouth opening. The head was mounted as described in Carter et al. [18] in 1 mM linalool and flushed with 2 mM reduced glutathione to trigger a feeding reaction. Video playback: 10fps. Scale bar: 100 μm.

S7 Movie. Linalool does not sufficiently immobilize polyps for long term imaging.
Shown first, an unconstrained animal in *Hydra* medium, which exits the field of view within 90 min of recording. In contrast, it is possible to take a 24 h time lapse movie of an unconstrained *Hydra* in 1 mM linalool. However, while linalool incubation significantly improves stability for imaging, the animal moves too much for experiments requiring cellular resolution. Video playback: 10 fps. Scale bar: 0.5 mm.

S8 Movie. Calcium activity in response to pinching.
Time-lapse movie showing calcium activity in epithelial GCaMP animal in response to pinching. Animal in *Hydra* medium (HM) shows the global contraction accompanied by calcium

activity in the entire body column. Animal incubated in linalool only shows calcium activity at the site of pinching. Video playback: 10 fps. Scale bar: 1 mm.

Table 4.S1: Coefficient of variation calculated for t-stacks of GCaMP animals imaged at 4x and z-stacks of GCaMP animals imaged at 60x., (**) indicates statistically significant difference from corresponding imaging in Hydra medium at p ¡ 0.01 as determined by a two-tailed t-test.

	***Hydra* medium**		**1 mM linalool**	
	4x	**60x**	**4x**	**60x**
	0.222	0.152	0.154	0.136
	0.168	0.199	0.145	0.149
	0.195	0.158	0.143	0.099
	0.176	0.183	0.147	0.113
	0.163	0.268	0.139	0.144
	0.172	0.170	0.137	0.084
	0.163		0.143	
	0.148		0.143	
	0.202		0.127	
	0.137		0.156	
mean	**0.175**	**0.188**	**0.143****	**0.121****
stdev	**0.025**	**0.042**	**0.008**	**0.026**

Chapter 5

Inheritance of parental body axis in regenerating *Hydra* fragments

5.1 A novel bilateral grafting technique for studying patterning in *Hydra*

5.1.1 Abstract

Control of patterning and the specification of body axes are fundamental aspects of animal development involving complex interactions between chemical, physical, and genetic signals. The freshwater polyp *Hydra* has long been recognized as a useful model system to address these questions due to its simple anatomy, optical transparency, and strong regenerative abilities, which enabled clever grafting experiments to alter and probe patterning. Reliable methods exist for the transplantation of small tissue pieces into the body column or the combination of sections cut perpendicular to the body axis, which can be used to

examine oral-aboral gradients and axis induction potential of tissue fragments. However, existing methods do not allow researchers to probe questions of axis alignment and lateral information exchange. We therefore developed a technique to produce chimeric animals split longitudinally along the body axis of the animal by anesthetizing the animals with the terpene linalool and threading the donor pieces onto pairs of fine glass needles. Our novel approach can be applied to study questions in *Hydra* research that have thus far been inaccessible, including patterning processes acting perpendicular to the oral-aboral axis and the extent of lateral cell migration.

5.1.2 Introduction

Hydra, a small freshwater cnidarian polyp, is a popular model organism for studying fundamental questions in regeneration and development [14]. Its simple anatomy, a hollow cylinder with a head on one end and an adhesive foot at the other, makes *Hydra* an attractive system to study axis specification and organismal patterning. Since the seminal work by Abraham Trembley in the 18^{th} century, *Hydra*'s potent healing and regenerative abilities have made grafts or transplants of various tissues and structures an invaluable tool for researchers.

Grafts have been utilized previously to investigate the mechanisms controlling axis formation, and more recently in conjunction with genetic engineering to create compound transgenic *Hydra* lines [17]. Established methods exist for the transplantation of small pieces of tissue [9] or for combining sections cut perpendicular to the body axis (e.g. [38]). These techniques have been key to our current understanding of *Hydra* patterning. Transplants of

the hypostome into the body column established the hypostome as the organizer directing head and body axis formation [9, 45]. Grafting pieces of tissue from varying locations along the body axis established that *Hydra* has both head activation and inhibition gradients and allowed an estimate of their dynamics [36, 25, 26]. Grafts constructed from segments of body column have been used to disrupt and reduce the gradients present along the body axis to study the impacts of gradients on patterning [1]. However, the geometry of these top/bottom body column grafts limited their applications to the study of differences along the oral-aboral body axis. The possibility of differences in tissue or biochemical properties perpendicular to the body axis has thus remained challenging to probe directly. This lack of experimental data has led to a tendency in the field to consider *Hydra* a one-dimensional system in both experiments and computational modeling (e.g. [16, 5]), which is a potential oversimplification that should be further investigated.

Here, we present a method for producing a chimera split longitudinally along the body axis of the polyp. The main difficulty in such a construct is securing the long interface of the graft long enough for the two halves to heal together smoothly. The method described below uses fixed pairs of glass needles and the anesthetic linalool [18] to immobilize the graft during healing, allowing for reliable production of bilateral grafts. Using live imaging and phalloidin staining, we show that bilateral grafts heal together smoothly. We have used this novel technique to compare lateral and oral/aboral cell migration in *Hydra*, and to alter the inherited body axis during regeneration of excised tissue.

5.1.3 Materials and Methods

Construction of the needle apparatus

The bilateral grafting procedure requires two parallel needles, which are used to hold the two ends of the graft in place during healing. The needles must be fixed in space as independent movement of the needles will destroy the graft. Glass needles are preferred over alternatives such as metal insect pins, as they are smooth, stiff, and can be hand pulled very thin.

To prepare the glass needles, a Bunsen burner was lit and adjusted to a produce a small flame. A glass capillary (e.g. 20 μL glass capillaries (21-164-2D, Fisher Scientific, Hampton NH)) was held at both ends with the middle of the capillary in the flame to soften the glass. The capillary was rotated during this process to ensure even heating. When the middle of the glass was softened and faintly glowing, the capillary was lifted from the flame while simultaneously pulling on both ends in one smooth, rapid motion, thus separating the two halves and producing a thin needle or thread of glass on each half. It is important to achieve a consistent diameter of 20–30 μm for the needles, as thicker needles will cause too much damage for a successful graft, while thinner ones are too flexible.

The finished needles were broken into pieces approximately 1 cm long using watchmaker's forceps, working over a smooth black benchtop to avoid losing the fragments. To create the needle apparatus, a small drop of liquid superglue (The Original Superglue, Ontario, CA) was placed 2–3 mm away from the long edge of a clean glass slide (e.g. 3" x 1" x 1 mm glass slides (12-544-1, Fisher Scientific)). A needle fragment was placed into the drop of glue using forceps, such that one end was held securely and the other projected over the

edge of the slide (Fig. 5.1A, and B). An overhang of about 0.5 cm is ideal. Too small of an overhang makes fitting the pieces of the graft onto the needles difficult, while too long an overhang makes the needles prone to breakage.

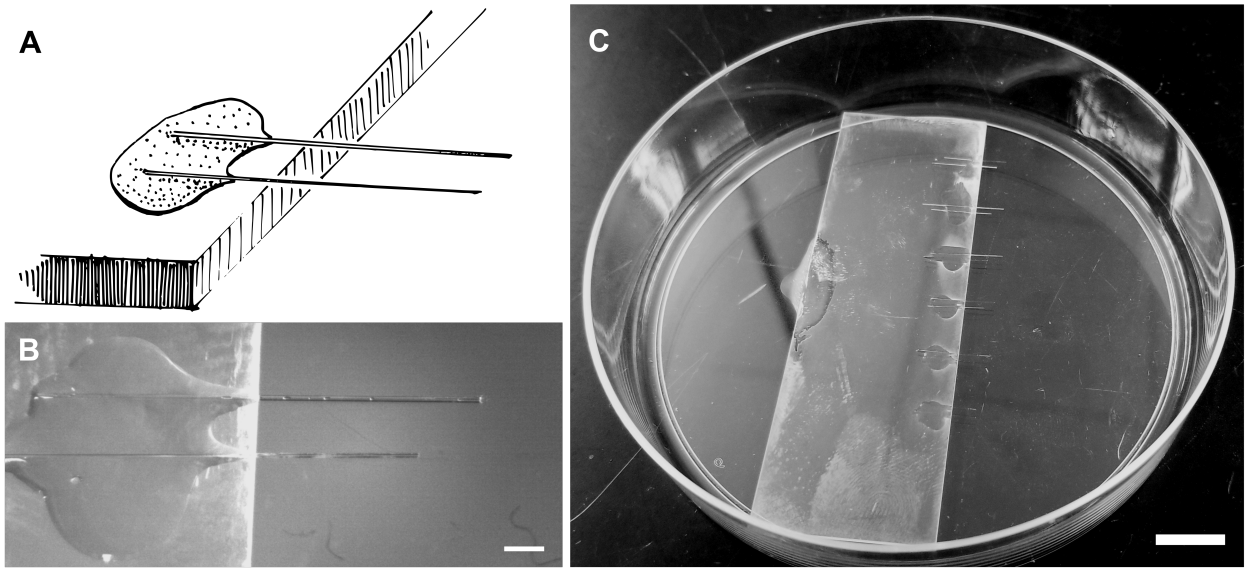

Figure 5.1: Construction of the needle apparatus. A. Schematic of a needle pair. B. Image of a completed needle pair, with the lower needle slightly shorter than the upper. Scale bar, 1 mm. C. Image of completed grafting dish. Scale bar, 1 cm.

A second needle was then added to the same drop of glue and positioned approximately 1 mm away and as close to parallel to the first as possible before the glue set. Subsequent grafting is easier if one needle is at least 1 mm shorter than the other. Spacing can be varied depending on the size of the *Hydra* polyps that will be used. The process is repeated at approximately 1–2 cm intervals on the slide to create more needle pairs, until the full length of the slide is utilized. It is important to leave sufficient space between each pair to allow maneuvering of the *Hydra* pieces with forceps. Once the glue has dried sufficiently for handling (5 min), the slide was placed in a 100 mm Petri dish (961–62084, Spectrum Chemical, New Brunswick NJ). A drop of superglue was placed under the back edge of the slide to secure it to the dish, and the glue was allowed to dry thoroughly for at least 1 h before use.

Grafting procedure

Polyps for grafting were chosen from two strains of *Hydra* that can be distinguished via imaging, e.g. watermelon (WM; GFP ectoderm and RFP endoderm [17]) and AEP (wild type [41, 28]), allowing the quality of the graft to be easily verified. Vital stains, such as neutral red [24] or India ink [10], may also work for this purpose. Two pairs of sharp Dumont forceps #5 (World Precision Instruments, Sarasota, FL) were used to manipulate the tissue pieces, and grafting was conducted under a stereo microscope (American Optical Corporation, Buffalo NY) at 20x magnification over a black background with reflected light.

The 100 mm dish containing the needle apparatus (grafting dish) was filled with approximately 25 mL of a solution of 1 mM linalool (L2602, Sigma-Aldrich) in *Hydra* medium. The solution was mixed by shaking vigorously for 1 min. Linalool is a harmless and re-

versible anesthetic that greatly facilitates manipulation of *Hydra* tissue [18]. Hydra medium (HM) consists of 1 mM $CaCl_2$ (Spectrum Chemical), 0.1 mM $MgCl_2$ (Sigma-Aldrich, St. Louis MO), 0.03 mM KNO_3 (Fisher Scientific), 0.5 mM $NaHCO_3$ (Fisher Scientific), and 0.08 mM $MgSO_4$ (Fisher Scientific), prepared in MilliQ water and adjusted to a final pH of 7–7.3 using sodium bicarbonate and 1 N hydrochloric acid. A second Petri dish was filled with approximately 25 mL of HM. A Kimwipe was cut into small pieces of approximately 2 $\times$ 2 mm.

One large *Hydra* without buds or gonads from each strain was selected, matching the sizes of the animals as closely as possible. Both animals were placed in the dish of HM. Animals were gently pinched or poked near the foot with forceps until mostly contracted, then bisected along the body axis with a no. 10 scalpel in a single cut to avoid ragged or uneven edges. Pieces were discarded if the cut edge was not smooth or if there was enough tissue damage to impact their overall structural integrity. The two halves were transferred to the grafting dish filled with linalool solution and placed near a needle pair.

A small square of Kimwipe was threaded simultaneously onto the two needles and pushed up against the glass slide. One of the *Hydra* halves was then threaded onto the needles, ectoderm side first. The tissue was positioned such that one needle was inserted near the foot and the other near the head, keeping the animal straight between them. This was accomplished by first impaling one end on the longer of the two needles and sliding the tissue down to the position of the second needle. One set of forceps was used to gently grip the free end of the tissue and stretch it over the end of the needle. The second set of forceps was then used to push the tissue onto the needle. Finally, the tissue was carefully pushed down the needles to secure it and make space for further operations. Common problems are

damaging or tearing the tissue with the forceps or snapping the glass needles. The process was repeated to thread the second *Hydra* half on endoderm first. A second piece of Kimwipe was then threaded onto both needles. At this point the pair of needles contained two *Hydra* halves with cut edges facing, sandwiched by two pieces of Kimwipe (Fig. 5.2).

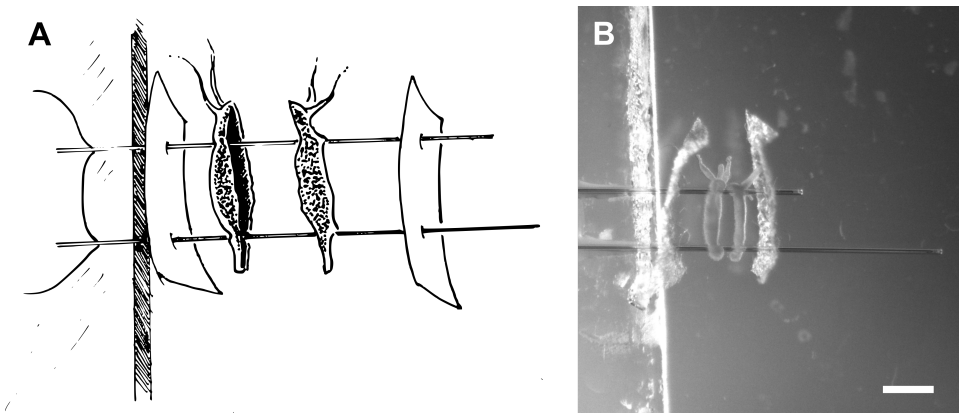

Figure 5.2: Bilateral grafting process. A. Schematic of Kimwipe and tissue on needles. B. Photograph of graft in progress. Scale bar 1 mm.

The second piece of Kimwipe was used to push the *Hydra* tissue against the glass slide, compressing the halves together and bringing the cut edges into contact. Kimwipes worked sufficiently well for our purposes, but sturdier alternatives for graft compression could be explored if Kimwipes are insufficient for a particular experiment. There should be no visible space between the halves along the length of the body column – aligning the head and foot in addition is possible, but more difficult and usually unnecessary. Alignment is easiest if the two animal halves are similarly extended and of similar sizes.

The graft was allowed to heal for approximately 1 h at room temperature. In successful grafts, the cut edges sealed together with no visible gaps between the halves. The outer piece of Kimwipe was then carefully removed and the grafted animal was gently pushed off the needles with Dumont forceps #5. Grafted animals were transferred to a glass dish containing fresh HM and allowed to heal overnight at 18°C.

Prior to use, the animals were examined under a stereo microscope. Any animals showing separation or clearly visible misalignment of the tissue halves were discarded. Animals showing normal body column morphology, with the two halves joined into one coherent hollow body column, were retained for further experiments. If imaging of a fluorescent graft is desired, this can be accomplished using a stereo microscope equipped with a fluorescent light source and the appropriate filters.

Quantification of graft interfaces

Bilateral grafts were made as described above and oral/aboral grafts were made as previously described [18]. Grafts were allowed to heal overnight at 18°C before being imaged. Imaging was conducted by anesthetizing the animal in 1 mM linalool, mounting on a tunnel

slide [18], and capturing an image of each side of the animal using a 4x objective on an EVOS FL Auto microscope (Thermo Fisher Scientific). Animals were imaged on days 1, 5 and 10 after grafting (n = 17 oral/aboral, n = 10 lateral). For long term evaluation of graft interfaces, we measured the length of the interface and divided it by the end-to-end distance, effectively calculating how straight the interface was. For a perfectly straight graft interface, this ratio would be 1; the more rugged the interface, the more this measure deviates from 1. All measurements were conducted manually using Fiji [34]. For oral/aboral grafts, the interface was measured over the full width of the animal. For bilateral grafts the image was rotated until the body axis was horizontal, cropped to a width of 450 pixels, and measurements were taken within this area. This was done to standardize the area being measured and to limit measurements to the body column. Ectoderm and endoderm were measured separately because tissue mismatch between the two layers was sometimes observed upon grafting, and the two epithelial layers have been shown to be displaced along the body axis at different rates [3]. Only non-budding, healthy animals that could be positioned properly were included in the analysis. No animals were excluded on days 1 and 5. 3/10 bilateral grafts and 5/17 oral/aboral grafts were excluded on day 10.

Alsterpaullone treatment

To study axial patterning, some animals were treated with 5 μM alsterpaullone (ALP) for 48 h as described in [8] prior to grafting. Bilateral grafts were then made between two untreated animals (control) or between one ALP-treated and one untreated animal (ALP lateral graft). To assess body column regeneration, the animals (control bilateral graft, ALP bilateral graft, or ungrafted ALP-treated animal) were cut to remove the head and

foot. Body columns were transferred to clean HM, incubated for 3 days at 18°C, and then anesthetized with linalool and imaged on an EVOS microscope.

5.1.4 Results and Discussion

Our method allows the reliable creation of bilateral grafted *Hydra*. One of the most challenging parts of the procedure is getting the two halves successfully onto the needles. Once this step is achieved, approximately 80% of the grafts heal properly. While the technique is difficult to master, with some practice a researcher can consistently produce animals with a clean graft boundary along the entire length of the body column (Fig. 5.3A). Separation of the head and foot above or below the placement of the needles is common and is not a disqualification for experiments requiring only body column tissue. The most common cause of graft failure is separation of the halves after removal from the needles, which can occur due to damage or misalignment of the grafted pieces or due to insufficient pressure on the two halves during healing.

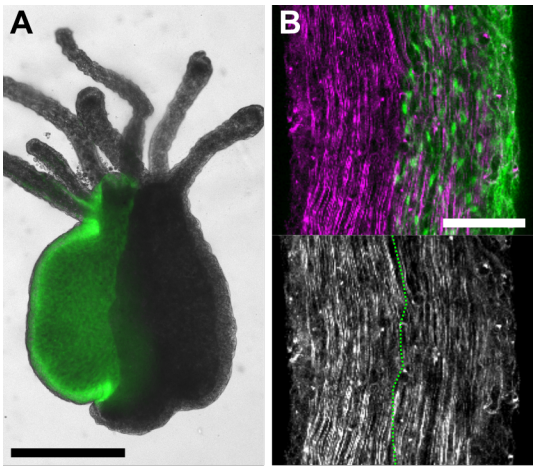

Figure 5.3: Successful grafts with a properly healed boundary. A. Healed bilateral graft with wild type and transgenic halves. Scale bar 0.5 mm. B. Phalloidin staining of healed graft, showing normal myoneme organization along the oral-aboral axis. Upper panel shows myonemes in magenta and transgenic tissue in green. Lower panel shows myonemes only. Scale bar 0.1 mm.

Successfully grafted animals appear to have normal tissue morphology at the graft interface. After 24 h, the halves are fully merged and do not separate when the animal is cut or manipulated. Phalloidin staining reveals normal myoneme organization at the graft boundary (Fig. 5.3B), suggesting that the tissue is structurally normal. Thus, the tissue around the graft boundary is useable in any experiments requiring body columns or tissue pieces. Exceptionally clean grafts with joining of the head and foot can be used in experiments requiring whole animals.

Bilaterally grafted *Hydra* have several applications. First, we explored the possibility of lateral epithelial cell displacement in individual *Hydra*. Previous work has established that *Hydra* cells multiply in the body column and are shed from the tentacles and peduncle in addition to tissue loss via budding [32]. It was additionally observed that cells are displaced as epithelial sheets rather than as individuals, with a "stationary zone" representing the boundary between upward and downward movement present in both endoderm and ectoderm [11, 3]. Logically this would imply that the majority of cell displacement in the animal occurs in the direction parallel to the body axis, with relatively little motion in the direction perpendicular to the body axis. However, lateral cell displacement of the epithelial sheets has never been measured.

By comparing bilaterally grafted animals to oral/aboral grafts, we have for the first time visualized the theorized differences in cell displacement patterns along these two directions. Over time, oral/aboral grafts showed a distinct pattern of widening probability density estimates in both the ectoderm and endoderm (Fig. 5.4Ai), indicating that the tissue displacement along the oral-aboral axis causes a distortion of the graft interface, as seen qualitatively in (Fig. 5.4ii, iii). In contrast, the probability density estimates of bilateral

grafts remain relatively stable over time in both epithelial layers (Fig. 5.4Bi) and the graft interface is observed to remain relatively straight and smooth (Fig. 5.4Bi, iii). Increasing deformation of the interface in oral/aboral but not bilateral grafts indicates that most tissue displacement occurs along the oral-aboral axis over the observed time scale. In addition, we do not observe migration and intermixing of individual cells in agreement with previous publications [11, 32, 3]. However, the presence of an observable distortion of the graft boundary in both tissue layers (see representative Fig. 5.4A iii) suggests that cell displacement of the epithelial layers along the oral-aboral axis does not occur in perfect synchrony. Thus our results agree with previous claims that circumferential movement of epithelial cells is minimal, despite the fact that endodermal cells divide preferentially perpendicular to the body axis [37].

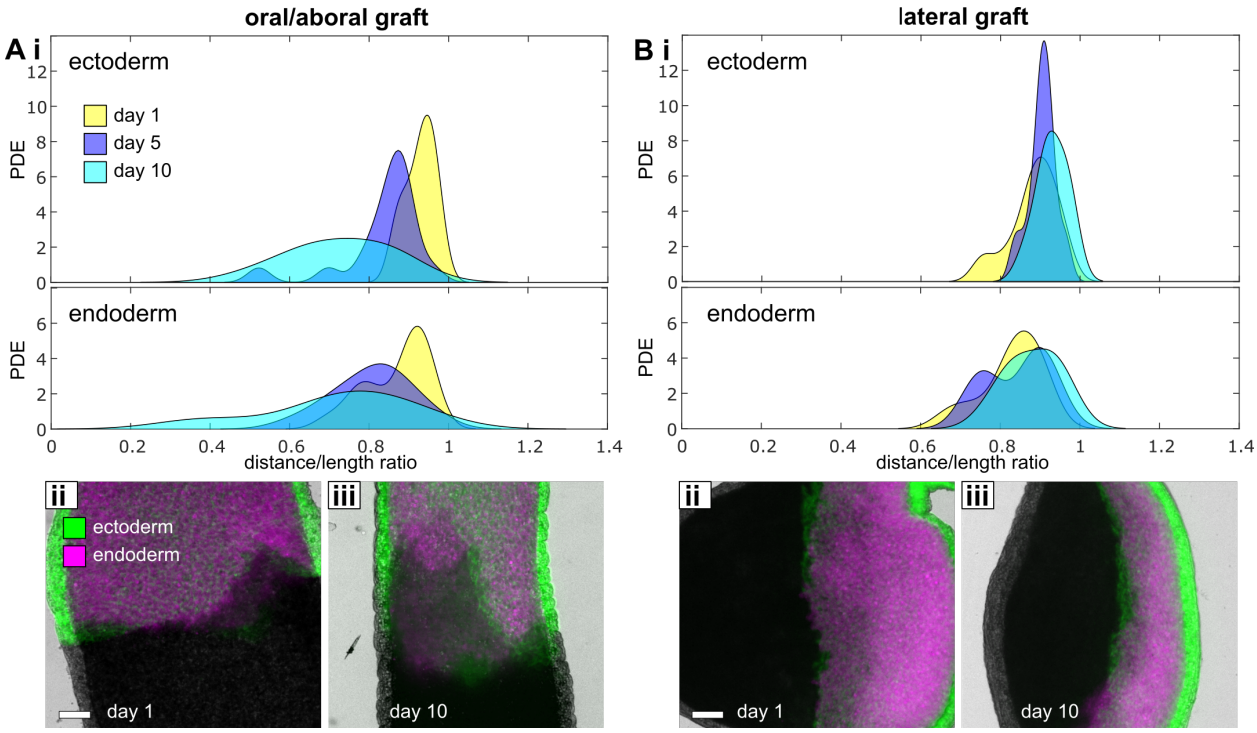

Figure 5.4: Tissue displacement is different in lateral and oral-aboral directions. A. Oral/aboral grafts between WM and AEP animals. i. Probability density estimates (PDE) of distance/length ratio of ectoderm and endoderm graft interfaces at days 1 (n = 17), 5 (n = 17) and 10 (n = 12). ii, iii. Representative images of graft interfaces at day 1 and day 10. Scale bar 100 μm. B. Bilateral grafts between WM and AEP animals. i. PDEs of distance/length ratio of ectoderm and endoderm graft interfaces at days 1 (n = 10), 5 (n = 10) and 10 (n = 8). ii, iii. Representative images of graft interfaces at day 1 and day 10. Scale bar 100 μm.

In the future, bilateral grafts could be used to study longitudinal migration of specific cell types of interest. Nematocytes could be tracked using previously shown *in vivo* staining of nematocysts [18], or interstitial cells and their descendants could be tracked as previously shown using vital dyes [42] or transgenic labeling [6].

As a second application, we investigated whether it was possible to redirect axis formation in a body column cut from a bilateral graft wherein one half was treated with ALP. ALP treatment induces ectopic Wnt expression throughout the animal, resulting in the formation of ectopic tentacles and head structures [8]. The body column of a control bilateral graft animal reliably regenerated with its axis parallel to that of the original animal, as expected if the grafting procedure does not alter normal patterning (Fig. 5.5A). The regenerated body columns of animals treated with ALP for 48 h prior to amputation form uniformly distributed ectopic head structures and sometimes lack an obvious body axis (Fig. 5.5B). By contrast, in bilaterally grafted body columns wherein one half was treated with ALP for 48 h prior to grafting, formation of ectopic head structures occurred mostly in the treated tissue and many of the regenerates showed elongation in a direction perpendicular to the original axis (Fig. 5.5C). This outcome is distinctly different from both control grafts and ungrafted ALP animals (Fig. 5.5).

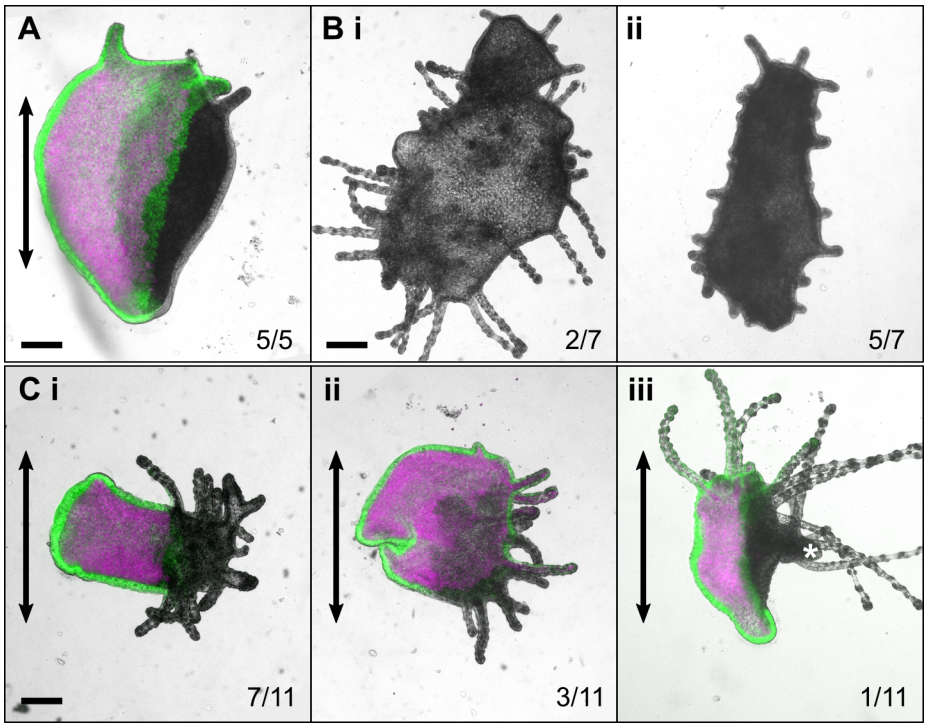

Figure 5.5: Regeneration outcomes of body columns. A. Control bilateral graft, showing retention of parental phenotype. Arrow indicates parental body axis. B. Alsterpaullone-treated animal. i. Numerous ectopic tentacles with no clearly defined body axis. ii. Ectopic tentacles with defined body axis. C. Bilateral graft between alsterpaullone treated (unlabeled) and untreated (WM) animals shows ectopic head structures arising from treated tissue. Arrows indicate direction of parental body axis. i. Elongation in direction perpendicular to parental axis. ii. No clear body axis. iii. Ectopic head (*) formed from ALP tissue, body axis parallel to parental axis. Scale bars 0.25 mm.

Taken together, these data suggest that it is possible to overwrite the endogenous axis orientation in body columns by applying a large domain of ectopic Wnt signaling perpendicular to the original axis. This ability is distinct from previous experiments which altered patterning by grafting a head organizer into the body column (e.g. [9]. Rather than inserting a point source of Wnt, we can create a region at the graft interface where the strongest decrease in Wnt signaling is uniformly perpendicular to the natural gradient. Isolating and studying this region could lead to novel insights into the mechanisms of pattern formation.

5.1.5 Conclusion

We present a detailed protocol for a novel method of generating bilateral grafts in *Hydra*, parallel to the oral-aboral body axis. Historically, grafting experiments have been used to probe the graded properties underlying *Hydra* patterning. While the advent of modern molecular biology and genetic manipulation has opened many new avenues of exploration, combining these new tools with advances in grafting has potential for addressing novel questions in *Hydra* research. In this paper we have shown proof of principle experiments using bilateral grafts to explore directional cell displacement and altered patterning. This technique could further be applied to observing movement of specific cell types or to probe the mechanisms of patterning during regeneration.

5.1.6 Acknowledgements

We thank Sara Martin for help with animal care and discussions, and Drs. Danielle Ireland and Robert Steele for comments on the manuscript. This work was supported by

NSF grant CMMI-1463572, the Research Corporation for Science Advancement, and the Gordon and Betty Moore Foundation.

5.2 Wnt signaling determines body axis polarity in regenerating *Hydra* tissue fragments

5.2.1 Abstract

How an animal establishes its body axis is a fundamental question in developmental biology. The freshwater cnidarian *Hydra* is an attractive model for studying axis formation because it is radially symmetric, with a single oral-aboral axis. It was recently proposed that the orientation of the new body axis in a regenerating Hydra polyp is determined by the oral-aboral orientation of the actin-myosin contractile processes (myonemes) in the animal's outer epithelial layer. However, it remained unclear how the oral-aboral polarity of the body axis would be defined. As Wnt signaling is known to control axis polarity in *Hydra* and bilaterians, we hypothesized that it plays a role in axis formation during regeneration of *Hydra* tissue pieces. We tested this hypothesis using pharmacological perturbations and novel grafting experiments to set Wnt signaling and myoneme orientation perpendicular to each other to determine which controls axis formation. Our results demonstrate that Wnt signaling is the dominant encoder of axis orientation and polarity, in line with its conserved role in axial patterning.

5.2.2 Introduction

The coordinated interplay of chemical and mechanical signaling is critical for patterning in metazoans (e.g. [27]), but the contribution of each type of signaling can be difficult to determine in a living animal. The freshwater cnidarian *Hydra* - with its ability to regen-

erate from excised tissue pieces and even from aggregates of cells [16] - has long been used to study pattern formation [29] and is now being developed as a model for biomechanical studies [23, 30, 44, 12], as it enables *in vivo* examination of the mechanochemical basis of pattern formation.

Patterning in *Hydra* has been shown in classical grafting experiments to involve graded properties, such as head activation and head inhibition [25]. These gradients, which are established by the head organizer [7], run parallel to the oral/aboral axis. The *Hydra* head organizer relies on the canonical Wnt signaling pathway [8, 21, 19, 31], and it is generally assumed that Wnt signaling is graded along the oral/aboral axis. However, it has not been possible to visualize and quantify biochemical gradients directly in the living animal. Thus, how the head organizer and the oral/aboral axis are established and maintained has yet to be conclusively determined and can only be addressed indirectly. Experiments with cell aggregates and small tissue fragments may be key to finding these answers. While larger *Hydra* tissue fragments such as rings or strips retain parental axis information [23, 39], both aggregates of cells [15] and small tissue fragments form hollow spheriods during regeneration, thus apparently losing axial asymmetry [39, 13]. Because the regenerating spheroids undergo large osmotically driven shape oscillations [20], it was proposed that crosstalk between mechanical forces and Wnt signaling governs patterning [30, 39]. While this is an attractive idea, *Hydra* patterning can be explained by the Gierer-Meinhardt reaction-diffusion model without the need for mechanical cues [16] and the role of mechanics in *Hydra* patterning remains to be shown experimentally.

However, it was recently shown that small tissue pieces retain domains of organized actin-myosin contractile elements (myonemes) in the ectoderm that persist through regener-

ation [23]. Phalloidin staining and *in vivo* observations of ectodermal myoneme orientation during regeneration using a LifeAct-ectoderm transgenic line revealed that the regenerated body axis was parallel to the initial myoneme orientation. Based on these findings, it was proposed that small pieces of *Hydra* tissue inherit the parental body axis through myonemes oriented parallel to the body axis in the ectoderm [23], and the mechanical forces they exert. While the work in [23] shows a correlation between myoneme orientation and axis orientation, it does not establish a causal link. Ectodermal myonemes run parallel to the parental body axis in the same manner as head activation and head inhibition gradients, which were not studied in [23]; therefore, the conclusion that "the inherited actin organization determines the body axis in regenerating tissues" [23] is in need of further experimental study. Moreover, the experiments presented in [23] do not address the question of how the oral/aboral polarity of the body axis is determined.

We therefore developed experiments to 1) investigate what sets axial polarity in small tissue pieces, and 2) uncouple the ectodermal myoneme orientation from a signaling gradient involved in axial patterning to determine which factor was key in establishing the body axis orientation in regenerating *Hydra* tissue spheroids. This is impossible using established grafting and manipulation techniques, but can be achieved using our novel technique of bilateral grafting to examine effects perpendicular to the body axis [43]. By using a combination of grafting experiments and manipulation of canonical Wnt signaling via alsterpaullone (ALP) treatment, we demonstrate that Wnt signaling defines axis polarity and directs myoneme orientation in regenerating *Hydra* tissue pieces.

5.2.3 Results and Discussion

First, we took advantage of a traditional *Hydra* grafting technique [18] to test polarity inheritance in regenerating tissue pieces. We generated oral-aboral grafts between a transgenic line expressing GFP in the ectoderm and DsRed 2 in the endoderm [17] and non-transgenic polyps, both bisected perpendicular to the body axis (Fig. 5.6A). Excising tissue pieces from the graft interface allowed us to determine the orientation of the regenerated axis relative to the axis of the grafted animal (Fig. 5.6A, B). Axis polarity was assayed by determining whether the tissue piece giving rise to the regenerated head was the same as that in the oral half of the grafted animal (Fig. 5.6Bi, ii). Of these grafts, 37/40 retained the polarity of the grafted animal and 3/40 reversed it (Fig. 5.6C). These data show that axis information is inherited in small tissue pieces, in agreement with [23]. Furthermore, these grafting experiments yield an additional new insight. They suggest that although the parental biochemical gradient may be distorted as tissue folds to form a spheroid [23], small intercellular differences in head competency are sufficient to set the polarity of the future axis.

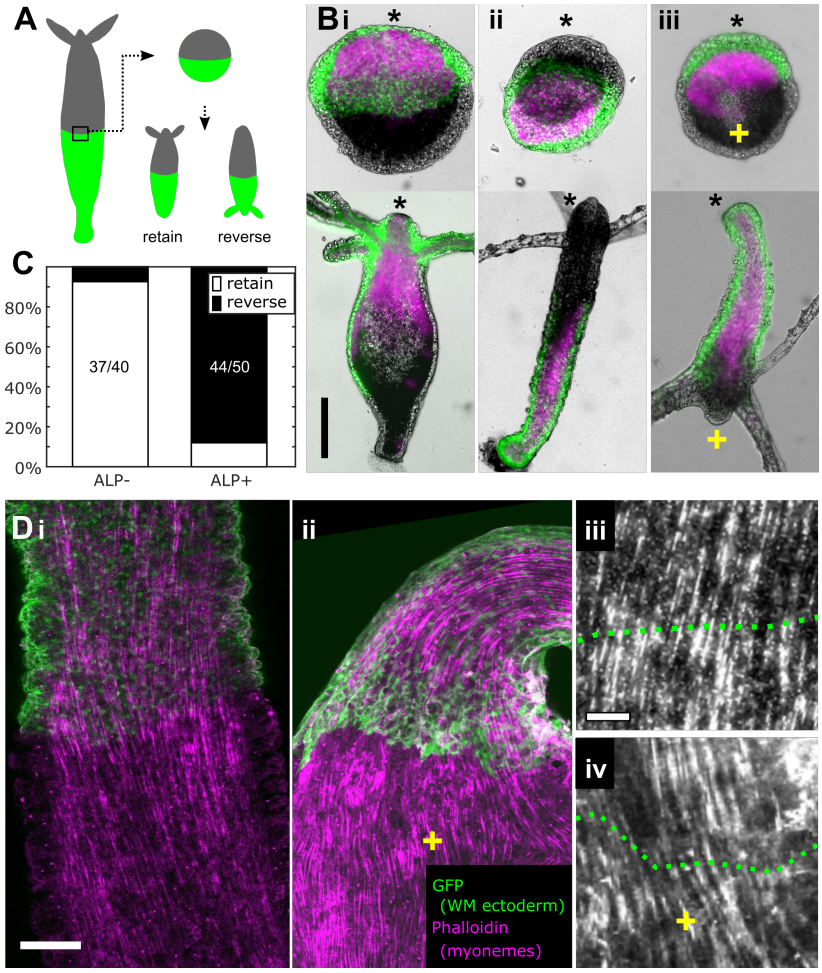

Figure 5.6: Inherited axial polarity can be reversed by ectopic Wnt signaling. A. Schematic of an oral/aboral graft and possible outcomes. B. Representative examples of tissue pieces from the interface of oral/aboral grafts, before (top) and after (bottom) regeneration, imaged at 4–5 days post excision. Asterisks indicate the direction of the parental head where known. Yellow crosses indicate ALP-treated tissue. (i) Control with fluorescent (WM; GFP ectoderm and RFP endoderm) head, (ii) control with WM foot and (iii) animal with WM head and ALP-treated foot (ALP+) and WM head. Scale bar is 200 μm. C. Axis polarity results for control (ALP-) and ALP+ oral/aboral grafts (p = 1.896e-15). Only images taken at the same time point (4 days post excision) were included in the statistical analysis. D. Phalloidin staining of oral/aboral grafts. i. ALP-, ii. ALP+. Scale bar is 100 μm iii. ALP-, iv. ALP+ show graft interface at higher magnification. Scale bar is 25 μm.

To further test this idea, we perturbed Wnt signaling by grafting the lower half of an ALP-treated polyp to the upper half of an untreated polyp. Normally *Hydra* expresses Wnt in the head organizer, while ALP causes ectopic Wnt signaling throughout the animal [8]. Grafted animals in this case have normal Wnt signaling in the oral half, and ectopic Wnt signaling in the aboral half (Fig. 5.6 Biii). Of these ALP+ grafts, 6/50 retained the original polarity while 44/50 reversed it, a significant difference from untreated grafts (p = 1.896e-15) (Fig. 5.6C). Myoneme organization at the graft interface was visualized using phalloidin [44] and appeared normal, with ectodermal myonemes parallel to the body axis in both ALP+ and ALP- grafts (Fig. 5.6D). Taken together, the data from these oral-aboral grafts demonstrate that while tissue pieces retain their original myoneme organization, their axis polarity can be reversed by ectopic Wnt signaling in the lower half of the grafted animal.

Because ectodermal myonemes and Wnt signaling are both oriented parallel to the body axis, existing experimental techniques such as oral/aboral grafts can only establish correlations between regeneration outcomes and one or both of these factors. To determine whether causality can be attributed to one of them, it was necessary to set myoneme orientation and Wnt signaling in direct conflict to ascertain their contributions to the inheritance of axis orientation and polarity.

We engineered such a situation using bilateral grafts (Fig. 5.7A and B), a newly developed technique that produces a chimeric animal split parallel to the body axis [43]. By combining a donor half treated with ALP with an untreated donor half, we created a chimera in which Wnt signaling is highest in the ALP-treated half of the animal, perpendicular to the body axis (Fig. 5.7B). While alignment of the ectodermal myonemes was parallel to the body axis in untreated control grafts, we observed some myoneme reorientation perpendicular to

the body axis in ALP+ grafts at < 24 h post-grafting (Fig. 5.7C), suggesting that Wnt signaling can redirect myoneme orientation.

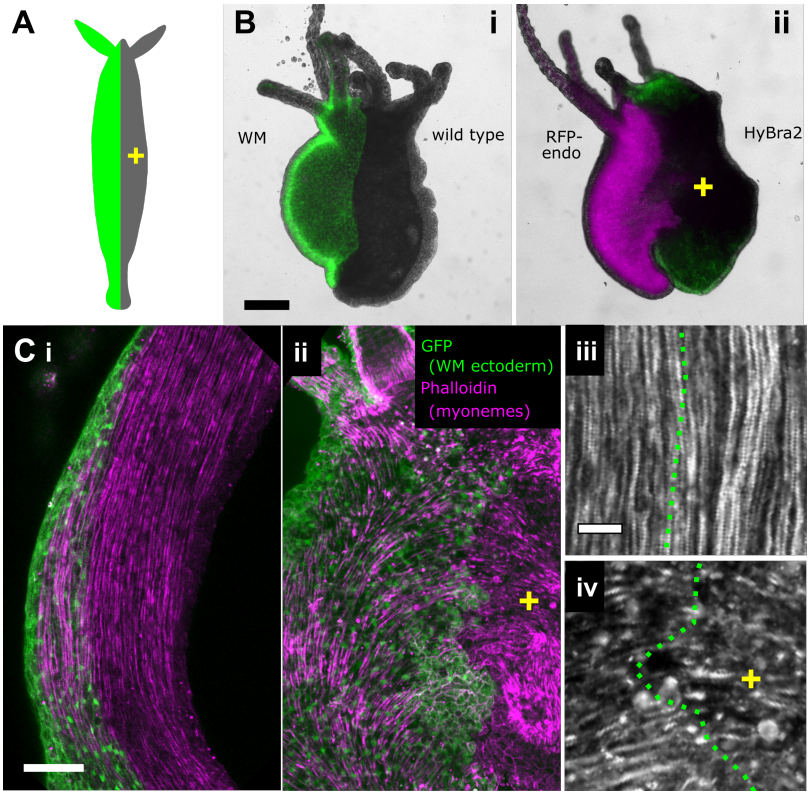

Figure 5.7: Bilateral grafting and ALP treatment allow setting axial gradients and myonemes perpendicular to each other. A. Schematic of a bilateral graft. B. Examples of live bilaterally grafted animals. i. Control graft between WM (left) and wild type (right) animals. ii. ALP+ graft between untreated RFP-endoderm (left) and treated HyBra2-GFP (right) animals. The HyBra2-GFP line contains a transgene in which the HyBra2 promoter drives expression of GFP [17]. HyBra2 is a T-box gene expressed in the hypostome and is used here as an early indicator of ectopic head structures [4]. Yellow cross indicates ALP-treated tissue. Scale bar 250 μm. C. Phalloidin staining of bilateral grafts. i. ALP-, ii. ALP+. Scale bar is 100 μm iii. ALP-, iv. ALP+ show graft interface at higher magnification. Scale bar is 25 μm.

This observation is in line with previous work, which showed that canonical Wnt signaling is essential for axial patterning and can redirect myoneme orientation. For example, during budding in *Hydra*, Wnt genes are consistently expressed as early as budding stage 1 [8], when reorientation of myonemes has not yet occurred [32]. More recent observations of the budding process suggest that actin reorientation occurs in response to biochemical cues [2] and show that noncanonical Wnt signaling defines the sites of tissue evagination where heads and tentacles will form [33]. Furthermore, in cell aggregates, which lack a head organizer or any preexisting myoneme structure, clearly defined patches of Wnt expression consistent with head organizers are observed by 48 h [19] whereas large domains of organized myonemes are not seen until 60 h [35]. Finally, head organizer tissue grafted into the body column induces an ectopic body axis (see e.g. [9]), which requires the reorientation of surrounding myonemes similar to what is observed during budding. This evidence that a change in Wnt signaling precedes myoneme orientation is consistent with our observation that myonemes reorient perpendicular to the graft interface in ALP+ bilateral grafts in less than 24 h (Fig. 5.7 Civ).

Therefore, based on our results from the oral-aboral grafts and the observed redirection of myoneme orientation in ALP+ bilateral grafts, we expect tissue pieces cut from the interface of bilateral grafts to form their body axes parallel to the inherited Wnt signaling differential - independent of parental myonemes.

Tissue pieces cut from the interface of ALP + bilateral chimeras (n = 23) were compared to those originating from bilateral grafts of untreated animals (n = 22) (Fig. 5.8). If initial myoneme orientation determines axis orientation without the involvement of Wnt signaling, tissue pieces from the interface of an ALP+ bilateral graft should regenerate with

a split between labeled and unlabeled tissue parallel to the body axis as seen in control bilateral grafts. Alternatively, if Wnt signaling determines axis orientation, they should show ALP+ tissue in the head (Fig. 5.8A).

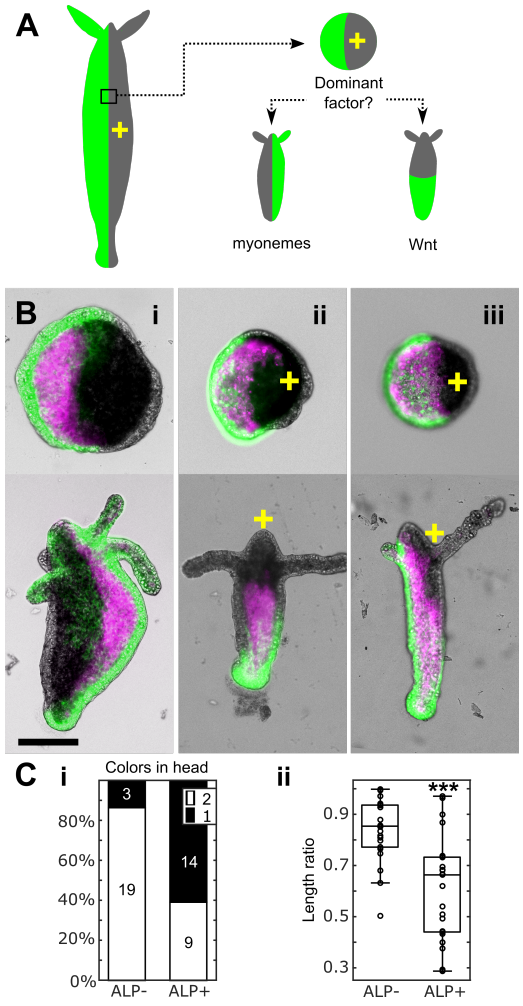

Figure 5.8: Wnt signaling overrides structural cues to set regenerated axis. A. Schematic of ALP+ bilateral graft and possible regeneration outcomes. B. Examples of tissue pieces from the interface of bilateral grafts before (top) and after (bottom) regeneration, showing observed outcomes. i. ALP- control. ii, iii. ALP+. Yellow crosses indicate ALP-treated tissue. Scale bar is 200 μm. C. Quantification of regeneration outcomes. i. Number of strains in head (p = 0.0018). ii. Interface/body length ratio (p = 1.5651e-04). ***p $<$ 0.001. Only images taken at the same time point (4 days post excision) were included in the statistical analysis.

Two scoring metrics were used to account for variability caused by the grafting procedure: number of tissue types (ALP treated/untreated) in the head and the ratio of the length of the interface between the two tissue types to body length (Methods). We found statistically significant differences between ALP+ and ALP- bilateral grafts ($p < 0.05$; Fig. 5.8B and C), demonstrating that Wnt signaling defines oral-aboral polarity and overrides the role of myonemes in setting body axis orientation.

One could argue that under physiologically relevant conditions, the body axis could be set by myoneme orientation, and that the high level of Wnt signaling induced by ALP treatment could override mechanical signals. To directly test whether physiological Wnt signaling levels can override preexisting myoneme orientation, we carried out "quadrant" bilateral grafts (Fig. 5.9A and B). These were created by matching the donor quadrant to the recipient half (control), or by using a mismatch (m) to appose tissue from the oral and aboral ends of two animals. Mismatch grafts exploit the physiological differences in Wnt signaling along the body axis [25, 26, 7] to create a Wnt signaling differential perpendicular to the body axis. The biochemical differences between the upper and lower halves of an animal are larger than those expected within an ungrafted small tissue fragment, but the process of bringing together mismatched domains of tissue can be considered analogous to what occurs during the folding and rounding of a fragment into a spheroid.

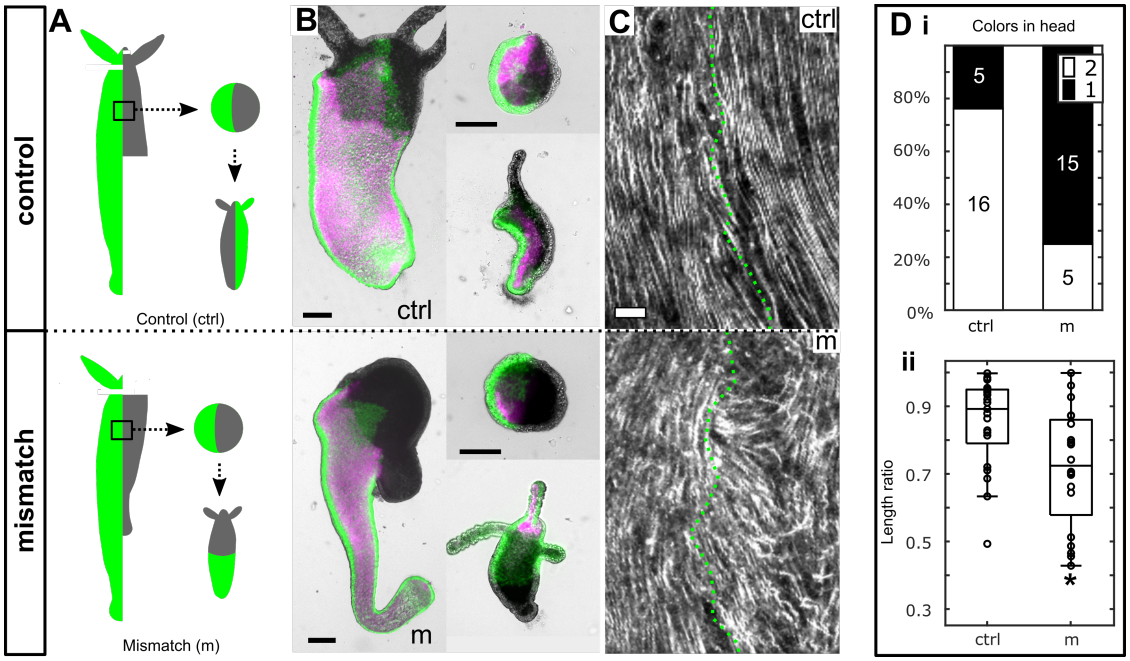

Figure 5.9: Physiological Wnt signaling differentials set the regenerated axis. A. Schematics of control (ctrl) and mismatch (m) quadrant bilateral grafts. B. Representative images of quadrant bilateral grafts. Scale bars 200 μm. C. Phalloidin staining of quadrant graft interfaces. Scale bar 25 μm. D. Quantification of control vs. mismatch quadrant grafts. i. Number of strains in head ($p = 0.0017$). ii. Interface/body length ratio ($p = 0.011$). *$p < 0.05$. Only images taken at the same time point (4 days post excision) were included in the statistical analysis.

While control grafts showed no misalignment of myonemes due to the grafting procedure, mismatch grafts showed signs of myoneme reorientation (Fig. 5.9C), similar to what we observed in ALP+ bilateral grafts (Fig. 5.7C). Therefore, we hypothesized that: 1) tissue pieces cut from the interface of control quadrant grafts would behave like those cut from full bilateral grafts, and 2) that if physiologically relevant Wnt differentials can override myoneme orientation to set a body axis, tissue pieces excised from mismatch grafts would behave similarly to those excised from ALP+ bilateral grafts. Alternatively, if our previous results were due to unnaturally high Wnt signaling in the ALP+ treated tissue, tissue pieces excised from mismatch quadrant grafts would behave similarly to those excised from control grafts or ALP- bilateral grafts.

We observed that tissue pieces cut from the interface of quadrant grafts without a mismatch were significantly different from those with a mismatch (Fig. 5.9D). In addition, mismatch quadrant grafts were statistically similar to ALP+ bilateral grafts while control quadrant grafts were similar to ALP- bilateral grafts (5.1). These results indicate that quadrant grafting does not alter regeneration, but that physiologically relevant differences in Wnt signaling can override structural cues in establishing a new axis.

Table 5.1: P-values resulting from statistical comparison of scoring metrics for regenerated tissue pieces from quadrant grafts. The grey shading represents $p < 0.05$.

	Number of strains in head	**Length ratio**
ALP+ vs. ALP-	0.0018	1.57E-04
ctrl quadrant vs. m quadrant	0.0017	0.011
ctrl quadrant vs. ALP-	0.4566	0.7065
ctrl quadrant vs. ALP+	0.0173	2.47E-04
m quadrant vs. ALP-	1.12E-04	0.0151
m quadrant vs. ALP+	0.3528	0.0735

Our findings disagree with previous claims that small tissue spheroids of the size used here lose all parental signaling differentials [39]. Parental Wnt signaling gradients are likely distorted by the folding and rounding of the tissue fragment [23]; however, domains with quantifiable differences in head induction potential ("head competency") within the spheroid remain sufficient to establish a new head, as shown in the oral/aboral graft experiments (Fig. 5.6C). In fact, MacWilliams showed that small pieces of body column tissue have different head induction potential depending on where they originated from along the body axis [25, 26]; the closer the graft's origin was to the donor head, the higher its potential for head formation in the recipient body column. In addition, the head formation frequency of the graft was shown to increase with increased distance from the recipient head. These experiments were independently confirmed by Takano and Sugiyama [40], who similarly showed that tissue fragments consisting of ∼5000 cells extracted from different positions along the body column of a donor animal had markedly different likelihoods of inducing ectopic head structures when grafted into a fixed body column location on a recipient animal (Fig. 5.10).

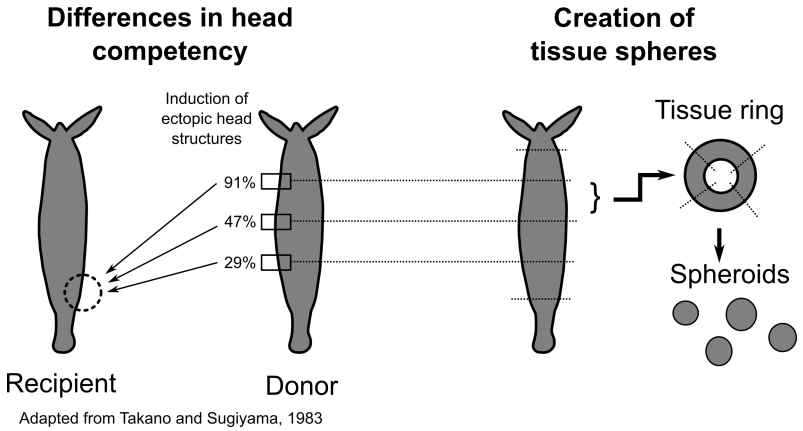

Figure 5.10: Schematic illustrating how tissue spheres excised from the body column can have different levels of Wnt signaling. The 3 donor sites within the body column have notably different probabilities of inducing ectopic head structures: 91%, 47% and 29%. Adapted from Takano and Sugiyama, 1983 [40]

Because these fragments were excised and inserted in exactly the same way, it is improbable that differences in outcome can be attributed to myoneme mismatches at the graft site. The three body column donor sites described in [40] are evenly spaced over the region we used for tissue pieces. Thus, the separation between the donor sites is roughly equivalent to the distance along the parental body axis spanned by one of our tissue fragments (Fig. 5.10; Methods). The observations in [25] and [40] and our data on axis inheritance are best explained by the small *Hydra* tissue fragments having Wnt signaling differentials that are sufficient to determine both the orientation and the polarity of the oral-aboral axis in *Hydra*.

In summary, our results demonstrate that ectodermal myoneme orientation in small tissue pieces of *Hydra* - claimed to govern axial patterning in [23] - is downstream of Wnt signaling. How mechanical cues, such as forces exerted by myonemes, may interact with Wnt signaling, either in the course of normal regeneration [30, 39] or in response to experimental perturbations [23] remains to be investigated. Further exploration of these phenomena will require the development of methods for directly measuring the distribution of Wnt protein along the *Hydra* body axis.

5.2.4 Materials and Methods

Hydra cultures were maintained using standard methods [22]. Oral/aboral grafts were performed as in [18] and bilateral grafts were performed as in [43] using the WM transgenic line [17], HyBra2 promoter:GFP transgenic line [17], and the non-transgenic AEP strain. The position (oral/aboral) of the lineages in the grafts was random, to account for possible

strain differences. Animals were treated with ALP (Sigma-Aldrich, St. Louis, MO) for 2 days as in [8]. Quadrant bilateral grafts were made by fixing one half of an animal on needles [43], followed by adding a quarter of a second animal to the needle fixing the aboral end. The tip of the hypostome was excised to remove the existing head organizer, which is the normal source of Wnt signaling. Tissue pieces were cut as previously described [23, 44]. In brief, the body column was cut into 3–4 rings, then each ring was cut into smaller fragments that form spheroids with a radius of $\sim$150–200 μm. Confocal microscopy was performed on an Olympus IX81 inverted microscope (Olympus Corporation, Tokyo, Japan) with an ORCA-ER camera (Hamamatsu Photonics, Hamamatsu, Japan) and Slidebook software version 5.0 (Intelligent Imaging Innovations, Denver, CO) as described in [18]. Images of oral/aboral grafts were manually scored for polarity retention by assessing if the lineage represented in the regenerated head matched that in the original animal. Bilateral graft regeneration was scored by two metrics: the number of strains represented in the regenerated head above the tentacle ring, and the ratio of the length of the interface between strains to the length of the animal measured down the midline from hypostome to foot. Measurements were conducted using Fiji [34]. Only regenerated animals able to feed after 4 days were included in the analysis. Raw data are available upon request. All data analysis was carried out in MATLAB (MathWorks, Natick, MA). Statistical significance was determined using Fisher's Exact Test for polarity retention and number of tissue types in the head, and the Mann-Whitney U Test for interface ratio. Statistical analysis using multiple metrics was used to account for uneven interfaces or inconsistencies in grafting and the impossibility of matching the biochemical signaling of two animals.

5.2.5 Acknowledgements

We thank Sara Martin, Stacy Guan, and Tapan Goel for experiments and discussions, and Drs. Danielle Ireland and Karl Willert for comments on the manuscript. Funding was provided by NSF grant CMMI-1463572, the Research Corporation for Science Advancement, and the Gordon and Betty Moore foundation.

Chapter 5, in full, is a reprint of material as it appears in Developmental Biology 2020. (Wang, R. and Collins, E.M.S. A novel lateral grafting technique for studying patterning in Hydra. Developmental Biology, 2020, and Wang, R., Steele, R.E., and Collins, E.M.S. Wnt signaling determines body axis polarity in regenerating Hydra tissue fragments. Developmental Biology, 2020). Use of these manuscripts in this dissertation is covered by the rights permitted to the authors by Elsevier. The dissertation author was the primary author of these papers.

Bibliography

[1] Hiroshi Ando, Yasuji Sawada, Hiroshi Shimizu, and Tsutomu Sugiyama. "Pattern formation in hydra tissue without developmental gradients". In: *Developmental Biology* 133.2 (June 1989), pp. 405–414. ISSN: 0012-1606. DOI: 10.1016/0012-1606(89)90044-4.

[2] Roland Aufschnaiter, Roland Wedlich-Söldner, Xiaoming Zhang, and Bert Hobmayer. "Apical and basal epitheliomuscular F-actin dynamics during Hydra bud evagination". In: *Biology Open* 6.8 (Aug. 2017), pp. 1137–1148. ISSN: 20466390. DOI: 10.1242/bio.022723.

[3] Roland Aufschnaiter, Evan A. Zamir, Charles D. Little, Suat Özbek, Sandra Münder, Charles N. David, Li Li, Michael P. Sarras, and Xiaoming Zhang. "In vivo imaging of basement membrane movement: ECM patterning shapes Hydra polyps". In: *Journal of Cell Science* 124.23 (Dec. 2011), pp. 4027–4038. ISSN: 00219533. DOI: 10.1242/jcs.087239.

[4] Holger Bielen, Sabine Oberleitner, Sylvain Marcellini, Lydia Gee, Patrick Lemaire, Hans R. Bode, Ralph Rupp, and Ulrich Technau. "Divergent functions of two ancient Hydra Brachyury paralogues suggest specific roles for their C-terminal domains in tissue fate induction". In: *Development* 134.23 (2007), pp. 4187–4197. ISSN: 09501991. DOI: 10.1242/dev.010173.

[5] Hans Bode. "Axis Formation in Hydra". In: *Annual Review of Genetics* 45.1 (Dec. 2011), pp. 105–117. ISSN: 0066-4197. DOI: 10.1146/annurev-genet-102209-163540.

[6] Anna Marei Boehm and Thomas C.G. Bosch. "Migration of multipotent interstitial stem cells in Hydra". In: *Zoology* 115.5 (Oct. 2012), pp. 275–282. ISSN: 09442006. DOI: 10.1016/j.zool.2012.03.004.

[7] Mariya Broun and Hans R. Bode. *Characterization of the head organizer in hydra.* 2002.

[8] Mariya Broun, Lydia Gee, Beate Reinhardt, and Hans R Bode. "Formation of the head organizer in hydra involves the canonical Wnt pathway". In: *Development* 132.12 (2005), pp. 2907–2916. DOI: 10.1242/dev.01848.

[9] Ethel Nicholson Browne. "The production of new hydranths in Hydra by the insertion of small grafts". In: *Journal of Experimental Zoology* 7.1 (Aug. 1909), pp. 1–23. ISSN: 0022-104X. DOI: 10.1002/jez.1400070102.

[10] R. D. Campbell. "Vital marking of single cells in developing tissues: Indian ink injection to trace tissue movements in hydra". In: *Journal of Cell Science* 13.3 (1973), pp. 651–661. ISSN: 00219533.

[11] Richard D. Campbell. "Tissue dynamics of steady state growth in hydra littoralis. III. Behavior of specific cell types during tissue movements". In: *Journal of Experi-*

mental Zoology 164.3 (Apr. 1967), pp. 379–391. ISSN: 1097010X. DOI: 10.1002/jez.1401640308.

[12] Olivier Cochet-Escartin, Tiffany T. Locke, Winnie H. Shi, Robert E. Steele, and Eva-Maria S. Collins. "Physical Mechanisms Driving Cell Sorting in Hydra". In: *Biophysical Journal* 113.12 (Dec. 2017), pp. 2827–2841. ISSN: 0006-3495. DOI: 10.1016/J.BPJ.2017.10.045.

[13] C Fütterer, C Colombo, F Jülicher, and A Ott. "Morphogenetic oscillations during symmetry breaking of regenerating ¡i¿Hydra vulgaris¡/i¿ cells". In: *Europhysics Letters (EPL)* 64.1 (2003), pp. 137–143. ISSN: 0295-5075. DOI: 10.1209/epl/i2003-00148-y.

[14] Brigitte Galliot. "The hydra model system". In: *International Journal of Developmental Biology* 56.6-8 (2012), pp. 407–409. ISSN: 02146282. DOI: 10.1387/ijdb.120094bg.

[15] A Gierer, S Berking, H Bode, C N David, K Flick, G Hansmann, H Schaller, and E Trenkner. "Regeneration of hydra from reaggregated cells". In: *Nature New Biology* 239.91 (1972), pp. 98–101. ISSN: 00900028. DOI: 10.1038/newbio239098a0.

[16] A. Gierer and Hans Meinhardt. "A theory of biological pattern formation". In: *Kybernetik* 12.1 (1972), pp. 30–39. ISSN: 03401200. DOI: 10.1007/BF00289234.

[17] K. M. Glauber, C. E. Dana, S. S. Park, D. A. Colby, Y. Noro, T. Fujisawa, A. R. Chamberlin, and R. E. Steele. "A small molecule screen identifies a novel compound that induces a homeotic transformation in Hydra". In: *Development* 142.11 (2015), pp. 2081–2081. ISSN: 0950-1991. DOI: 10.1242/dev.126235.

[18] Tapan Goel, Rui Wang, Sara Martin, Elizabeth Lanphear, and Eva Maria S. Collins. "Linalool acts as a fast and reversible anesthetic in Hydra". In: *PLoS ONE* 14.10 (Mar. 2019), p. 584946. ISSN: 19326203. DOI: 10.1371/journal.pone.0224221.

[19] Bert Hobmayer, Fabian Rentzsch, Kerstin Kuhn, Christoph M Happel, Christoph Cramer Von Laue, Petra Snyder, Ute Rothbächer, and Thomas W Holstein. "WNT signalling molecules act in axis formation in the diploblastic metazoan Hydra". In: *Nature* 407.6801 (2000), pp. 186–189. ISSN: 00280836. DOI: 10.1038/35025063.

[20] Michael Kücken, Jordi Soriano, Pramod A. Pullarkat, Albrecht Ott, and Ernesto M. Nicola. "An osmoregulatory basis for shape oscillations in regenerating Hydra". In: *Biophysical Journal* 95.2 (July 2008), pp. 978–985. ISSN: 15420086. DOI: 10.1529/biophysj.107.117655.

[21] Tobias Lengfeld, Hiroshi Watanabe, Oleg Simakov, Dirk Lindgens, Lydia Gee, Lee Law, Heiko A Schmidt, Suat Özbek, Hans Bode, and Thomas W Holstein. "Multiple Wnts are involved in Hydra organizer formation and regeneration". In: *Developmental Biology* 330.1 (2009), pp. 186–199. DOI: http://dx.doi.org/10.1016/j.ydbio.2009.02.004.

[22] Howard M. Lenhoff and Ray DuBois Brown. “Mass culture of hydra: an improved method and its application to other aquatic invertebrates”. In: *Laboratory Animals* 4.1 (Apr. 1970), pp. 139–154. ISSN: 0023-6772. DOI: 10.1258/002367770781036463.

[23] Anton Livshits, Lital Shani-Zerbib, Yonit Maroudas-Sacks, Erez Braun, and Kinneret Keren. “Structural Inheritance of the Actin Cytoskeletal Organization Determines the Body Axis in Regenerating Hydra”. In: *Cell Reports* 18.6 (Feb. 2017), pp. 1410–1421. ISSN: 22111247. DOI: 10.1016/j.celrep.2017.01.036.

[24] Martin Macklin. “Reversal of cell layers in Hydra: a critical re-appraisal”. In: *The Biological Bulletin* 134.3 (1968), pp. 465–472. ISSN: 0028-0836. DOI: 10.2307/1539864.

[25] Harry K. MacWilliams. “Hydra transplantation phenomena and the mechanism of Hydra head regeneration. I. Properties of the head inhibition”. In: *Developmental Biology* 96.1 (Mar. 1983), pp. 217–238. ISSN: 00121606. DOI: 10.1016/0012-1606(83)90324-X.

[26] Harry K. MacWilliams. “Hydra transplantation phenomena and the mechanism of Hydra head regeneration. II. Properties of the head activation”. In: *Developmental Biology* 96.1 (Mar. 1983), pp. 239–257. ISSN: 00121606. DOI: 10.1016/0012-1606(83)90325-1.

[27] Tadanori Mammoto and Donald E Ingber. “Mechanical control of tissue and organ development.” In: *Development (Cambridge, England)* 137.9 (May 2010), pp. 1407–20. ISSN: 1477-9129. DOI: 10.1242/dev.024166.

[28] V J Martin, C L Littlefield, W E Archer, and H R Bode. “Embryogenesis in hydra.” In: *The Biological bulletin* 192.3 (June 1997), pp. 345–63. ISSN: 0006-3185. DOI: 10.2307/1542745.

[29] Hans Meinhardt. “Modeling pattern formation in hydra: a route to understanding essential steps in development”. In: *Int. J. Dev. Biol.* 56 (2012), pp. 447–462. DOI: 10.1387/ijdb.113483hm.

[30] Moritz Mercker, Alexandra Köthe, and Anna Marciniak-Czochra. “Mechanochemical Symmetry Breaking in Hydra Aggregates”. In: *Biophysical Journal* 108.9 (2015), pp. 2396–2407. ISSN: 15420086. DOI: 10.1016/j.bpj.2015.03.033.

[31] Yukio Nakamura, Charisios D Tsiairis, Suat Özbek, and Thomas W Holstein. “Autoregulatory and repressive inputs localize Hydra Wnt3 to the head organizer.” In: *Proceedings of the National Academy of Sciences of the United States of America* 108.22 (2011), pp. 9137–42. ISSN: 1091-6490. DOI: 10.1073/pnas.1018109108.

[32] Joann J. Otto. “Orientation and behavior of epithelial cell muscle processes during Hydra budding”. In: *Journal of Experimental Zoology* 202.3 (1977), pp. 307–321. ISSN: 1097010X. DOI: 10.1002/jez.1402020303.

[33] Isabelle Philipp, Roland Aufschnaiter, Suat Özbek, Stefanie Pontasch, Marcell Jenewein, Hiroshi Watanabe, Fabian Rentzsch, Thomas W. Holstein, and Bert Hobmayer.

"Wnt/β-Catenin and noncanonical Wnt signaling interact in tissue evagination in the simple eumetazoan Hydra". In: *Proceedings of the National Academy of Sciences of the United States of America* 106.11 (Mar. 2009), pp. 4290–4295. ISSN: 00278424. DOI: 10.1073/pnas.0812847106.

[34] Johannes Schindelin, Ignacio Arganda-Carreras, Erwin Frise, Verena Kaynig, Mark Longair, Tobias Pietzsch, Stephan Preibisch, Curtis Rueden, Stephan Saalfeld, Benjamin Schmid, Jean-Yves Tinevez, Daniel James White, Volker Hartenstein, Kevin Eliceiri, Pavel Tomancak, and Albert Cardona. "Fiji: an open-source platform for biological-image analysis". In: *Nature Methods* 9.7 (July 2012), pp. 676–682. ISSN: 1548-7091. DOI: 10.1038/nmeth.2019.

[35] Anna Seybold, Willi Salvenmoser, and Bert Hobmayer. "Sequential development of apical-basal and planar polarities in aggregating epitheliomuscular cells of Hydra". In: *Developmental Biology* 412.1 (Apr. 2016), pp. 148–159. ISSN: 1095564X. DOI: 10.1016/j.ydbio.2016.02.022.

[36] Hiroshi Shimizu. "Transplantation analysis of developmental mechanisms in Hydra". In: *The International Journal of Developmental Biology* 56.6-7-8 (June 2012), pp. 463–472. ISSN: 0214-6282. DOI: 10.1387/ijdb.123498hs.

[37] Hiroshi Shimizu, Patricia M. Bode, and Hans R. Bode. "Patterns of oriented cell division during the steady-state morphogenesis of the body column in hydra". In: *Developmental Dynamics* 204.4 (Dec. 1995), pp. 349–357. ISSN: 10588388. DOI: 10.1002/aja.1002040402.

[38] Hiroshi Shimizu and Yasuji Sawada. "Transplantation phenomena in hydra: Cooperation of position-dependent and structure-dependent factors determines the transplantation result". In: *Developmental Biology* 122.1 (July 1987), pp. 113–119. ISSN: 0012-1606. DOI: 10.1016/0012-1606(87)90337-X.

[39] Jordi Soriano, Cyril Colombo, and Albrecht Ott. "Hydra molecular network reaches criticality at the symmetry-breaking axis-defining moment". In: *Physical Review Letters* 97.25 (2006). ISSN: 00319007. DOI: 10.1103/PhysRevLett.97.258102.

[40] Jun Takano and Tsutomu Sugiyama. "Genetic analysis of developmental mechanisms in hydra. VIII. Head-activation and head-inhibition potentials of a slow-budding strain (L4)". In: *Development* 78.1 (1983).

[41] Ulrich Technau, Michael A Miller, Diane Bridge, and Robert E Steele. "Arrested apoptosis of nurse cells during Hydra oogenesis and embryogenesis". In: *Developmental Biology* 260.1 (Aug. 2003), pp. 191–206. ISSN: 0012-1606. DOI: 10.1016/S0012-1606(03)00241-0.

[42] Carolyn K. Teragawa and Hans R. Bode. "Migrating interstitial cells differentiate into neurons in hydra". In: *Developmental Biology* 171.2 (Oct. 1995), pp. 286–293. ISSN: 00121606. DOI: 10.1006/dbio.1995.1281.

[43] Rui Wang and Eva Maria S. Collins. "A novel bilateral grafting technique for studying patterning in Hydra". In: *Developmental Biology* 462.1 (Mar. 2020), pp. 60–65. ISSN: 1095564X. DOI: 10.1016/j.ydbio.2020.03.006.

[44] Rui Wang, Tapan Goel, Kate Khazoyan, Ziad Sabry, Heng J. Quan, Patrick H. Diamond, and Eva Maria S. Collins. "Mouth Function Determines the Shape Oscillation Pattern in Regenerating Hydra Tissue Spheres". In: *Biophysical Journal* 117.6 (Sept. 2019), pp. 1145–1155. ISSN: 15420086. DOI: 10.1016/j.bpj.2019.07.051.

[45] T. Yao. "Studies on the organizer problem in Pelmatohydra oligactis. I. The induction potency of the implants and the nature of the induced hydranth". In: *J. Exp. Biol* 21.1 (1945), pp. 147–150.

Chapter 6

Creation of new transgenic reporter strains

6.1 Introduction

Fluorescent reporter strains are robust and widely used in *Hydra* research, as demonstrated in previous chapters. These are created by microinjection of *Hydra* embryos with plasmid constructs [8]. While existing strains represent a powerful set of tools, they have several critical limitations with regards to the study of pattern formation in *Hydra*. Understanding and accurately modeling the patterning process requires *in vivo* quantitative study of the biochemical gradients that define the body axis and head organizer. Extant transgenic strains largely do not offer the ability to track protein localization, and are incapable of providing quantitative measurements of protein concentration.

The issue of protein localization can be addressed by driving expression of a fluorescently tagged protein rather than a fluorescent protein (FP) alone. Previous work has

demonstrated the expression of fusion proteins in *Hydra*. A β-catenin-GFP fusion is stable, but is driven by the actin promoter to produce an overexpression strain [3] and is thus of limited utility in determining the native localization of β-catenin. Another study showed expression of an Innexin-1 (Inx1)-GFP fusion protein via a plasmid construct delivered into adult animals using a gene gun [2]. The tagged protein produced localized correctly to cell membranes, but was only transiently expressed in addition to being driven by the actin promoter. While these studies strongly suggest that expression of fusion proteins is a viable approach, the use of constitutive promoters makes them unsuitable for quantitative study of *Hydra*'s natural state. At the time of writing, no fusion protein strains driven by a native promoter have been reported.

The ideal method of quantifying native protein concentration would be to knock a FP into the genomic locus of a target gene. CRISPR gene editing has not been widely implemented in *Hydra*, but has been used to this effect in other model systems [10, 20]. If successful, editing of the genomic locus would allow precise tracking and quantification of the native protein. This approach faces several challenges - namely, the necessity of optimizing the approach for use in *Hydra*, and the possibility that the addition of a fluorescent tag may impact protein function or localization to produce an unwanted phenotype. Depending on the gene of interest, using the existing plasmid-based approach to introduce a copy of the fusion protein driven by its native promoter could also prove viable. This approach represents a slight overexpression, which is potentially problematic for powerful signaling molecules like Wnt3 but less concerning in more widely expressed downstream genes. Introducing an additional labeled copy may prove to be an advantage over editing the genomic locus in proteins such as Inx1, where correct function requires assembly of multiple proteins and

labeling every molecule could introduce steric hindrance.

A promising target gene is Sp5, which has been shown to antagonize Wnt in human stem cells [7], and to additionally to impact development and patterning in mouse [6, 9] and zebrafish [23]. Recently, it has also been shown to interact with Wnt signaling in *Hydra* [21]. Early reaction-diffusion quantitative models of *Hydra* patterning [4] predicted the presence of a biochemical inhibitor, which has not been experimentally identified. Later models focused on the possibility of other factors such as mechanical cues covering some of the functions of the predicted inhibitor [17, 12]. While Sp5 does not fulfill all of the predicted criteria (notably, it is not secreted and thus cannot diffuse), observing its activity has the potential to validate or disprove key assumptions made in the models. This is especially true if coupled with labeling of Wnt3, in which case both the activator and a possible inhibitor could be observed simultaneously.

Creating transgenic strains that express fluorescent fusion proteins driven by their native promoters, whether by editing of the genomic locus or by introducing an additional copy via plasmid, will allow *in vivo* visualization and quantification of genes relevant to development and regeneration. This will prove key to any attempt to fully understand patterning in *Hydra*.

6.2 Materials and Methods

6.2.1 *Hydra* culture and screening

Adult animals of the strain AEP-SS1 were fed *Artemia* nauplii and maintained at 18°C in *Hydra* medium (HM) as previously described [22]. To encourage sexual reproduction, they were fed 3 times per week and starved for 1 week prior to harvesting embryos.

Injected embryos were placed in clean Petri dishes of HM for 48 h. Surviving cuticle-stage embryos were then transferred individually to wells of a 48 well plate with 0.5 mL of HM, and kept at room temperature on the benchtop with daily screening and weekly water changes. Any hatchlings found were transferred to wells of a 24 well plate with 1 mL of HM and fed 3 times a week. Hatchlings were screened for fluorescent cells using an EVOS microscope (Thermo Fisher Scientific) beginning after their second feeding. Mosaic animals were maintained in 24 well plates until reaching adult size and screened twice weekly for fluorescence.

6.2.2 Plasmid constructs

The actin promoter :: YPet construct was made using the pHyVec2 plasmid from the Steele lab (Addgene #34790) as a backbone to provide the *Hydra* actin 5' and 3' flanking sequences. YPet was cloned from YPet-N1 (Addgene #54637), with restriction sites added to the primers (Table 6.1). The YPet insert was then restriction cloned into pHyVec2 using the EcoRI and NsiI sites.

The Sp5 promoter-driven constructs were assembled from PCR-amplified segments. All constructs use pHyVec2 as a backbone and pGL3-*HySp5*-2992 (previously published [21],

provided by the Galliot lab) as a source for the Sp5 promoter. Primers were designed to add overhangs of approximately 30 bp (Table 6.1), and amplified with either Taq or Phusion polymerase. Default conditions were 98°C/90 s, (98°C/30 s, 65°C/30 s, 72°C/3 min) x 39, 72°C/10 min for Phusion, and 94°C/3 min, (94°C/45 s, 50°C/1 min, 60°C/6 min) x 39, 60°C/10 min for Taq. Any adjustments to these conditions are noted in Table 6.1 Fragments were joined using the NEB HiFi assembly kit (New England Biolabs, Ipswitch MA).

The Sp5 promoter :: YPet construct was made using YPet amplified from YPet-N1. The Sp5 promoter :: Sp5-FP fusion constructs used the full Sp5 coding sequence amplified from extracted mRNA, and either YPet-N1 or the Wnt3-mNG knockin template as a source for the FP.

Full sequences of all constructs are provided in Appendix B.

Table 6.1: Primers for plasmid-based transgenics. Upper case indicates priming region. Symbols (*, **, †, ‡, indicate uses of the same primer.

Construct	**Template**	**Primer sequence (5' to 3')**	**Conditions**
actin promoter:: YPet	YPet-N1	caaaatgcatATGGTGAGCAAAGGCG ttgtgaattcGGCCGCTTTACTTATAGAG	Phusion 90 s extend
Sp5 promoter:: YPet	pHyVec2	catcaccgagggcatgaacgagctctataagtaaCATCCCGGGTGAATTCACAATTCG ctttgcgaacgtaatagagctaaattagaactagCCAATTCGCCCTATAGTGAGTC	Taq
	pGL3-*HySp5*-2992	gcgtaatacgactcactatagggcgaattggCTAGTTCTAATTTAGCTCTATTACGTTC cggtgaacagctcttcgcctttgctcaccatGAAACCGCCATCTTATCTTAAATAGCTTC	Taq
	YPet-N1	ccgaagctatttaagataagatggcggtttcATGGTGAGCAAAGGCGAAG atataatcgaattgtgaattcacccgggatgTTACTTATAGAGCTCGTTCATGCCCTC	Phusion 90 s extend
Sp5 promoter:: Sp5-mNG	pHyVec2	gatgtgatgggcatggacgagctgtacaagtaaCATCCCGGGTGAATTCACAATTCG ctttgcgaacgtaatagagctaaattagaactagCCAATTCGCCCTATAGTGAGTC *	Taq
	pGL3-*HySp5*-2992	gcgtaatacgactcactatagggcgaattggCTAGTTCTAATTTAGCTCTATTACGTTC ** tggaacacgacttggaggtgacatgaaaccgccatcTTATCTTAAATAGCTTC †	Taq
	Sp5 mRNA	ccgaagctatttaagataagatggcggtttcATGTCACCTCCAAGTCGTGTTCC ‡ tatcctcctcgcccttgctcaccataccaccaccGTTTTCAACGTTTACTTCAAGTTCC	Phusion
	mNG	tatggaacttgaagtaaacgttgaaaacggtggtggtATGGTGAGCAAGGGCGAG atataatcgaattgtgaattcacccgggatgTTACTTGTACAGCTCGTCCATGC	Phusion 90 s extend
Sp5 promoter:: Sp5-YPet	pHyVec2	catcaccgagggcatgaacgagctctataagtaaCATCCCGGGTGAATTCACAATTCG ctttgcgaacgtaatagagctaaattagaactagCCAATTCGCCCTATAGTGAGTC *	Taq
	pGL3-*HySp5*-2992	gcgtaatacgactcactatagggcgaattggCTAGTTCTAATTTAGCTCTATTACGTTC ** tggaacacgacttggaggtgacatgaaaccgccatcTTATCTTAAATAGCTTC †	Taq
	Sp5 mRNA	ccgaagctatttaagataagatggcggtttcATGTCACCTCCAAGTCGTGTTCC ‡ aacagctcttcgcctttgctcaccataccaccaccGTTTTCAACGTTTACTTCAAGTTCC	Phusion
	YPet-N1	tatggaacttgaagtaaacgttgaaaacggtggtggtATGGTGAGCAAAGGCGAAGAGC atataatcgaattgtgaattcacccgggatgTTACTTATAGAGCTCGTTCATGCCCTC	Phusion 90 s extend

6.2.3 Embryo microinjection

Production and injection of embryos were conducted according to a previously published protocol [8]. Embryos were injected at the 2-cell stage.

Plasmid DNA was prepared using a Qiagen midiprep kit. The plasmid was then further concentrated by ethanol precipitation. The yield from the kit was mixed with 1/10 volume of 3 M sodium acetate and 3 volumes of 100% ethanol in a 1.7 mL microcentrifuge tube, and frozen overnight at -20°C. The tube was spun at maximum speed in a microcentrifuge at 4°C for 30 minutes, supernatant carefully removed, and the pellet air-dried at room temperature for 15-30 min. The pellet was then resuspended in nuclease-free water to a final concentration of 1-2 mg/μL.

6.2.4 CRISPR-Cpf1 editing

A template construct to insert the coding sequence of mNeonGreen (mNG) after exon 2 of HyWnt3 and the associated guide RNA were designed, tested *in vitro* for correct cutting of the genomic sequence, and provided by Dr. Thomas Kuhlman.

Dr. Karl Willert confirmed expression and secretion of Hydra Wnt3-mNG in HEK293 cells.

The Cpf1 guide RNA (TTGATTGATGAACGTGGCCTGGAT) and Alt-R A.s. Cpf1 nuclease 2NLS were ordered from Integrated DNA Technologies.

Guide RNA was resuspended to a concentration of 100 μM. The mixture for injection was prepared using 0.8 μL guide RNA, 1 μL Cpf1 nuclease, and 0.7 μL nuclease free water. The mixture was incubated for 15 min at room temperature, then mixed 1:1 with a 10%

solution of phenol red in nuclease free water as a tracer dye.

Injection into embryos and rearing and screening of hatchlings was conducted as previously described for plasmid constructs.

6.2.5 Tissue recombination

Grafts between the upper and lower halves of animals of different strains were conducted as previously described [5]. Grafted animals were cultured normally after 24 hours of healing, and screened using an EVOS microscope as needed.

In order to recombine the epithelial layers of two different strains, the top and bottom halves of animals from the parental strains were grafted together and the resulting animals were maintained long term. When regular screening revealed an animal with a sizable misalignment between the interface between parental tissues in the endoderm and the ectoderm, the animal was cut to extract the misaligned region. This was then cut to create tissue fragments as previously described [22]. The fragments were allowed to heal and regenerate, and the resulting animals carefully raised to adult size. Cutting to extract the desired combination of epithelial tissues was repeated if necessary until a pure recombined animal was obtained.

Transfer of GFP interstitial cells from WM to a recipient strain was accomplished in two stages. First, A10 animals [16] were heat shocked at 30°C for 3 days to eliminate their interstitial cells. These animals were raised for 2 additional days to allow the interstitial cells to die and the animals to begin to become nerve free (NF), then grafted with WM animals. Grafted animals were further maintained for up to 2 weeks to allow migration

of GFP interstitial stem cells into the NF tissue before being cut. Animals showing GFP neurons and nematocysts, unlabeled ectoderm, unlabeled or dsRed2 endoderm, and a rescue of the bloated, nonfeeding NF phenotype were cultured as normal and screened to select the animals with the greatest proportion of GFP cells. These donor animals will be used in future work to transfer GFP interstitial cells into recipient animals by a similar grafting process. Colchicine treatment [19] will be used to render the recipient strain NF prior to grafting.

6.2.6 Imaging

An Invitrogen EVOS FL Auto 2 microscope (Thermo Fisher Scientific) was used for screening of transgenic animals and imaging of the resulting strains. A YFP filter cube was used to visualize YPet, a GFP cube for eGFP and mNG, and an RFP cube for dsRed.

A Leica MZ 16 FA microscope was used to observe fluorescent strains during cutting and manipulation.

6.3 Results and Discussion

Two approaches to generating transgenic animals were attempted: CRISPR-Cpf1 editing to knock a FP in at the genomic locus of Wnt3, and plasmid constructs to test and deploy a new FP in *Hydra*.

152 embryos were injected with a CRISPR-Cpf1 editing mix aimed at creating a Wnt3-mNeonGreen fusion protein. The hatchlings from this attempt were all maintained until they had budded several times. None showed green fluorescence. As the guide RNA and

template had been shown to produce correct editing *in vitro*, the most likely explanation is that some difficulty occurs within the injected mixture or in the *Hydra* embryo after injection.

During oogenesis, *Hydra* incorporates the contents of hundreds of nurse cells to form the oocyte. The nuclei of the nurse cells are also incorporated. They remain dormant but intact, and can be visualized in the embryo until after hatching [18] These persisting nuclei represent a possible failure mode for CRISPR-based gene editing: the many additional copies of the genome may be viable targets for the injected nuclease and thus decrease the chances of editing the egg nucleus. If this is the case, successful editing may require larger numbers of injected embryos, or an increase in the concentrations of nuclease, guide RNA, and template RNA injected.

Due to ongoing difficulties implementing CRISPR genome editing, the decision was made to pursue established plasmid-based methods in parallel. As a proof of concept, a transgenic strain consisting of the actin promoter driving a fluorescent protein was created (Fig. 6.1A). The yellow fluorescent protein YPet [13] was selected for its brightness and lack of significant spectral overlap with the green and red fluorescent proteins already used in transgenic *Hydra*, with the end goal of creating a tricolored transgenic strain in which all three stem cell lineages could be visualized simultaneously.

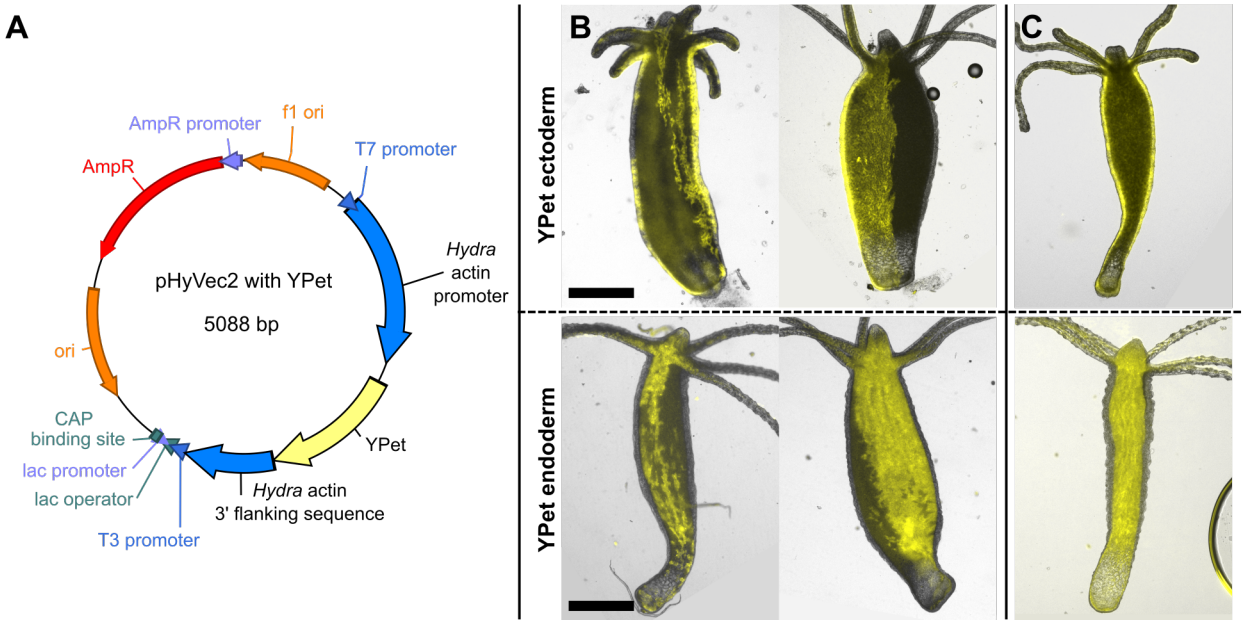

Figure 6.1: Actin promoter::YPet transgenic strains. A. Plasmid map of injected construct, with YPet driven by the *Hydra* actin promoter. B. Images of mosaic animals from injected embryos. C. Images of fully transgenic animals.

A total of 69 injected embryos survived to the cuticle stage. Of these 31 hatched, resulting in 5 animals with mosaic expression of YPet in epithelial tissue (Fig. 6.1B). Of these, the two brightest were selected for further propagation and gave rise to a YPet-ectoderm strain (ghidorah) and a YPet-endoderm strain (softboiled). (Fig. 6.1C).

As a demonstration of simultaneous imaging of 3 FPs *in vivo*, a test tricolored animal was created by grafting segments from ghidorah, a donor strain with GFP interstitial cells, and Frank. We were thus able to confirm that both epithelial layers and the interstitial cells could be visualized simultaneously with minimal bleedthrough. (Fig. 6.2)

Current work is focused on combining one of the YPet strains with existing transgenic lines to create a tri-colored animal, which will allow *in vivo* imaging and differentiation of all three of *Hydra*'s stem cell lineages. An i-cell donor strain was first established by grafting heat-shocked A10 with WM animals to isolate actin promoter::eGFP interstitial stem cells as described in Methods. Simultaneously, grafts between ghidorah and WM animals were used to create a strain with YPet ectoderm and dsRed2 endoderm. Currently this strain is undergoing selection to achieve full labeling. Once this is completed and it has been propagated to sufficient numbers, animals will be treated with colchicine to eliminate the interstitial lineage and grafted to the eGFP i-cell donor strain. Migration of eGFP i-cells across the graft interface will then complete the tricolored strain.

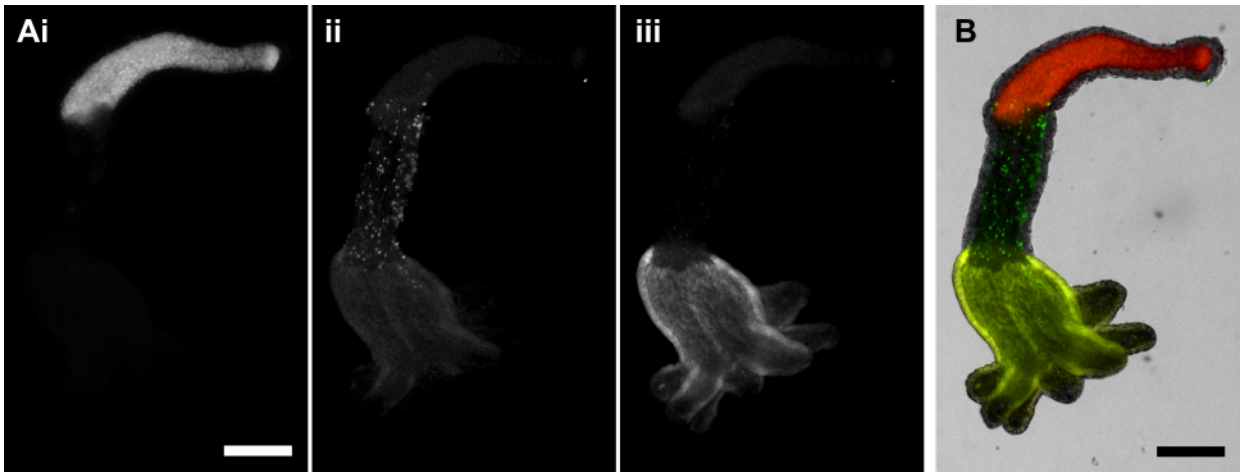

Figure 6.2: Tricolored animal proof of concept. A. Individual channels: i. dsRed2, ii. eGFP, iii. YPet. B. Composite image.

At the time of writing, fusion proteins are less widely used in the literature than promoter::FP constructs. The existing examples are largely driven by the actin promoter for an overexpression strain [11]. A fusion protein construct driven by the gene's own promoter offers the possibility of tracking protein localization *in vivo*. While the addition of an extra copy of the gene and the possibility of missing regulatory elements means that a plasmid-based approach would not be a fully accurate quantification of native protein behavior, such a construct would still permit visualization of biochemical signaling gradients in a way that has not previously been possible.

The putative Wnt inhibitor Sp5 was chosen as a target both for the potential for significant contributions to the study of patterning, and for being a more amenable target for editing than Wnt3. The published expression pattern of Sp5 is a broad gradient strongest just below the head and decreasing gradually down the body column. This wider expression domain will make the screening and selection of mosaic animals easier to accomplish. In addition, the presence of larger quantities of protein in the animal makes unwanted effects from the introduction of an additional copy less likely to occur.

A series of constructs driven by the Sp5 promoter were designed to allow a range of visualization approaches. The Sp5 promoter :: YPet construct is analogous to many existing reporter strains utilizing the promoter of a gene of interest to drive an FP. The activity of the promoter has been verified by using it to drive a luciferase reporter in HEK293 cells [21], so this should represent an effective reporter for Sp5 expression.

Two plasmids encoding the Sp5 promoter driving an Sp5-FP fusion protein were designed. YPet was initially selected as the FP to allow possible co-imaging with existing red and green FP reporters. However, in imaging of strains with YPet driven by the actin

promoter in epithelial cells, YPet appeared significantly dimmer than equivalent eGFP or dsRed-expressing epithelial cells. Therefore, an alternate construct using mNG was also designed. mNG is likely to be brighter, which will make detection, testing, and quantitative imaging of the transgene easier in singly labeled animals.

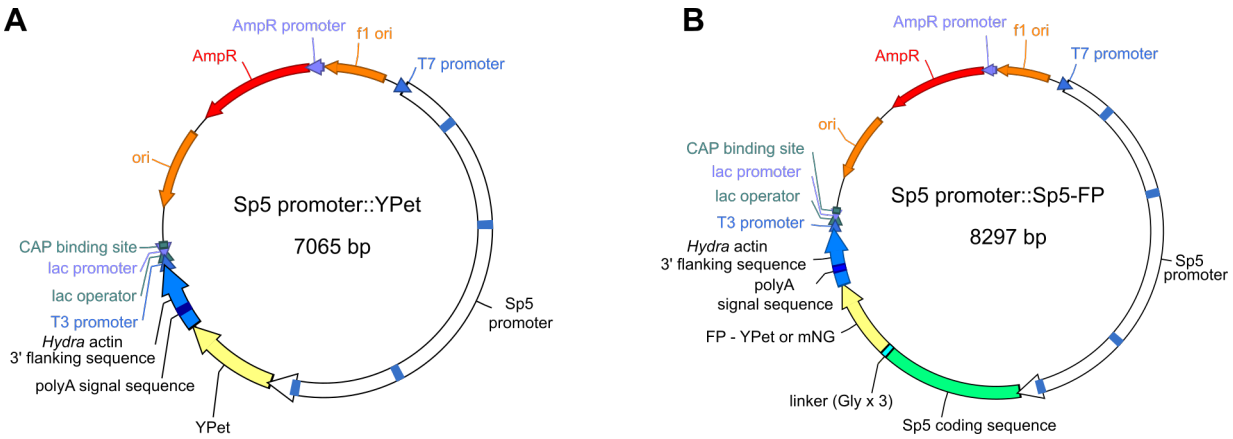

Figure 6.3: Sp5 promoter-driven constructs. A. Plasmid map for construct using Sp5 promoter to drive YPet. B. Plasmid map for construct using Sp5 promoter to drive an Sp5-FP fusion protein. Blue rectangles on Sp5 promoter represent putative TCF binding sites.

The Sp5 promoter :: YPet construct has been made, and correct assembly verified by Sanger sequencing of the junctions between fragments. The Sp5 promoter :: mNG construct has also been made. Several clones have been verified as correctly assembled, and screened for sequence correctness by Sanger sequencing. The most promising of these will be tested *in vitro* by transfecting mammalian cells prior to *Hydra* embryo microinjection. This will allow us to confirm that the fusion protein is produced, and confirm that it is fluorescent.

Combining multiple reporter constructs would allow *in vivo* visualization of multiple proteins simultaneously. This can be done in several ways.

Existing methods allow the recombination of stem cell lineages from different strains, which is sufficient if the genes to be co-visualized are expressed exclusively in different lineages. A theoretical maximum of 3 genes can be visualized in this way. If the expression patterns overlap, the transgenic constructs will need to be combined by other methods. Obtaining a strain in which one construct is transmitted through the germline and using this as a starting strain for the injection of additional constructs is one approach. There is precedent for a reporter expressed in the interstitial cell lineage being made to appear in gametes [14]. Nishimiya-Fujisawa and Kobayashi show that within the interstitial lineage, multipotent and germline stem cells are separate populations under normal conditions and that a reporter expressed in descendants of multipotent interstitial stem cells (neurons, gland cells, etc) may not be expressed in the gonads. However, by cutting small tissue fragments, they find that one can force new germline stem cells to be created and thus obtain gametes expressing the transgene.

Furthermore, the transmission of reporter constructs via sexual reproduction has been documented in a preprint [15]. In this study the authors inject embryos with reporter

constructs consisting of promoters specific to specific neuron subpopulations driving the calcium indicator GCaMP6s. Some of the strains used in the study are derived from these F0 animals, while others, including a double reporter, result from F1 crosses. It would therefore appear that the production of transgenic gametes for either crossbreeding or as starting material for microinjection is possible, though screening and establishing an interstitial cell reporter line is more challenging than an epithelial reporter line.

Alternatively, a construct could be made that incorporates multiple reporters. This has been implemented with a promoter of interest driving eGFP and the actin promoter driving RFP to enable easier selection of edited tissue [1]. While viable, this approach is likely to suffer from limitations as the length of the construct increases. Thus it may not be workable for larger numbers of reporters, or for the greater length needed to express fusion proteins rather than FPs alone. Co-injection of multiple separate constructs is unlikely to be practical, but obtaining a germline-transmissible reporter and iterating to add further reporters could potentially prove workable if CRISPR genome editing were successfully adapted for use in *Hydra*.

6.4 Conclusions

The continued development and utilization of transgenic strains in *Hydra* patterning research will enable the field to validate and fully utilize quantitative modeling. *Hydra* is a powerful system due to ease of manipulation and observation, but easily observed milestones of development and regeneration are lacking and quantitative measurements of protein expression and localization have proved elusive. Thus, while models that accurately repro-

duce observable regeneration and patterning behaviors have been developed, they cannot be confirmed as fully accurate. Quantitative measurements of morphogen gradients should be possible using modern imaging technology if appropriate reporter strains can be developed.

Future work towards this goal should focus first on the creation of fusion protein reporter strains, so that protein localization can be measured *in vivo*. While plasmid-based constructs such as those shown here would represent an improvement over FP-only constructs that can only show localization, they introduce an extra copy of the gene of interest at an unknown genomic location. Thus, they cannot fully show the behavior of the native protein. This problem can be bypassed by successful genome editing, for which reason the adaptation of editing methods such as CRISPR should be prioritized as well.

Once this is achieved, multiple reporters should be combined in a single strain to fully visualize the interplay between multiple gradients. This type of data will enable definitive testing of existing quantitative models of pattern formation, or the construction of new models based more firmly in experimental data. Thus the field will be able to realize *Hydra*'s full potential as a model system that shares many core biochemical processes with higher organisms while being simple enough to be described by mathematical modeling.

6.5 Acknowledgments

I would like to thank Dr. Karl Willert and Dr. Thomas Kuhlman for providing reagents and for discussion of the work, and Dr. Robert E. Steele for additional discussion and suggestions.

Bibliography

[1] Anna Marei Boehm and Thomas C.G. Bosch. "Migration of multipotent interstitial stem cells in Hydra". In: *Zoology* 115.5 (Oct. 2012), pp. 275–282. ISSN: 09442006. DOI: 10.1016/j.zool.2012.03.004.

[2] Angelika Böttger, Olga Alexandrova, Mihai Cikala, Marsha Schade, Michaela Herold, and Charles N. David. "GFP expression in Hydra: Lessons from the particle gun". In: *Development Genes and Evolution* 212.6 (2002), pp. 302–305. ISSN: 0949944X. DOI: 10.1007/s00427-002-0245-0.

[3] Lydia Gee, Julia Hartig, Lee Law, Jörg Wittlieb, Konstantin Khalturin, Thomas C.G. G Bosch, and Hans R. Bode. "β-catenin plays a central role in setting up the head organizer in hydra". In: *Developmental Biology* 340.1 (Apr. 2010), pp. 116–124. ISSN: 0012-1606.

[4] A. Gierer and Hans Meinhardt. "A theory of biological pattern formation". In: *Kybernetik* 12.1 (1972), pp. 30–39. ISSN: 03401200. DOI: 10.1007/BF00289234.

[5] Tapan Goel, Rui Wang, Sara Martin, Elizabeth Lanphear, and Eva Maria S. Collins. "Linalool acts as a fast and reversible anesthetic in Hydra". In: *PLoS ONE* 14.10 (Mar. 2019), p. 584946. ISSN: 19326203. DOI: 10.1371/journal.pone.0224221.

[6] Stephen M. Harrison, Denis Houzelstein, Sally L. Dunwoodie, and Rosa S.P. Beddington. "Sp5, a new member of the Sp1 family, is dynamically expressed during development and genetically interacts with Brachyury". In: *Developmental Biology* 227.2 (Nov. 2000), pp. 358–372. ISSN: 00121606. DOI: 10.1006/dbio.2000.9878.

[7] Ian J. Huggins, Tomas Bos, Olivia Gaylord, Christina Jessen, Brianna Lonquich, Angeline Puranen, Jenna Richter, Charlotte Rossdam, David Brafman, Terry Gaasterland, and Karl Willert. "The WNT target SP5 negatively regulates WNT transcriptional programs in human pluripotent stem cells". In: *Nature Communications* 8.1 (Dec. 2017), pp. 1–14. ISSN: 20411723. DOI: 10.1038/s41467-017-01203-1.

[8] Celina E. Juliano, Haifan Lin, and Robert E. Steele. "Generation of Transgenic Hydra by Embryo Microinjection". In: *Journal of Visualized Experiments* 91 (2014), e51888. ISSN: 1940-087X. DOI: 10.3791/51888.

[9] Mark W. Kennedy, Ravindra B. Chalamalasetty, Sara Thomas, Robert J. Garriock, Parthav Jailwala, Terry P. Yamaguchi, and Roeland Nusse. "Sp5 and Sp8 recruit β-catenin and Tcf1-Lef1 to select enhancers to activate Wnt target gene transcription". In: *Proceedings of the National Academy of Sciences of the United States of America* 113.13 (Mar. 2016), pp. 3545–3550. ISSN: 10916490. DOI: 10.1073/pnas.1519994113.

[10] Yukiko Kimura, Yu Hisano, Atsuo Kawahara, and Shin Ichi Higashijima. "Efficient generation of knock-in transgenic zebrafish carrying reporter/driver genes by CRISPR/Cas9-mediated genome engineering". In: *Scientific Reports* 4.1 (Oct. 2014), pp. 1–7. ISSN: 20452322. DOI: 10.1038/srep06545.

[11] Alexander Klimovich, Jörg Wittlieb, and Thomas C.G. Bosch. "Transgenesis in Hydra to characterize gene function and visualize cell behavior". In: *Nature Protocols* 14.7 (July 2019), pp. 2069–2090. ISSN: 17502799. DOI: 10.1038/s41596-019-0173-3.

[12] Moritz Mercker, Alexandra Köthe, and Anna Marciniak-Czochra. "Mechanochemical Symmetry Breaking in Hydra Aggregates". In: *Biophysical Journal* 108.9 (2015), pp. 2396–2407. ISSN: 15420086. DOI: 10.1016/j.bpj.2015.03.033.

[13] Annalee W. Nguyen and Patrick S. Daugherty. "Evolutionary optimization of fluorescent proteins for intracellular FRET". In: *Nature Biotechnology* 23.3 (Mar. 2005), pp. 355–360. ISSN: 10870156. DOI: 10.1038/nbt1066.

[14] Chiemi Nishimiya-Fujisawa and Satoru Kobayashi. "Germline stem cells and sex determination in Hydra". In: *The International Journal of Developmental Biology* 56.6-7-8 (June 2012), pp. 499–508. ISSN: 0214-6282. DOI: 10.1387/ijdb.123509cf.

[15] Yukihiko Noro, Hiroshi Shimizu, Katsuhiko Mineta, and Takashi Gojobori. "A single neuron subset governs a single coactive neuron circuit in Hydra vulgaris, representing a prototypic feature of neural evolution". In: *bioRxiv* (Nov. 2020), p. 2020.11.22.392985. DOI: 10.1101/2020.11.22.392985.

[16] Hiroshi Shimizu, Osamu Koizumi, and Toshitaka Fujisawa. "Three digestive movements in Hydra regulated by the diffuse nerve net in the body column". In: *Journal of Comparative Physiology A* 190.8 (Aug. 2004), pp. 623–630. ISSN: 0340-7594. DOI: 10.1007/s00359-004-0518-3.

[17] Jordi Soriano, Cyril Colombo, and Albrecht Ott. "Hydra molecular network reaches criticality at the symmetry-breaking axis-defining moment". In: *Physical Review Letters* 97.25 (2006). ISSN: 00319007. DOI: 10.1103/PhysRevLett.97.258102.

[18] Ulrich Technau, Michael A Miller, Diane Bridge, and Robert E Steele. "Arrested apoptosis of nurse cells during Hydra oogenesis and embryogenesis". In: *Developmental Biology* 260.1 (Aug. 2003), pp. 191–206. ISSN: 0012-1606. DOI: 10.1016/S0012-1606(03)00241-0.

[19] Cassidy M. Tran, Sharon Fu, Trevor Rowe, and Eva Maria S. Collins. "Generation and long-term maintenance of nerve-free hydra". In: *Journal of Visualized Experiments* 2017.125 (2017). ISSN: 1940087X. DOI: 10.3791/56115.

[20] Takeshi Uemura, Takuma Mori, Taiga Kurihara, Shiori Kawase, Rie Koike, Michiru Satoga, Xueshan Cao, Xue Li, Toru Yanagawa, Takayuki Sakurai, Takayuki Shindo, and Katsuhiko Tabuchi. "Fluorescent protein tagging of endogenous protein in brain neurons using CRISPR/Cas9-mediated knock-in and in utero electroporation techniques". In: *Scientific Reports* 6.1 (Oct. 2016), pp. 1–13. ISSN: 20452322. DOI: 10.1038/srep35861.

[21] Matthias C. Vogg, Leonardo Beccari, Laura Iglesias Ollé, Christine Rampon, Sophie Vriz, Chrystelle Perruchoud, Yvan Wenger, and Brigitte Galliot. "An evolutionarily-

conserved Wnt3/β-catenin/Sp5 feedback loop restricts head organizer activity in Hydra". In: *Nature Communications* 10.1 (Dec. 2019), pp. 1–15. ISSN: 20411723. DOI: 10.1038/s41467-018-08242-2.

[22] Rui Wang, Tapan Goel, Kate Khazoyan, Ziad Sabry, Heng J. Quan, Patrick H. Diamond, and Eva Maria S. Collins. "Mouth Function Determines the Shape Oscillation Pattern in Regenerating Hydra Tissue Spheres". In: *Biophysical Journal* 117.6 (Sept. 2019), pp. 1145–1155. ISSN: 15420086. DOI: 10.1016/j.bpj.2019.07.051.

[23] Gilbert Weidinger, Chris J. Thorpe, Katrin Wuennenberg-Stapleton, John Ngai, and Randall T. Moon. "The Sp1-related transcription factors sp5 and sp5-like act downstream of Wnt/β-catenin signaling in mesoderm and neuroectoderm patterning". In: *Current Biology* 15.6 (Mar. 2005), pp. 489–500. ISSN: 09609822. DOI: 10.1016/j.cub.2005.01.041.

Chapter 7

Innexins as possible targets of Wnt signaling

7.1 Introduction

Previous chapters of this thesis illustrate a critical flaw in current attempts to advance quantitative modeling of *Hydra*: models and their predictions are generally very difficult to definitively prove or disprove, because there are very few reliably quantifiable milestones of regeneration and development and the morphogen gradients themselves cannot yet be observed *in vivo*. Continuing to experimentally test individual aspects of these models (ex. [46], [45]) is helpful. However, as such efforts have consistently revealed that key assumptions were flawed, we must consider that the core premise of a mechanotransduction pathway driving pattern formation may need to be revisited. Current experimental results cannot definitively confirm a role for mechanical force in *Hydra* patterning. In light of the possibility that mechanotransduction is not involved, or is present but not the sole factor, it becomes

important to explore other potential mechanisms of patterning regulation. Some notable proposed alternatives include actin structure [23] and electric fields [7].

Based on findings in other model systems, gap junctions represent a promising candidate for an unexplored regulator of Wnt signaling in *Hydra*. Gap junctions connect the cytoplasm of two adjacent cells via dense arrays of membrane channels on the adjoining cell membranes. [4] These channels are permeable to a wide range of molecules and signals including ions, voltage, and small proteins, and are thus critical to intercellular communication within an organism. Each cell produces hemichannels on its membrane, which are composed of multiple copies of a gap junction protein. These then pair with a hemichannel on an adjacent cell to form a full channel. Clusters of channels compose the full gap junction. The proteins that compose gap junctions are connexins and pannexins in vertebrates, and innexins in invertebrates [30]. The different families of gap junction proteins are believed to have evolved convergently. [2]

Connexins and innexins share almost no primary sequence similarity. The hemichannels differ in the number of subunits (6 for connexins, 8 for innexins). Both intracellular gap and channel spacing are larger in innexin-based gap junctions than in their connexin-based counterparts [36]. Nevertheless, the similarities between the two protein families are striking. Their membrane topology is similar - for example, both have 4 transmembrane domains with conserved cysteines in the extracellular loops [24]. The permeability of the channels is approximately equivalent, both can be inhibited by long-chain alcohols such as octanol, and their voltage sensitivity and gating characteristics are similar [36]. Therefore, while connexins are vastly better-studied, it is not unreasonable to theorize that behaviors observed in connexins may also be present in innexins.

In vertebrate systems there is strong evidence for interactions between Wnt signaling and gap junctions. A range of studies has showed Wnt signaling to impact connexin expression and gap junction function in various systems. In *Xenopus* embryos, injection of Wnt1 protein was showed to increase gap junction communication. [25] In mammals a great deal of work has focused on connexin-43 (Cx43), which is expressed in most cell types and participates in both gap junctional and other forms of intercellular communication [32]. In several human cell lines Wnt1 was showed to increase chemical and electrical coupling as well as increasing the expression of Cx43. This effect was limited to Cx43 and not observed in several other connexins [43]. In cultured rat cardiac myocytes, Wnt1 increased Cx43 transcripts and protein [1]. Thus it seems clear that Cx43 expression and function can be directly regulated by Wnt signaling.

In human neural progenitor cells, Cx43 was shown to inhibit β-catenin expression and transcriptional activity [33]. This represents evidence of the inverse relationship, in which Cx43 feeds back into Wnt signaling via β-catenin to form a feedback loop.

Finally, Wnt signaling has also been shown to affect cellular localization of Cx43 in mammalian cells. Nuclear localization increases 8 to 10-fold with a corresponding decrease in membrane and cytosolic Cx43 when cells are treated with recombinant Wnt protein. The altered localization could be reversed by shRNA knockdown of β-catenin. In addition, it was shown that Cx43 physically interacts with β-catenin, and that a Cx43 knockdown results in reduced nuclear localization of β-catenin [19]. This is further compelling evidence that Cx43 interacts with β-catenin to play a major role in Wnt signaling.

In other invertebrate systems, innexins have been shown to be linked to patterning. For example, studies of planarians have revealed a link between gap junctions and patterning

[29]. Blocking of gap junctions using octanol during specific time windows early in regeneration resulted in severe patterning defects when worms were amputated in certain ways [27]. Critically, regeneration defects could also be observed following triple RNAi against 3 central nervous system-associated innexins (*Dj-inx5, 12* and *13*) [27]. These are distinct from a separate planarian innexin, *smedinx-11*, which is neoblast-specific and has been shown to be necessary for regeneration and stem cell renewal [26]. Furthermore, studies in *Drosophila* have showed *Drosophila* Inx2 (no sequence similarity to *Hydra* Inx2) expression to be regulated by Wingless signaling [3], and found that *Drosophila* Inx2 is a downstream target of dWnt4 in somatic encapsulation of female germline stem cells [42]. Therefore, it is highly likely that a link between Wnt signaling and gap junction proteins exists in invertebrates as well.

Based on established connections between Wnt signaling, patterning, and gap junctions in both vertebrate and invertebrate systems, we theorize that there could be a crosstalk between innexins and canonical Wnt signaling during pattern formation in *Hydra*. Sequencing of the *Hydra* genome has identified at least 17 putative innexin sequences [10]. Of these, only innexin 2 (Inx2) has been thoroughly studied. Whole mount *in situ* hybridization (WISH) has showed that it is expressed exclusively in neurons making up the nerve ring in the peduncle, which are responsible for contraction burst behavior [39]. While full expression patterns for the remaining innexins have not been published, transcriptomic analysis of sections of body column reveals that several innexins are more highly expressed in the head [48] and are thus candidates for potential biochemical interactions with the head organizer. The most direct support for a possible link to Wnt signaling is a 1987 study that shows an antibody against a rat liver connexin can block *Hydra* cell coupling, and observes

that antibody treatment interferes with the head inhibition gradient in grafting experiments [11]. Existing evidence for a Wnt-gap junction link in *Hydra* is circumstantial at best, but the range of unexplored candidate innexins and a published report of altered patterning in response to gap junction perturbation are promising.

If a link between innexins and patterning exists, there should be quantifiable changes in innexin expression and/or localization upon perturbing Wnt signaling. Here we utilize multiple published techniques, and obtain preliminary results showing changes to innexin expression in response to both upregulation and downregulation of Wnt signaling.

7.2 Materials and Methods

7.2.1 *Hydra* strains and maintenance

Hydra cultures were maintained using standard methods [22]. Existing strains used were as follows: WM transgenic line [12] (actin promoter::eGFP ectoderm/actin promoter::dsRed2 endoderm), HyBra transgenic line (HyBra2 promoter:GFP) [12], Frank transgenic line (actin promoter::dsRed2 endoderm) [13] and the non-transgenic AEP strain.

7.2.2 Riboprobe cloning and synthesis

mRNA was extracted using the RNeasy Mini Kit (QIAGEN, Germantown, MD, USA) including a DNase treatment. Source material was whole AEP animals, or heads only for head-specific genes with relatively low expression. cDNA was synthesized using the SuperScript® III First-Strand Synthesis System (Invitrogen, Carlsbad, CA, USA) following

the manufacturer's protocol. cDNA was used as template material for PCR using the primer pairs in Table 7.1. Successful amplifications were cloned using the TOPO® TA Cloning® Kit for Sequencing (Invitrogen). Plasmids were evaluated by Sanger sequencing to confirm the correct sequence and to determine the direction of the insert. The Wnt3 riboprobe was a gift from Bert Hobmayer [18].

DNA template was amplified from the plasmids using T3 and T7 primers (Inx1, Inx4, Inx5) or T7 and Sp6 primers (Wnt3). PCR product was ethanol precipitated, then *in vitro* transcription was conducted using T3, T7, or Sp6 polymerase (Thermo Fisher) and DIG RNA Labeling Mix (Roche, Mannheim, Germany). The probe was treated with DNAse to remove the template, ethanol precipitated, and resuspended in hybridization buffer to a concentration of 50 ng/μL. For use in WISH, this stock solution was diluted 1:100 in hybridization buffer.

Full riboprobe synthesis protocol is provided in Appendix A.

Table 7.1: Riboprobe cloning primers. See Appendix B for full riboprobe sequences.

Gene	**Direction**	**Primer Sequence (5'-3')**
Inx1	F	ATGGGAATAAGCTGGTTCAATG
	R	AGGAGACAAATTCGCCATTAAG
Inx4	F	ATGTCTATCATTACCGGAAACC
	R	CTGTTTGGTGGGTTTATCTGG
Inx5	F	ATGTCAACTATTACCAACGATATC
	R	ATCGCTATTCACATATCGGAATAG
Sp5	F	AATTACTCACAAAAA
	R	TAAGGTGACTAGTTTTACC

7.2.3 Whole mount *in situ* hybridization

WISH was conducted using an adaptation of a previously published *Hydra* protocol [34] with AP development adapted from Pearson [28]. See Appendix A for the full protocol as used.

7.2.4 Alsterpaullone treatment

Alsterpaullone (ALP) (Sigma-Aldrich, St. Louis, MO) treatment was conducted as previously described [8]. Animals were incubated in 5 μM ALP for 48 h with changes of solution every 24 h.

7.2.5 Lithium chloride treatment

LiCl (Sigma-Aldrich) treatment was conducted as previously described [16]. In brief, animals were treated with 1mM LiCl in the medium described by Hassel et al. (0.01 mM Tris, 1 mM $CaCl_2$, 0.1 mM KCl, 0.01 mM $MgCl_2$, 0.02 mM EDTA-Na_2). Intact animals were incubated in the solution for 6 days with one feeding on day 3, then harvested for use in experiments.

7.2.6 iCRT14 treatment

Stock iCRT14 (Sigma-Aldrich, St. Louis, MO, USA) solution was prepared at 1 mM in DMSO, and stored in the dark at -20°C.

Animals were incubated in 2.5 or 5 μM iCRT14. The HM formulation used for iCRT14 treatment was as previously described by Gufler *et al.* [15]: 1 mM $CaCl_2$, 0.1 mM $MgCl_2$,

0.1 mM KCl, 1mM $NaHCO_3$.

7.2.7 Wnt-C59 treatment

Stock Wnt-C59 (C59) (Millipore Sigma, Burlington, MA, USA) solution was prepared at 0.1 mM in DMSO, and stored in the dark at -20°C.

Whole or decapitated animals were placed in 1 μM C59, in a final concentration of 1% DMSO in HM. 1% DMSO was used as a positive control. The medium was changed every 24 h. Animals were washed with HM and harvested for experiments after 72 h.

7.2.8 qPCR

mRNA was extracted from whole *Hydra* using the RNEasy Mini Kit (QIAGEN) including a DNAse treatment. cDNA was synthesized using iScript^{TM} Reverse Transcription Supermix for RT-qPCR (Bio-Rad, Hercules, CA, USA) with 1 μg of RNA per reaction. qPCR primers were designed using Primer3 [41] and parameters as described in [40]. Primer sequences are provided in Table 7.2.

Table 7.2: qPCR primer sequences. Source paper is listed if relevant; n/a indicates primers designed by the author.

Gene	**Primer**	**Sequence (5' to 3')**	**Reference**
γ-tubulin	F	CTGCTTGTGTAGCATACTTTGAAAT	[ref lommel 2018]
	R	TCATGTTCAGCTACAAGAAATTCAC	
Wnt3	F	ATTACAACAGCCAGCAGAGAAAG	[ref petersen 2015]
	R	TTATCGCAACGACAGTGGAC	
Inx1	F	AATGCTTAGTACCAGGGGTCAACGC	n/a
	R	ACCAAAATAACCAACCTCGCTTGATCT	
Inx4	F	CTCGGTTTGCTTTACTATTTTCCGT	n/a
	R	TCTGTTTGGTGGGTTTATCTGGTA	
Inx5	F	AAAAGAGACAGTAGAAACAGGACCG	n/a
	R	TAACAAGACGCTCACCAACATAGT	

qPCR was run in a CFX96 Touch Real-Time PCR Detection System (Bio-Rad) using PerfeCTa® SYBR® Green FastMix® (Quantabio, Beverly, MA, USA). Technical triplicates were run for all reactions within an experiment. Analysis of relative expression for the genes of interest was performed using the ΔΔCt method.

7.2.9 siRNA

Previously published siRNA sequences and elecroporation protocol were used to knock down Sp5 and β-catenin in *Hydra*. [44] Animals were starved 12 h prior to the first electroporation on day 0, then fed on alternating days between electroporations. Animals used for WISH were fixed on day 3, while morphological phenotypes were evaluated on day 9.

7.3 Results and Discussion

7.3.1 Characterization of 3 *Hydra* innexins

Roughly 17 innexins have been identified in *Hydra* based on its sequenced genome [10]. Of these, only Inx2 has been characterized to reveal its expression pattern and role in controlling contraction bursts [39]. To select candidate innexins for further characterization, we utilized three resources: 1. a study that compared the number of transcripts for various genes in sections from different positions along the body column [48], 2. the *Hydra* 2.0 genome project [20], and 3. an online database of single-cell sequencing data [35].

Inx1 was reported to have slightly higher expression near the head, and single-cell data showed it was expressed in nearly all cell types. We theorized that this might represent

a near ubiquitous gap junction similar to the role Cx43 plays in vertebrates, with a possibility for directly reproducing reported interactions between Cx43 and Wnt signaling. Inx4 and Inx5 both appeared to have clearly graded expression along the body column based on the sections and were chosen for the potential of direct interactions with the head organizer.

To confirm the feasibility of innexins as downstream targets of Wnt, we located the genomic sequences of the three candidate innexins in the *Hydra* 2.0 Genome Portal [20] and used the ATAC-seq data to identify probable promoter sequences. We then examined these promoters for putative TCF binding sites based on published consensus sequences [9]. We were able to locate varying numbers of putative TCF binding sites in all promoters examined (Fig. 7.1A), indicating that it is theoretically possible that innexin expression is directly regulated by canonical Wnt signaling.

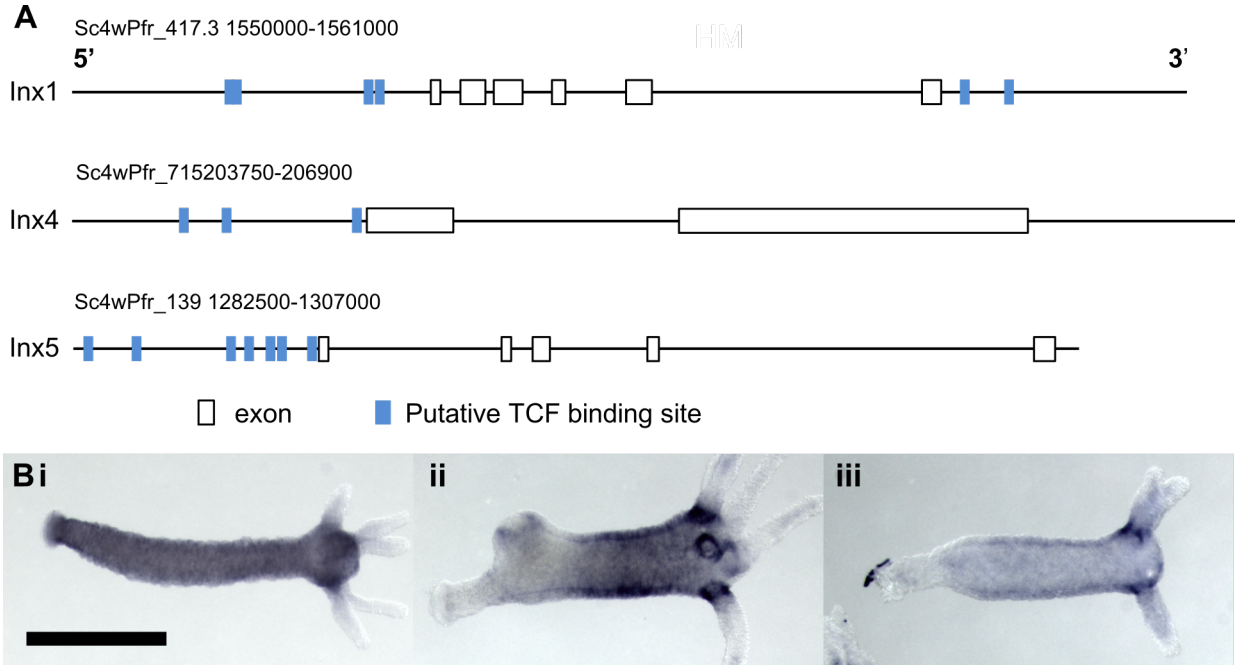

Figure 7.1: Expression patterns of 3 *Hydra* innexins. A. Genomic loci of Inx1, Inx4 and Inx5. Blue boxes represent putative TCF binding sites. white boxes represent exons. B. Expression profiles established using colorimetric WISH. i. Inx1. ii. Inx4. iii. Inx5.

We then cloned riboprobes for Inx1, Inx4, and Inx5, and established expression patterns via colorimetric WISH. The observed expression patterns align well with both the published RNA-seq of sectioned animals and with the cell type data from the single cell portal. Inx1 shows strong expression throughout the body with a slight increase around the bases of the tentacles (Fig. 7.1 Bi), in line with its transcripts appearing in almost all cell types and slightly stronger expression from sections near the head. Inx4 was reported to have graded expression strongest near the head and weakest near the foot, and to be expressed mostly in ectodermal cells. WISH results show domains of strong expression at the tentacle bases, and a fainter ectodermal gradient fading out down the length of the body. Interestingly, expression appears to be entirely absent in the head above the tentacle ring, a result that could not be intuited from existing information. This behavior is also clearly observed in buds prior to the formation of tentacles (Fig. 7.1 Bii), implying that the inhibition in the head is by the head organizer rather than by the tentacles themselves. Inx5 was likewise reported to have graded expression and to be ectodermal. WISH shows a faint ectodermal gradient strongest near the head, but with fainter and more poorly defined tentacle-base expression compared to Inx4. (Fig. 7.1 Biii)

Knowledge of where transcription occurs is valuable information, but fully characterizing these proteins ideally requires observing their expression and localization *in vivo* and perturbing them to determine their function. Proof of concept exists for both approaches. An Inx1-GFP fusion protein has been transiently expressed via gene gun, and showed correct localization to the cell membrane. [6] Thus, a strain stably expressing an innexin fusion protein should be possible, and could reveal protein localization. Intracellular localization is of particular interest given results suggesting that Cx43 can localize to the nucleus and

may act as a transcription factor. [19] Electroporated siRNA knockdown of various genes has been demonstrated in *Hydra* (e.g. [44]) and could reveal aspects of gene function via knockdown phenotypes. Antibodies represent a way to target innexins after translation: Takaku *et al.* developed an anti-Inx2 monoclonal antibody, and were able to show that treated animals lost contraction behavior [39]. Fraser *et al.* showed a change in patterning behavior following treatment with an antibody against a rat connexin [11]. This indicates that blocking antibodies may be a viable approach to perturbing gap junction connectivity without altering innexin expression or localization.

7.3.2 Innexin expression changes in response to Wnt upregulation

We utilized two approaches to upregulate canonical Wnt signaling: the small-molecule inhibitor alsterpaullone (ALP), and lithium chloride. Both are known to upregulate canonical Wnt signaling by inhibiting GSK3-β - ALP has been verified to work in this way in *Hydra* [8], while lithium has been widely used to this effect in other systems [17]. The impact on both Wnt3 and various innexins was assessed by WISH and by qPCR.

WISH represents a qualitative readout, but comparisons can be made between multiple samples using the same probe by stopping development at a set time. In this way, we can observe a dramatic increase in Inx1 expression in alsterpaullone-treated animals. (Fig. 7.2A) Inx4 and Inx5 are more challenging to interpret but appear to show decreased expression.

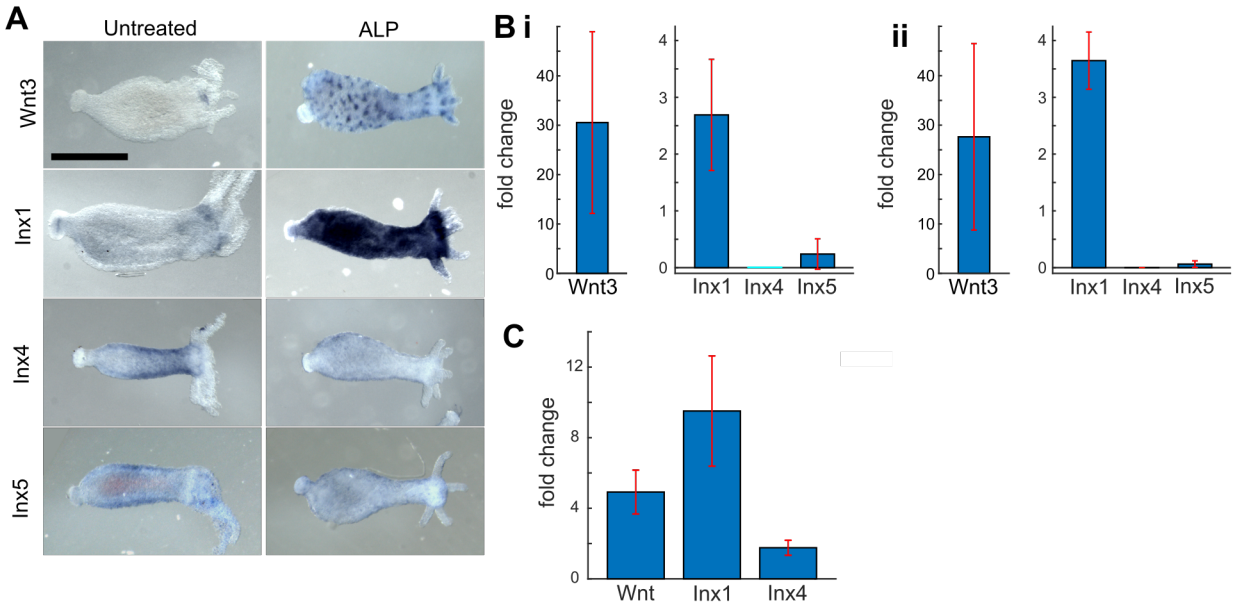

Figure 7.2: Wnt upregulation impacts innexin expression. A. WISH showing sharp upregulation of Inx1 and downregulation of Inx4 in response to ALP treatment. Scale bar 0.5 mm. B. qPCR results verifying the effect under Wnt upregulation by ALP. Inx4 represents a single successful replicate in i. and two successful replicates in ii. C. qPCR showing similar changes to innexin expression in response to LiCl treatment. For each qPCR treatment, biological replicates are shown separately. Error bars represent standard deviation among replicates.

qPCR was employed to obtain a quantitative readout with γ-tubulin as a reference gene. This confirms the WISH results: Inx1 is sharply upregulated, while Inx4 and Inx5 are downregulated (Fig. 7.2B).

Inx1 upregulation is of interest due to its near-ubiquitious expression, which makes it the most potentially similar of the *Hydra* innexins to Cx43. Such a dramatic upregulation in response to a specific inhibitor of GSK3-β is the strongest evidence we have yet uncovered for a crosstalk between innexins and Wnt signaling in *Hydra*. Inx4 downregulation is likewise consistent with WISH results (Fig. 7.1B). The reduction in expression was severe across both biological replicates. In Fig. 7.2Bi, only one of the technical triplicates amplified at a detectable level. As we believe this represents a very low number of transcripts rather than failed reactions, normalization was carried out using the one readable reaction and the means of triplicates for all other reactions. This value is displayed without an error bar. In Fig. 7.2Bii, one reaction failed to read and thus normalization was carried out with the remaining two replicates. Untreated animals show that Inx4 expression is natively low or nonexistent in the head above the tentacle ring, suggesting it may be inhibited by the head organizer. ALP causes widespread upregulation of Wnt signaling and eventually results in the formation of numerous ectopic head structures, so the reduction in both expression domain and overall number of transcripts of Inx4 in treated animals is somewhat expected.

Lithium ions in *Hydra* are a slightly more complex case: early publications observed that certain treatment protocols induced ectopic foot tissue, and theorized that this was due to downregulation of the head activator or upregulation of the head inhibitor [16]. Later work observes that treatment with antioxidants abolishes the ectopic foot phenotype, suggesting that the formation of ectopic tissue is a response to oxidative stress rather than the result of a

direct interaction with morphogen signaling [21]. The qPCR results shown here (Fig. 7.2C) clearly show an increase in Wnt3 expression, similar to but much less dramatic than in ALP-treated animals. This serves as quantitative validation that LiCl treatments do not induce ectopic foot tissue via inhibition of Wnt signaling, and strongly suggests that LiCl increases Wnt signaling by inhibiting GSK3-β in *Hydra* as it does in other organisms. Notably, there has been an observation of LiCl treatment leading to an upregulation of Cx43 in human cell lines [43]. This lends further weight to the observed upregulation of Inx1. The differences in Inx4 and Inx5 results compared to ALP may be explained by the lower specificity of Li^+ ions in comparison, but would require further exploration and study to confirm. Regardless, the consistent impact on innexin expression seen with multiple methods of Wnt signaling upregulation suggests that Wnt signaling does in fact impact innexin expression.

7.3.3 Wnt pathway inhibitors block head regeneration

iCRT14 is a thiazolidinedione that inhibits canonical Wnt signaling by destabilizing the β-catenin-TCF complex [14]. It has previously been used in *Hydra* to block regeneration of the head or foot [15], and to inhibit bud formation [47].

C59 is a small-molecule inhibitor of Porcupine (PORCN), a membrane bound O - acyltransferase required for palmitoylation and subsequent secretion of Wnt proteins. [38] Inhibition of PORCN results in reduction of Wnt/β-catenin signaling and activation of downstream genes, as well as processes reliant on Wnt signaling such as bone regrowth in zebrafish or certain cancers in mice [31, 37].

By utilizing two Wnt inhibitors with different targets, we can presume that any

impact observed in both treatments is indeed due to inhibition of Wnt signaling rather than an unknown side effect.

A reporter strain that uses the HyBra2 promoter to drive eGFP was used as an approximate *in vivo* readout of Wnt signaling during inhibitor treatments. HyBra2 is a T-box gene expressed in the hypostome [5].

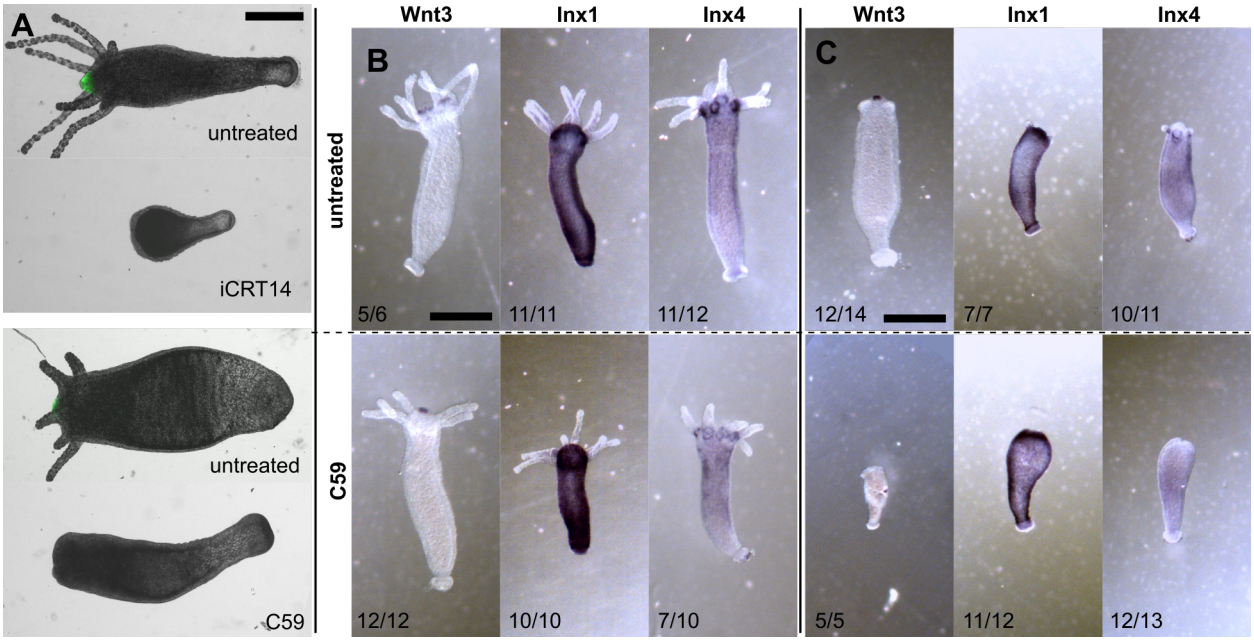

Figure 7.3: Wnt inhibitors block head regeneration. A. Live images of HyBra animals 72 h after decapitation showing inhibition of head regeneration and HyBra2 expression by iCRT14 and C59. Scale bar 0.5 mm. B. WISH results on intact animals comparing untreated to 72 h C59 incubation. C. WISH results on decapitated animals comparing untreated to 72 h C59 incubation. Scale bars 0.5 mm; numbers indicate how many animals within the experiment resemble the example.

The previously reported head inhibition phenotype of iCRT14 was successfully reproduced, and a similar head inhibition phenotype was established for C59. (Fig. 7.3A) For both inhibitors head regeneration is suppressed for up to 72 h, and resumes within 48 h of the animals being transferred back to HM. No HyBra signal can be observed, suggesting that the formation of the head organizer itself is blocked rather than solely the formation of visible head structures.

We then used WISH to qualitatively observe the impact of inhibitor treatment on both intact and decapitated animals. There was not a visible reduction of expression of Wnt in intact animals. (Fig. 7.3B) WISH of decapitated animals at 72 h verified that no head organizer is formed, but was otherwise uninformative. (Fig. 7.3C)

Likewise, we did not observe clear impacts on innexin expression. Inx1 expression appeared entirely unaffected. Inx4 expression may be slightly decreased in intact C59-treated animals, particularly at the tentacle bases. (Fig. 7.3B) In decapitated C59-treated animals, Inx4 expression appears reduced at the oral end of the animal rather than extending the gradient seen in intact animals. (Fig. 7.3C) However, the WISH results are not clear enough on their own to support a claim of changed innexin expression.

We attempted to quantify innexin expression using qPCR, but encountered technical difficulties with both the machine and certain housekeeping genes and were not able to complete the asssay in the time available. Verification of the effects of iCRT14 and C59 on both innexins and Wnt pathway genes is a high priority for the future of this project.

The WISH results on decapitated vs. intact animals combined with the head regeneration phenotype strongly suggests that disrupting a new head organizer as it forms is significantly easier than abolishing an established one. Models of the head organizer indicate

it is quite strongly self-sustaining, and the published iCRT14 result looked at inhibition of budding rather than trying to abolish the existing organizer, so this proposal is consistent with existing knowledge.

7.3.4 siRNA against Wnt pathway genes

Previous work showed successful use of electroporated siRNA to knock down Sp5 and β-catenin [44], resulting in clearly observable phenotypes. We utilized the published siRNA sequences and electroporation protocol as an alternate method of inhibiting specific parts of the Wnt signaling pathway. Knockdown of the Wnt inhibitor Sp5 should roughly parallel the Wnt overexpression of ALP, while knockdown of β-catenin should be analogous to blocking or inhibiting Wnt signaling.

The published phenotypes for these siRNA knockdowns after 3 electroporations and 2 further days of recovery are ectopic head structures below the existing head for Sp5, and lumps on the body axis for β-catenin. [44] We were able to accurately reproduce the Sp5 phenotype, though ectopic heads were observed earlier in the siRNA protocol and more frequently in general on buds compared to the parental axis. We did not consistently observe the lump phenotype for β-catenin, though we did note that the animals were consistently stumpy and appeared generally stressed compared to the scramble siRNA treatment. (Fig. 7.4Aii) Given that the Sp5 phenotype seems accurate and the animals are clearly responding to the knockdown in a way different to scramble siRNA, we tentatively conclude that this difference is due to variability between strains and populations of *Hydra* or in experimental conditions.

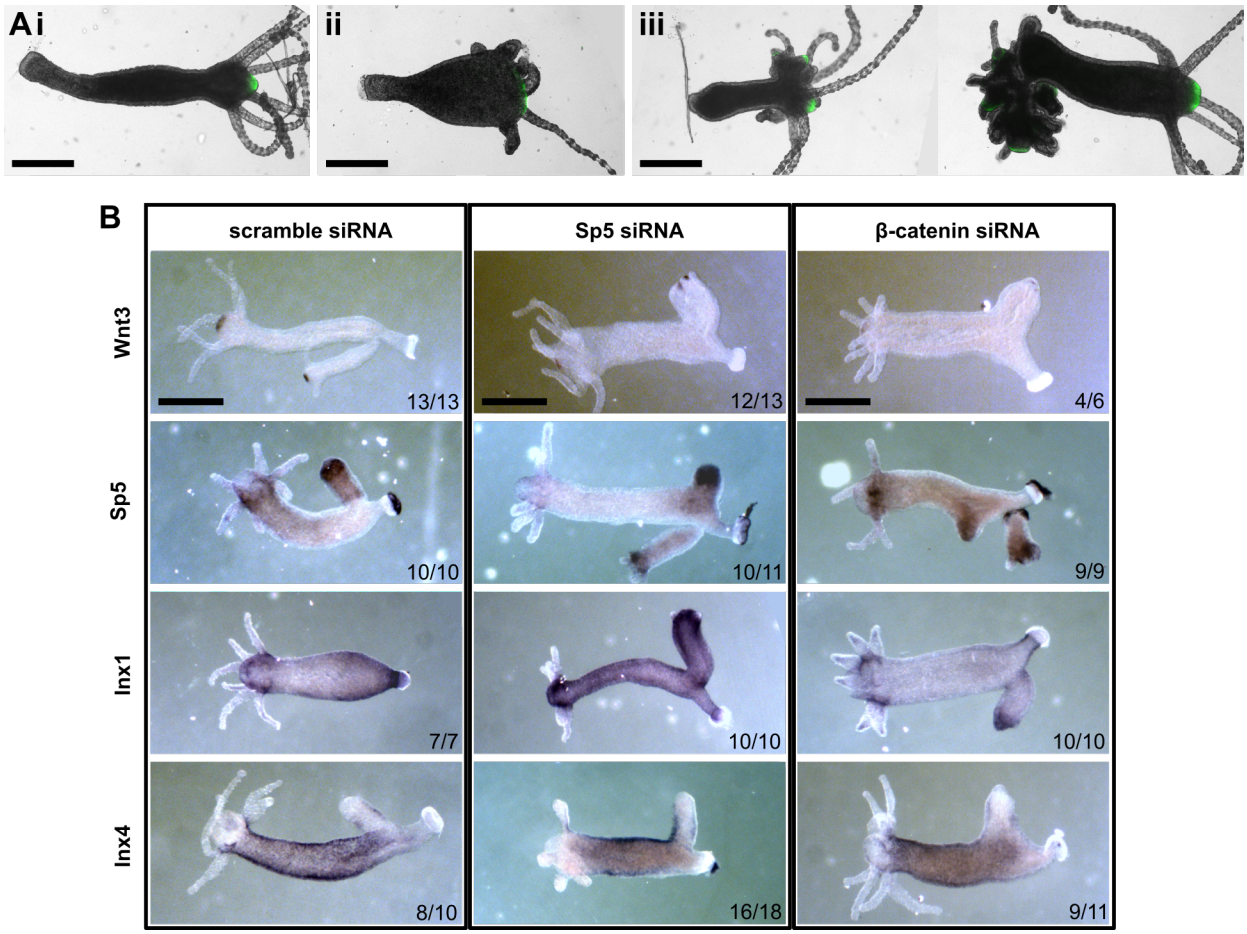

Figure 7.4: siRNA knockdown of Wnt pathway genes. A. Live imaging of HyBra-GFP animals. i. Scramble siRNA. ii. β-catenin siRNA, showing contracted phenotype. iii. Sp5 siRNA, showing ectopic heads on both the main body axis and on a bud. Scale bars 0.5 mm. B. Representative WISH images. Scale bars 0.5 mm; numbers indicate how many animals within the experiment resemble the example.

WISH was conducted on animals fixed on day 3 of the siRNA protocol, after the second electroporation. This was because marked morphological phenotypes were sometimes observed as early as the third electroporation, rendering interpretation challenging. Results are varied. Sp5 siRNA clearly increases Wnt expression, with multiple head organizer-like patches appearing well in advance of observable ectopic head structures. However, the impacts on Sp5 itself are less clear - there is possibly a decrease in expression level on the main body axis, but this is inconsistent and expression domain does not appear to be altered. (Fig. 7.4B) It is possible that once ectopic head organizers are formed they rapidly establish downstream gene expression including Sp5, which would render the effects of the initial knockdown transient and difficult to observe by WISH. β-catenin siRNA is more challenging to interpret. There may be a slight reduction in Wnt expression, although again this is somewhat ambiguous and inconsistent. (Fig. 7.4B) There do not appear to be changes to Sp5 expression.

Innexin expression may be subtly impacted by both knockdowns. Inx1 expression appears to be strengthened by Sp5 siRNA, and slightly reduced by β-catenin siRNA. Inx4 expression appears to be altered by Sp5 siRNA, with loss of the strong expression around tentacle bases and expansion of the clear zone in the head. (Fig. 7.4B) If we presume that Sp5 knockdown is analogous to upregulation of Wnt signaling and β-catenin knockdown resembles a downregulation of Wnt signaling, these results are consistent with the changes seen in ALP-treated animals. We attempted to verify these results by qPCR, and obtained some very preliminary results that appear consistent with the WISH. However, due to the ongoing nature of our aforementioned difficulties, further work is needed before quantitative conclusions can be drawn.

7.4 Conclusions

We have amassed a reasonably broad collection of preliminary evidence suggesting that perturbations to Wnt signaling can alter innexin expression in *Hydra*. The wide range of methods used strongly suggests that the impacts seen are not experimental artifacts. However, significant work remains to be done to conclusively establish and properly characterize this link.

To confirm the preliminary results presented here, it will be necessary to obtain a better quantitative understanding of how each of the perturbations (pharmacological activation or inhibition of Wnt signaling, siRNA knockdowns) impacts expression of both Wnt pathway genes and innexins. This can be achieved by further qPCR to strengthen the preliminary data presented here with further technical and biological replicates, or by RNA-seq to obtain a more complete picture of the transcriptome.

To fully explore the nature of the Wnt-innexin link, direct work on innexins will be necessary. Our results clearly demonstrate that innexin expression can be impacted by Wnt signaling. If innexins are truly a component of the signaling pathway rather than simply downstream targets, perturbing innexin function will result in Wnt signaling and patterning defects. The most promising strategies for gap junction blocking are developing antibodies as seen in some previous *Hydra* publications, or applying siRNA knockdown to innexins directly.

Carrying out some or all of this additional work to establish and further study the canonical Wnt signaling - gap junction connection in *Hydra* has the potential to close a major gap in our knowledge of pattern formation in this model system. More generally, it would

extend knowledge of gap junction proteins as a component of the Wnt signaling pathway from vertebrate to invertebrate models.

7.5 Acknowledgements

I would like to thank Christina Rabeler for assistance with qPCR, and Dr. Robert E. Steele for suggestions and discussions regarding this work.

Bibliography

[1] Zhaowei Ai, Avi Fischer, David C. Spray, Anthony M.C. Brown, and Glenn I. Fishman. "Wnt-1 regulation of connexin43 in cardiac myocytes". In: *Journal of Clinical Investigation* 105.2 (Jan. 2000), pp. 161–171. ISSN: 00219738. DOI: 10.1172/JCI7798.

[2] Haris Alexopoulos, Angelika Böttger, Sylvia Fischer, Alice Levin, Alexander Wolf, Toshitaka Fujisawa, Shiho Hayakawa, Takashi Gojobori, Jane A. Davies, Charles N. David, and Jonathan P. Bacon. "Evolution of gap junctions: the missing link?" In: *Current Biology* 14.20 (Oct. 2004), R879–R880. ISSN: 09609822. DOI: 10.1016/j.cub.2004.09.067.

[3] Reinhard Bauer, Corinna Lehmann, Bernhard Fuss, Franka Eckardt, and Michael Hoch. "The Drosophila gap junction channel gene innexin 2 controls foregut development in response to Wingless signalling". In: *Journal of Cell Science* 115.9 (2002), pp. 1859–1867. ISSN: 00219533.

[4] Eric C Beyer, David L Paul, and Daniel A Goodenough. *Connexin family of gap junction proteins*. 1990. DOI: 10.1007/BF01868459.

[5] Holger Bielen, Sabine Oberleitner, Sylvain Marcellini, Lydia Gee, Patrick Lemaire, Hans R. Bode, Ralph Rupp, and Ulrich Technau. "Divergent functions of two ancient Hydra Brachyury paralogues suggest specific roles for their C-terminal domains in tissue fate induction". In: *Development* 134.23 (2007), pp. 4187–4197. ISSN: 09501991. DOI: 10.1242/dev.010173.

[6] Angelika Böttger, Olga Alexandrova, Mihai Cikala, Marsha Schade, Michaela Herold, and Charles N. David. "GFP expression in Hydra: Lessons from the particle gun". In: *Development Genes and Evolution* 212.6 (2002), pp. 302–305. ISSN: 0949944X. DOI: 10.1007/s00427-002-0245-0.

[7] Erez Braun and Hillel Ori. "Electric-Induced Reversal of Morphogenesis in Hydra". In: *Biophysical Journal* 117.8 (Oct. 2019), pp. 1514–1523. ISSN: 15420086. DOI: 10.1016/j.bpj.2019.09.007.

[8] Mariya Broun, Lydia Gee, Beate Reinhardt, and Hans R Bode. "Formation of the head organizer in hydra involves the canonical Wnt pathway". In: *Development* 132.12 (2005), pp. 2907–2916. DOI: 10.1242/dev.01848.

[9] Ken M. Cadigan and Marian L. Waterman. "TCF/LEFs and Wnt signaling in the nucleus". In: *Cold Spring Harbor Perspectives in Biology* 4.11 (Nov. 2012). ISSN: 19430264. DOI: 10.1101/cshperspect.a007906.

[10] Jarrod A. Chapman, Ewen F. Kirkness, Oleg Simakov, Steven E. Hampson, Therese Mitros, Thomas Weinmaier, Thomas Rattei, Prakash G. Balasubramanian, Jon Borman, Dana Busam, Kathryn Disbennett, Cynthia Pfannkoch, Nadezhda Sumin, Granger G. Sutton, Lakshmi Devi Viswanathan, Brian Walenz, David M. Goodstein, Uffe Hellsten, Takeshi Kawashima, Simon E. Prochnik, Nicholas H. Putnam,

Shengquiang Shu, Bruce Blumberg, Catherine E. Dana, Lydia Gee, Dennis F. Kibler, Lee Law, Dirk Lindgens, Daniel E. Martinez, Jisong Peng, Philip A. Wigge, Bianca Bertulat, Corina Guder, Yukio Nakamura, Suat Ozbek, Hiroshi Watanabe, Konstantin Khalturin, Georg Hemmrich, André Franke, René Augustin, Sebastian Fraune, Eisuke Hayakawa, Shiho Hayakawa, Mamiko Hirose, Jung Shan Hwang, Kazuho Ikeo, Chiemi Nishimiya-Fujisawa, Atshushi Ogura, Toshio Takahashi, Patrick R.H. Steinmetz, Xiaoming Zhang, Roland Aufschnaiter, Marie Kristin Eder, Anne Kathrin Gorny, Willi Salvenmoser, Alysha M. Heimberg, Benjamin M. Wheeler, Kevin J. Peterson, Angelika Böttger, Patrick Tischler, Alexander Wolf, Takashi Gojobori, Karin A. Remington, Robert L. Strausberg, J. Craig Venter, Ulrich Technau, Bert Hobmayer, Thomas C.G. Bosch, Thomas W. Holstein, Toshitaka Fujisawa, Hans R. Bode, Charles N. David, Daniel S. Rokhsar, and Robert E. Steele. "The dynamic genome of Hydra". In: *Nature* 464.7288 (2010), pp. 592–596. ISSN: 00280836. DOI: 10.1038/nature08830.

[11] Scorr E. Fraser, Colin R. Green, Hans R. Bode, and Norton B. Gilula. "Selective disruption of gap junctional communication interferes with a patterning process in hydra". In: *Science* 237.4810 (July 1987), pp. 49–55. ISSN: 00368075. DOI: 10.1126/science.3037697.

[12] K. M. Glauber, C. E. Dana, S. S. Park, D. A. Colby, Y. Noro, T. Fujisawa, A. R. Chamberlin, and R. E. Steele. "A small molecule screen identifies a novel compound that induces a homeotic transformation in Hydra". In: *Development* 142.11 (2015), pp. 2081–2081. ISSN: 0950-1991. DOI: 10.1242/dev.126235.

[13] Tapan Goel, Rui Wang, Sara Martin, Elizabeth Lanphear, and Eva Maria S. Collins. "Linalool acts as a fast and reversible anesthetic in Hydra". In: *PLoS ONE* 14.10 (Mar. 2019), p. 584946. ISSN: 19326203. DOI: 10.1371/journal.pone.0224221.

[14] Foster C. Gonsalves, Keren Klein, Brittany B. Carson, Shauna Katz, Laura A. Ekas, Steve Evans, Robert Nagourney, Timothy Cardozo, Anthony M.C. Brown, and Ramanuj Das Gupta. "An RNAi-based chemical genetic screen identifies three small-molecule inhibitors of the Wnt/wingless signaling pathway". In: *Proceedings of the National Academy of Sciences of the United States of America* 108.15 (Apr. 2011), pp. 5954–5963. ISSN: 10916490. DOI: 10.1073/pnas.1017496108.

[15] S. Gufler, B. Artes, H. Bielen, I. Krainer, M. K. Eder, J. Falschlunger, A. Bollmann, T. Ostermann, T. Valovka, M. Hartl, K. Bister, U. Technau, and B. Hobmayer. "β-Catenin acts in a position-independent regeneration response in the simple eumetazoan Hydra". In: *Developmental Biology* 433.2 (Jan. 2018), pp. 310–323. ISSN: 1095564X. DOI: 10.1016/j.ydbio.2017.09.005.

[16] Monika Hassel, Kerstin Albert, and Sonja Hofheinz. "Pattern formation in Hydra vulgaris is controlled by lithium-sensitive processes". In: *Developmental Biology* 156.2 (1993), pp. 362–371. ISSN: 00121606. DOI: 10.1006/dbio.1993.1083.

[17] Chester M. Hedgepeth, Leslee J. Conrad, Jie Zhang, Hui Chuan Huang, Virginia M.Y. Lee, and Peter S. Klein. "Activation of the Wnt signaling pathway: A molecular mech-

anism for lithium action". In: *Developmental Biology* 185.1 (May 1997), pp. 82–91. ISSN: 00121606. DOI: 10.1006/dbio.1997.8552.

[18] Bert Hobmayer, Fabian Rentzsch, Kerstin Kuhn, Christoph M Happel, Christoph Cramer Von Laue, Petra Snyder, Ute Rothbächer, and Thomas W Holstein. "WNT signalling molecules act in axis formation in the diploblastic metazoan Hydra". In: *Nature* 407.6801 (2000), pp. 186–189. ISSN: 00280836. DOI: 10.1038/35025063.

[19] Xiaoming Hou, Mohammad R. A. Khan, Mark Turmaine, Christopher Thrasivoulou, David L Becker, and Aamir Ahmed. "Wnt signaling regulates cytosolic translocation of connexin 43". In: *American Journal of Physiology-Regulatory, Integrative and Comparative Physiology* 317.2 (Aug. 2019), R248–R261. ISSN: 0363-6119. DOI: 10.1152/ajpregu.00268.2018.

[20] *Hydra 2.0 Web Portal*.

[21] H. Jantzen, M. Hassel, and I. Schulze. "Hydroperoxides mediate lithium effects on regeneration in Hydra". In: *Comparative Biochemistry and Physiology - C Pharmacology Toxicology and Endocrinology* 119.2 (Feb. 1998), pp. 165–175. ISSN: 07428413. DOI: 10.1016/S0742-8413(97)00204-1.

[22] Howard M. Lenhoff and Ray DuBois Brown. "Mass culture of hydra: an improved method and its application to other aquatic invertebrates". In: *Laboratory Animals* 4.1 (Apr. 1970), pp. 139–154. ISSN: 0023-6772. DOI: 10.1258/002367770781036463.

[23] Anton Livshits, Lital Shani-Zerbib, Yonit Maroudas-Sacks, Erez Braun, and Kinneret Keren. "Structural Inheritance of the Actin Cytoskeletal Organization Determines the Body Axis in Regenerating Hydra". In: *Cell Reports* 18.6 (Feb. 2017), pp. 1410–1421. ISSN: 22111247. DOI: 10.1016/j.celrep.2017.01.036.

[24] William D. Marks and I. Martha Skerrett. "Role of amino terminus in voltage gating and junctional rectification of Shaking B innexins". In: *Journal of Neurophysiology* 111.6 (Mar. 2014), pp. 1383–1395. ISSN: 15221598. DOI: 10.1152/jn.00385.2013.

[25] Daniel J. Olson, Jan L. Christian, and Randall T. Moon. "Effect of Wnt-1 and related proteins on gap junctional communication in Xenopus embryos". In: *Science* 252.5009 (1991), pp. 1173–1176.

[26] Néstor J. Oviedo and Michael Levin. "Smedinx-11 is a planarian stem cell gap junction gene required for regeneration and homeostasis". In: *Development* 134.17 (Sept. 2007), pp. 3121–3131. ISSN: 09501991. DOI: 10.1242/dev.006635.

[27] Néstor J. Oviedo, Junji Morokuma, Peter Walentek, Ido P. Kema, Man Bock Gu, Joo Myung Ahn, Jung Shan Hwang, Takashi Gojobori, and Michael Levin. "Long-range neural and gap junction protein-mediated cues control polarity during planarian regeneration". In: *Developmental Biology* 339.1 (Mar. 2010), pp. 188–199. ISSN: 1095564X. DOI: 10.1016/j.ydbio.2009.12.012.

[28] Bret J. Pearson, George T. Eisenhoffer, Kyle A. Gurley, Jochen C. Rink, Diane E. Miller, and Alejandro Sánchez Alvarado. "Formaldehyde-based whole-mount in situ hybridization method for planarians". In: *Developmental Dynamics* 238.2 (Feb. 2009), pp. 443–450. ISSN: 10588388. DOI: 10.1002/dvdy.21849.

[29] T. Harshani Peiris and Néstor J. Oviedo. *Gap junction proteins: Master regulators of the planarian stem cell response to tissue maintenance and injury*. Jan. 2013. DOI: 10.1016/j.bbamem.2012.03.005.

[30] Pauline Phelan and Todd A. Starich. *Innexins get into the gap*. May 2001. DOI: 10.1002/bies.1057.

[31] Kyle David Proffitt, Babita Madan, Zhiyuan Ke, Vishal Pendharkar, Lijun Ding, May Ann Lee, Rami N. Hannoush, and David M. Virshup. "Pharmacological inhibition of the Wnt acyltransferase PORCN prevents growth of WNT-driven mammary cancer". In: *Cancer Research* 73.2 (Jan. 2013), pp. 502–507. ISSN: 00085472. DOI: 10.1158/0008-5472.CAN-12-2258.

[32] Teresa M. Ribeiro-Rodrigues, Tânia Martins-Marques, Sandrine Morel, Brenda R. Kwak, and Henrique Girão. *Role of connexin 43 in different forms of intercellular communication - gap junctions, extracellular vesicles and tunnelling nanotubes*. Nov. 2017. DOI: 10.1242/jcs.200667.

[33] F. Rinaldi, E. M. Hartfield, L. A. Crompton, J. L. Badger, C. P. Glover, C. M. Kelly, A. E. Rosser, J. B. Uney, and M. A. Caldwell. "Cross-regulation of Connexin43 and β-catenin influences differentiation of human neural progenitor cells." In: *Cell death & disease* 5.1 (2014), e1017. ISSN: 20414889. DOI: 10.1038/cddis.2013.546.

[34] Stefan Siebert, Jeffrey A. Farrell, Jack F. Cazet, Yashodara Abeykoon, Abby S. Primack, Christine E. Schnitzler, and Celina E. Juliano. "Stem cell differentiation trajectories in Hydra resolved at single-cell resolution". In: *Science* 365.6451 (July 2019). ISSN: 10959203. DOI: 10.1126/science.aav9314.

[35] *Single Cell Portal*.

[36] I. Martha Skerrett and Jamal B. Williams. *A structural and functional comparison of gap junction channels composed of connexins and innexins*. May 2017. DOI: 10.1002/dneu.22447.

[37] Scott Stewart, Alan W. Gomez, Benjamin E. Armstrong, Astra Henner, and Kryn Stankunas. "Sequential and Opposing Activities of Wnt and BMP Coordinate Zebrafish Bone Regeneration". In: *Cell Reports* 6.3 (2014), pp. 482–498. ISSN: 2211-1247. DOI: https://doi.org/10.1016/j.celrep.2014.01.010.

[38] Ritsuko Takada, Yoshinori Satomi, Tomoko Kurata, Naoto Ueno, Shigemi Norioka, Hisato Kondoh, Toshifumi Takao, and Shinji Takada. "Monounsaturated Fatty Acid Modification of Wnt Protein: Its Role in Wnt Secretion". In: *Developmental Cell* 11.6 (Dec. 2006), pp. 791–801. ISSN: 15345807. DOI: 10.1016/j.devcel.2006.10.003.

[39] Yasuharu Takaku, Jung Shan Hwang, Alexander Wolf, Angelika Böttger, Hiroshi Shimizu, Charles N. David, and Takashi Gojobori. "Innexin gap junctions in nerve cells coordinate spontaneous contractile behavior in Hydra polyps". In: *Scientific Reports* 4.1 (Jan. 2014), pp. 1–8. ISSN: 20452322. DOI: 10.1038/srep03573.

[40] Brenda Thornton and Chhandak Basu. "Real-time PCR (qPCR) primer design using free online software". In: *Biochemistry and Molecular Biology Education* 39.2 (Mar. 2011), pp. 145–154. ISSN: 14708175. DOI: 10.1002/bmb.20461.

[41] Andreas Untergasser, Ioana Cutcutache, Triinu Koressaar, Jian Ye, Brant C. Faircloth, Maido Remm, and Steven G. Rozen. "Primer3-new capabilities and interfaces". In: *Nucleic Acids Research* 40.15 (Aug. 2012), e115. ISSN: 03051048. DOI: 10.1093/nar/gks596.

[42] Maitreyi Upadhyay, Yesenia Martino Cortez, SiuWah Wong-Deyrup, Leticia Tavares, Sean Schowalter, Pooja Flora, Corinne Hill, Mohamad Ali Nasrallah, Sridar Chittur, and Prashanth Rangan. "Transposon Dysregulation Modulates dWnt4 Signaling to Control Germline Stem Cell Differentiation in Drosophila". In: *PLOS Genetics* 12.3 (Mar. 2016). Ed. by Erika L. Matunis, e1005918. ISSN: 1553-7404. DOI: 10.1371/journal.pgen.1005918.

[43] Marcel A.G. Van der Heyden, Martin B. Rook, Monique M.P. Hermans, Gert Rijksen, Johannes Boonstra, Libert H.K. Defize, and Olivier H.J. Destrée. "Identification of connexin43 as a functional target for Wnt signalling". In: *Journal of Cell Science* 111.12 (May 1998), pp. 1741–1749. ISSN: 00219533.

[44] Matthias C. Vogg, Leonardo Beccari, Laura Iglesias Ollé, Christine Rampon, Sophie Vriz, Chrystelle Perruchoud, Yvan Wenger, and Brigitte Galliot. "An evolutionarily-conserved Wnt3/β-catenin/Sp5 feedback loop restricts head organizer activity in Hydra". In: *Nature Communications* 10.1 (Dec. 2019), pp. 1–15. ISSN: 20411723. DOI: 10.1038/s41467-018-08242-2.

[45] Rui Wang and Eva Maria S. Collins. "A novel bilateral grafting technique for studying patterning in Hydra". In: *Developmental Biology* 462.1 (Mar. 2020), pp. 60–65. ISSN: 1095564X. DOI: 10.1016/j.ydbio.2020.03.006.

[46] Rui Wang, Tapan Goel, Kate Khazoyan, Ziad Sabry, Heng J. Quan, Patrick H. Diamond, and Eva Maria S. Collins. "Mouth Function Determines the Shape Oscillation Pattern in Regenerating Hydra Tissue Spheres". In: *Biophysical Journal* 117.6 (Sept. 2019), pp. 1145–1155. ISSN: 15420086. DOI: 10.1016/j.bpj.2019.07.051.

[47] Hiroshi Watanabe, Heiko A. Schmidt, Anne Kuhn, Stefanie K. Höger, Yigit Kocagöz, Nico Laumann-Lipp, Suat Özbek, and Thomas W. Holstein. "Nodal signalling determines biradial asymmetry in Hydra". In: *Nature* 515.7525 (Nov. 2014), pp. 112–115. ISSN: 14764687. DOI: 10.1038/nature13666.

[48] Y. Wenger, W. Buzgariu, and B. Galliot. "Loss of neurogenesis in Hydra leads to compensatory regulation of neurogenic and neurotransmission genes in epithelial cells". In: *Philosophical Transactions of the Royal Society B: Biological Sciences* 371.1685 (Jan. 2016), p. 20150040. ISSN: 14712970. DOI: 10.1098/rstb.2015.0040.

Chapter 8

Conclusions and Future Directions

The work presented here makes significant improvements to the field's knowledge. I have combined new advances with creative adaptation of old methods to test two persistent assumptions utilized in the construction of mathematical models of patterning. This led to the discovery that a shift in oscillation pattern shift is not a marker of axis specification, and that tissue fragments inherit a body axis and thus cannot be used to model *de novo* pattern formation. I have additionally implemented a new fluorescent protein in *Hydra*, and laid groundwork for the development of new transgenic strains that will enable *in vivo* visualization of Wnt and Sp5 localization. Finally I provide preliminary data suggesting that gap junction proteins may interact with Wnt signaling in *Hydra*, similar to the cross-regulation observed in other model organisms. These findings open the door for a variety of further investigations.

For instance, establishing that several core assumptions of existing models were inaccurate does not necessarily disprove their central premise. It is possible that tissue strain does play a role in patterning in the absence of an inherited morphogen gradient. Future

studies in this area should therefore shift exclusively to cell aggregates. One key concern to address is that we currently assume that aggregates must set their body axis and associated biochemical gradients from a completely isotropic state. However, we cannot say for certain that this is the case - the axis or head organizer could be influenced by cues not lost during reaggregation, such as cell polarity, or they could be established following another currently unknown event or process. Therefore, we should prioritize first confirming that cell aggregates do not inherit axis information, followed by direct study of axis formation. The potential crosstalk between morphogen signaling and mechanical force could be tested via a combination of mechanical perturbation using microfluidics, and pharmacological perturbation of biochemical patterning.

My preliminary data showing possible regulation of innexin expression by Wnt signaling also requires significant additional confirmation. Future efforts in this area will focus on quantifying the impacts of Wnt signaling on innexins via qPCR or RNA-seq, and testing for patterning defects or impacts on Wnt signaling when innexins are perturbed. Gap junction communication can be inhibited via methods such as drugs or blocking antibodies, or innexin proteins can be targeted directly via siRNA knockdown. If and when a Wnt-innexin feedback is firmly established, determining whether this interaction was relevant to forming a Wnt signaling gradient would once again require carefully designed studies in cell aggregates.

With the previous two points in mind, it becomes clear that many potential major advances in the study of *Hydra* patterning hinge on improving our ability to observe biochemistry in the living animal. Both avenues of study require the use of cell aggregates, and the ability to determine with relative precision the timings of biochemical events. Ideally, visualization of endogenous proteins and their spatial and temporal interactions would enable

direct observations of axis and pattern formation *in vivo*, which we currently lack the tools to accomplish. To this end I believe that the most important aspect of any continuation of this work is the development of fluorescent fusion protein reporter strains. In the short term, the most efficient targets are likely those genes that can be visualized well with the existing plasmid microinjection method - innexins do not require every molecule to be tagged to accurately visualize localization, and more broadly expressed proteins such as Sp5 will be more easily imaged and less sensitive to the introduction of an additional copy of the coding sequence.

The long term goal should be the optimization of genome editing techniques for *Hydra*, and knocking fluorescent proteins into the genomic loci of genes of interest. One approach is further optimization of existing embryo microinjection protocols for the delivery of CRISPR reagents. Alternatively, we could attempt to exploit *Hydra*'s regenerative prowess by developing methods for genomic editing in either an intact animal or in cell suspension, followed by isolation of the desired transgenic from the resultant mosaic. For example, electroporation has been shown to be effective in delivery of siRNA into adult *Hydra*, and is a known method of delivering CRISPR reagents into cultured cells. Other established transfection methods could also be explored.

In summary, this work presents valuable experimental insights into axis specification in *Hydra*, and establishes several useful methods and tools as a basis for further quantitative study. I sincerely hope that future researchers can utilize these results to realize *Hydra*'s full potential as a model organism.

Appendix A

Protocols and Scripts

A.1 Riboprobe Synthesis

This protocol begins with a template plasmid containing the riboprobe sequence, flanked by RNA polymerase binding sites. Select appropriate primers to generate an amplicon containing both the probe sequence and the binding sites.

1. Amplify template fragment by PCR.

2. Confirm PCR amplification by nanodrop and/or gel electrophoresis.

3. Ethanol precipitate PCR product.

    - Add 55 μL nuclease-free water to remaining PCR product and transfer to a clean 1.7 mL microcentrifuge tube.
    - Add 33 μL 7.5M ammonium acetate (stored at 4°C) and tap or gently vortex to mix.

- Add 200 μL cold 100% ethanol and vortex gently to mix.
- Incubate at -20°C for at least 30 min.
- Centrifuge at 18000xg, 4°C, 20 min.
- Gently pipet out supernatant without disturbing pellet.
- Add 100 μL cold 80% ethanol and tap gently or invert once to mix.
- Centrifuge at 18000xg, 4°C, 5 min.
- Gently remove all supernatant without disturbing pellet.
- Air dry pellet at room temperature for 5-10 min. Pellet should appear slightly gummy with no remaining liquid, but should not be allowed to dry completely.
- Resuspend in 20 μL DEPC-treated water.

4. Spec cleaned template on nanodrop - concentration should be 40-100 ng/μL.

5. *in vitro* transcription reaction. From this point forwards, use RNAse-free tips and reagents.

   Reaction mix:

2.5 μL	5X transcription buffer (Thermo Fisher)
X μL	200 ng PCR product (or max volume 5 μL)
0.5 μL	RNAseOUT
1 μL	polymerase (ex. T3, T7, Sp6)
1.25 μL	10X DIG RNA labeling mix
to 12.5 μL	DEPC-treated H_2O

   - Flick tube to mix, then place in 37°C water bath for 2 h.
   - Add 0.75 μL RQ1 DNAse, flick gently to mix, and incubate for 15 min in 37°C water bath.

- Place reaction on ice.

6. Ethanol precipitate probe to clean for use.

    - Add 12.5 μL DEPC water to *in vitro* transcription reaction.
    - Add 2.5 μL chilled 4M LiCl. (Solution stored at 4°C.) Tap tube to mix.
    - Add 75 μL cold 100% ethanol. Tap tube to mix, then place at -80°C 1-2 h, or overnight.
    - Centrifuge at 18000xg and 4°C for 30 min. Gently remove the supernatant, being careful not to disturb the pellet. Keep pellet on ice while working.
    - Add 100 μL cold 70% ethanol (diluted with DEPC water) and tap gently or invert once to mix.
    - Centrifuge at 18000xg, 4°C, for 7 min. Aspirate supernatant without disturbing pellet.
    - Air dry pellet for 5 min at room temperature, or until pellet is slighly gummy with no visible liquid. Do not overdry.
    - Resuspend in 25 μL DEPC-treated water and mix gently. Move tube back to ice and keep cold.

7. Spec and resuspend in hybridization buffer.

    - If desired, quality check probe by running 5 μL on a gel with settings optimized for RNA.
    - Spec sample on nanodrop. Concentration should be 200-400 ng/μL.

- Resuspend to a concentration of 50 ng/μL in hybridization buffer. Store probe at -20°C.

A.2 Colorimetric Whole-mount In Situ Hybridization

WIP

Fixation

1. Relax animals in 1 mM linalool in *Hydra* medium (HM) for 5 minutes
2. Fix in 4% paraformaldehyde (PFA) in HM for 1 hour at room temperature
3. Remove PFA with 3 quick washes in PBSTx
4. Transfer animals to methanol for bleaching
    - 1x 5 min wash in 33% methanol
    - 1x 5 min wash in 66% methanol
    - Transfer to 100% methanol
5. Animals can either be incubated in methanol at room temperature until all color is removed for immediate use, or stored in methanol at -20°C for later use

Hybridization

1. Rehydrate animals via methanol gradient
    - 1x 5 min wash in 66% methanol
    - 1x 5 min wash in 33% methanol

- Transfer to PBSTx

2. 3x 10 min washes in PBSTx
3. If necessary, separate animals into 1.7 mL microcentrifuge tubes for each probe with up to 15 animals per tube. Subsequent washes use 200 μL of liquid each.
4. Treat with 10 μg/μL proteinase K in PBSTx for 5 minutes at room temperature
5. Stop digestion with quick wash in 4 mg/mL glycine in PBSTx, followed by 1x 10 min wash in glycine
6. 3x 10 min washes in PBSTx
7. 2x 10 min washes in triethanolamine (662 μL in 50 mL PBSTx)
8. 5 min wash in 3 μL/mL acetic anhydride in triethanolamine (add acetic anhydride to triethanolamine immediately before use, and shake vigorously to dissolve)
9. 5 min wash in 6 μL/mL acetic anhydride in triethanolamine
10. 3x 5 min washes in PBSTx
11. Refix in 4% PFA for 1 h at room temperature
12. 3x 5-10 min washes in PBSTx
13. 2x 5 min washes in 2X SSCTx
14. 10 min wash in 50% 2X SSCTx/50% prehyb. Start at room temperature and transfer to 60°C.

15. 10 min wash with prewarmed prehyb at 60°C

16. Prehybridize in fresh change of prewarmed prehyb for 2 h at 60°C

17. Add riboprobe

    - Dilute probe 1:100 in hyb buffer on first use
    - Denature probe for 5 min at 85°C
    - Remove prehyb, and add denatured probe solution

18. Hybridize at 60°C for 2.5 days

Antibody labeling Steps 1-5 use solutions prewarmed to 60°C.

1. 10 min wash in prehyb

    - Carefully remove as much of riboprobe solution as possible and store in sealed tubes at -20°C for reuse

2. 10 min wash in 66% prehyb/33% 2X SSCTx

3. 10 min wash in 33% prehyb/66% 2X SSCTx

4. 2x 30 min wash in 2X SSCTx. Second wash begins at 60°C and transitions to room temperature.

5. 4x 10 min wash in MABT

6. 1x 2h wash in blocking buffer (80% MABT/10% sheep serum)

7. Incubate overnight in 1:2000 solution of anti-DIG-AP (src) in blocking buffer at 4°C

Development

1. 2x quick washes in MABT to remove antibody solution, then 6-10x washes in MABT over 2-4 h at room temperature
2. 1x wash in AP buffer (make AP buffer fresh before use)
3. Transfer the contents of each tube to a well of a 24-well plate using a cut P1000 tip to avoid damaging the animals
4. Develop in the dark in AP buffer with 3.5 μL/mL BCIP () and 4.5 μL/mL NBT (Nitro-blue tet....???). Monitor development carefully.
5. When probe is well developed but background staining has not yet appeared, remove AP buffer and stop development with 3x quick washes in PBSTx
6. Refix for 10-20 min in 4% PFA
7. 1x wash with PBSTx
8. Wash in 100% ethanol to remove nonspecific background. Monitor closely.
9. 1x wash with PBSTx to remove ethanol
10. Clear overnight in 80% glycerol, then mount on slides for imaging. Slides can be stored long term in slide boxes at 4°C.

Solutions

PBSTx - 0.3% TritonX-100 in phosphate-buffered saline (PBS).

2X SSCTx - 20X SSC diluted to 2X with milliQ water. Autoclave, then add 0.1% TritonX-100.

MABT - 150 mM NaCl, 100 mM maleic acid, 0.1% Tween-20, pH 7.5.

Hybridization buffer (hyb) - 50% formamide, 5X SSC, 100 μg/mL heparin, 1X Denhardt's, 0.1% CHAPS, 0.1% Tween-20, 5% dextran sulfate, 0.1 mg/mL yeast torula RNA. Store at -20°C.

Prehybridization buffer - hybridization buffer without yeast torula RNA and dextran sulfate. Store at -20°C.

AP buffer - 100mM NaCl, 50 mM $MgCl_2$, 100 mM Tris pH 9.5, 0.1% Tween-20, all in 10% polyvinyl alcohol in distilled water. Developer is made fresh from stock solutions of the individual components immediately prior to use.

A.3 qPCR analysis script

This script takes a spreadsheet and user input in order to normalize qPCR data to a housekeeping gene and a control condition, then plot the output. It currently does not support multiple housekeeping genes or multiple biological replicates.

```
% This is an automated qPCR analysis script.
% Written in MATLAB R2020b by Rui Wang

% assumes triplicates
% assumes same number of genes for each condition
% Best to run section by section

% input requirements:
% well names in column 1
% C(t) in column 6
% read but not used: efficiency in column 5

```

```
%% Specify input
disp('Check input requirements before using!');
disp('==========');
prompt = 'What is the file name of the input?  ';
[~,~, rawdata] = xlsread(input(prompt));

disp('==========');

%% Create and populate structure array of data

% Get info on how many conditions and how many genes
prompt = 'How many conditions?  ';
numConditions = input(prompt);
prompt = 'How many genes, including housekeeping?  ';
numGenes = input(prompt);
% multiply to get overall number of samples
num = numConditions*numGenes;

% initialize string for list of conditions with NaNs
hasNaN = '';

%preallocate struct array
data = struct('condition', cell(1,num), 'gene', cell(1,num), '
    efficiency',...
    cell(1,num), 'Ct', cell(1,num), 'ddCt', cell(1,num), '
        avg_ddCt', cell(1,num));

for counter = 1:num
    disp(append('Reading in data for sample number ',...
        num2str(counter), ' of ', num2str(num), '?  '));
    prompt = 'Condition?  ';
    data(counter).condition = input(prompt, 's');
    prompt = 'Gene?  ';
    data(counter).gene = input(prompt, 's');

    % Read in efficiency and Ct, calculate ddCt for each
        triplicate
    prompt = 'First of triplicates: ';
    val = input(prompt, 's');
    ind = getIndex(rawdata, val);
    data(counter).efficiency(1) = sanitizeBad(rawdata{ind,5});
    data(counter).Ct(1) = sanitizeBad(rawdata{ind,6});
    data(counter).ddCt(1) = 2^(40-data(counter).Ct(1));

    prompt = 'Second of triplicates: ';
```

```
55      val = input(prompt, 's');
56      ind = getIndex(rawdata, val);
57      data(counter).efficiency(2) = sanitizeBad(rawdata{ind,5});
58      data(counter).Ct(2) = sanitizeBad(rawdata{ind,6});
59      data(counter).ddCt(2) = 2^(40-data(counter).Ct(2));
60
61      prompt = 'Third of triplicates: ';
62      val = input(prompt, 's');
63      ind = getIndex(rawdata, val);
64      data(counter).efficiency(3) = sanitizeBad(rawdata{ind,5});
65      data(counter).Ct(3) = sanitizeBad(rawdata{ind,6});
66      data(counter).ddCt(3) = 2^(40-data(counter).Ct(3));
67
68      % fill in average ddCt
69      data(counter).avg_ddCt = nanmean(data(counter).ddCt);
70
71      %add to string if there are bad wells
72      if sum(isnan(data(counter).ddCt))~= 0
73          hasNaN = append(hasNaN, data(counter).condition, ' ',...
74              data(counter).gene, ' - ');
75      end
76  end
77
78  disp('The following conditions have NaNs: ')
79  disp(hasNaN);
80  disp('==========');
81
82  %% normalize each condition to housekeeping gene
83
84  % get lists of conditions and genes from input array
85  conditionsList = unique({data.condition});
86
87      % ask which gene to normalize to
88      disp('Normalize each condition to single housekeeping gene
            .');
89      disp('Output is in housekeepNorm.normalized as struct
            arrays');
90      disp('Note: name given must match EXACTLY');
91      prompt = 'Normalize to which gene?  ';
92      housekeeper = input(prompt, 's');
93
94      housekeepNorm = struct('normalized', cell(1,length(
            conditionsList)));
95
96      % housekeepNorm is a struct array
```

```
97      % housekeepNorm(n).normalized is a struct array
98      % fields: condition, gene, normalized_mean_ddCt,
99      % normalized_individual_ddCt
100
101     for condNum = 1:length(conditionsList) %for each condition
102         cond = conditionsList(condNum); %which condition are
                we dealing with
103         temp_index = ismember({data.condition}, cond);
104         % structure containing all genes for given condition
105         temp_struct = data(temp_index);
106         % Sort all of these by .gene before adding
107         tempTable = struct2table(normalizeQ(housekeeper,
                temp_struct));
108         tempTable_sort = sortrows(tempTable, 'gene');
109         housekeepNorm(condNum).normalized = ...
110             table2struct(tempTable_sort);
111     end
112
113 disp('==========');
114
115 %% Normalize to control condition (after normalizing to
    housekeeping)
116
117 prompt = 'Normalize to which condition? ';
118 ctrl = input(prompt, 's');
119
120 % loop through housekeepNorm and get normalized_mean_ddCt for
    control
121 for n = 1:numConditions
122     if strcmp(housekeepNorm(n).normalized(1).condition, ctrl)
123         % normalize means - retained for cross checking
124         ctrl_norm_ddCt = ...
125             [housekeepNorm(n).normalized.normalized_mean_ddCt
                ];
126         % individual normalized values
127         ctrl_norm_ddCt_ind = cell(1,length(ctrl_norm_ddCt));
128         for i = 1:length(ctrl_norm_ddCt)
129             ctrl_norm_ddCt_ind{i} = ...
130                 [housekeepNorm(n).normalized(i).
                    normalized_individual_ddCt];
131         end
132     end
133 end
134
135 % get the list of genes in their sorted order for plotting
```

```
    purposes
geneNames = [{housekeepNorm(1).normalized.gene}];

%  update this value
numGenes = length(geneNames);

% initialize list of conditions
conditionNames = strings(1,numConditions-1);

% initialize output array for bar plot
% each row is a gene, each column is a condition
plottingArray_individual = zeros(numGenes, numConditions-1);
errorbars = zeros(numGenes, numConditions-1);

conditionCounter = 1;
for x = 1:numConditions
    if strcmp(ctrl, housekeepNorm(x).normalized(1).condition)
        %ignore the control condition
    else
        % normalize each gene to corresponding gene in control
            condition
        % and add result to output array
        for y = 1:numGenes
            % normalize each replicate
            ind_norm_temp = ...
                housekeepNorm(x).normalized(y).
                    normalized_individual_ddCt...
                ./ctrl_norm_ddCt_ind{y};
            % calculate mean and standard deviation for
                plotting
            plottingArray_individual(y, conditionCounter) = ...
                nanmean(ind_norm_temp);
            errorbars(y,conditionCounter) = std(ind_norm_temp,
                'omitnan');
        end
        % add condition name to the array for plotting
        conditionNames(conditionCounter) =...
            housekeepNorm(x).normalized.condition;
        % increment the counter
        conditionCounter = conditionCounter+1;
    end
end

disp('==========');

```

```
%% plot with error bars

 figure;
 bar(plottingArray_individual);
 set(gca, 'XTickLabel',geneNames);
 hold on;

% Plot error bars so they appear centered on the bars
ngroups = size(plottingArray_individual, 1);
nbars = size(plottingArray_individual, 2);
% Calculating the width for each bar group
groupwidth = min(0.8, nbars/(nbars + 1.5));
for i = 1:nbars
    x = (1:ngroups) - groupwidth/2 + (2*i-1) * groupwidth /
       (2*nbars);
    errorbar(x, plottingArray_individual(:,i), errorbars(:,i),
        '.');
end
hold off

 clear title;
 clear xlabel;
 clear ylabel;
 legend(conditionNames);
 title(append('Normalized to ', housekeeper, ' then to ', ctrl
    ));
 xlabel('Genes');
 ylabel('fold change');


 disp('done!');
 disp('=');

%% functions

% search through input for a cell designation, return index of
    that row
function index = getIndex(dataArray, well)
arguments
    dataArray
    well string
end
placeholder = NaN;
arraySize = size(dataArray);
for x = 1:arraySize(1)
```

```
    if well == string(dataArray(x,1))
        placeholder = x;
    end
end
index = placeholder;
end

% Designate one item in an array and normalize everything else to that
% used ONLY when normalizing to housekeeping gene
function outArray = normalizeQ(target, inArray)
arguments
    target string %name of gene to normalize to; must be in inArray
    inArray struct
    %data array containing the info as generated earlier in this file
end
arraySize = size(inArray);
num = arraySize(2) - 1;

%initialize output struct array
outArray = struct('condition', cell(1,num), 'gene', cell(1,num),...
    'normalized_mean_ddCt', cell(1,num),'normalized_individual_ddCt',cell(1,num));

%get the mean ddCt value to normalize to
for x = 1:arraySize(2)
    if inArray(x).gene == target
        normTo = inArray(x).avg_ddCt;
        normTo_individual = inArray(x).ddCt;
    end
end

counter = 1;
for x = 1:arraySize(2)
    if inArray(x).gene == target
        % pass over the gene to be normalized
    else
        % normalize the mean values
        outArray(counter).condition = inArray(x).condition;
        outArray(counter).gene = inArray(x).gene;
        outArray(counter).normalized_mean_ddCt = ...
            inArray(x).avg_ddCt/normTo;
```

```
257         %normalize the individual values
258         outArray(counter).normalized_individual_ddCt = ...
259             inArray(x).ddCt./normTo_individual;
260         counter = counter + 1;
261     end
262 end
263 end
264
265 % convert strings to NaN to handle 'N/A' from failed cells
266 function value = sanitizeBad(cellInput)
267 if ischar(cellInput)
268     value = NaN;
269 else
270     value = cellInput;
271 end
272
273 end
```

Appendix B

DNA sequences and constructs

B.1 Constructs from other labs

B.1.1 Wnt3-mNeonGreen knockin template

Sequence is cloned into pCSJ1027, which is a pCS2 expression vector carrying a FZD9-mCherry transgene.

gagtctttatcaatgtttttgatattaaaattgattttaacatggttacttaaatatttttaaaatatttttttcggtgaaggt
atcagtttaaatgaaaagagtgcatggctaaaaaaaaaaaaactaatgtaataagcgagtaaggagttacggatctataatgataa
taataatatgtataaatacttttttcgaacaaaatttttttgaaaataaaagcatttcaaacaaataaaaaaaactgcaaggtaatattt
gttaggcaaaaaagtttatttagggtaagatttatttggtttagattttatttgagacaaagtaattatttaggacttaaatgaggta
tggtttatactgagtaaagttcaggctatggtatgtgtggagtaacgttcaggtttttattgcttataaattaatgtatgatatggta
tacagaaattttacttacgatgcttttacctacgattacttacgaaagcttacgattgataatttaacttacaataatcaagtacata
aaaaatctattttataaaaagattttataaagcataacaaatacataaactaattaaaaactataatgaatcaaaaacagcaaaa
atataaaaatttgtaaatttgtctagacataacttgattgttttgagtatttttatttacataatataaaagaaaataatttaaaatt

attgagaaactaccactagtaaaaactaattaaatggtaatgatgcctatctaaccttaagcgcccatctaaccctaacagacagtt

caaattaaagtaaaactaaaaaaaaacaaccgtaaagtaaataatttttattgacattcttgaaaataatacccatttgttgaaaa

aatttcttttattaaagaccatgtaaggtagtattagccatagagttgagatgctcaaaatttaattcacctaatgtgtttatacata

agggcgcttgggacgcaaacgtcagcaattgaatccaggccacgttcatcaatcaatatggtgagcaagggcgaggaggataaca

tggcctctctcccagcgacacatgagttacacatctttggctccatcaacggtgtggactttgacatggtgggtcagggcaccggca

atccaaatgatggttatgaggagttaaacctgaagtccaccaagggtgacctccagttctccccctggattctggtccctcatatcg

ggtatggcttccatcagtacctgccctaccctgacgggatgtcgcctttccaggccgccatggtagatggctccggataccaagtcc

atcgcacaatgcagtttgaagatggtgcctcccttactgttaactaccgctacacctacgagggaagccacatcaaaggagaggcc

caggtgaaggggactggtttccctgctgacggtcctgtgatgaccaactcgctgaccgctgcggactggtgcaggtcgaagaagac

ttaccccaacgacaaaaccatcatcagtacctttaagtggagttacaccactggaaatggcaagcgctaccggagcactgcgcgga

ccacctacacctttgccaagccaatggcggctaactatctgaagaaccagccgatgtacgtgttccgtaagacggagctcaagcac

tccaagaccgagctcaacttcaaggagtggcaaaaggcctttaccgatgtgatgggcatggacgagctgtacaagaaaaatttat

gtcgagcgctttatcttcatcactaccaaagaacggtatgtttaaattacactgatctaatgttaagcgttgcagaaggaatacgac

tgggaattgacgaatgtcaagttcaatttaagcaccgtaaatggaattgtacgataaacgaacatggaacatccgtttttggccca

attattacaacaggtttttaattttaactattataataacaggtcgtcaattttatacggcttgttttatatatgtatttttttaactatt

tttttacttgtactgtagaacttacatatttaattctgaaacttatttttagccagcagagaaagtgcatttattagtggaattatatc

tgcgggagttgcgttttcagtgactgagtcatgtgcagaaggaaaatctgtccactgtcgttgcgataatagtgtacgaggtcaaa

cggacgaaggttggcgctggggaggttgtaacaggccaatcacatatggtatatggttttcgcagttatttattgatcaagtagaa

aaaattgtaaaaaaaagaaaagatccacgaaaaataatgaatcttcataacaacaaggctggacgagaggtttttaaattaaaat

tatttatttagaaagcaatactaaaataaaattaaaaagttttcttggatatctctaaaagccctattaaaggatcaaaaactagaa

tcatttatagaaataatagatatttaacaaatatttaacttaaaattatatttaggtaataaaaaaccttttacagactgaatgtaa

atgccacggaacatcaggaaactgcaacttaaaaacatgctggcgttcacagccccacttcagtgaggtaatttttcacatcacag

cctcacttcagtgaggtaatttttcttaaaataaaaattatatgcaaaaaatgatttttttttaaaaaataaaagcgcttaatacttt

attctttgttttatagaaaccaagtcttttaaaagctggactc

B.1.2 pGL3-*HySp5*-2992

Promoter sequence:

GGTACCCTAGTTCTAATTTAGCTCTATTACGTTCGCAAAGTTGACAAAG
TCGCAAATTTTTTTCTTTTTCAAAAGACCTCCCATTCATTTTAATAAAGACTGG
TTCTAATTTTGCTTTATCACGCTTATAAAAATTGACAAAGTCGCAAGTACTTTG
TTTTTTAAAAGACCTCCCATTCATTGAGATAAATACTAGTTATTTTCATGTATC
ATTGAAATAGTAAACAATTCATTCTAGTTTTTATTTGTCTAGGGCAGTATTTC
ACACCTTCCACAAGTGCGAAACGTTTTATTTACTTGATTGAGTAAATTAATTTA
AAATAAAATAAAAAAATAAGAACTTAATGTGAAAAAAAAAACAAAACAAAAAC
AATAAAAAAAAAAACAATGTAAAATATTTCTCATAGCTGTTGAAATATTAAAA
AGACGGAAGGAAAAATATAACGGCAAAGCTAAATTCTTTTCTGCGTATTGCTT
TTTATCTCTTTATTGTCTGTTTGTTGCTTTTCACTGCATTCTATTTTGTGCTTA
ATAAATCTCAATCGATTTTAAGGAATGACTAGGATGTTTCATTTTGTATATAT
CAATAACTGAAATATTAAAAATCTCCTCAGTGCATCCGTTCGTTAGACAATTG
GGGGTATTAACTCAATTATTTCCTGAATATAAACTCAACAAGTAAAAAAGTTT
CATCCGTAAGCAAGCAAGAATAACGACACTTGTTTACATTTAAGAATTTCTTA
ACTTTATGTAAAAAACAATTCTTAGTTAAAAACGAAGTAAAAGGGTTTTAATT
TTTTGTTTTTTAGTTGAAAACAAATTGCTAAATAAAACTTAATTTAAAAAAAA
AAAACCAAATATTTAAAATGATAAACTGGTTAAAATTAATAGATTATACAAAC
CATTGTAAGCATTTAAAAACAATTTTTTTTTTATAAAAACAACAACAAAAAAAT

TTCACCTAATTACTCCGCCTTTGTTAATAAAACCTCCGTTTTACAGTTAAAAGT

AATGTATGAACCGTAATCCCTATTACAAAAAAATGGTATATTGTTTATAAAGA

CGTTTTGATGATTGTAGCTTATTTTATATTTTTGTTGCTTTTGTTTGTTTTCCT

TGTTGTTGTTTTTAATTTGATTAGTTATATTCTTACGGCCTTACGACCACGTTT

GCTGTTTTAAATCGCGAGCGTTGCTTTGACTTTACACGAAGCCTCTAAAACAA

ACATAAAGAGAATTCATCGAAAGTAAAAAAAATCATGCTGACCTTCGGTGATC

CGTAATTGAAATTGATATATATTTTCTCCCTATTTTGACATATAAATGGTTAAA

GTTAATCTTTTTTATTAAACTCAATCAATTTCAACAAAATAAGTGTCAAGTTTAC

TGCTTATTTCAAGTAACAAATAAGTCTTATTGTAAATAAAGTTATTGTTTAAAA

GGGATTGAAACTTCAATCATTATTGTAATAAAGAAGAATTTCATGTAAGATTT

GTATTTATTAAAATTAAATAAACTAAATGAAACAAAAGCGCTACGTCAAATTT

ATATTTTGATTATTAAGAGGAATTTTTTTACCTAATGTAAAACTACTGTAAAAA

TCGACTGAATCAATAAGGTCAGAGAGACTAGGTCAGCGAGTTTGGATCATTAA

AATCGATAACAATAATTAACGATATAGTTTATAATGATAGGAAACTTACACTT

GACATTTAAATGGGAAGTCCTGAGGCTATAACGTTCGTTTGTCGTGGGTAGAT

AAGCCAATTGACAAAACCATCATCTTATATTTTTATGGGCGCCAAATGTTTATC

ATGTTTAATTTCTTTTATATAAATGATAAAAACATTTAACCACAAATTATTTTT

TTTATCTCCAAATGAAATCAAGAACTTTTAAGTCATAAAAAGTAGCGACAGCG

CCAGTGATAATCATAGACAAGTGTACACATTAGCTTATCAAAAAGTACGCTAG

AGTAAAGCTTATTGTTTTGTTTTGGCTAGGATATATCCTTCTCGTTAAAATAA

TTTGTCCTACTTTTATATACGATATTCATATTTTTAGGTTTCTTGTTTCGATAT

ATATATATATTTCGTTATGTTTGTATGTATATATGTGTTTGTTTGTATGTGTAT

GTAAAAATATGAAATATACTTTTTGCAAATCTTTGTAGAAGTTTAATAAATAA

AGTATCAAGTTTAAAAATTCCTTCGATATTTTTAAAGCTTCAATTTGGTTGGG

CGTAGACACATTAGTAATTGCGGTAAAGATCAGTAAGAATTCTAAATAGACGT

TAATTTTAAAACCTGGCCTGCCCCTTGATTATTTAATTTGAAATTTTTAAGCTG

TCTCCATTTCAACCACAGTATCAATGGGTCGGCAAAAAAAGAAAGATTGAACG

TTTTATCAATTTTACCAACGAAAAACACTTAACAAATATTGTAGTACTTTTTTA

AGTTTAAATGTTTTTTGTAAAACTGTTATTTTTAAAATAAACCTTTTACTTCTT

TTTTTTTTTTTTTGAAATCGTTTTAAACTGATATTTAATAAAAGCTTAAATATA

AATGTGGTAAAGTTCGTAAAACCAATGAGGCAGGTGCCGGCATAGATGAAAGT

GAAAGAACAATTTTTTTTATTGAACTTCACATTTACTGTGGATTGTCGGAATG

TTTTACTATTAAGTTGATTTGAAGTCAAAAACAAAATAACAAAATCAACCAAT

GAACTTCCTTAGAAATTGTTTAATCATAAACCAATCAAATAGCGTTTTATATCT

TTTAACCAATAAGATAACAATTTTATTGTTTTGTCGGCATCTTAAGATATTAAA

AGTTAATATCTTTTCCGCCTTACGTATTCTGTTTATCACCGCCTCTTAGACCAT

CCCATTTGTACGTAAACAGAGAAAATATGATCGCAACGCGCCATTTCTCAGTC

AGAGGCGTGACATTAACCCCTTATCAAAGAAGCCGAAGCTATTTAAGATAAgatg

gcggtttc

B.2 Transgenic constructs for embryo microinjection

B.2.1 actin promoter::YPet

ctaaattgtaagcgttaatattttgttaaaattcgcgttaaatttttgttaaatcagctcatttttttaaccaataggccgaa

atcggcaaaatcccttataaatcaaaagaatagaccgagatagggttgagtgttgttccagtttggaacaagagtccactattaaa

gaacgtggactccaacgtcaaagggcgaaaaaccgtctatcagggcgatggcccactacgtgaaccatcaccctaatcaagttttt

tggggtcgaggtgccgtaaagcactaaatcggaaccctaaagggagcccccgatttagagcttgacggggaaagccggcgaacgt

ggcgagaaaggaagggaagaaagcgaaaggagcgggcgctagggcgctggcaagtgtagcggtcacgctgcgcgtaaccacca

cacccgccgcgcttaatgcgccgctacagggcgcgtcccattcgccattcaggctgcgcaactgttgggaagggcgatcggtgcgg

gcctcttcgctattacgccagctggcgaaaggggatgtgctgcaaggcgattaagttgggtaacgccagggttttcccagtcacg

acgttgtaaaacgacggccagtgagcgcgcgtaatacgactcactatagggcgaattggttttaagccgagatgcaggattctgaa

tgaaaaagaaaaaaagaagtctcggtagagtaaaagtgatcggtttgcaactgtaaaatttattgaagtaccaataatttttattta

aaataaaactgaaatataaagttaaagttgctgttctataagtttaccgaattttaaaaccattgtaacgctagagtaatatttgag

tctactaagttagtccccgcacttttttaatcaagcaataaatacccaaactttgcttattcaaatcaataaaccaatatatctcttaa

aataaagtaaaaacttctgaaattctataaaaaaaaaatttaatttcgaaatatcaaatgtaacttcaacaccgcactattttctttta

aacaactgatatagtaattacttctcaaaaacgttatctcaaggtttgtgatgtacttaaaaccactcctattttgttacgcgtttaa

aaaagcaaacataagttggtttctattgatgaatgagaacatatttcatttaaagttaaaatcctaccagtggtttcactgtacgta

aacaccgtcaaaaaaacaggaacgtttttaaagattaataattgaagtaaaaaaaatttaataccgggggttaaaaaaatctttta

aaataattataaatatatatattaaaatttataaatttttaaacacatttaaaatatatattaagtataataaaagtaatattataa

aaaaaaatttaattttataattatttttattaaatttataaataataggtaaaacttacatatccgttttatttttcttaataaaata

acgcgtgcaaatttttgtccatataaagacctttcgaacaataacttttttgcttagccgtttttttcttatatggtcaaaaaagcg

ctcaagcgattcaccataaaaagcgcaattagttcagcgttcgttattcagaagcttcagctttgcttgatactcagctcttctcttt

taaacaaaacacttaatcaaaatgcatATGGTGAGCAAAGGCGAAGAGCTGTTCACCGGCGTG

GTGCCCATCCTGGTGGAGCTGGACGGCGACGTGAACGGCCACAAGTTCAGCGT

GAGCGGCGAGGGCGAGGGCGACGCCACCTACGGCAAGCTGACCCTGAAGCTGC

TGTGCACCACCGGCAAGCTGCCCGTGCCCTGGCCCACCCTGGTGACCACCCTG

GGCTACGGCGTGCAGTGCTTCGCCCGGTACCCCGACCACATGAAGCAGCACGA

CTTCTTCAAGAGCGCCATGCCCGAGGGCTACGTGCAGGAGCGGACCATCTTCT

TCAAGGACGACGGCAACTACAAGACCCGGGCCGAGGTGAAGTTCGAGGGCGAC

ACCCTGGTGAACCGGATCGAGCTGAAGGGCATCGACTTCAAGGAGGACGGCAA

CATCCTGGGCCACAAGCTGGAGTACAACTACAACAGCCACAACGTGTACATCA

CCGCCGACAAGCAGAAGAACGGCATCAAGGCCAACTTCAAGATCCGGCACAAC

ATCGAGGACGGCGGCGTGCAGCTGGCCGACCACTACCAGCAGAACACCCCCAT

CGGCGACGGCCCCGTGCTGCTGCCCGACAACCACTACCTGAGCTACCAGAGCG

CCCTGTTCAAGGACCCCAACGAGAAGCGGGACCACATGGTGCTGCTGGAGTTC

CTGACCGCCGCCGGCATCACCGAGGGCATGAACGAGCTCTATAAGTAAAGCGG

CCgaattcacaattcgattatatttatactggactatttttacatctgttcggttattttcacatttatttttctatatatatcttataa

acgttttaaaacccatgtaatttttgttaagctgtaatataaaagacgtcctaacaaacttcttttattactgaatttcctttaattat

aataaataacaagttttaaaataaattcaggcaattaaggcgctcctgaggtactaaaattaatgtaaacatttaaaattaacttg

gatggtcttaagtactgtactcgtgattttgttatactttattattagaaaagtcgtctattaacttttgttccttaatttacttgatt

aaattgtcgcttaatttatcaaatcaggttttgcgcgttattttagagaaaaacttattagaaaaatgaataagcaaagtttaggct

aacatgtttttttattattttaaatagttcaagtcaatgacgtataaaccagcttttgttccctttagtgagggttaattgcgcgcttg

gcgtaatcatggtcatagctgtttcctgtgtgaaattgttatccgctcacaattccacacaacatacgagccggaagcataaagtgt

aaagcctggggtgcctaatgagtgagctaactcacattaattgcgttgcgctcactgcccgctttccagtcgggaaacctgtcgtgc

cagctgcattaatgaatcggccaacgcgcggggagaggcggtttgcgtattgggcgctcttccgcttcctcgctcactgactcgctg

cgctcggtcgttcggctgcggcgagcggtatcagctcactcaaaggcggtaatacggttatccacagaatcaggggataacgcag

gaaagaacatgtgagcaaaaggccagcaaaaggccaggaaccgtaaaaaggccgcgttgctggcgtttttccataggctccgccc

ccctgacgagcatcacaaaaatcgacgctcaagtcagaggtggcgaaacccgacaggactataaagataccaggcgtttccccct

ggaagctccctcgtgcgctctcctgttccgaccctgccgcttaccggatacctgtccgcctttctcccttcgggaagcgtggcgctttc

tcatagctcacgctgtaggtatctcagttcggtgtaggtcgttcgctccaagctgggctgtgtgcacgaacccccgttcagcccga

ccgctgcgccttatccggtaactatcgtcttgagtccaacccggtaagacacgacttatcgccactggcagcagccactggtaacag

gattagcagagcgaggtatgtaggcggtgctacagagttcttgaagtggtggcctaactacggctacactagaaggacagtatttg

gtatctgcgctctgctgaagccagttaccttcggaaaaagagttggtagctcttgatccggcaaacaaaccaccgctggtagcggt

ggtttttttgtttgcaagcagcagattacgcgcagaaaaaaaggatctcaagaagatcctttgatcttttctacggggtctgacgct

cagtggaacgaaaactcacgttaagggattttggtcatgagattatcaaaaaggatcttcacctagatccttttaaattaaaaatg

aagttttaaatcaatctaaagtatatatgagtaaacttggtctgacagttaccaatgcttaatcagtgaggcacctatctcagcgat

ctgtctatttcgttcatccatagttgcctgactccccgtcgtgtagataactacgatacgggagggcttaccatctggccccagtgct

gcaatgataccgcgagacccacgctcaccggctccagatttatcagcaataaaccagccagccggaagggccgagcgcagaagtg

gtcctgcaactttatccgcctccatccagtctattaattgttgccgggaagctagagtaagtagttcgccagttaatagtttgcgcaa

cgttgttgccattgctacaggcatcgtggtgtcacgctcgtcgtttggtatggcttcattcagctccggttcccaacgatcaaggcga

gttacatgatcccccatgttgtgcaaaaaagcggttagctccttcggtcctccgatcgttgtcagaagtaagttggccgcagtgttat

cactcatggttatggcagcactgcataattctcttactgtcatgccatccgtaagatgcttttctgtgactggtgagtactcaaccaa

gtcattctgagaatagtgtatgcggcgaccgagttgctcttgcccggcgtcaatacgggataataccgcgccacatagcagaacttt

aaaagtgctcatcattggaaaacgttcttcggggcgaaaactctcaaggatcttaccgctgttgagatccagttcgatgtaacccac

tcgtgcacccaactgatcttcagcatcttttactttcaccagcgtttctgggtgagcaaaaacaggaaggcaaaatgccgcaaaaa

agggaataagggcgacacggaaatgttgaatactcatactcttccttttcaatattattgaagcatttatcagggttattgtctcat

gagcggatacatatttgaatgtatttagaaaaataaacaaatagggttccgcgcacatttccccgaaaagtgccac

B.2.2 Sp5 promoter::YPet

ctaaattgtaagcgttaatattttgttaaaattcgcgttaaatttttgttaaatcagctcatttttaaccaataggccgaa

atcggcaaaatcccttataaatcaaaagaatagaccgagatagggttgagtgttgttccagtttggaacaagagtccactattaaa

gaacgtggactccaacgtcaaagggcgaaaaaccgtctatcagggcgatggcccactacgtgaaccatcaccctaatcaagtttt

ttggggtcgaggtgccgtaaagcactaaatcggaaccctaaagggagcccccgatttagagcttgacggggaaagccggcgaac

gtggcgagaaaggaagggaagaaagcgaaaggagcgggcgctagggcgctggcaagtgtagcggtcacgctgcgcgtaaccac

cacacccgccgcgcttaatgcgccgctacagggcgcgtcccattcgccattcaggctgcgcaactgttgggaagggcgatcggtgc

gggcctcttcgctattacgccagctggcgaaaggggatgtgctgcaaggcgattaagttgggtaacgccagggttttcccagtca

cgacgttgtaaaacgacggccagtgagcgcgcgtaatacgactcactatagggcgaattggCTAGTTCTAATTTAG

CTCTATTACGTTCGCAAAGTTGACAAAGTCGCAAATTTTTTTCTTTTTCAAAAG

ACCTCCCATTCATTTTAATAAAGACTGGTTCTAATTTTGCTTTATCACGCTTAT

AAAAATTGACAAAGTCGCAAGTACTTTGTTTTTTAAAAGACCTCCCATTCATTG

AGATAAATACTAGTTATTTTCATGTATCATTGAAATAGTAAACAATTCATTCTA

GTTTTTATTTGTCTAGGGCAGTATTTCACACCTTCCACAAGTGCGAAACGTTTT

ATTTACTTGATTGAGTAAATTAATTTAAAATAAAATAAAAAAATAAGAACTTA

ATGTGAAAAAAAAAACAAAACAAAAACAATAAAAAAAAAAACAATGTAAAATA

TTTCTCATAGCTGTTGAAATATTAAAAAGACGGAAGGAAAAATATAACGGCAA

AGCTAAATTCTTTTCTGCGTATTGCTTTTTATCTCTTTATTGTCTGTTTGTTGC

TTTTCACTGCATTCTATTTTGTGCTTAATAAATCTCAATCGATTTTAAGGAATG

ACTAGGATGTTTCATTTTGTATATATCAATAACTGAAATATTAAAAATCTCCTC

AGTGCATCCGTTCGTTAGACAATTGGGGGTATTAACTCAATTATTTCCTGAAT

ATAAACTCAACAAGTAAAAAAGTTTCATCCGTAAGCAAGCAAGAATAACGACA

CTTGTTTACATTTAAGAATTTCTTAACTTTATGTAAAAAACAATTCTTAGTTAA

AAACGAAGTAAAAGGGTTTTAATTTTTTGTTTTTTAGTTGAAAACAAATTGCT

AAATAAAACTTAATTTAAAAAAAAAAAACCAAATATTTAAAATGATAAACTGG

TTAAAATTAATAGATTATACAAACCATTGTAAGCATTTAAAAACAATTTTTTTT

TTATAAAAACAACAACAAAAAAATTTCACCTAATTACTCCGCCTTTGTTAATAA

AACCTCCGTTTTACAGTTAAAAGTAATGTATGAACCGTAATCCCTATTACAAAA

AAATGGTATATTGTTTATAAAGACGTTTTGATGATTGTAGCTTATTTTATATT

TTTGTTGCTTTTGTTTGTTTTCCTTGTTGTTGTTTTTAATTTGATTAGTTATAT

TCTTACGGCCTTACGACCACGTTTGCTGTTTTAAATCGCGAGCGTTGCTTTGA

CTTTACACGAAGCCTCTAAAACAAACATAAAGAGAATTCATCGAAAGTAAAAA

AAATCATGCTGACCTTCGGTGATCCGTAATTGAAATTGATATATATTTTCTCCC

TATTTTGACATATAAATGGTTAAAGTTAATCTTTTTATTAAACTCAATCAATTT

CAACAAAATAAGTGTCAAGTTTACTGCTTATTTCAAGTAACAAATAAGTCTTAT

TGTAAATAAAGTTATTGTTTAAAAGGGATTGAAACTTCAATCATTATTGTAAT

AAAGAAGAATTTCATGTAAGATTTGTATTTATTAAAATTAAATAAACTAAATG

AAACAAAAGCGCTACGTCAAATTTATATTTTGATTATTAAGAGGAATTTTTTT

ACCTAATGTAAAACTACTGTAAAAATCGACTGAATCAATAAGGTCAGAGAGAC

TAGGTCAGCGAGTTTGGATCATTAAAATCGATAACAATAATTAACGATATAGT

TTATAATGATAGGAAACTTACACTTGACATTTAAATGGGAAGTCCTGAGGCTA

TAACGTTCGTTTGTCGTGGGTAGATAAGCCAATTGACAAAACCATCATCTTAT

ATTTTTATGGGCGCCAAATGTTTATCATGTTTAATTTCTTTTATATAAATGATA

AAAACATTTAACCACAAATTATTTTTTTTATCTCCAAATGAAATCAAGAACTTT

TAAGTCATAAAAAGTAGCGACAGCGCCAGTGATAATCATAGACAAGTGTACAC

ATTAGCTTATCAAAAAGTACGCTAGAGTAAAGCTTATTGTTTTGTTTTGGCTA

GGATATATCCTTCTCGTTAAAATAATTTGTCCTACTTTTATATACGATATTCAT

ATTTTTAGGTTTCTTGTTTCGATATATATATATATTTCGTTATGTTTGTATGTA

TATATGTGTTTGTTTGTATGTGTATGTAAAAATATGAAATATACTTTTTGCAA

ATCTTTGTAGAAGTTTAATAAATAAAGTATCAAGTTTAAAAATTCCTTCGATAT

TTTTAAAGCTTCAATTTGGTTGGGCGTAGACACATTAGTAATTGCGGTAAAGA

TCAGTAAGAATTCTAAATAGACGTTAATTTTAAAACCTGGCCTGCCCCTTGATT

ATTTAATTTGAAATTTTTAAGCTGTCTCCATTTCAACCACAGTATCAATGGGTC

GGCAAAAAAAGAAAGATTGAACGTTTTATCAATTTTACCAACGAAAAACACTT

AACAAATATTGTAGTACTTTTTTAAGTTTAAATGTTTTTTGTAAAACTGTTATT

TTTAAAATAAACCTTTTACTTCTTTTTTTTTTTTTTTGAAATCGTTTTAAACTG

ATATTTAATAAAAGCTTAAATATAAATGTGGTAAAGTTCGTAAAACCAATGAG

GCAGGTGCCGGCATAGATGAAAGTGAAAGAACAATTTTTTTTATTGAACTTCA

CATTTACTGTGGATTGTCGGAATGTTTTACTATTAAGTTGATTTGAAGTCAAA

AACAAAATAACAAAATCAACCAATGAACTTCCTTAGAAATTGTTTAATCATAAA

CCAATCAAATAGCGTTTTATATCTTTTAACCAATAAGATAACAATTTTATTGTT

TTGTCGGCATCTTAAGATATTAAAAGTTAATATCTTTTCCGCCTTACGTATTCT

GTTTATCACCGCCTCTTAGACCATCCCATTTGTACGTAAACAGAGAAAATATG

ATCGCAACGCGCCATTTCTCAGTCAGAGGCGTGACATTAACCCCTTATCAAAG

AAGCCGAAGCTATTTAAGATAAgatggcggtttcATGGTGAGCAAAGGCGAAGAGCT

GTTCACCGGCGTGGTGCCCATCCTGGTGGAGCTGGACGGCGACGTGAACGGCC

ACAAGTTCAGCGTGAGCGGCGAGGGCGAGGGCGACGCCACCTACGGCAAGCTG

ACCCTGAAGCTGCTGTGCACCACCGGCAAGCTGCCCGTGCCCTGGCCCACCCT

GGTGACCACCCTGGGCTACGGCGTGCAGTGCTTCGCCCGGTACCCCGACCACA

TGAAGCAGCACGACTTCTTCAAGAGCGCCATGCCCGAGGGCTACGTGCAGGAG

CGGACCATCTTCTTCAAGGACGACGGCAACTACAAGACCCGGGCCGAGGTGAA

GTTCGAGGGCGACACCCTGGTGAACCGGATCGAGCTGAAGGGCATCGACTTCA

AGGAGGACGGCAACATCCTGGGCCACAAGCTGGAGTACAACTACAACAGCCAC

AACGTGTACATCACCGCCGACAAGCAGAAGAACGGCATCAAGGCCAACTTCAA

GATCCGGCACAACATCGAGGACGGCGGCGTGCAGCTGGCCGACCACTACCAGC

AGAACACCCCCATCGGCGACGGCCCCGTGCTGCTGCCCGACAACCACTACCTG

AGCTACCAGAGCGCCCTGTTCAAGGACCCCAACGAGAAGCGGGACCACATGGT

GCTGCTGGAGTTCCTGACCGCCGCCGGCATCACCGAGGGCATGAACGAGCTCT

ATAAGTAAcatcccgggtgaattcacaattcgattatatttatactggactatttttacatctgttcggttattttcacatttat

ttttctatatatatcttataaacgttttaaaacccatgtaatttttgttaagctgtaatataaaagacgtcctaacaaacttcttttatt

actgaatttcctttaattataataaataacaagttttaaaataaattcaggcaattaaggcgctcctgaggtactaaaattaatgta

aacatttaaaattaacttggatggtcttaagtactgtactcgtgattttgttatactttattattagaaaagtcgtctattaacttttt

gttccttaatttacttgattaaattgtcgcttaatttatcaaatcaggttttgcgcgttattttagagaaaaacttattagaaaaatga

ataagcaaagtttaggctaacatgttttttttattattttaaatagttcaagtcaatgacgtataaaccagcttttgttccctttagtga

gggttaattgcgcgcttggcgtaatcatggtcatagctgtttcctgtgtgaaattgttatccgctcacaattccacacaacatacgag

ccggaagcataaagtgtaaagcctggggtgcctaatgagtgagctaactcacattaattgcgttgcgctcactgcccgctttccagt

cgggaaacctgtcgtgccagctgcattaatgaatcggccaacgcgcggggagaggcggtttgcgtattgggcgctcttccgcttcct

cgctcactgactcgctgcgctcggtcgttcggctgcggcgagcggtatcagctcactcaaaggcggtaatacggttatccacagaat

caggggataacgcaggaaagaacatgtgagcaaaaggccagcaaaaggccaggaaccgtaaaaaggccgcgttgctggcgtttt

tccataggctccgccccctgacgagcatcacaaaaatcgacgctcaagtcagaggtggcgaaacccgacaggactataaagata

ccaggcgtttcccccctggaagctccctcgtgcgctctcctgttccgaccctgccgcttaccggatacctgtccgcctttctcccttcgg

gaagcgtggcgctttctcatagctcacgctgtaggtatctcagttcggtgtaggtcgttcgctccaagctgggctgtgtgcacgaac

cccccgttcagcccgaccgctgcgccttatccggtaactatcgtcttgagtccaacccggtaagacacgacttatcgccactggcag

cagccactggtaacaggattagcagagcgaggtatgtaggcggtgctacagagttcttgaagtggtggcctaactacggctacact

agaaggacagtatttggtatctgcgctctgctgaagccagttaccttcggaaaaagagttggtagctcttgatccggcaaacaaac

caccgctggtagcggtggttttttgtttgcaagcagcagattacgcgcagaaaaaaaggatctcaagaagatcctttgatcttttc

tacggggtctgacgctcagtggaacgaaaactcacgttaagggattttggtcatgagattatcaaaaaggatcttcacctagatcc

ttttaaattaaaaatgaagttttaaatcaatctaaagtatatatgagtaaacttggtctgacagttaccaatgcttaatcagtgagg

cacctatctcagcgatctgtctatttcgttcatccatagttgcctgactccccgtcgtgtagataactacgatacgggagggcttacc

atctggccccagtgctgcaatgataccgcgagacccacgctcaccggctccagatttatcagcaataaaccagccagccggaaggg

ccgagcgcagaagtggtcctgcaactttatccgcctccatccagtctattaattgttgccgggaagctagagtaagtagttcgccag

ttaatagtttgcgcaacgttgttgccattgctacaggcatcgtggtgtcacgctcgtcgtttggtatggcttcattcagctccggttcc

caacgatcaaggcgagttacatgatcccccatgttgtgcaaaaaagcggttagctccttcggtcctccgatcgttgtcagaagtaag

ttggccgcagtgttatcactcatggttatggcagcactgcataattctcttactgtcatgccatccgtaagatgcttttctgtgactgg

tgagtactcaaccaagtcattctgagaatagtgtatgcggcgaccgagttgctcttgcccggcgtcaatacgggataataccgcgc

cacatagcagaactttaaaagtgctcatcattggaaaacgttcttcggggcgaaaactctcaaggatcttaccgctgttgagatcca

gttcgatgtaacccactcgtgcacccaactgatcttcagcatcttttactttcaccagcgtttctgggtgagcaaaaacaggaaggc

aaaatgccgcaaaaaagggaataagggcgacacggaaatgttgaatactcatactcttccttttcaatattattgaagcatttatc

agggttattgtctcatgagcggatacatatttgaatgtatttagaaaaataaacaaatagggttccgcgcacatttccccgaaaa

gtgccac

B.2.3 Sp5 promoter::Sp5-mNeonGreen

ctaaattgtaagcgttaatattttgttaaaattcgcgttaaatttttgttaaatcagctcatttttaaccaataggccgaa

atcggcaaaatcccttataaatcaaaagaatagaccgagatagggttgagtgttgttccagtttggaacaagagtccactattaaa

gaacgtggactccaacgtcaaagggcgaaaaaccgtctatcagggcgatggcccactacgtgaaccatcaccctaatcaagtttt

ttggggtcgaggtgccgtaaagcactaaatcggaaccctaaagggagcccccgatttagagcttgacggggaaagccggcgaac

gtggcgagaaaggaagggaagaaagcgaaaggagcgggcgctagggcgctggcaagtgtagcggtcacgctgcgcgtaaccac

cacacccgccgcgcttaatgcgccgctacagggcgcgtcccattcgccattcaggctgcgcaactgttgggaagggcgatcggtgc

gggcctcttcgctattacgccagctggcgaaaggggatgtgctgcaaggcgattaagttgggtaacgccagggttttcccagtca

cgacgttgtaaaacgacggccagtgagcgcgcgtaatacgactcactatagggcgaattggCTAGTTCTAATTTAG

CTCTATTACGTTCGCAAAGTTGACAAAGTCGCAAATTTTTTTCTTTTTCAAAAG

ACCTCCCATTCATTTTAATAAAGACTGGTTCTAATTTTGCTTTATCACGCTTAT

AAAAATTGACAAAGTCGCAAGTACTTTGTTTTTTAAAAGACCTCCCATTCATTG

AGATAAATACTAGTTATTTTCATGTATCATTGAAATAGTAAACAATTCATTCTA

GTTTTTATTTGTCTAGGGCAGTATTTCACACCTTCCACAAGTGCGAAACGTTTT

ATTTACTTGATTGAGTAAATTAATTTAAAATAAAATAAAAAAATAAGAACTTA

ATGTGAAAAAAAAAACAAAACAAAAACAATAAAAAAAAAAACAATGTAAAATA

TTTCTCATAGCTGTTGAAATATTAAAAAGACGGAAGGAAAAATATAACGGCAA

AGCTAAATTCTTTTCTGCGTATTGCTTTTTATCTCTTTATTGTCTGTTTGTTGC

TTTTCACTGCATTCTATTTTGTGCTTAATAAATCTCAATCGATTTTAAGGAATG

ACTAGGATGTTTCATTTTGTATATATCAATAACTGAAATATTAAAAATCTCCTC

AGTGCATCCGTTCGTTAGACAATTGGGGGTATTAACTCAATTATTTCCTGAAT

ATAAACTCAACAAGTAAAAAAGTTTCATCCGTAAGCAAGCAAGAATAACGACA

CTTGTTTACATTTAAGAATTTCTTAACTTTATGTAAAAAACAATTCTTAGTTAA

AAACGAAGTAAAAGGGTTTTAATTTTTTGTTTTTTAGTTGAAAACAAATTGCT

AAATAAAACTTAATTTAAAAAAAAAAAACCAAATATTTAAAATGATAAACTGG

TTAAAATTAATAGATTATACAAACCATTGTAAGCATTTAAAAACAATTTTTTTT

TTATAAAAACAACAACAAAAAAATTTCACCTAATTACTCCGCCTTTGTTAATAA

AACCTCCGTTTTACAGTTAAAAGTAATGTATGAACCGTAATCCCTATTACAAAA

AAATGGTATATTGTTTATAAAGACGTTTTGATGATTGTAGCTTATTTTATATT

TTTGTTGCTTTTGTTTGTTTTCCTTGTTGTTGTTTTTAATTTGATTAGTTATAT

TCTTACGGCCTTACGACCACGTTTGCTGTTTTAAATCGCGAGCGTTGCTTTGA

CTTTACACGAAGCCTCTAAAACAAACATAAAGAGAATTCATCGAAAGTAAAAA

AAATCATGCTGACCTTCGGTGATCCGTAATTGAAATTGATATATATTTTCTCCC

TATTTTGACATATAAATGGTTAAAGTTAATCTTTTTTATTAAACTCAATCAATTT

CAACAAAATAAGTGTCAAGTTTACTGCTTATTTCAAGTAACAAATAAGTCTTAT

TGTAAATAAAGTTATTGTTTAAAAGGGATTGAAACTTCAATCATTATTGTAAT

AAAGAAGAATTTCATGTAAGATTTGTATTTATTAAAATTAAATAAACTAAATG

AAACAAAAGCGCTACGTCAAATTTATATTTTGATTATTAAGAGGAATTTTTTT

ACCTAATGTAAAACTACTGTAAAAATCGACTGAATCAATAAGGTCAGAGAGAC

TAGGTCAGCGAGTTTGGATCATTAAAATCGATAACAATAATTAACGATATAGT

TTATAATGATAGGAAACTTACACTTGACATTTAAATGGGAAGTCCTGAGGCTA

TAACGTTCGTTTGTCGTGGGTAGATAAGCCAATTGACAAAACCATCATCTTAT

ATTTTTATGGGCGCCAAATGTTTATCATGTTTAATTTCTTTTATATAAATGATA

AAAACATTTAACCACAAATTATTTTTTTTATCTCCAAATGAAATCAAGAACTTT

TAAGTCATAAAAAGTAGCGACAGCGCCAGTGATAATCATAGACAAGTGTACAC

ATTAGCTTATCAAAAAGTACGCTAGAGTAAAGCTTATTGTTTTGTTTTGGCTA

GGATATATCCTTCTCGTTAAAATAATTTGTCCTACTTTTATATACGATATTCAT

ATTTTTAGGTTTCTTGTTTCGATATATATATATATTTCGTTATGTTTGTATGTA

TATATGTGTTTGTTTGTATGTGTATGTAAAAATATGAAATATACTTTTTGCAA

ATCTTTGTAGAAGTTTAATAAATAAAGTATCAAGTTTAAAAATTCCTTCGATAT

TTTTAAAGCTTCAATTTGGTTGGGCGTAGACACATTAGTAATTGCGGTAAAGA

TCAGTAAGAATTCTAAATAGACGTTAATTTTAAAACCTGGCCTGCCCCTTGATT

ATTTAATTTGAAATTTTTAAGCTGTCTCCATTTCAACCACAGTATCAATGGGTC

GGCAAAAAAAGAAAGATTGAACGTTTTATCAATTTTACCAACGAAAAACACTT

AACAAATATTGTAGTACTTTTTTAAGTTTAAATGTTTTTTGTAAAACTGTTATT

TTTAAAATAAACCTTTTACTTCTTTTTTTTTTTTTTTGAAATCGTTTTAAACTG

ATATTTAATAAAAGCTTAAATATAAATGTGGTAAAGTTCGTAAAACCAATGAG

GCAGGTGCCGGCATAGATGAAAGTGAAAGAACAATTTTTTTTATTGAACTTCA

CATTTACTGTGGATTGTCGGAATGTTTTACTATTAAGTTGATTTGAAGTCAAA

AACAAAATAACAAAATCAACCAATGAACTTCCTTAGAAATTGTTTAATCATAAA

CCAATCAAATAGCGTTTTATATCTTTTAACCAATAAGATAACAATTTTATTGTT

TTGTCGGCATCTTAAGATATTAAAAGTTAATATCTTTTCCGCCTTACGTATTCT

GTTTATCACCGCCTCTTAGACCATCCCATTTGTACGTAAACAGAGAAAATATG

ATCGCAACGCGCCATTTCTCAGTCAGAGGCGTGACATTAACCCCTTATCAAAG

AAGCCGAAGCTATTTAAGATAAgatggcggtttcatgtcacctccaagtcgtgttccaacaacaatcagccca

aactttaaaagtcaacatcattgtcttaaagaacatattaagtattcaccgttggcattacttgcagcaacctgtaaaaaaaattgga

cggcctatcagcccattagaacaaacatctcctaaaaaaatttttcaaccatggaatcacacgtttgaatcacacaattatgacaca

cctatttcaccaaatagcaaagtgagacactttctagagacaaatttctcgcttccaccaagtcctccattaaaatcagagatagta

aaagttcccccaacaataagaccaatgccgatgacgaatgtaatgcaagaaaaagcgactttaaattactcacaaaaactttctc

cacctccgtgtctcgcatgttcagctggtcaaaagtgcaatggaataaataaaatatctccagttttgctttctccgcctgcctcgcc

aatctcatggttatttcctcaaaatattattcaatctcatccttctaaagtatcaattaacgagcaccacataaaagaatattccgaa

cattctcaagctgatccaacgcgttttgtaaactacgtttacaaaaacgtcgactcttctcaagcaaaacctaatctaataattcga

cacgataacatgatctcctctacacaatcgtataacaatcgtatattctcatcttcgccacatttaactacaacatcccacatatatt

caatgtctacatcaattcctgctcaatcgcatgcagttataccgaacagcgttgcaacccgaagatgtcgtcgctgtaaatgcccaa

actgcatatcaggacaacaatctgagccaaataaacccaagcagcacgtatgtcatattccagggtgcggaaaggtttatggtaa

aactagtcaccttaaagctcatttaagatggcatgctggattgcgtccattcgtttgtaattggttattttgcaacaaatcctttactc

gttctgatgaactccaacgtcacttgcgaacacatacgggcgaaaagcgatttgcctgtcaagattgcggcaaacgttttactcgtt

ccgaccatttatcgaaacatatgaaaacacaccaaaataaaaaacaagaaaacacatttgtaaaagatactgtcatagaagtgat

taaagacaatgtcgatgaaaattgcgatgagaatgttatggaacttgaagtaaacgttgaaaacGGTGGTGGTATGG

TGAGCAAGGGCGAGGAGGATAACATGGCCTCTCTCCCAGCGACACATGAGTTA

CACATCTTTGGCTCCATCAACGGTGTGGACTTTGACATGGTGGGTCAGGGCAC

CGGCAATCCAAATGATGGTTATGAGGAGTTAAACCTGAAGTCCACCAAGGGTG

ACCTCCAGTTCTCCCCCTGGATTCTGGTCCCTCATATCGGGTATGGCTTCCATC

AGTACCTGCCCTACCCTGACGGGATGTCGCCTTTCCAGGCCGCCATGGTAGAT

GGCTCCGGATACCAAGTCCATCGCACAATGCAGTTTGAAGATGGTGCCTCCCT

TACTGTTAACTACCGCTACACCTACGAGGGAAGCCACATCAAAGGAGAGGCCC

AGGTGAAGGGGACTGGTTTCCCTGCTGACGGTCCTGTGATGACCAACTCGCTG

ACCGCTGCGGACTGGTGCAGGTCGAAGAAGACTTACCCCAACGACAAAACCAT

CATCAGTACCTTTAAGTGGAGTTACACCACTGGAAATGGCAAGCGCTACCGGA

GCACTGCGCGGACCACCTACACCTTTGCCAAGCCAATGGCGGCTAACTATCTG

AAGAACCAGCCGATGTACGTGTTCCGTAAGACGGAGCTCAAGCACTCCAAGAC

CGAGCTCAACTTCAAGGAGTGGCAAAAGGCCTTTACCGATGTGATGGGCATGG

ACGAGCTGTACAAGTAAcatcccgggtgaattcacaattcgattatatttatactggactatttttacatctgttcgg

ttattttcacatttatttttctatatatatcttataaacgttttaaaacccatgtaatttttgttaagctgtaatataaaagacgtccta

acaaacttcttttattactgaatttcctttaattataataaataacaagttttaaaataaattcaggcaattaaggcgctcctgaggt

actaaaattaatgtaaacatttaaaattaacttggatggtcttaagtactgtactcgtgattttgttatactttattattagaaaagt

cgtctattaacttttgttccttaatttacttgattaaattgtcgcttaatttatcaaatcaggttttgcgcgttattttagagaaaaac

ttattagaaaaatgaataagcaaagtttaggctaacatgtttttttattattttaaatagttcaagtcaatgacgtataaaccagctt

ttgttccctttagtgagggttaattgcgcgcttggcgtaatcatggtcatagctgtttcctgtgtgaaattgttatccgctcacaattc

cacacaacatacgagccggaagcataaagtgtaaagcctggggtgcctaatgagtgagctaactcacattaattgcgttgcgctca

ctgcccgctttccagtcgggaaacctgtcgtgccagctgcattaatgaatcggccaacgcgcggggagaggcggtttgcgtattgg

gcgctcttccgcttcctcgctcactgactcgctgcgctcggtcgttcggctgcggcgagcggtatcagctcactcaaaggcggtaat

acggttatccacagaatcaggggataacgcaggaaagaacatgtgagcaaaaggccagcaaaaggccaggaaccgtaaaaagg

ccgcgttgctggcgtttttccataggctccgccccctgacgagcatcacaaaaatcgacgctcaagtcagaggtggcgaaacccg

acaggactataaagataccaggcgtttccccctggaagctccctcgtgcgctctcctgttccgaccctgccgcttaccggatacctgt

ccgcctttctcccttcgggaagcgtggcgctttctcatagctcacgctgtaggtatctcagttcggtgtaggtcgttcgctccaagct

gggctgtgtgcacgaaccccccgttcagcccgaccgctgcgccttatccggtaactatcgtcttgagtccaacccggtaagacacga

cttatcgccactggcagcagccactggtaacaggattagcagagcgaggtatgtaggcggtgctacagagttcttgaagtggtggc

ctaactacggctacactagaaggacagtatttggtatctgcgctctgctgaagccagttaccttcggaaaaagagttggtagctctt

gatccggcaaacaaaccaccgctggtagcggtggtttttttgtttgcaagcagcagattacgcgcagaaaaaaaggatctcaaga

agatcctttgatcttttctacggggtctgacgctcagtggaacgaaaactcacgttaagggattttggtcatgagattatcaaaaag

gatcttcacctagatccttttaaattaaaaatgaagttttaaatcaatctaaagtatatatgagtaaacttggtctgacagttaccaa

tgcttaatcagtgaggcacctatctcagcgatctgtctatttcgttcatccatagttgcctgactccccgtcgtgtagataactacgat

acgggagggcttaccatctggccccagtgctgcaatgataccgcgagacccacgctcaccggctccagatttatcagcaataaacc

agccagccggaagggccgagcgcagaagtggtcctgcaactttatccgcctccatccagtctattaattgttgccgggaagctaga

gtaagtagttcgccagttaatagtttgcgcaacgttgttgccattgctacaggcatcgtggtgtcacgctcgtcgtttggtatggctt

cattcagctccggttcccaacgatcaaggcgagttacatgatcccccatgttgtgcaaaaaagcggttagctccttcggtcctccga

tcgttgtcagaagtaagttggccgcagtgttatcactcatggttatggcagcactgcataattctcttactgtcatgccatccgtaag

atgcttttctgtgactggtgagtactcaaccaagtcattctgagaatagtgtatgcggcgaccgagttgctcttgcccggcgtcaat

acgggataataccgcgccacatagcagaactttaaaagtgctcatcattggaaaacgttcttcggggcgaaaactctcaaggatct

taccgctgttgagatccagttcgatgtaacccactcgtgcacccaactgatcttcagcatcttttactttcaccagcgtttctgggtga

gcaaaaacaggaaggcaaaatgccgcaaaaaagggaataagggcgacacggaaatgttgaatactcatactcttccttttcaat

attattgaagcatttatcagggttattgtctcatgagcggatacatatttgaatgtatttagaaaaataaacaaatagggttccgc

gcacatttccccgaaaagtgccac

B.2.4 Sp5 promoter::Sp5-YPet

ctaaattgtaagcgttaatattttgttaaaattcgcgttaaatttttgttaaatcagctcatttttaaccaataggccgaa
atcggcaaaatcccttataaatcaaaagaatagaccgagatagggttgagtgttgttccagtttggaacaagagtccactattaaa
gaacgtggactccaacgtcaaagggcgaaaaaccgtctatcagggcgatggcccactacgtgaaccatcaccctaatcaagtttt
ttggggtcgaggtgccgtaaagcactaaatcggaaccctaaagggagcccccgatttagagcttgacggggaaagccggcgaac
gtggcgagaaaggaagggaagaaagcgaaaggagcgggcgctagggcgctggcaagtgtagcggtcacgctgcgcgtaaccac
cacacccgccgcgcttaatgcgccgctacagggcgcgtcccattcgccattcaggctgcgcaactgttgggaagggcgatcggtgc
gggcctcttcgctattacgccagctggcgaaaggggatgtgctgcaaggcgattaagttgggtaacgccagggttttcccagtca
cgacgttgtaaaacgacggccagtgagcgcgcgtaatacgactcactatagggcgaattggCTAGTTCTAATTTAG
CTCTATTACGTTCGCAAAGTTGACAAAGTCGCAAATTTTTTTCTTTTTCAAAAG
ACCTCCCATTCATTTTAATAAAGACTGGTTCTAATTTTGCTTTATCACGCTTAT
AAAAATTGACAAAGTCGCAAGTACTTTGTTTTTTAAAAGACCTCCCATTCATTG
AGATAAATACTAGTTATTTTCATGTATCATTGAAATAGTAAACAATTCATTCTA
GTTTTTATTTGTCTAGGGCAGTATTTCACACCTTCCACAAGTGCGAAACGTTTT
ATTTACTTGATTGAGTAAATTAATTTAAAATAAAATAAAAAAATAAGAACTTA
ATGTGAAAAAAAAAACAAAACAAAAACAATAAAAAAAAAAACAATGTAAAATA
TTTCTCATAGCTGTTGAAATATTAAAAAGACGGAAGGAAAAATATAACGGCAA
AGCTAAATTCTTTTCTGCGTATTGCTTTTTATCTCTTTATTGTCTGTTTGTTGC
TTTTCACTGCATTCTATTTTGTGCTTAATAAATCTCAATCGATTTTAAGGAATG
ACTAGGATGTTTCATTTTGTATATATCAATAACTGAAATATTAAAAATCTCCTC

AGTGCATCCGTTCGTTAGACAATTGGGGGTATTAACTCAATTATTTCCTGAAT

ATAAACTCAACAAGTAAAAAAGTTTCATCCGTAAGCAAGCAAGAATAACGACA

CTTGTTTACATTTAAGAATTTCTTAACTTTATGTAAAAAACAATTCTTAGTTAA

AAACGAAGTAAAAGGGTTTTAATTTTTTGTTTTTTAGTTGAAAACAAATTGCT

AAATAAAACTTAATTTAAAAAAAAAAAACCAAATATTTAAAATGATAAACTGG

TTAAAATTAATAGATTATACAAACCATTGTAAGCATTTAAAAACAATTTTTTTT

TTATAAAAACAACAACAAAAAAATTTCACCTAATTACTCCGCCTTTGTTAATAA

AACCTCCGTTTTACAGTTAAAAGTAATGTATGAACCGTAATCCCTATTACAAAA

AAATGGTATATTGTTTATAAAGACGTTTTGATGATTGTAGCTTATTTTATATT

TTTGTTGCTTTTGTTTGTTTTCCTTGTTGTTGTTTTTAATTTGATTAGTTATAT

TCTTACGGCCTTACGACCACGTTTGCTGTTTTAAATCGCGAGCGTTGCTTTGA

CTTTACACGAAGCCTCTAAAACAAACATAAAGAGAATTCATCGAAAGTAAAAA

AAATCATGCTGACCTTCGGTGATCCGTAATTGAAATTGATATATATTTTCTCCC

TATTTTGACATATAAATGGTTAAAGTTAATCTTTTTATTAAACTCAATCAATTT

CAACAAAATAAGTGTCAAGTTTACTGCTTATTTCAAGTAACAAATAAGTCTTAT

TGTAAATAAAGTTATTGTTTAAAAGGGATTGAAACTTCAATCATTATTGTAAT

AAAGAAGAATTTCATGTAAGATTTGTATTTATTAAAATTAAATAAACTAAATG

AAACAAAAGCGCTACGTCAAATTTATATTTTGATTATTAAGAGGAATTTTTTT

ACCTAATGTAAAACTACTGTAAAAATCGACTGAATCAATAAGGTCAGAGAGAC

TAGGTCAGCGAGTTTGGATCATTAAAATCGATAACAATAATTAACGATATAGT

TTATAATGATAGGAAACTTACACTTGACATTTAAATGGGAAGTCCTGAGGCTA

TAACGTTCGTTTGTCGTGGGTAGATAAGCCAATTGACAAAACCATCATCTTAT

ATTTTTATGGGCGCCAAATGTTTATCATGTTTAATTTCTTTTATATAAATGATA

AAAACATTTAACCACAAATTATTTTTTTTATCTCCAAATGAAATCAAGAACTTT

TAAGTCATAAAAAGTAGCGACAGCGCCAGTGATAATCATAGACAAGTGTACAC

ATTAGCTTATCAAAAAGTACGCTAGAGTAAAGCTTATTGTTTTGTTTTGGCTA

GGATATATCCTTCTCGTTAAAATAATTTGTCCTACTTTTATATACGATATTCAT

ATTTTTAGGTTTCTTGTTTCGATATATATATATATTTCGTTATGTTTGTATGTA

TATATGTGTTTGTTTGTATGTGTATGTAAAAATATGAAATATACTTTTTGCAA

ATCTTTGTAGAAGTTTAATAAATAAAGTATCAAGTTTAAAAATTCCTTCGATAT

TTTTAAAGCTTCAATTTGGTTGGGCGTAGACACATTAGTAATTGCGGTAAAGA

TCAGTAAGAATTCTAAATAGACGTTAATTTTAAAACCTGGCCTGCCCCTTGATT

ATTTAATTTGAAATTTTTAAGCTGTCTCCATTTCAACCACAGTATCAATGGGTC

GGCAAAAAAAGAAAGATTGAACGTTTTATCAATTTTACCAACGAAAAACACTT

AACAAATATTGTAGTACTTTTTTAAGTTTAAATGTTTTTTGTAAAACTGTTATT

TTTAAAATAAACCTTTTACTTCTTTTTTTTTTTTTTTGAAATCGTTTTAAACTG

ATATTTAATAAAAGCTTAAATATAAATGTGGTAAAGTTCGTAAAACCAATGAG

GCAGGTGCCGGCATAGATGAAAGTGAAAGAACAATTTTTTTTATTGAACTTCA

CATTTACTGTGGATTGTCGGAATGTTTTACTATTAAGTTGATTTGAAGTCAAA

AACAAAATAACAAAATCAACCAATGAACTTCCTTAGAAATTGTTTAATCATAAA

CCAATCAAATAGCGTTTTATATCTTTTAACCAATAAGATAACAATTTTATTGTT

TTGTCGGCATCTTAAGATATTAAAAGTTAATATCTTTTCCGCCTTACGTATTCT

GTTTATCACCGCCTCTTAGACCATCCCATTTGTACGTAAACAGAGAAAATATG

ATCGCAACGCGCCATTTCTCAGTCAGAGGCGTGACATTAACCCCTTATCAAAG

AAGCCGAAGCTATTTAAGATAAgatggcggtttcatgtcacctccaagtcgtgttccaacaacaatcagccca

aactttaaaagtcaacatcattgtcttaaagaacatattaagtattcaccgttggcattacttgcagcaacctgtaaaaaaattgga

cggcctatcagcccattagaacaaacatctcctaaaaaaatttttcaaccatggaatcacacgtttgaatcacacaattatgacac

acctatttcaccaaatagcaaagtgagacactttctagagacaaatttctcgcttccaccaagtcctccattaaaatcagagatagt

aaaagttcccccaacaataagaccaatgccgatgacgaatgtaatgcaagaaaaagcgactttaaattactcacaaaaactttct

ccacctccgtgtctcgcatgttcagctggtcaaaagtgcaatggaataaataaaatatctccagttttgctttctccgcctgcctcgc

caatctcatggttatttcctcaaaatattattcaatctcatccttctaaagtatcaattaacgagcaccacataaaagaatattccga

acattctcaagctgatccaacgcgttttgtaaactacgtttacaaaaacgtcgactcttctcaagcaaaacctaatctaataattcg

acacgataacatgatctcctctacacaatcgtataacaatcgtatattctcatcttcgccacatttaactacaacatcccacatatat

tcaatgtctacatcaattcctgctcaatcgcatgcagttataccgaacagcgttgcaacccgaagatgtcgtcgctgtaaatgccca

aactgcatatcaggacaacaatctgagccaaataaacccaagcagcacgtatgtcatattccagggtgcggaaaggtttatggta

aaactagtcaccttaaagctcatttaagatggcatgctggattgcgtccattcgtttgtaattggttattttgcaacaaatcctttac

tcgttctgatgaactccaacgtcacttgcgaacacatacgggcgaaaagcgatttgcctgtcaagattgcggcaaacgttttactcg

ttccgaccatttatcgaaacatatgaaaacacaccaaaataaaaaacaagaaaacacatttgtaaaagatactgtcatagaagtg

attaaagacaatgtcgatgaaaattgcgatgagaatgttatggaacttgaagtaaacgttgaaaacGGTGGTGGTATG

GTGAGCAAAGGCGAAGAGCTGTTCACCGGCGTGGTGCCCATCCTGGTGGAGCT

GGACGGCGACGTGAACGGCCACAAGTTCAGCGTGAGCGGCGAGGGCGAGGGC

GACGCCACCTACGGCAAGCTGACCCTGAAGCTGCTGTGCACCACCGGCAAGCT

GCCCGTGCCCTGGCCCACCCTGGTGACCACCCTGGGCTACGGCGTGCAGTGCT

TCGCCCGGTACCCCGACCACATGAAGCAGCACGACTTCTTCAAGAGCGCCATG

CCCGAGGGCTACGTGCAGGAGCGGACCATCTTCTTCAAGGACGACGGCAACTA

CAAGACCCGGGCCGAGGTGAAGTTCGAGGGCGACACCCTGGTGAACCGGATCG

AGCTGAAGGGCATCGACTTCAAGGAGGACGGCAACATCCTGGGCCACAAGCTG

GAGTACAACTACAACAGCCACAACGTGTACATCACCGCCGACAAGCAGAAGAA

CGGCATCAAGGCCAACTTCAAGATCCGGCACAACATCGAGGACGGCGGCGTGC

AGCTGGCCGACCACTACCAGCAGAACACCCCCATCGGCGACGGCCCCGTGCTG

CTGCCCGACAACCACTACCTGAGCTACCAGAGCGCCCTGTTCAAGGACCCCAA

CGAGAAGCGGGACCACATGGTGCTGCTGGAGTTCCTGACCGCCGCCGGCATCA

CCGAGGGCATGAACGAGCTCTATAAGTAAcatcccgggtgaattcacaattcgattatatttatactgg

actatttttacatctgttcggttattttcacatttatttttctatatatatcttataaacgttttaaaacccatgtaatttttgttaagct

gtaatataaaagacgtcctaacaaacttcttttattactgaatttcctttaattataataaataacaagttttaaaataaattcaggc

aattaaggcgctcctgaggtactaaaattaatgtaaacatttaaaattaacttggatggtcttaagtactgtactcgtgattttgtta

tactttattattagaaaagtcgtctattaacttttgttccttaatttacttgattaaattgtcgcttaatttatcaaatcaggttttgc

gcgttattttagagaaaaacttattagaaaaatgaataagcaaagtttaggctaacatgtttttttattattttaaatagttcaagtc

aatgacgtataaaccagcttttgttccctttagtgagggttaattgcgcgcttggcgtaatcatggtcatagctgtttcctgtgtgaa

attgttatccgctcacaattccacacaacatacgagccggaagcataaagtgtaaagcctggggtgcctaatgagtgagctaactc

acattaattgcgttgcgctcactgcccgctttccagtcgggaaacctgtcgtgccagctgcattaatgaatcggccaacgcgcgggg

agaggcggtttgcgtattgggcgctcttccgcttcctcgctcactgactcgctgcgctcggtcgttcggctgcggcgagcggtatcag

ctcactcaaaggcggtaatacggttatccacagaatcaggggataacgcaggaaagaacatgtgagcaaaaggccagcaaaagg

ccaggaaccgtaaaaaggccgcgttgctggcgtttttccataggctccgccccctgacgagcatcacaaaaatcgacgctcaagt

cagaggtggcgaaacccgacaggactataaagataccaggcgtttccccctggaagctccctcgtgcgctctcctgttccgaccctg

ccgcttaccggatacctgtccgcctttctcccttcgggaagcgtggcgctttctcatagctcacgctgtaggtatctcagttcggtgta

ggtcgttcgctccaagctgggctgtgtgcacgaaccccccgttcagcccgaccgctgcgccttatccggtaactatcgtcttgagtcc

aacccggtaagacacgacttatcgccactggcagcagccactggtaacaggattagcagagcgaggtatgtaggcggtgctacag

agttcttgaagtggtggcctaactacggctacactagaaggacagtatttggtatctgcgctctgctgaagccagttaccttcggaa

aaagagttggtagctcttgatccggcaaacaaaccaccgctggtagcggtggttttttgtttgcaagcagcagattacgcgcaga

aaaaaaggatctcaagaagatcctttgatcttttctacggggtctgacgctcagtggaacgaaaactcacgttaagggattttggtc

atgagattatcaaaaaggatcttcacctagatccttttaaattaaaaatgaagttttaaatcaatctaaagtatatatgagtaaact

tggtctgacagttaccaatgcttaatcagtgaggcacctatctcagcgatctgtctatttcgttcatccatagttgcctgactccccgt

cgtgtagataactacgatacgggagggcttaccatctggccccagtgctgcaatgataccgcgagacccacgctcaccggctccag

atttatcagcaataaaccagccagccggaagggccgagcgcagaagtggtcctgcaactttatccgcctccatccagtctattaatt

gttgccgggaagctagagtaagtagttcgccagttaatagtttgcgcaacgttgttgccattgctacaggcatcgtggtgtcacgct

cgtcgtttggtatggcttcattcagctccggttcccaacgatcaaggcgagttacatgatcccccatgttgtgcaaaaaagcggtta

gctccttcggtcctccgatcgttgtcagaagtaagttggccgcagtgttatcactcatggttatggcagcactgcataattctcttac

tgtcatgccatccgtaagatgcttttctgtgactggtgagtactcaaccaagtcattctgagaatagtgtatgcggcgaccgagttg

ctcttgcccggcgtcaatacgggataataccgcgccacatagcagaactttaaaagtgctcatcattggaaaacgttcttcggggc

gaaaactctcaaggatcttaccgctgttgagatccagttcgatgtaacccactcgtgcacccaactgatcttcagcatcttttacttt

caccagcgtttctgggtgagcaaaaacaggaaggcaaaatgccgcaaaaaagggaataagggcgacacggaaatgttgaatact

catactcttccttttcaatattattgaagcatttatcagggttattgtctcatgagcggatacatatttgaatgtatttagaaaaata

aacaaataggggttccgcgcacatttccccgaaaagtgccac

B.3 Riboprobe sequences

Inx1

ATGGGAATAAGCTGGTTCAATGACTCTGTTAAATGCTTAGTACCAGGGGTCAA

CGCCGTCGATGGCGGATTTGTTTCGCAAGCTTGTTGGATACAAGGGGTGTATG

TATACAAGGAGTTAATGTACAGATCAAGCGAGGTTGGTTATTTTGGTATTCCT

AAAGACATGGACAATGATGGTATGCTTGCTTCTGGAGAATTATGTTCGACTAC

GCCTAAATTTGGGGTTGTCAATGATAAATGCAAGCCAATGCAGAAAACATTCT

TTTTACAGTATCAATGGATGCCTTTTTTAATTGCTGCGTTGTCCATACTCTATT

ATTTGCCTTACATTGGCTTTCGTTCGGCTAACAGCGATCTTATCAGTCTTAAAA

ATACTATTAAAGGTGGAACAGCTAATGCTGAAAAAATTGCCAAAAACTTCTTT

GACAGACATTCAAACCCATCTCGCAATATGACATTGAGAGTGGTGTTCAATAT

TTTAATTAAAGTATTGTACATTGTTGCCAACTTGGTGGCTTTTTTGGGCCTCG

ATAATCTTCTTAATGGCGAATTTGTCTCCT

Inx4

ATGTCTATCATTACCGGAAACCTTAAGTCGTTACTTACAATTAAGTTCAAACCA

AGACATGATACGTTTACAGATCAATTTAATCGTATTTTTATGGTGAAAATGGC

TATGGTCGCATCATTTTTACTTGGTTTAAATTGGTTTAAAGATACAATTACAT

GTATTGTTCCTGCATCAGCTGGAATAGATAAAGGTTATGTTGCTCAGGGTTGT

TGGATCCAAGGTTTTTATATTTACAAAGAGCTTAAACGAGTTCCTGGTCTTCT

TGGCTATTACGGTGTACCAAAAGATATATATCAAGACGGAATGTTTGAGGATG

GTACTCTTTGCAAAACTAGCGAAAAAAACTGCATTCCAATGACAAAAACATTT

TATTTACAGTACCAATGGTTTCCTTTTTATATTGCTAGTCTCGGTTTGCTTTAC

TATTTTCCGTACATTGTTTTCCGTTTCGTAAATACCGACTTGATCAGTTTGAGA

ACTAGTATTAAAGCCATAAACGTAAACATCGATGATTTAGTGAAAAACTACTT

TAATTACCAGATAAACCCACCAAACAG

Inx5

ATGTCAACTATTACCAACGATATCAAAAAGTTAATAAATTTTAAGTACAAGTC

AAGAAACGACTCGATAACAGATCAGTTTAATCGAGTATTGATGATGAAAATAA

TGCTTATTGGTGCATTTTTGACTGGAATGAGCTGGTACAAGGATGAAATTAAA

TGTCTTGCTCCGAAAACGCCAAACGATCACATAAAATTATTTTCTTCACAAGCG

TGCTGGATTAACGGATTTTACATCTATAAAGAGCTAAAAACAAAGAGCAACTT

TTTTGGCTATTATGGTGTACCAATTGACATGAACCACAATGGAACAACATTGA

GTAACGAAACATGCGTGGCATTAGGTGGCCTATCGAAGCGATGTAAGCCAATG

ACTAAACTTTTCTATCTTCAATTTCAATGGTTTCCATTCTTTCTTGGAATTCTT

GCTTTGTCTTTTTATCTTCCGTATTTACTATTCCGATATGTGAATAGCGAT

Sp5

AATTACTCACAAAAACTTTCTCCACCTCCGTGTCTCGCATGTTCAGCTGGTCAA

AAGTGCAATGGAATAAATAAAATATCTCCAGTTTTGCTTTCTCCGCCTGCCTCG

CCAATCTCATGGTTATTTCCTCAAAATATTATTCAATCTCATCCTTCTAAAGTA

TCAATTAACGAGCACCACATAAAAGAATATTCCGAACATTCTCAAGCTGATCCA

ACGCGTTTTGTAAACTACGTTTACAAAAACGTCGACTCTTCTCAAGCAAAACCT

AATCTAATAATTCGACACGATAACATGATCTCCTCTACACAATCGTATAACAAT

CGTATATTCTCATCTTCGCCACATTTAACTACAACATCCCACATATATTCAATG

TCTACATCAATTCCTGCTCAATCGCATGCAGTTATACCGAACAGCGTTGCAACC

CGAAGATGTCGTCGCTGTAAATGCCCAAACTGCATATCAGGACAACAATCTGA

GCCAAATAAACCCAAGCAGCACGTATGTCATATTCCAGGGTGCGGAAAGGTTT

ATGGTAAAACTAGTCACCTTA